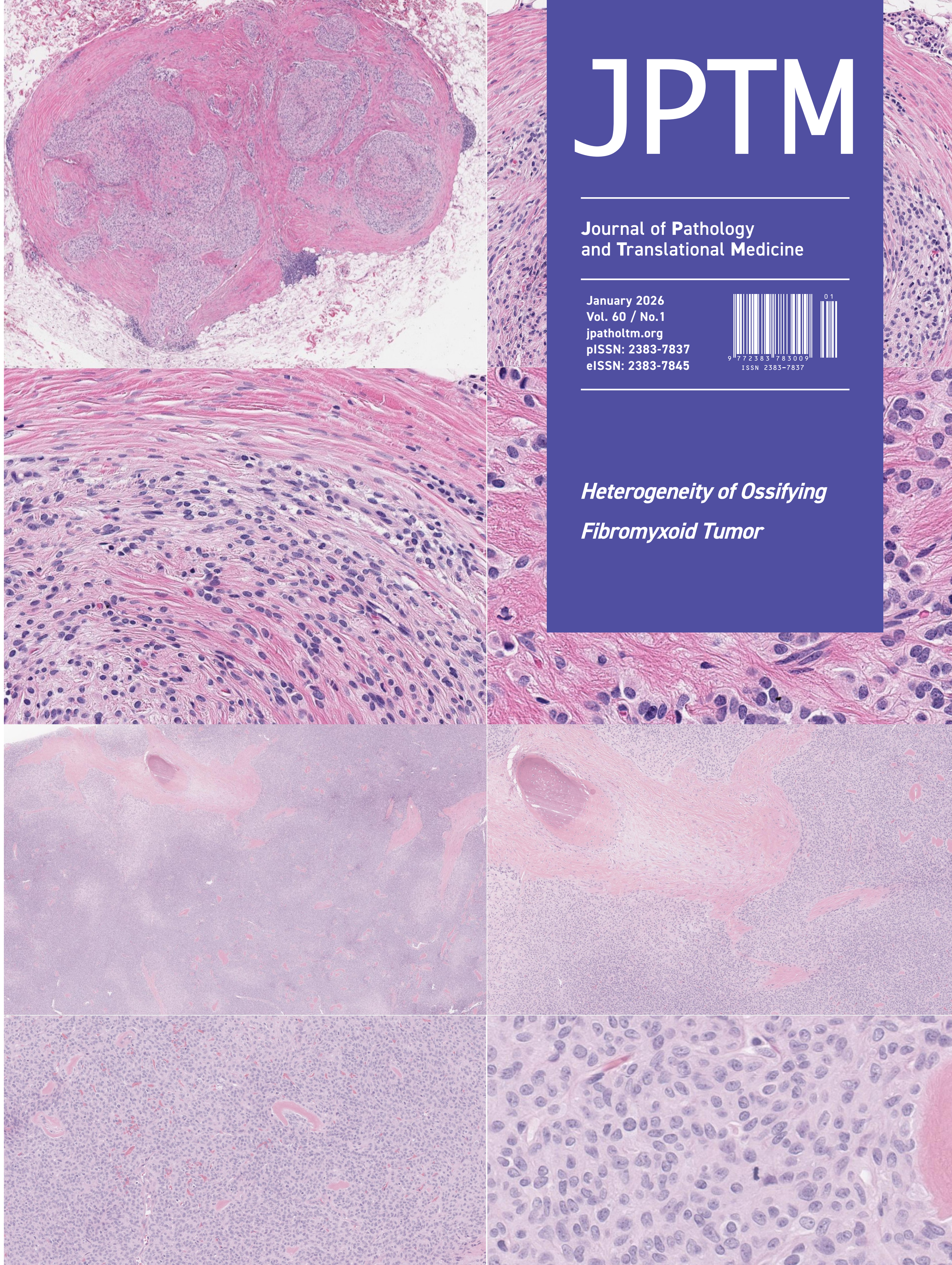

JPTM

Journal of Pathology
and Translational Medicine

January 2026
Vol. 60 / No.1
jpatholtm.org
pISSN: 2383-7837
eISSN: 2383-7845

01
9 772383 783009
ISSN 2383-7837

Heterogeneity of Ossifying Fibromyxoid Tumor

Journal of Pathology and Translational Medicine

Vol. 60, No.1, pp 1-128, January 2026

JPTM
Journal of Pathology and
Translational Medicine

JPTM

jpatholtm.org
pISSN 2383-7837 · eISSN 2383-7845

Vol. 60, No.1, January 2026

Published on 15 January 2026

Aims & Scope

The Journal of Pathology and Translational Medicine is an open venue for the rapid publication of major achievements in various fields of pathology, cytopathology, and biomedical and translational research. The Journal aims to share new insights into the molecular and cellular mechanisms of human diseases and to report major advances in both experimental and clinical medicine, with a particular emphasis on translational research. The investigations of human cells and tissues using high-dimensional biology techniques such as genomics and proteomics will be given a high priority. Articles on stem cell biology are also welcome. The categories of manuscript include original articles, review and perspective articles, case studies, brief case reports, and letters to the editor.

Subscription Information

To subscribe to this journal, please contact the Korean Society of Pathologists/the Korean Society for Cytopathology. Full text PDF files are also available at the official website (https://jpatholtm.org). *Journal of Pathology and Translational Medicine* is indexed by Emerging Sources Citation Index (ESCI), PubMed, PubMed Central, Scopus, KoreaMed, KoMCI, WPRIM, Directory of Open Access Journals (DOAJ), and CrossRef. Circulation number per issue is 50.

Contact the Korean Society of Pathologists/the Korean Society for Cytopathology

Publishers: Kang, Gyeong Hoon, MD; Choi, Yoon Jung, MD
Editors-in-Chief: Jung, Chan Kwon, MD; Park, So Yeon, MD
Published by the Korean Society of Pathologists/the Korean Society for Cytopathology

Editorial Office
Suite 706, 217 Saechang-ro, Yongsan-gu, Seoul 04376, Korea
Tel: +82-2-795-3094 Fax: +82-2-790-6635 E-mail: office@jpatholtm.org
#1508 Renaissancetower, 14 Mallijae-ro, Mapo-gu, Seoul 04195, Korea
Tel: +82-2-593-6943 Fax: +82-2-593-6944 E-mail: office@jpatholtm.org

Printed by M2PI
#805, 26 Sangwon 1-gil, Seongdong-gu, Seoul 04779, Korea
Tel: +82-2-6966-4930 Fax: +82-2-6966-4945 E-mail: support@m2-pi.com

Manuscript Editing by InfoLumi Co.
210-202, 421 Pangyo-ro, Bundang-gu, Seongnam 13522, Korea
Tel: +82-70-8839-8800 E-mail: infolumi.chang@gmail.com

Front cover image: Histologic spectrum of ossifying fibromyxoid tumor from nearly classic to malignant (p. 8, p. 11)

© 2026 The Korean Society of Pathologists/The Korean Society for Cytopathology
Ⓒ Journal of Pathology and Translational Medicine is an Open Access journal under the terms of the Creative Commons Attribution Non-Commercial License (https://creativecommons.org/licenses/by-nc/4.0).
∞ This paper meets the requirements of KS X ISO 9706, ISO 9706-1994 and ANSI/NISO Z.39.48-1992 (Permanence of Paper).

This work was supported by the Korean Federation of Science and Technology Societies Grant funded by the Korean Government (Ministry of Education).

VENTANA

Roche

VENTANA
Kappa and Lambda Dual ISH
mRNA Probe Cocktail

Dual Staining, High Sensitivity on One Slide

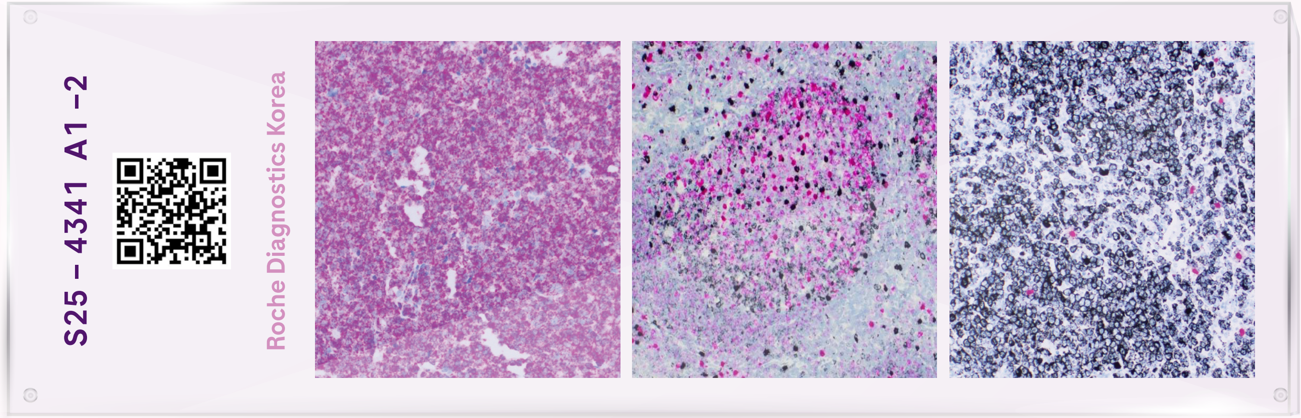

이점	Kappa and Lambda Dual ISH	IHC, ISH 단일 검사 (Kappa, Lambda 개별 슬라이드)	유세포 분석법 (Flow Cytometry)
하나의 슬라이드에서 다중 분석 가능	✓		
포르말린 고정 조직 호환 가능	✓	✓	
제한된 조직량으로 검사 가능	✓	✓	
백그라운드 염색 감소 가능	✓		
형태학적 해석 가능	✓	✓	
높은 민감도로 B세포 림프종과 형질세포 신생물 진단 가능	✓		✓

Roche
한국로슈진단(주)
서울특별시 강남구 테헤란로 108길 22 서경빌딩 2층(06174)
Tel 02-550-3300 | Fax 02-501-6666 | https://diagnostics.roche.com/kr/ko

VENTANA Kappa and Lambda Dual ISH mRNA Probe Cocktail
체외 수인 25-4191호
MC-KR-01894

Editorial Board

Editors–in-Chief

Jung, Chan Kwon, MD (*The Catholic University of Korea, Korea*) https://orcid.org/0000-0001-6843-3708
Park, So Yeon, MD (*Seoul National University, Korea*) https://orcid.org/0000-0002-0299-7268

Associate Editors

Bychkov, Andrey, MD (*Kameda Medical Center, Japan; Nagasaki University Hospital, Japan*) https://orcid.org/0000-0002-4203-5696
Kim, Haeryoung, MD (*Seoul National University, Korea*) https://orcid.org/0000-0002-4205-9081
Lee, Hee Eun, MD (*Mayo Clinic, USA*) https://orcid.org/0000-0001-6335-7312
Shin, Eunah, MD (*Yongin Severance Hospital, Yonsei University, Korea*) https://orcid.org/0000-0001-5961-3563

Editorial Board

Avila-Casado, Maria del Carmen, MD (*University of Toronto, Toronto General Hospital UHN, Canada*)
Bae, Jeong Mo, MD (*Seoul National University, Korea*)
Bae, Young Kyung, MD (*Yeungnam University, Korea*)
Bongiovanni, Massimo, MD (*Lausanne University Hospital, Switzerland*)
Bova, G. Steven, MD (*University of Tampere, Finland*)
Choi, Joon Hyuk, MD (*Yeungnam University, Korea*)
Chong, Yo Sep, MD (*The Catholic University of Korea, Korea*)
Chung, Jin-Haeng, MD (*Seoul National University, Korea*)
Fadda, Guido, MD (*Catholic University of Rome-Foundation Agostino Gemelli University Hospital, Italy*)
Fukushima, Noriyoshi, MD (*Jichi Medical University, Japan*)
Go, Heounjeong, MD (*University of Ulsan, Korea*)
Hong, Soon Won, MD (*Yonsei University, Korea*)
Jain, Deepali, MD (*All India Institute of Medical Sciences, India*)
Kakudo, Kennichi, MD (*Izumi City General Hospital, Japan*)
Kim, Jang-Hee, MD (*Ajou University, Korea*)
Kim, Jung Ho, MD (*Seoul National University, Korea*)
Kim, Se Hoon, MD (*Yonsei University, Korea*)
Kim, Young Hoon, MD (*The Catholic University of Korea, Korea*)
Komuta, Mina, MD (*Keio University, Tokyo, Japan*)
Lai, Chiung-Ru, MD (*Taipei Veterans General Hospital, Taiwan*)
Lee, C. Soon, MD (*University of Western Sydney, Australia*)
Lee, Hwajeong, MD (*Albany Medical College, USA*)
Lee, Sung Hak, MD (*The Catholic University of Korea, Korea*)
Liu, Zhiyan, MD (*Shanghai Jiao Tong University, China*)
Lkhagvadorj, Sayamaa, MD (*Mongolian National University of Medical Sciences, Mongolia*)
Lo, Regina, MD (*The University of Hong Kong, Hong Kong*)
Moran, Cesar, MD (*MD Anderson Cancer Center, U.S.A.*)
Paik, Jin Ho, MD (*Seoul National University, Korea*)
Park, Jeong Hwan, MD (*Seoul National University, Korea*)
Sakhuja, Puja, MD (*Govind Ballabh Pant Hospital, India*)
Shahid, Pervez, MD (*Aga Khan University, Pakistan*)
Song, Joon Seon, MD (*University of Ulsan, Korea*)
Tan, Puay Hoon, MD (*National University of Singapore, Singapore*)
Than, Nandor Gabor, MD (*Semmelweis University, Hungary*)
Tse, Gary M., MD (*The Chinses University of Hong Kong, Hong Kong*)
Yatabe, Yasushi, MD (*Aichi Cancer Center, Japan*)
Zhu, Yun, MD (*Jiangsu Institution of Nuclear Medicine, China*)

Ethic Editor

Choi, In-Hong, MD (*Yonsei University, Korea*)
Huh, Sun, MD (*Hallym University, Korea*)

Statistics Editors

Kim, Dong Wook (*National Health Insurance Service Ilsan Hospital, Korea*)
Lee, Hye Sun (*Yonsei University, Korea*)

Manuscript Editor

Chang, Soo-Hee (*InfoLumi Co., Korea*)

Layout Editor

Jeong, Eun Mi (*M2PI, Korea*)

Website and JATS XML File Producers

Choi, Min Young (*M2PI, Korea*)

Administrative Assistants

Lee, Hye jin (*The Korean Society of Pathologists*)
Kim, Song Yeun (*The Korean Society for Cytopathology*)

© 2026 The Korean Society of Pathologists/The Korean Society for Cytopathology

JPTM

jpatholtm.org
pISSN 2383-7837 · eISSN 2383-7845

Contents

Vol. 60, No.1, January 2026

EDITORIAL

REVIEW ARTICLES

ORIGINAL ARTICLES

CASE STUDY

© 2026 The Korean Society of Pathologists/The Korean Society for Cytopathology

JPTM

EDITORIAL

pISSN 2383-7837 · eISSN 2383-7845

Journal of Pathology and Translational Medicine 2026; 60: 1-5
https://doi.org/10.4132/jptm.2025.12.08

Advancing pathology through sixty volumes: reflections and future directions

Chan Kwon Jung[1], So Yeon Park[2], Soon Won Hong[3]

[1]Department of Hospital Pathology, College of Medicine, The Catholic University of Korea, Seoul, Korea
[2]Department of Pathology, Seoul National University College of Medicine, Seoul, Korea
[3]Department of Pathology, Yonsei University College of Medicine, Seoul, Korea

INTRODUCTION

The publication of Volume 60 of the *Journal of Pathology and Translational Medicine* (JPTM) represents a distinguished scholarly milestone—one that invites both commemoration and renewed commitment. Sixty volumes of continuous publication embody more than chronological achievement; they reflect decades of scientific effort, organizational dedication, and a sustained aspiration to contribute meaningfully to the advancement of pathology.

A BRIEF HISTORICAL REFLECTION

The origins of JPTM date to 1967, when *The Korean Journal of Pathology* was founded as the official journal of the Korean Society of Pathologists [1,2]. For many years, it served as the primary venue for surgical pathology and experimental pathology research within Korea. In response to the growing importance of cytology as a diagnostic discipline, the Korean Journal of Cytopathology was launched in 1990, and the two journals were published in parallel for nearly two decades [3].

A major structural transformation occurred in 2009, when the two journals were unified into a single publication representing both the Korean Society of Pathologists and the Korean Society for Cytopathology [3]. As part of the merger agreement, the unified journal retained the name *The Korean Journal of Pathology*, preserving continuity and reflecting the longer publishing history of the parent title [3]. A dual editorial leadership system was introduced, with each society appointing its own Editor-in-Chief—one responsible for manuscripts in surgical and experimental pathology, and the other responsible for manuscripts in cytopathology [3]. This structure ensured a balanced representation of both disciplines. The two academic societies also agreed to jointly support publication and operational costs in a 7:3 ratio, reflecting the proportional distribution of content.

A significant milestone in international visibility came earlier, when the journal was indexed in the Science Citation Index Expanded (SCIE) with Volume 41, Issue 1 in 2007 [4], a status maintained through Volume 47, Issue 6 in 2013. Although the journal was later removed from the SCIE list, this experience underscored the importance of heightened editorial rigor and deeper international engagement.

A series of transformative changes followed. The adoption of an all-English format in 2011 broadened international accessibility and encouraged global submissions. In 2015, the journal adopted its present title, the *Journal of Pathology and Translational Medicine* (JPTM), signaling an expanded scope encompassing pathology, molecular diagnostics, and translational science. In 2017, JPTM was indexed in the Emerging Sources Citation Index (ESCI), reinforcing its growing international standing and improving its discoverability within global scholarly databases.

These developments were not merely administrative adjustments; instead, they mirrored broader shifts across pathology, including the rise of molecular diagnostics, integrated trans-

Received: December 8, 2025 **Revised:** December 8, 2025 **Accepted:** December 8, 2025

Corresponding Author: Chan Kwon Jung, MD, PhD
Department of Pathology, Seoul St. Mary's Hospital, College of Medicine, The Catholic University of Korea, 222 Banpo-daero, Seocho-gu, Seoul 06591, Korea
Tel: +82-2-2258-1622, Fax: +82-2-2258-1627, E-mail: ckjung@catholic.ac.kr

This is an Open Access article distributed under the terms of the Creative Commons Attribution Non-Commercial License (https://creativecommons.org/licenses/by-nc/4.0/) which permits unrestricted non-commercial use, distribution, and reproduction in any medium, provided the original work is properly cited.
© 2026 The Korean Society of Pathologists/The Korean Society for Cytopathology

lational research, and the adoption of advanced imaging and computational technologies. Throughout these transitions, the journal refined its identity to reflect the evolving scientific landscape. Notably, since its inaugural issue, JPTM has upheld an uninterrupted tradition of timely publication, releasing every issue on schedule for six decades—an achievement made possible by the sustained dedication of its editorial leadership and contributing societies.

Now in Volume 60, JPTM stands on 60 years of continuous publication. Recent progress reflects steady and measurable growth. The journal is currently indexed in ESCI and has achieved a 2024 Journal Impact Factor of 3.0 and a 2024 CiteScore of 3.4. These metrics indicate that JPTM's publications are increasingly cited by researchers worldwide and that their relevance within the global pathology community continues to deepen.

In addition to these measurable indicators of growth, the journal's trajectory over the past 60 years has been significantly shaped by the dedication and scholarly leadership of its Editors-in-Chief (Table 1). Their collective efforts have guided JPTM through major transitions, including the integration of cytopathology, the unification of the two journals in 2009, the shift to an all-English format, the adoption of the current title, and its evolution into a globally recognized open-access platform. The continuity, stability, and integrity of JPTM are largely due to the vision, commitment, and stewardship of these individuals.

As JPTM continues to strengthen its scientific presence, it does so within a broader publishing ecosystem marked by substantial geographic imbalances.

THE CRUCIAL ROLE OF JPTM IN A WESTERN-DOMINATED PUBLISHING WORLD

Although numerous pathology journals exist worldwide, the global publishing environment remains heavily concentrated in North America and Western Europe, where long-established academic societies and commercial publishers shape both editorial standards and scientific priorities. This concentration has notable implications for researchers outside these regions, particularly those in Asia, who often face structural barriers to gaining representation in high-impact Western journals. Differences in disease epidemiology, clinical practice patterns, research priorities, and writing conventions can reduce the likelihood that regionally meaningful studies are prioritized or accepted. The rapid growth of biomedical research in Asia, driven by large patient populations, diverse disease profiles, and advancing technological capabilities, often outpaces the capacity of Western-centered publication systems to accommodate it.

Economic barriers add further inequities. The global shift to open-access publishing has increased scientific accessibility, yet the associated article processing charges are frequently prohibitive for authors without substantial institutional or governmental support. These costs disproportionately burden early-career investigators and scientists working in resource-limited environments.

Within this landscape, JPTM fulfills an essential and irreplaceable role. As a fully open-access journal, JPTM publishes manuscripts without cost to authors—or at only minimal cost for specific categories such as case studies—thereby ensuring that access to publication is determined by scientific merit rather than financial capacity. At the same time, the journal maintains rigorous peer review, broad scientific scope, and growing international reach, providing a high-quality platform for research across all areas of pathology and translational medicine.

By lowering both structural and economic barriers, JPTM enhances the global visibility of scientific work originating in Asia, enriches international literature with findings relevant to diverse populations and clinical environments, supports early-career researchers seeking an equitable pathway into global publishing, and contributes to a more balanced and representative scientific dialogue. In this regard, JPTM is not merely another pathology journal; it is an essential platform that counterbalances Western-dominated publication structures and advances global scientific communication.

SUSTAINING INTERNATIONAL REACH AND CROSS-REGIONAL DIALOGUE

Although the journal's origins are rooted in Korea, its mission has long been global in scope. The rapid evolution of pathology as an international discipline requires scholarly platforms that can sustain scientific exchange across regions with distinct clinical environments, disease patterns, and research priorities. JPTM is well-positioned to serve as such a platform, as evidenced by its growing international authorship representing Asia, Europe, the Americas, Africa, and Oceania.

Looking ahead, the journal seeks to deepen its contribution to cross-regional dialogue through initiatives such as thematic

https://doi.org/10.4132/jptm.2025.12.08

Table 1. Editors-in-Chief of the *Journal of Pathology and Translational Medicine*

Year of service	Editor-in-Chief	Affiliation	Associate Editor	Affiliation
1967 to 1970	Sang In Kim	Seoul National University	-	-
1970 to 1971	Soo Young Lee	The Catholic University of Korea	-	-
1971 to 1972	Yoo Bock Lee	Yonsei University	-	-
1972 to 1973	Sang Kook Lee	Seoul National University	-	-
1973 to 1976	Yong Il Kim	Seoul National University	-	-
1976 to 1977	Eui Keun Ham	Seoul National University	-	-
1978 to 1978	Jung Dal Lee	Korea Hospital	-	-
1978 to 1979	Han Ik Cho	Seoul National University	-	-
1979 to 1980	In Jun Choi	Yonsei University	-	-
1980 to 1981	Jung Dal Lee	Kyung Hee University	-	-
1981 to 1984	In Jun Choi	Yonsei University	-	-
1984 to 1986	Jung Dal Lee	Hanyang University	-	-
1986 to 1990	Yong Il Kim	Seoul National University	-	-
1991 to 1992	Chanil Park	Yonsei University	-	-
1993 to 1994	Song Kye Yong	Chung-Ang University	-	-
1995 to 1996	Nam Hee Won	Korea University	Han Kyeom Kim	Korea University
1997 to 1998	Moon Hyang Park	Hanyang University	Eun Kyung Hong	Hanyang University
1999 to 2000	Geung Hwan Ahn	Sungkyunkwan University	Cheol Keun Park	Sungkyunkwan University
2001 to 2002	Yeon-Lim Suh	Sungkyunkwan University	Sangyong Song	Sungkyunkwan University
2003 to 2004	Jae Yoon Ro	University of Ulsan	Eunsil Yu	University of Ulsan
			Jung-Sun Kim	Sungkyunkwan University
2005 to 2006	Eunsil Yu	University of Ulsan	Kyung-Ja Cho	University of Ulsan
2007 to 2008	Jeong-Wook Seo	Seoul National University	Kyung-Ja Cho	University of Ulsan
			Chan-Sik Park	University of Ulsan
2009 to 2012	Kyung-Ja Cho	University of Ulsan	Jin-Haeng Chung	Seoul National University
	So-Young Jin	Soonchunhyang University	Jee Young Han	Inha University
2013 to 2014	Soon Won Hong	Yonsei University	Jin-Haeng Chung	Seoul National University
	Kyung-Ja Cho	University of Ulsan	Jee Young Han	Inha University
2015 to 2016	Soon Won Hong	Yonsei University	Yoon Jung Choi	National Health Insurance Service Ilsan Hospital
	Chong Jai Kim	University of Ulsan	Jee Young Han	Inha University
2017 to 2018	Soon Won Hong	Yonsei University	Chan Kwon Jung	The Catholic University of Korea
	Chong Jai Kim	University of Ulsan	So Yeon Park	Seoul National University
2019 to present	Chan Kwon Jung	The Catholic University of Korea	Eunah Shin	Yonsei University
	So Yeon Park	Seoul National University	Haeryoung Kim	Seoul National University
			Andrey Bychkov[a]	Kameda Medical Center
			Hee Eun Lee[a]	Mayo Clinic

The journal was published under the title *The Korean Journal of Pathology* from its founding in 1967 until 2014; it was renamed the *Journal of Pathology and Translational Medicine* in 2015, under which title it continues to the present.

[a] Andrey Bychkov has served as Associate Editor since 2022, and Hee Eun Lee since 2023.

special issues developed in collaboration with global experts, invited reviews that synthesize emerging ideas from diverse geographic settings, and editorial partnerships that connect researchers working on complementary scientific challenges across continents. The planned expansion of the editorial board to include a broader range of international scholars will further reinforce these efforts.

JPTM aims to cultivate an environment in which scientific perspectives from globally diverse contexts are equitably represented. Such inclusivity enriches the global understanding of disease, particularly in pathology, where variations in epidemiology, genetics, and environment underscore the need for knowledge drawn from multiple regions.

CURRENT POSITION AND STRENGTHS OF JPTM

Today, JPTM occupies a position of growing international prominence. Submissions come from across Asia, Europe, and the Americas, reflecting a readership and contributor base that extends well beyond the journal's national origins. Its multidisciplinary scope encompasses surgical pathology, cytopathology, molecular pathology, digital pathology, tumor biology, translational oncology, and the full spectrum of organ-based diagnostic specialties. Editorial processes have been strengthened through careful oversight, ethical rigor, and consistent application of peer-review standards. Coupled with an uninterrupted publication record and rising citation metrics, these developments demonstrate that JPTM has matured into a stable, credible, and internationally relevant journal.

LOOKING AHEAD: PRIORITIES FOR THE NEXT DECADE

As pathology continues to evolve toward deeper integration with molecular medicine, spatial and single-cell technologies, advanced imaging, and computational science, JPTM must remain responsive to this changing landscape. Future priorities include strengthening the journal's focus on studies that bridge diagnostic pathology with translational and mechanistic research, expanding the publication of clinically impactful investigations, enhancing editorial transparency and adherence to global ethical standards, and supporting early-career investigators through an accessible and equitable publication model. International participation should continue to grow through collaborative initiatives and themed issues that highlight emerging areas of scientific importance. A long-term aspiration remains the journal's eventual re-indexing in SCIE, achieved through continuous improvements in scientific quality, editorial governance, and international engagement.

UPHOLDING EDITORIAL INTEGRITY IN THE ERA OF ARTIFICIAL INTELLIGENCE

As artificial intelligence (AI) becomes more deeply integrated into scientific research and clinical practice, the scholarly publishing ecosystem faces new ethical and procedural challenges. AI-assisted writing tools, algorithmic data analysis, automated figure generation, and large language models offer powerful capabilities but also pose risks related to authorship responsibility, data authenticity, image manipulation, plagiarism, and the erosion of scientific accountability.

Recognizing these challenges, JPTM has strengthened its editorial policies to ensure the responsible, transparent, and ethically governed use of AI in scientific publishing. AI tools cannot be listed as authors, as they cannot assume responsibility for the integrity of published work. Any use of generative AI or algorithmic assistance in writing, image processing, or data analysis must be clearly disclosed in the manuscript, including the tool used, the purpose for its use, and the extent of its contribution. Undisclosed AI-generated content constitutes a breach of publication ethics.

As AI continues to advance, JPTM will maintain a flexible, adaptive policy framework, regularly update author guidelines, provide ongoing training for editors and reviewers, and align with global standards such as Committee on Publication Ethics, International Committee of Medical Journal Editors, and Council of Science Editors. By proactively addressing AI-related ethical issues, JPTM seeks to uphold the highest standards of trust, rigor, and accountability while embracing innovations that enhance the publication process.

CONCLUSION

Sixty volumes of continuous publication reflect a remarkable legacy of dedication by authors, reviewers, editors, and the academic societies that have supported JPTM since its inception. The journal's evolution, from a nationally focused publication to a platform of growing international stature, illustrates how scholarly publishing must adapt to new technological, scientific, and ethical realities while upholding enduring commitments to quality, accessibility, and integrity. As JPTM moves into its next decade, it remains committed to advancing the science and practice of pathology, fostering global dialogue, and providing a fair and rigorous venue for the dissemination of research in pathology and translational medicine. The achievements of the past sixty volumes form a shared foundation, and the promise of the future rests on our collective commitment to sustaining and elevating the journal's contributions to the worldwide pathology community.

ORCID

Chan Kwon Jung	https://orcid.org/0000-0001-6843-3708
So Yeon Park	https://orcid.org/0000-0002-0299-7268
Soon Won Hong	https://orcid.org/0000-0002-0324-2414

https://doi.org/10.4132/jptm.2025.12.08

Conflicts of Interest

The authors declare that they have no potential conflicts of interest.

REFERENCES

1. Kim SH, Kim CJ, Hong S. History of the official journal published by the Korean Society of Pathologists: from *The Korean Journal of Pathology* to the *Journal of Pathology and Translational Medicine*. J Pathol Transl Med 2017; 51: 1-6.
2. Chi JG. *The Korean Journal of Pathology*: a review of the first 25 years. Korean J Pathol 1991; 25: 497-508.
3. Jin SY, Kang CS. The Korean Journal of Cytopathology: from foundation to unification with *The Korean Journal of Pathology*. Korean J Pathol 2009; 43: 1-3.
4. Seo JW, Cho KJ, Kim HK, Kang DY. *The Korean Journal of Pathology* is selected for coverage in Science Citation Index Expanded and Journal Citation Reports by Thomson Reuters. Korean J Pathol 2008; 42: 131-3.

https://doi.org/10.4132/jptm.2025.12.08

JPTM

REVIEW ARTICLE

pISSN 2383-7837 · eISSN 2383-7845

Journal of Pathology and Translational Medicine 2026; 60: 6-19
https://doi.org/10.4132/jptm.2025.10.02

A comprehensive review of ossifying fibromyxoid tumor: insights into its clinical, pathological, and molecular landscape

Kyriakos Chatzopoulos[1], Antonia Syrnioti[1], Mohamed Yakoub[2], Konstantinos Linos[2]

[1]Department of Pathology, Aristotle University of Thessaloniki, Thessaloniki, Greece
[2]Department of Pathology and Laboratory Medicine, Memorial Sloan Kettering Cancer Center, New York, NY, USA

Ossifying fibromyxoid tumor (OFMT) is a rare mesenchymal neoplasm first described in 1989. It typically arises in the superficial soft tissues of the extremities as a slow-growing, painless mass. Histologically, it is commonly characterized by a multilobular architecture composed of uniform epithelioid cells embedded in a fibromyxoid matrix, often surrounded by a rim of metaplastic bone. While classic cases are readily identifiable, the tumor's histopathological heterogeneity can mimic a range of benign and malignant neoplasms, posing significant diagnostic challenges. Molecularly, most OFMTs harbor *PHF1* rearrangements, commonly involving fusion partners such as *EP400*, *MEAF6*, or *TFE3*. This review underscores the importance of an integrated diagnostic approach–incorporating histopathological, immunohistochemical, and molecular data-to accurately classify OFMT and distinguish it from its mimics. Expanding awareness of its morphologic and molecular spectrum is essential for precise diagnosis, optimal patient management, and a deeper understanding of this enigmatic neoplasm.

Keywords: Ossifying fibromyxoid tumor; PHF1; Soft tissue neoplasms; Molecular pathology

INTRODUCTION

Ossifying fibromyxoid tumor (OFMT) is a rare soft tissue neoplasm of uncertain histogenesis, typically arising in the soft tissues of the extremities and often in the subcutaneous tissue [1]. First described by Enzinger et al. in 1989 [2], OFMT displays a wide spectrum of morphological findings and biological behavior. While typical histopathological presentations usually pose little diagnostic challenge, the tumor's morphological variability can complicate diagnosis. This includes cases exhibiting chondroid or lipoblastic differentiation [3], clear cell morphology or collagen entrapment [4], which may mimic other soft tissue neoplasms. Furthermore, hypercellular and mitotically active tumors with significant cellular atypia can demonstrate metastatic potential [5], underscoring the importance of accurate and timely diagnosis. The majority of OFMTs have recurrent molecular alterations, most frequently *PHF1* rearrangements [6], and molecular pathology can serve as a valuable adjunct in diagnosing challenging cases [4]. This review aims to provide a comprehensive overview of the clinical, pathological, and molecular characteristics of OFMT, educating the readers on this enigmatic entity.

EPIDEMIOLOGY AND CLINICAL PRESENTATION

Despite the rarity of OFMT, multiple case series have described its clinical and pathologic findings in thorough detail. In most cases, OFMT presents as a long-existing, slow-growing, painless mass, with a median duration of ~4 years before patients seek medical attention and treatment [7]. In the original case series of 59 patients published by Enzinger et al. in 1989 [2], OFMT

Received: March 4, 2025 **Revised:** August 4, 2025 **Accepted:** September 24, 2025

Corresponding Author: Konstantinos Linos, MD
Department of Pathology and Laboratory Medicine, Memorial Sloan Kettering Cancer Center, 1275 York Avenue, New York, NY 10065, USA
Tel: +1-212-639-5905, Fax: +1-212-557-0531, E-mail: linosk@mskcc.org

This is an Open Access article distributed under the terms of the Creative Commons Attribution Non-Commercial License (https://creativecommons.org/licenses/by-nc/4.0/) which permits unrestricted non-commercial use, distribution, and reproduction in any medium, provided the original work is properly cited.
© 2026 The Korean Society of Pathologists/The Korean Society for Cytopathology

was diagnosed more frequently in males than females, with age range spanning from 14 to 79 years. In the series of 70 patients published by Folpe and Weiss [5], OFMT was primarily observed in middle-aged adults, with a slight male predominance, and a propensity to arise in the soft tissues of the extremities. These findings were corroborated by a subsequent study of 104 patients from the Armed Forces Institute of Pathology, which highlighted a median age of 50 years at diagnosis, along with a male-to-female-ratio of 1.5:1 [7], as well as the study by Graham et al on 46 patients with a median age of 52 years and male-to-female ratio of 1.7:1 [8]. Apart from the extremities, OFMT frequently arises in various locations of the head and neck region [9-18]. Intracranial involvement [19,20], occasionally with transcranial extension [21], as well as paraspinal [22] or spinal extradural involvement [23] have been described. Other unusual locations include the retroperitoneum [24], the breast [25], and the genitourinary (GU) tract [26]. Pediatric cases, although uncommon, have been reported [27,28], including a 3-week-old male neonate with a left nasal mass [29].

MACROSCOPIC FINDINGS

OFMT typically presents as a well-circumscribed, ovoid, small soft tissue mass, with a rubbery to firm texture, and a glistening, white cut surface. It often features a peripheral hard shell, which can be appreciated on imaging as irregular bone [7,8,30]. Most tumors are small to medium-sized, with a median size of 3–5 cm, although large tumors measuring up to 17 cm or even 21 cm have been reported [5,7,8]. In the appropriate clinico-radiological setting, this finding can occasionally complicate the differential diagnosis with parosteal osteosarcoma [31]. The tumors are most often subcutaneous, although rarely, they may arise within the skeletal muscle, particularly in the head and neck area [7].

MICROSCOPIC FINDINGS

Microscopically, OFMT exhibits a multilobular architecture, with a pressure effect on the superficial component of the overlying skin, occasionally associated with cutaneous ulceration [7]. The tumor is lined by a pseudocapsule with metaplastic lamellar or woven bone, sometimes interspersed with adipocytes between bony trabeculae, but lacking hematopoietic cells. However, it's worth noting that the absence of the peripheral bone shell is reported in ~25%–40% of OFMT [8,32]. Additionally, osteoid material is commonly observed in central regions of the tumor [33], which raises the possibility of osteosarcoma in the differential diagnosis [34]. Pericapsular aggregates of lymphocytes are not uncommon [5,35]. Within a collagenous or myxoid matrix with perivascular hyalinization, the tumor cells are uniform and epithelioid, featuring pale to eosinophilic cytoplasm, round nuclei with even chromatin distribution, delicate nucleoli, inconspicuous clefts or pseudoinclusions, and low mitotic activity [5,7,35] (Fig. 1).

Unusual findings described in OFMT include breakdown of lamellar bone with osteoclasts, central hemorrhagic infarction [7], satellite microscopic nodules, mucinous microscopic cysts, microcalcification, crushing artifact, and paucity or absence of myxoid matrix, as well as chondroid differentiation (Fig. 2) with atypical binucleated cells [36]. Additional unusual findings are predominance of clear cell morphology, extravasated red blood cells, collagen entrapment and interdigitating fibrocollagenous and fibromyxoid stromal bundles [4] (Figs. 3, 4). A recent study also described two OFMTs with prominent lipoblastic differentiation [3].

An OFMT characterized by high nuclear grade or increased cellularity, and mitotic activity exceeding 2 mitoses per 50 high power fields can be classified as malignant [5] (Figs. 5–8). Additionally, necrosis and an infiltrative pattern may be present [8]. Patients with malignant OFMT are more likely to develop distant metastases, most often to the lungs [37]. Although overtly sarcomatous changes in OFMT are uncommon, they have been documented [38], with reported cases including osteosarcoma arising from OFMT after multiple recurrences [39].

HISTOGENESIS

The histogenesis of OFMT remains enigmatic. Initially it was thought to be a neoplasm of Schwannian origin [40] with possible incomplete neural or cartilaginous differentiation, a hypothesis supported by the commonly observed S100 protein immunoreactivity [7]. However, electron microscopy findings largely resemble those seen in pleomorphic adenomas or myoepithelial tumors [41], including paucity of organelles and aggregates of intermediate filaments with reduplicated basal lamina material [41-43]. Therefore, myoepithelial origin or differentiation is a plausible hypothesis, supported by case reports of tumors displaying intermediate characteristics between OFMT and myoepithelial neoplasms, as discussed below.

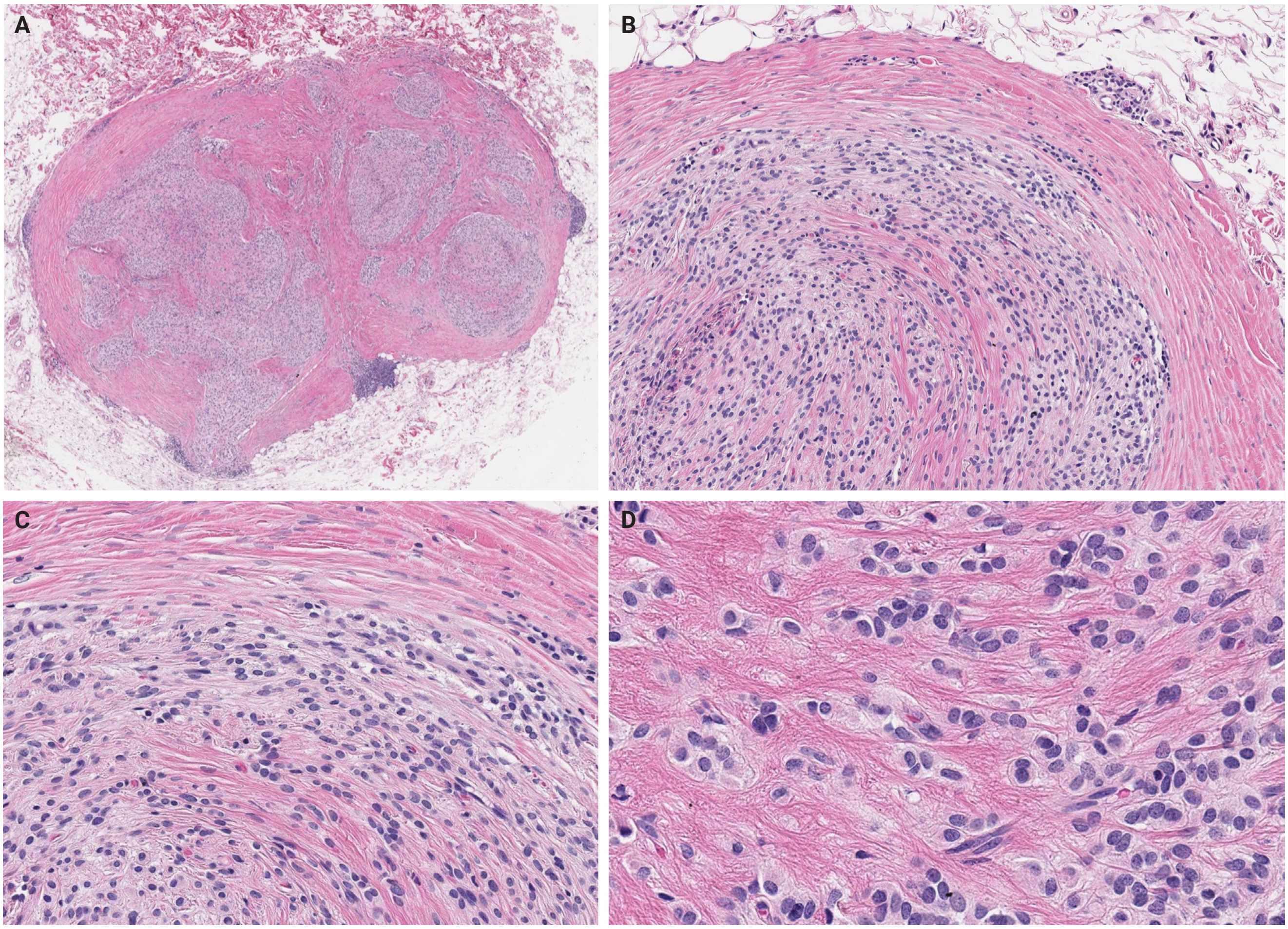

Fig. 1. A right inferior breast ossifying fibromyxoid tumor displaying nearly classic histologic features (except the peripheral metaplastic bone). This case harbors the classic *EP400*::*PHF1* fusion. (A) At low magnification, the tumor appears as a well-demarcated, multilobulated mass located within the subcutis. (B, C) Tumor cells are arranged in cords and sheets within collagenous stroma. (D) High power view depicting ovoid tumor cells, featuring pale to eosinophilic cytoplasm, and round, regular nuclei.

CYTOPATHOLOGY

The diagnosis of OFMT on cytology specimens is very challenging, both because of its rarity and the non-specific cytomorphology of the cellular component [44]. However, the presence of a fine fibrillary [45] or myxoid matrix [46], with occasional rosette-like structures [44,45] and particularly osteoid-like material [47] can guide cytopathologists to include OFMT in the differential diagnosis of a soft tissue mass. In addition, the presence of nuclear atypia, including features such as prominent nucleoli, chromatin clumping and irregular nuclear contours, may raise the possibility of malignant OFMT [46].

IMMUNOHISTOCHEMISTRY

OFMT typically expresses S100 protein [7,8] and is frequently positive for excitatory amino acid transporter 4 (EAAT4) [8,38], desmin, neurofilament, CD56 [8], CD10 [7], and insulinoma-associated protein 1 (INSM1) [48]. OFMT often displays mosaic expression of integrase interactor 1 (INI1), due to a commonly present underlying alteration of the *SMARCB1* gene, as mentioned in detail below [8,38,49]. Transcription factor E3 (TFE3) nuclear expression is typically seen in OFMT harboring a *PHF1*::*TFE3* fusion [50,51].

Expression of keratins, collagen IV, glial fibrillary acidic protein (GFAP), epithelial membrane antigen (EMA), smooth muscle actin (SMA) [7], CD99 [52], MUC4 (not diffuse) [8] or

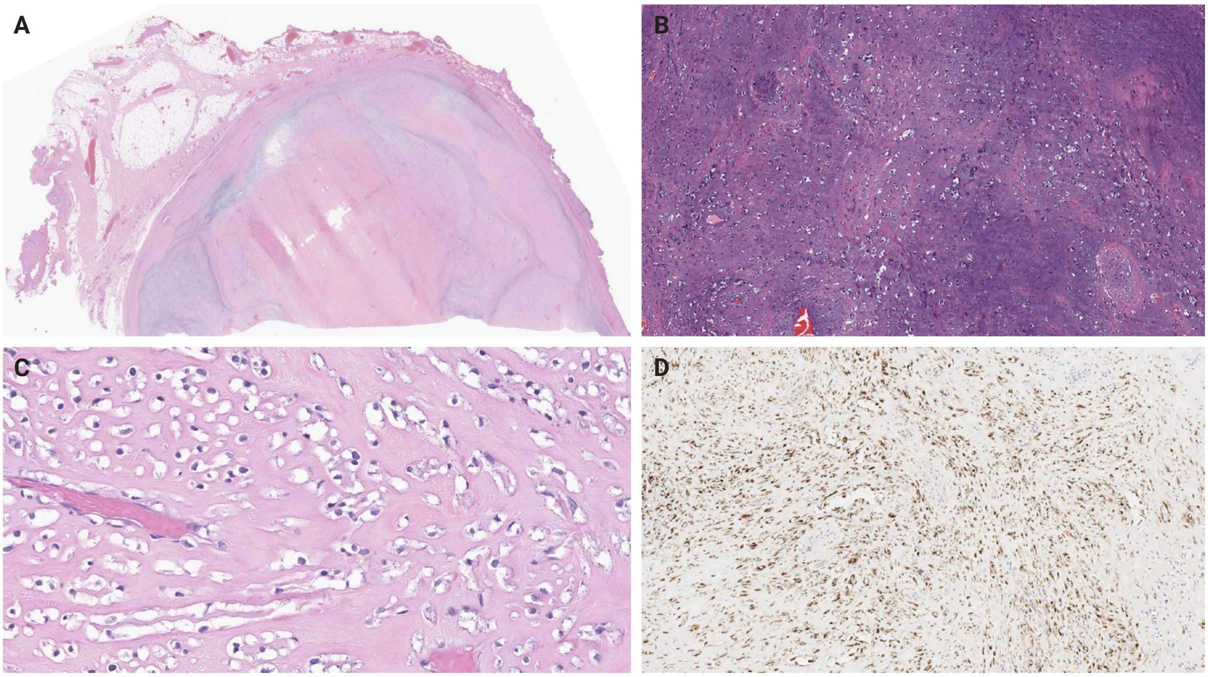

Fig. 2. A lower back ossifying fibromyxoid tumor, harboring a *CREBBP*::*BCORL1* fusion. (A) Low-power view depicting a well-delineated, pseudoencapsulated tumor, featuring prominent central stromal hyalinization. (B, C) Extensive chondroid differentiation and focal clear cell morphology are appreciated. (D) Tumor cells exhibit positivity for S100 on immunohistochemical staining.

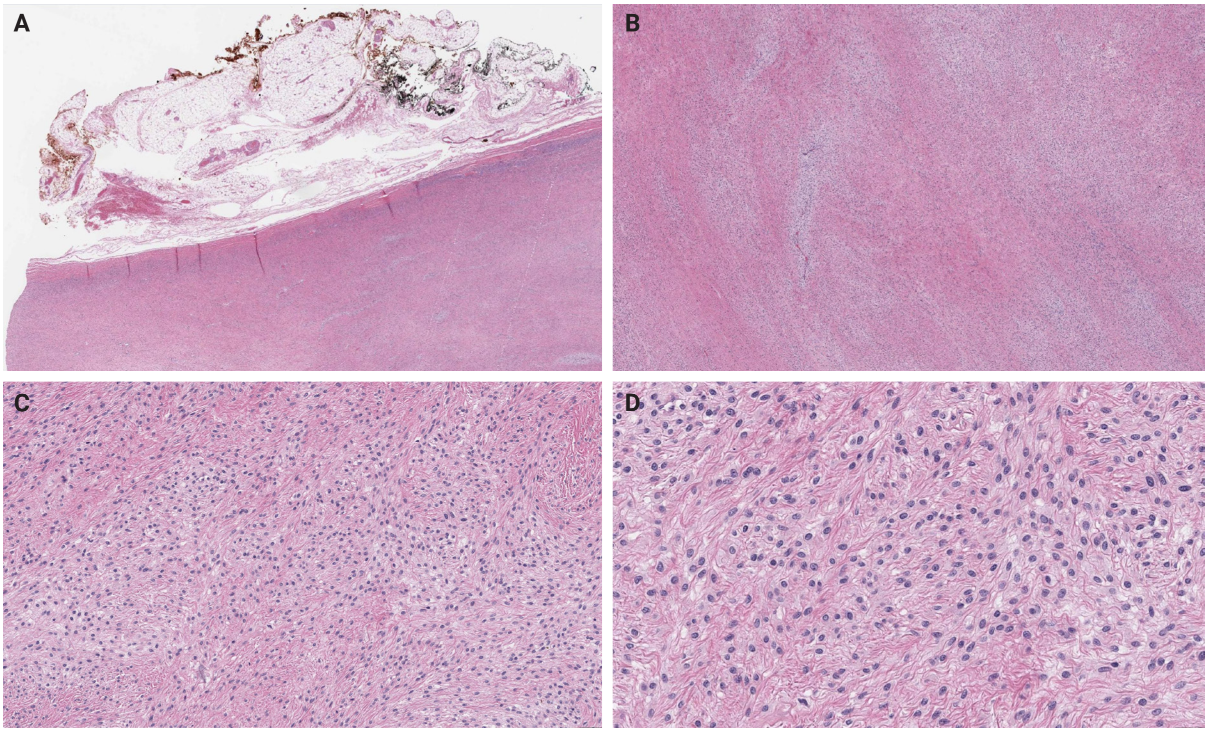

Fig. 3. A left axillary ossifying fibromyxoid tumor harboring an *EP400*::*PHF1* fusion. (A) At low magnification, the tumor is well-defined and distinctly bordered by adjacent adipose tissue. (B) Tumor cells are set within a stromal matrix that transitions between fibrocollagenous and fibromyxoid areas in a geographically interwoven pattern. (C, D) Cords and sheets of spindle-to-ovoid tumor cells with uniform, ovoid nuclei and pale to eosinophilic cytoplasm are noted.

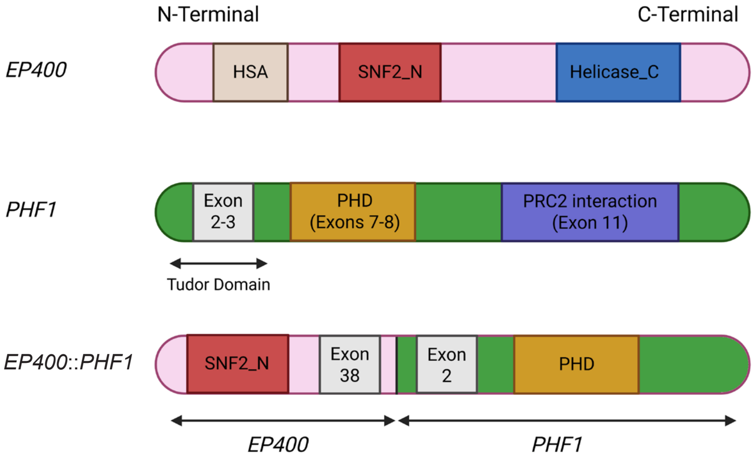

Fig. 4. The *EP400*::*PHF1* fusion, detected in the case depicted in Fig. 3, preserves SNF2_N from *EP400* and fuses to *PHF1* exon 2 and the PHD domain, altering chromatin regulation via recruitment to new loci [53]. HAS, actin-binding domain in chromatin remodelers; SNF2_N, ATP-binding subdomain of SNF2 helicase; Helicase_C, catalytic helicase subdomain; PHD, zinc finger "reader" domain binding histone marks; PRC2 interaction, region mediating interaction with the PRC2 complex (Illustrations are created by Biorender https://app.biorender.com).

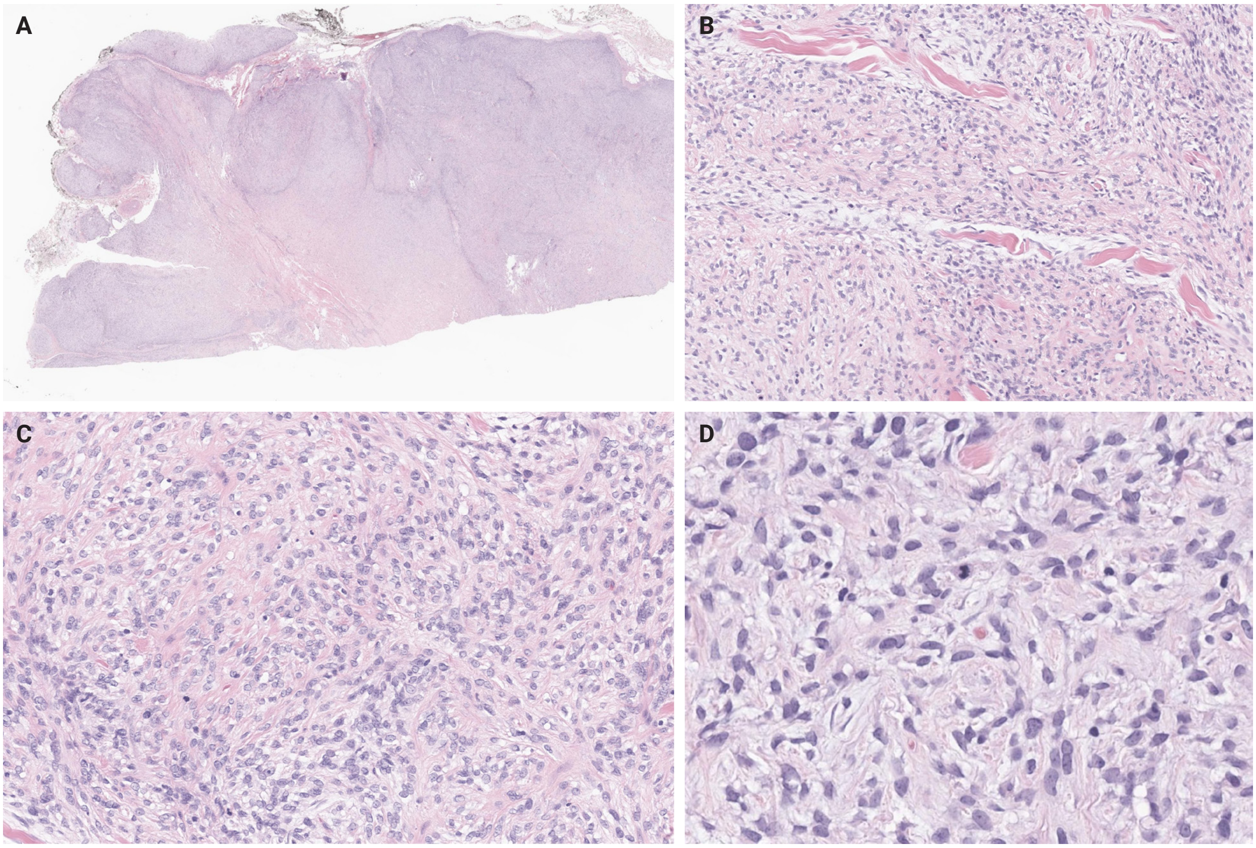

Fig. 5. A malignant, right-back ossifying fibromyxoid tumor harboring an *EPC1*::*SUZ12* fusion. (A) At low magnification, the tumor appears multilobulated and highly cellular. (B, C) Sheets and trabeculae of tumor cells are seen infiltrating the collagen bundles. (D) Areas of increased mitotic activity are observed, with no evidence of pleomorphism or necrosis.

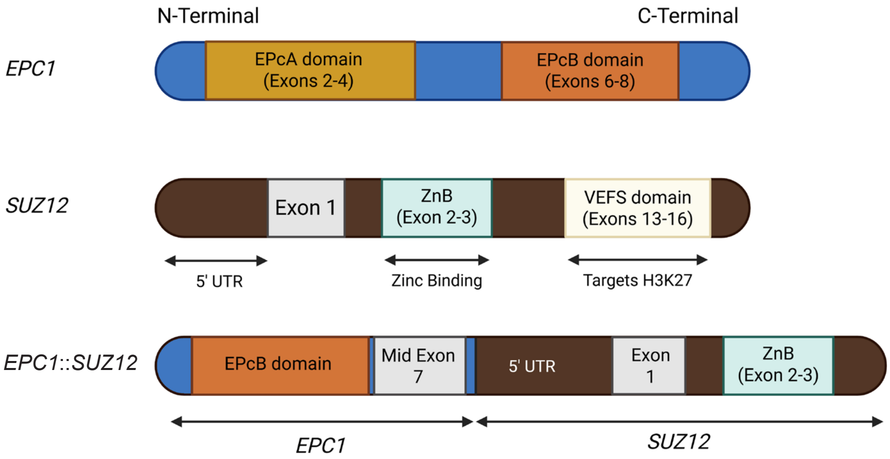

Fig. 6. *EPC1*::*SUZ12* fusion, detected in the case depicted in Fig. 5, joins the EPcB domain of *EPC1* to *SUZ12* 5′-UTR, reprogramming PRC2 recruitment and function with loss of H3K27 trimethylation [54]. EPcA/EPcB domains, EPC1 domains that scaffold chromatin modifiers; ZnB, Zinc-binding domain (complex assembly function); VEFS, Domain that interacts with EZH2/EED and targets H3K27 (Illustrations are created by Biorender https://app.biorender.com).

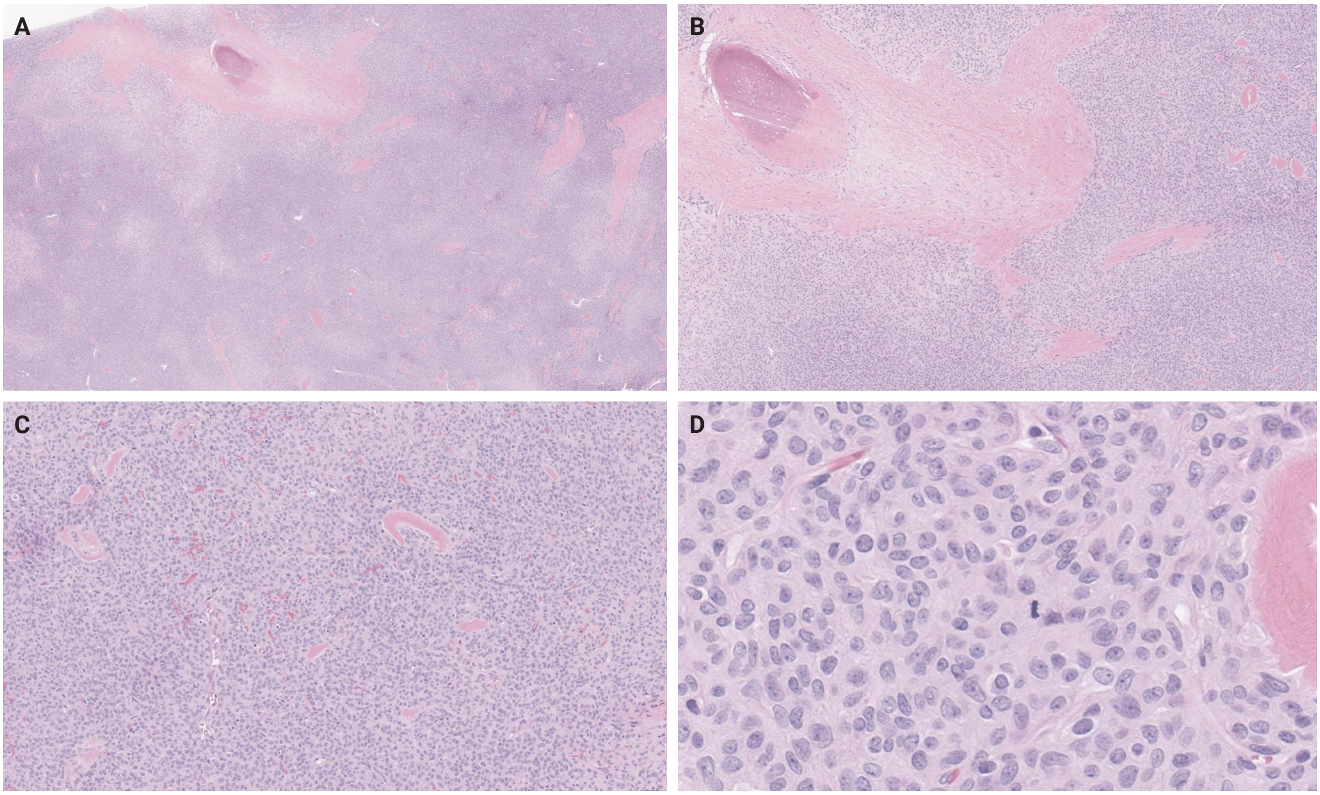

Fig. 7. A malignant right parapharyngeal ossifying fibromyxoid tumor with the very rare *PHF1*::*FOXR2* fusion. (A, B) At low magnification, the tumor appears highly cellular, with metaplastic bone present within the fibrous septae. (C) Tumor cells form cords, nests, and sheets, scattered throughout a collagenous to hyalinized background. (D) The tumor cells are predominantly ovoid to spindle-shaped, with a high nucleus-to-cytoplasm ratio, round to ovoid nuclei featuring occasional small nucleoli, and increased mitotic activity. The patient subsequently developed lung metastases.

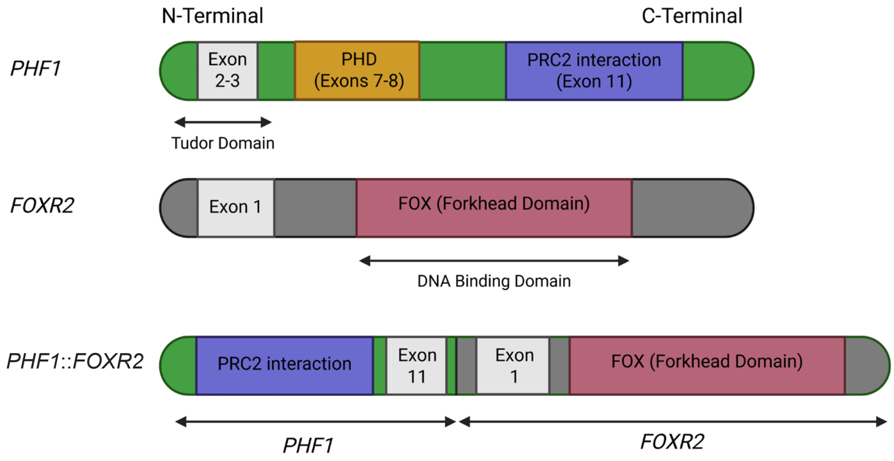

Fig. 8. The *PHF1*::*FOXR2* fusion, detected in the case depicted in Fig. 7, combines PRC2 recruitment ability (*PHF1*) with the transcriptional targeting domain of *FOXR2*, redirecting epigenetic silencing to FOX-bound genomic loci and mislocalization of chromatin-modifying complexes [55]. PHD, histone reader domain; FOX (Forkhead domain), DNA-binding domain of FOXR2, found in FOX transcription factors (Illustrations are created by Biorender https://app.biorender.com).

calponin [56] has occasionally been reported, while OFMT is consistently negative for HMB45, CD34 [7], SOX10 [33], and preferentially expressed antigen in melanoma (PRAME) [57]. Interestingly, estrogen receptor and progesterone receptor (PR) expression has been described in a *PHF1*-rearranged OFMT of the breast, which also co-expressed STAT6 [25], as well as in a *PHF1*-rearranged OFMT of the axillary soft tissues [4], while isolated diffuse PR expression was seen in two OFMTs of the extremities with *BCOR* and *TFE3* rearrangements [51].

Of note, expression of pan-tropomyosin receptor kinase (pan-TRK) by immunohistochemistry has been reported in *BCOR*-rearranged OFMT [58,59]. Given the efficacy of targeted neurotrophic tyrosine receptor kinase (NTRK) inhibition for patients with *NTRK*-fused tumors [60], this finding is of potential clinical interest. Although the exact mechanism of pan-TRK expression has not been fully elucidated, it seems that it occurs due to underlying *NTRK3* mRNA overexpression [58].

Finally, it is worth mentioning that malignant OFMT can show an atypical immunophenotype, with attenuation or complete absence of S100 protein expression [61]. Absence of S100 expression was also demonstrated in all four GU OFMTs described by Argani et al. [26], two of which were classified as malignant based on mitotic count.

MOLECULAR GENETICS

The presence of clonal chromosomal alterations such as aneusomies, unbalanced translocations [62] and complex karyotypes [63], including marker chromosomes [64], was highlighted in early studies. Complex karyotypes have been particularly associated with malignant OFMT cases exhibiting metastases [63]. A relatively recurrent finding is hemizygous deletion of chromosome 22 or 22q, leading to hemizygous loss of *SMARCB1*, an alteration corresponding to the mosaic immunohistochemical pattern of INI1 expression frequently observed, as mentioned above [8]. Another recurrent finding most often seen in atypical and malignant OFMT is loss of the *RB1* tumor suppressor gene, observed in almost a third of cases [55].

The molecular hallmark of OFMT is the presence of recurrent rearrangements of *PHF1*, which are seen in approximately 80%–85% of tumors [6]. The *PHF1* gene encodes a protein which interacts with polycomb-repressive complex 2 (PRC2), an important regulator of chromatin structure and developmental gene expression [65], ultimately controlling histone H3K27 methylation status [66]. Rearrangement of *PHF1* typically occurs in the form of a reciprocal translocation, resulting in gene fusion, with *EP400* being the most common fusion partner (Fig. 4) [67]. Other *PHF1* fusion partners include *EPC1*, *MEAF6* [68], *TFE3* [69], *FOXR1*, *FOXR2* (Fig. 8) [70], *CREBZF* [34], *TP53* [71], and *JAZF1* [3].

Non-*PHF1* fusions have also been described, including *MEAF6*::*SUZ12* [72], *EPC1*::*SUZ12* (Fig. 6) [4], *CREBBP*::*BCORL1*, *KDM2A*::*WWTR1* [73], *ZC3H7B*::*BCOR* [59], *CSMD1*::*MEAF6* [55], and *EPC1*::*PHC1* [3]. The common denominator of these fusions is that they function as tumor drivers, inducing significant epigenetic changes via histone modification, a process currently regarded as the major molecular mechanism of OFMT pathogenesis [55]. Of note, a non-fused malignant OFMT with a *BCOR* internal tandem duplication has been reported in a pediatric patient with a lateral neck mass and subsequent local and metastatic recurrences [74].

Interestingly, certain of the above mentioned fusions, particularly *JAZF1*::*PHF1*, *EPC1*::*PHF1*, *MEAF6*::*PHF1*, *ZC3H7*::*BCOR*, and *EPC1*::*SUZ12* [75,76] have been previously described in low-grade endometrial stromal sarcoma (ESS), a finding explaining why certain OFMT may cluster with ESSs by DNA methylation analysis [4]. The latter fact may limit the utility of DNA methylation assay in the work-up of OFMT.

Given the frequency of *PHF1* rearrangements, a reasonable approach includes morphological assessment with confirmation of *PHF1* alteration by break-apart fluorescent in situ hybridization (FISH) [77]. However, in cases with unusual morphological findings and non-*PHF1* rearrangements, the final diagnosis may need to be deferred until molecular testing by next generation sequencing (NGS) is performed [4].

DIFFERENTIAL DIAGNOSIS

The broad spectrum of the differential diagnosis for OFMT often encompasses myoepithelial neoplasms [78]. In challenging cases, testing for *EWSR1* rearrangements in these neoplasms can provide valuable insights. However, it's essential to acknowledge that *EWSR1* rearrangements are detected in only around 50% of soft tissue myoepithelial neoplasms [79], making the test informative when positive, but less conclusive when negative.

The most frequent pitfall in the differential diagnosis of OFMT is low-grade fibromyxoid sarcoma (LGFMS) [80]. Also known as “Evans tumor” [81], LGFMS is a low-grade sarcoma arising in the extremities of young adults, although as many as 20% of cases occur in patients younger than 18 years old. It consists of spindle to epithelioid cells arranged in alternating hyalinized and myxoid areas, with occasional hyaline rosettes [82]. These morphologic features, along with lack of S100 expression and strong and diffuse MUC4 positivity, usually suffice for distinguishing LGFMS from OFMT. Molecular detection of the characteristic *FUS*::*CREB3L2* or *EWSR1*::*CREB3L1* fusions confirms the diagnosis of LGFMS in the appropriate morphologic context [83].

Sclerosing epithelioid fibrosarcoma (SEF) or hybrid SEF-LGFMS tumors are also frequently included in the differential diagnosis. SEF is a rare aggressive variant of fibrosarcoma, characterized by small epithelioid cells arranged in cords and nests within a densely sclerotic stroma [84]. However, unlike OFMT, SEF primarily arises in deep soft tissues and lacks S100 expression [85]. The diagnosis of SEF can be confirmed through molecular studies that identify the characteristic *EWSR1*::*CREB3L1* fusion [86].

The differential diagnosis also includes the newly described *YAP1*::*KMTA2*-rearranged sarcoma, an aggressive soft tissue malignancy, notorious for its propensity to mimic benign or low-grade neoplasms, such as schwannoma, fibromatosis or LGFMS [87]. Initially thought to represent a MUC4-negative subtype of SEF, the identification of recurrent *YAP1* and *KMT2A* rearrangements [88,89], along with distinctive morphologic features [89] and a unique DNA methylation profile [87], has established *YAP1*::*KMT2A* rearranged sarcoma as a novel entity. These tumors usually exhibit an infiltrative growth pattern with areas of variable cellularity, where monomorphic epithelioid or bland, fibroma-like spindle cells are embedded in a densely collagenous matrix. Mitotic activity is generally low and high-grade features, such as necrosis are usually absent [89]. Immunohistochemically, these tumors are consistently negative for MUC4 and usually negative for S100 protein, but may show variable EMA or CD34 expression [86]. Despite its deceptively low-grade histomorphology, *YAP1*::*KMT2A*-rearranged sarcoma can follow an aggressive clinical course, with local recurrence and metastatic disease developing in up to 50% of patients [86].

Other entities to consider in the differential diagnosis include schwannoma [90], malignant peripheral nerve sheath tumor (MPNST) [78], extraskeletal myxoid chondrosarcoma (EMC) [48], and extraskeletal osteosarcoma [78]. Schwannoma arises from the peripheral nerve sheath and is characteristically strongly and diffusely positive for S100 protein, in contrast to OFMT, where S100 expression may be weak or absent. Schwannomas also lack the peripheral ossification and cytomorphologic features typical of OFMT [90]. MPNST typically arises in deep soft tissues, often in association with major nerves, and does not exhibit peripheral ossification. While MPNST may show attenuated S100 positivity, it can also express other neural markers such as neurofilament and GFAP [78]. Importantly, loss of H3K27me3 expression—frequently seen in MPNST—can help distinguish it from OFMT, in which H3K27me3 expression is consistently retained [91,92]. EMC is characterized by a lobular architecture with fibrous septa and uniform tumor cells showing eosinophilic cytoplasm, occasional spindling, and inconspicuous nucleoli in a myxoid background. EMC typically expresses INSM1, synaptophysin, and sometimes other neuroendocrine or neural markers such as chromogranin, PGP9.5, microtubule-associated protein 2, class III β-tubulin, and peripherin [48]. Genetically, EMC is defined by *NR4A3* rearrangements, most commonly with *EWSR1*, but also involving partners such as *TAF15*, *TCF12*, *TFG*, *FUS*, *HSPA8*, *LSM14A*, or *SMARCA2* [48]. Extraskeletal osteosarcoma is exceedingly rare in the skin or subcutis and typically represents metastatic disease, making clinical history essential. Helpful distinguishing features include lack of S100 expression and the presence of marked nuclear atypia [78].

Notably, primary bone OFMT has also been described, which may be extremely challenging to distinguish from osteosarcoma [93]. In tumors with lipoblastic differentiation, distinction from benign and malignant lipomatous tumors such as chondroid lipoma or myxoid liposarcoma can be challenging [3]. The differential diagnosis can be particularly challenging in tumors with uncommon microscopic features, where the final diagnosis can be confidently rendered only by confirming a characteristic molecular alteration [4].

PRACTICAL DIAGNOSTIC APPROACH

Diagnosing OFMT requires an integrative approach, as the tumor's morphologic and immunophenotypic spectrum is broad and overlaps with several benign and malignant entities. In classic presentations—characterized by uniform ovoid cells embedded in a fibromyxoid matrix and surrounded by a peripheral shell of metaplastic bone—the diagnosis may be straightforward, particularly when supported by strong S100 protein and desmin expression. However, in atypical or malignant variants, these features may be attenuated or absent. For instance, malignant OFMTs frequently lack ossification, exhibit increased cellularity and mitotic activity, and may show reduced or completely lost S100 expression. Ancillary studies are essential in such cases. FISH is widely used and can detect gene rearrangements or amplifications in formalin-fixed paraffin-embedded tissue with good sensitivity, but it is restricted to one locus per assay and, in the case of break-apart probes, cannot identify the fusion partner. Furthermore, cryptic or complex rearrangements may go undetected. Reverse-transcriptase polymerase chain reaction (RT-PCR) offers high sensitivity and relatively low cost for detecting known fusion transcripts, but it requires prior knowledge of the partner genes and thus cannot identify novel fusions. Targeted RNA sequencing and broader NGS panels overcome these limitations by interrogating multiple loci simultaneously, allowing both confirmation of established fusions and discovery of novel ones. Although more resource-intensive, NGS has emerged as the most reliable method for characterizing OFMT at the molecular level, particularly in diagnostically challenging cases [94].

In clinical practice, the diagnostic work-up of a suspected OFMT typically begins with a panel of broad immunohistochemical stains, including S100, SOX10, desmin, SMA, and a broad-spectrum cytokeratin. In tumors with classic morphology, the combination of S100 and desmin positivity is generally sufficient to establish a confident diagnosis. In cases with very suggestive morphology but incomplete immunophenotypic support—for example, when S100 or desmin expression is weak or focal—*PHF1* break-apart FISH is the logical next step, as approximately 80%–85% of OFMTs harbor *PHF1* rearrangements. If *PHF1* testing is negative but the pretest probability remains high, RT-PCR, targeted RNA sequencing or broad-panel NGS can help identify rarer fusions, such as *CREBBP*::*BCORL1*, *EPC1*::*SUZ12*, or *ZC3H7B*::*BCOR* amongst others.

In atypical or malignant cases, where classic immunohistochemical markers such as S100 and desmin are diminished or absent, a diagnosis of OFMT may still be appropriate if the tumor contains areas reminiscent of conventional OFMT. In such instances, *PHF1* FISH remains useful. However, in malignant tumors that lack both morphologic and immunophenotypic features suggestive of OFMT, comprehensive molecular testing via NGS is often the only practical means of confirming the diagnosis.

Emerging evidence supports a correlation between specific gene fusions and atypical or malignant histologic features of OFMT. In a synthesis of reported cases across the literature, approximately 26 OFMTs with non-*PHF1* fusions or *PHF1* fusions involving uncommon partners (e.g., *TP53*, *FOXR1/2*, *CREBZF*, *ZC3H7B*, *EPC1*) have been compiled and analyzed. Of these, 18 tumors (69%) were classified as atypical or malignant, indicating a strong association between rare fusion events and aggressive histologic behavior. Moreover, certain fusion types—such as *TP53*::*PHF1*, *PHF1*::*FOXR2*, *ZC3H7B*::*BCOR*, and *EPC1*::*SUZ12*—have been reported almost exclusively in malignant cases, further supporting their potential as molecular indicators of high-grade disease. While these rare fusions do not inherently define malignancy, their frequent occurrence in morphologically aggressive tumors suggests they may play a role in driving dedifferentiation or loss of canonical OFMT features.

These atypical/malignant variants also tend to show marked loss of conventional immunophenotypic markers. In the pooled dataset, S100 expression was retained in only four of 15 cases (27%), often in a focal or patchy distribution, and desmin was expressed in just two of 14 cases (14%). In contrast, classic OFMTs show S100 positivity in ~70% and desmin in ~50% of cases. Additionally, the characteristic peripheral ossified shell was frequently absent in these high-grade tumors, further complicating diagnosis.

Together, these findings highlight the importance of recognizing non-classic morphologic and immunohistochemical presentations and maintaining a low threshold for molecular testing—especially in tumors lacking both classic architecture and marker expression [71].

TREATMENT AND PROGNOSIS

OFMT is treated surgically with local marginal or wide excision and rarely amputation, particularly when a large tumor arises on a digit [7]. Local recurrence is more likely to occur in patients whose tumors show increased mitotic activity [7]. Tumors fulfilling the microscopic criteria of malignancy, should be regarded as sarcomas for treatment purposes, as they tend to display more aggressive clinical behavior, including the potential for distant metastasis [5,95]. These patients may be candidates for adjuvant radiation therapy, particularly after being diagnosed with local recurrence [5]. Similarly, patients with metastatic disease may be eligible for chemotherapy [96]. When malignant OFMT metastasizes, it typically spreads to the lung [8,37,96], although unusual locations such as the thyroid gland have been reported [97].

CONCLUSION

OFMT is a rare mesenchymal neoplasm that can occasionally complicate the differential diagnosis of a soft tissue mass, leading to diagnostic uncertainty. Given that certain tumors behave in a clinically aggressive manner, pathologists should consider OFMT in the differential diagnosis of an unusual soft tissue tumor and triage cases for molecular testing where appropriate, as rendering an accurate diagnosis is the cornerstone of effective patient management.

Ethics Statement

Not applicable.

Availability of Data and Material

The datasets generated or analyzed during the study are available from the corresponding author on reasonable request.

Code Availability

Not applicable.

ORCID

Kyriakos Chatzopoulos	https://orcid.org/0000-0001-6769-6952
Antonia Syrnioti	https://orcid.org/0000-0002-9232-6715
Mohamed Yakoub	https://orcid.org/0000-0002-6400-660X
Konstantinos Linos	https://orcid.org/0000-0001-9462-652X

Author Contributions

Conceptualization: KL. Data curation: all authors. Formal analysis: all authors. Funding acquisition: KL. Investigation: all authors. Methodology: all authors. Project administration: KL. Resources: KL. Supervision: KL. Validation: KL. Writing—original draft: KC. Writing—review & editing: all authors. Approval of final manuscript: all authors.

Conflicts of Interest

The authors declare that they have no potential conflicts of interest.

Funding Statement

This work was supported by MSK NIH Funded Grant# P30 CA08748.

REFERENCES

1. Endo M, Miettinen M, Mertens F. Ossifying fibromyxoid tumor. In: WHO Classification of Tumours Editorial Board, ed. WHO classification of tumours: soft tissue and bone tumours. 5th ed. Lyon: International Agency for Research on Cancer, 2020; 274-6.

2. Enzinger FM, Weiss SW, Liang CY. Ossifying fibromyxoid tumor of soft parts: a clinicopathological analysis of 59 cases. Am J Surg Pathol 1989; 13: 817-27.
3. Klubickova N, Billings S, Dermawan JK, Molligan JF, Fritchie K. Ossifying fibromyxoid tumours with lipomatous and cartilaginous differentiation: a diagnostic pitfall. Histopathology 2025; 86: 891-9.
4. Syrnioti A, Chatzopoulos K, Kerr DA, et al. A potential conundrum in dermatopathology: molecularly confirmed superficial ossifying fibromyxoid tumors with unusual histomorphologic findings and a novel fusion. Virchows Arch 2024; 485: 1063-73.
5. Folpe AL, Weiss SW. Ossifying fibromyxoid tumor of soft parts: a clinicopathologic study of 70 cases with emphasis on atypical and malignant variants. Am J Surg Pathol 2003; 27: 421-31.
6. Pozas J, Thway K, Lindsay D, et al. Ossifying fibromyxoid tumours: a case series. Eur J Cancer 2025; 217: 115229.
7. Miettinen M, Finnell V, Fetsch JF. Ossifying fibromyxoid tumor of soft parts: a clinicopathologic and immunohistochemical study of 104 cases with long-term follow-up and a critical review of the literature. Am J Surg Pathol 2008; 32: 996-1005.
8. Graham RP, Dry S, Li X, et al. Ossifying fibromyxoid tumor of soft parts: a clinicopathologic, proteomic, and genomic study. Am J Surg Pathol 2011; 35: 1615-25.
9. Park DJ, Miller NR, Green WR. Ossifying fibromyxoid tumor of the orbit. Ophthalmic Plast Reconstr Surg 2006; 22: 87-91.
10. Blum A, Back W, Naim R, Hormann K, Riedel F. Ossifying fibromyxoid tumor of the nasal septum. Auris Nasus Larynx 2006; 33: 325-7.
11. Tanna N, Chadha N, Sharma RR, Goodman JF, Sadeghi N. Malignant ossifying fibromyxoid tumor of the parapharyngeal space. Ear Nose Throat J 2012; 91: E15-7.
12. Perez-de-Oliveira ME, Morais TM, Lopes MA, de Almeida OP, van Heerden WF, Vargas PA. Ossifying fibromyxoid tumor of the oral cavity: rare case report and long-term follow-up. Autops Case Rep 2021; 11: e2020216.
13. Ohta K, Taki M, Ogawa I, et al. Malignant ossifying fibromyxoid tumor of the tongue: case report and review of the literature. Head Face Med 2013; 9: 16.
14. Sharif MA, Mushtaq S, Mamoon N, Khadim MT. Ossifying fibromyxoid tumor of oral cavity. J Coll Physicians Surg Pak 2008; 18: 181-2.
15. Nonaka CF, Pacheco DF, Nunes RP, Freitas Rde A, Miguel MC. Ossifying fibromyxoid tumor in the mandibular gingiva: case report and review of the literature. J Periodontol 2009; 80: 687-92.
16. Mollaoglu N, Tokman B, Kahraman S, Cetiner S, Yucetas S, Uluoglu O. An unusual presentation of ossifying fibromyxoid tumor of the mandible: a case report. J Clin Pediatr Dent 2006; 31: 136-8.
17. Titsinides S, Nikitakis NG, Tasoulas J, Daskalopoulos A, Goutzanis L, Sklavounou A. Ossifying fibromyxoid tumor of the retromolar trigone: a case report and systematic review of the literature. Int J Surg Pathol 2017; 25: 526-32.
18. Mashkova TA, Panchenko IG, Maltsev AB, Shaposhnikova IV. A clinical observation of laryngeal ossifying fibromyxoid tumor. Vestn Otorinolaringol 2021; 86: 82-4.
19. Dhawan S, Lal T, Pandey PN, Saran R, Singh A. Synchronous occurrence of colloid cyst with intracranial ossifying fibromyxoid tumor masquerading as meningioma. Cureus 2020; 12: e10662.
20. Beyer S, Sebastian NT, Prasad RN, et al. Malignant ossifying fibromyxoid tumor of the brain treated with post-operative fractionated stereotactic radiation therapy: a case report and literature review. Surg Neurol Int 2021; 12: 588.
21. Hachmann JT, Graham RS. Malignant ossifying fibromyxoid tumor of the calvaria: illustrative case. J Neurosurg Case Lessons 2021; 2: CASE21346.
22. Sangala JR, Park P, Blaivas M, Lamarca F. Paraspinal malignant ossifying fibromyxoid tumor with spinal involvement. J Clin Neurosci 2010; 17: 1592-4.
23. Lu Q, Ho CL. A case of an 82-year-old man with a spinal extradural malignant ossifying fibromyxoid tumor. Am J Case Rep 2023; 24: e939408.
24. Motoyama T, Ogose A, Watanabe H. Ossifying fibromyxoid tumor of the retroperitoneum. Pathol Int 1996; 46: 79-83.
25. Gajdzis P, Lae M, Choussy O, Lavigne M, Klijanienko J. Fine-needle aspiration features of ossifying fibromyxoid tumor in the breast: a case report and literature review. Diagn Cytopathol 2019; 47: 711-5.
26. Argani P, Dickson BC, Gross JM, Matoso A, Baraban E, Antonescu CR. Ossifying fibromyxoid tumor of the genitourinary tract: report of 4 molecularly confirmed cases of a diagnostic pitfall. Am J Surg Pathol 2023; 47: 709-16.
27. Aminudin CA, Sharaf I, Hamzaini AH, Salmi A, Aishah MA. Ossifying fibromyxoid tumour in a child. Med J Malaysia 2004; 59 Suppl F: 49-51.
28. Ijiri R, Tanaka Y, Misugi K, Sekido K, Nishi T. Ossifying fibromyxoid tumor of soft parts in a child: a case report. J Pediatr Surg 1999; 34: 1294-6.
29. Al-Mazrou KA, Mansoor A, Payne M, Richardson MA. Ossifying fibromyxoid tumor of the ethmoid sinus in a newborn: report of a case and literature review. Int J Pediatr Otorhinolaryngol 2004;

68: 225-30.

30. Schaffler G, Raith J, Ranner G, Weybora W, Jeserschek R. Radiographic appearance of an ossifying fibromyxoid tumor of soft parts. Skeletal Radiol 1997; 26: 615-8.
31. Ogose A, Otsuka H, Morita T, Kobayashi H, Hirata Y. Ossifying fibromyxoid tumor resembling parosteal osteosarcoma. Skeletal Radiol 1998; 27: 578-80.
32. Schneider N, Fisher C, Thway K. Ossifying fibromyxoid tumor: morphology, genetics, and differential diagnosis. Ann Diagn Pathol 2016; 20: 52-8.
33. Carter CS, Patel RM. Ossifying fibromyxoid tumor: a review with emphasis on recent molecular advances and differential diagnosis. Arch Pathol Lab Med 2019; 143: 1504-12.
34. Sharma AE, Dermawan JK, Sherrod AE, Chopra S, Maki RG, Antonescu CR. When molecular outsmarts morphology: malignant ossifying fibromyxoid tumors masquerading as osteosarcomas, including a novel *CREBZF*::*PHF1* fusion. Genes Chromosomes Cancer 2024; 63: e23206.
35. WHO Classification of Tumours Editorial Board. WHO classification of tumours: soft tissue and bone tumours. 5th ed. Lyon: International Agency for Research on Cancer, 2020.
36. Zamecnik M, Michal M, Simpson RH, et al. Ossifying fibromyxoid tumor of soft parts: a report of 17 cases with emphasis on unusual histological features. Ann Diagn Pathol 1997; 1: 73-81.
37. Sarraj A, Duarte J, Dominguez L, Pun YW. Resection of metastatic pulmonary lesion of ossifying fibromyxoid tumor extending into the left atrium and ventricle via pulmonary vein. Eur J Echocardiogr 2007; 8: 384-6.
38. Dantey K, Schoedel K, Yergiyev O, McGough R, Palekar A, Rao UN. Ossifying fibromyxoid tumor: a study of 6 cases of atypical and malignant variants. Hum Pathol 2017; 60: 174-9.
39. Shelekhova KV, Kazakov DV, Michal M. Extraosseous osteosarcoma arising in recurrent ossifying fibromyxoid tumor of soft tissue: a case report. Arkh Patol 2013; 75: 24-8.
40. Donner LR. Ossifying fibromyxoid tumor of soft parts: evidence supporting Schwann cell origin. Hum Pathol 1992; 23: 200-2.
41. Min KW, Seo IS, Pitha J. Ossifying fibromyxoid tumor: modified myoepithelial cell tumor? Report of three cases with immunohistochemical and electron microscopic studies. Ultrastruct Pathol 2005; 29: 535-48.
42. Miettinen M. Ossifying fibromyxoid tumor of soft parts: additional observations of a distinctive soft tissue tumor. Am J Clin Pathol 1991; 95: 142-9.
43. Hirose T, Shimada S, Tani T, Hasegawa T. Ossifying fibromyxoid tumor: invariable ultrastructural features and diverse immunophenotypic expression. Ultrastruct Pathol 2007; 31: 233-9.
44. Goyal P, Sehgal S, Agarwal R, Singh S, Gupta R, Kumar A. Ossifying fibromyxoid tumor: diagnostic challenge for a cytopathologist. Cytojournal 2012; 9: 17.
45. Lax S, Langsteger W. Ossifying fibromyxoid tumor misdiagnosed as follicular neoplasia: a case report. Acta Cytol 1997; 41: 1261-4.
46. Minami R, Yamamoto T, Tsukamoto R, Maeda S. Fine needle aspiration cytology of the malignant variant of ossifying fibromyxoid tumor of soft parts: a case report. Acta Cytol 2001; 45: 745-55.
47. Mohanty SK, Srinivasan R, Rajwanshi A, Vasishta RK, Vignesh PS. Cytologic diagnosis of ossifying fibromyxoid tumor of soft tissue: a case report. Diagn Cytopathol 2004; 30: 41-5.
48. Yoshida A, Makise N, Wakai S, Kawai A, Hiraoka N. INSM1 expression and its diagnostic significance in extraskeletal myxoid chondrosarcoma. Mod Pathol 2018; 31: 744-52.
49. Tajima S, Koda K. Atypical ossifying fibromyxoid tumor unusually located in the mediastinum: report of a case showing mosaic loss of INI-1 expression. Int J Clin Exp Pathol 2015; 8: 2139-45.
50. Suurmeijer AJ, Song W, Sung YS, et al. Novel recurrent *PHF1-TFE3* fusions in ossifying fibromyxoid tumors. Genes Chromosomes Cancer 2019; 58: 643-9.
51. Linos K, Kerr DA, Baker M, et al. Superficial malignant ossifying fibromyxoid tumors harboring the rare and recently described *ZC3H7B-BCOR* and *PHF1-TFE3* fusions. J Cutan Pathol 2020; 47: 934-45.
52. Miliaras D, Meditskou S, Ketikidou M. Ossifying fibromyxoid tumor may express CD56 and CD99: a case report. Int J Surg Pathol 2007; 15: 437-40.
53. Sudarshan D, Avvakumov N, Lalonde ME, et al. Recurrent chromosomal translocations in sarcomas create a megacomplex that mislocalizes NuA4/TIP60 to polycomb target loci. Genes Dev 2022; 36: 664-83.
54. Przybyl J, Kidzinski L, Hastie T, Debiec-Rychter M, Nusse R, van de Rijn M. Gene expression profiling of low-grade endometrial stromal sarcoma indicates fusion protein-mediated activation of the Wnt signaling pathway. Gynecol Oncol 2018; 149: 388-93.
55. Hofvander J, Jo VY, Fletcher CD, et al. PHF1 fusions cause distinct gene expression and chromatin accessibility profiles in ossifying fibromyxoid tumors and mesenchymal cells. Mod Pathol 2020; 33: 1331-40.
56. Squillaci S, Tallarigo F, Cazzaniga R, Capitanio A. Ossifying fibromyxoid tumor with atypical histological features: a case report. Pathologica 2009; 101: 248-52.
57. Cammareri C, Beltzung F, Michal M, et al. PRAME immunohistochemistry in soft tissue tumors and mimics: a study of 350

cases highlighting its imperfect specificity but potentially useful diagnostic applications. Virchows Arch 2023; 483: 145-56.

58. Kao YC, Sung YS, Argani P, et al. NTRK3 overexpression in undifferentiated sarcomas with *YWHAE* and *BCOR* genetic alterations. Mod Pathol 2020; 33: 1341-9.
59. Linos K, Kerr DA, Sumegi J, Bridge JA. Pan-Trk immunoexpression in a superficial malignant ossifying fibromyxoid tumor with *ZC3H7B-BCOR* fusion: A potential obfuscating factor in the era of targeted therapy. J Cutan Pathol 2021; 48: 340-2.
60. Farago AF, Demetri GD. Larotrectinib, a selective tropomyosin receptor kinase inhibitor for adult and pediatric tropomyosin receptor kinase fusion cancers. Future Oncol 2020; 16: 417-25.
61. Foster-Davies H, Jessop ZM, Clancy RM, et al. Reduced S100 protein expression in malignant ossifying fibromyxoid tumors: a case report. Plast Reconstr Surg Glob Open 2021; 9: e3482.
62. Sovani V, Velagaleti GV, Filipowicz E, Gatalica Z, Knisely AS. Ossifying fibromyxoid tumor of soft parts: report of a case with novel cytogenetic findings. Cancer Genet Cytogenet 2001; 127: 1-6.
63. Nishio J, Iwasaki H, Ohjimi Y, et al. Ossifying fibromyxoid tumor of soft parts. Cytogenetic findings. Cancer Genet Cytogenet 2002; 133: 124-8.
64. Kawashima H, Ogose A, Umezu H, et al. Ossifying fibromyxoid tumor of soft parts with clonal chromosomal aberrations. Cancer Genet Cytogenet 2007; 176: 156-60.
65. Gebre-Medhin S, Nord KH, Moller E, et al. Recurrent rearrangement of the *PHF1* gene in ossifying fibromyxoid tumors. Am J Pathol 2012; 181: 1069-77.
66. Sarma K, Margueron R, Ivanov A, Pirrotta V, Reinberg D. Ezh2 requires PHF1 to efficiently catalyze H3 lysine 27 trimethylation in vivo. Mol Cell Biol 2008; 28: 2718-31.
67. Endo M, Kohashi K, Yamamoto H, et al. Ossifying fibromyxoid tumor presenting *EP400-PHF1* fusion gene. Hum Pathol 2013; 44: 2603-8.
68. Antonescu CR, Sung YS, Chen CL, et al. Novel *ZC3H7B-BCOR*, *MEAF6-PHF1*, and *EPC1-PHF1* fusions in ossifying fibromyxoid tumors: molecular characterization shows genetic overlap with endometrial stromal sarcoma. Genes Chromosomes Cancer 2014; 53: 183-93.
69. Zou C, Ru GQ, Zhao M. A *PHF1-TFE3* fusion atypical ossifying fibromyxoid tumor with prominent collagenous rosettes: case report with a brief review. Exp Mol Pathol 2021; 123: 104686.
70. Srivastava P, Zilla ML, Naous R, et al. Expanding the molecular signatures of malignant ossifying fibromyxoid tumours with two novel gene fusions: *PHF1*::*FOXR1* and *PHF1*::*FOXR2*. Histopathology 2023; 82: 946-52.
71. Bigot NJ, Neyaz A, Alani A, et al. Malignant ossifying fibromyxoid tumour with *TP53*::*PHF1* fusion: report of three cases suggesting an association between rare fusions and malignant phenotypes. Histopathology 2025; 87: 332-7.
72. Killian K, Leckey BD, Naous R, McGough RL, Surrey LF, John I. Novel *MEAF6-SUZ12* fusion in ossifying fibromyxoid tumor with unusual features. Genes Chromosomes Cancer 2021; 60: 631-4.
73. Kao YC, Sung YS, Zhang L, Chen CL, Huang SC, Antonescu CR. Expanding the molecular signature of ossifying fibromyxoid tumors with two novel gene fusions: *CREBBP-BCORL1* and *KDM2A-WWTR1*. Genes Chromosomes Cancer 2017; 56: 42-50.
74. McEvoy MT, Blessing MM, Fisher KE, et al. A novel case of malignant ossifying fibromyxoid tumor with a *BCOR* internal tandem duplication in a child. Pediatr Blood Cancer 2023; 70: e29972.
75. Micci F, Panagopoulos I, Bjerkehagen B, Heim S. Consistent rearrangement of chromosomal band 6p21 with generation of fusion genes *JAZF1/PHF1* and *EPC1/PHF1* in endometrial stromal sarcoma. Cancer Res 2006; 66: 107-12.
76. Dickson BC, Lum A, Swanson D, et al. Novel *EPC1* gene fusions in endometrial stromal sarcoma. Genes Chromosomes Cancer 2018; 57: 598-603.
77. Graham RP, Weiss SW, Sukov WR, et al. *PHF1* rearrangements in ossifying fibromyxoid tumors of soft parts: a fluorescence in situ hybridization study of 41 cases with emphasis on the malignant variant. Am J Surg Pathol 2013; 37: 1751-5.
78. Atanaskova Mesinkovska N, Buehler D, McClain CM, Rubin BP, Goldblum JR, Billings SD. Ossifying fibromyxoid tumor: a clinicopathologic analysis of 26 subcutaneous tumors with emphasis on differential diagnosis and prognostic factors. J Cutan Pathol 2015; 42: 622-31.
79. Antonescu CR, Zhang L, Chang NE, et al. *EWSR1-POU5F1* fusion in soft tissue myoepithelial tumors: a molecular analysis of sixty-six cases, including soft tissue, bone, and visceral lesions, showing common involvement of the *EWSR1* gene. Genes Chromosomes Cancer 2010; 49: 1114-24.
80. Thway K, Chisholm J, Hayes A, Swansbury J, Fisher C. Pediatric low-grade fibromyxoid sarcoma mimicking ossifying fibromyxoid tumor: adding to the diagnostic spectrum of soft tissue tumors with a bony shell. Hum Pathol 2015; 46: 461-6.
81. Reid R, de Silva MV, Paterson L, Ryan E, Fisher C. Low-grade fibromyxoid sarcoma and hyalinizing spindle cell tumor with giant rosettes share a common t(7;16)(q34;p11) translocation. Am J

Surg Pathol 2003; 27: 1229-36.
82. Guillou L, Benhattar J, Gengler C, et al. Translocation-positive low-grade fibromyxoid sarcoma: clinicopathologic and molecular analysis of a series expanding the morphologic spectrum and suggesting potential relationship to sclerosing epithelioid fibrosarcoma: a study from the French Sarcoma Group. Am J Surg Pathol 2007; 31: 1387-402.
83. Mohamed M, Fisher C, Thway K. Low-grade fibromyxoid sarcoma: clinical, morphologic and genetic features. Ann Diagn Pathol 2017; 28: 60-7.
84. Meis-Kindblom JM, Kindblom LG, Enzinger FM. Sclerosing epithelioid fibrosarcoma: a variant of fibrosarcoma simulating carcinoma. Am J Surg Pathol 1995; 19: 979-93.
85. Warmke LM, Meis JM. Sclerosing epithelioid fibrosarcoma: a distinct sarcoma with aggressive features. Am J Surg Pathol 2021; 45: 317-28.
86. Arbajian E, Puls F, Magnusson L, et al. Recurrent *EWSR1-CREB3L1* gene fusions in sclerosing epithelioid fibrosarcoma. Am J Surg Pathol 2014; 38: 801-8.
87. Warmke LM, Ameline B, Fritchie KJ, et al. *YAP1*::*KMT2A*-rearranged sarcomas harbor a unique methylation profile and are distinct from sclerosing epithelioid fibrosarcoma and low-grade fibromyxoid sarcoma. Virchows Arch 2025; 486: 457-77.
88. Kao YC, Lee JC, Zhang L, et al. Recurrent *YAP1* and *KMT2A* gene rearrangements in a subset of MUC4-negative sclerosing epithelioid fibrosarcoma. Am J Surg Pathol 2020; 44: 368-77.
89. Puls F, Agaimy A, Flucke U, et al. Recurrent fusions between *YAP1* and *KMT2A* in morphologically distinct neoplasms within the spectrum of low-grade fibromyxoid sarcoma and sclerosing epithelioid fibrosarcoma. Am J Surg Pathol 2020; 44: 594-606.
90. Martinez-Rodriguez M, Subramaniam MM, Calatayud AM, Ramos D, Navarro S, Llombart-Bosch A. Ossifying fibromyxoid tumor of soft parts mimicking a schwannoma with uncommon histology: a potential diagnostic pitfall. J Cutan Pathol 2009; 36: 71-3.
91. Schaefer IM, Fletcher CD, Hornick JL. Loss of H3K27 trimethylation distinguishes malignant peripheral nerve sheath tumors from histologic mimics. Mod Pathol 2016; 29: 4-13.
92. Prieto-Granada CN, Wiesner T, Messina JL, Jungbluth AA, Chi P, Antonescu CR. Loss of H3K27me3 expression is a highly sensitive marker for sporadic and radiation-induced MPNST. Am J Surg Pathol 2016; 40: 479-89.
93. Sbaraglia M, Bellan E, Gambarotti M, et al. Primary malignant ossifying fibromyxoid tumour of the bone: a clinicopathologic and molecular report of two cases. Pathologica 2020; 112: 184-90.
94. Wang XQ, Goytain A, Dickson BC, Nielsen TO. Advances in sarcoma molecular diagnostics. Genes Chromosomes Cancer 2022; 61: 332-45.
95. Kilpatrick SE, Ward WG, Mozes M, Miettinen M, Fukunaga M, Fletcher CD. Atypical and malignant variants of ossifying fibromyxoid tumor: clinicopathologic analysis of six cases. Am J Surg Pathol 1995; 19: 1039-46.
96. Provenzano S, Raimondi A, Bertulli RM, et al. Response to isolated limb perfusion and chemotherapy with epirubicin plus ifosfamide in a metastatic malignant ossifying fibromyxoid tumor. Clin Sarcoma Res 2017; 7: 20.
97. Lastra RR, Newman JG, Brooks JS, Huang JH. Ossifying fibromyxoid tumor metastatic to the thyroid: a case report and review of the literature. Ear Nose Throat J 2014; 93: 221-3.

JPTM

REVIEW ARTICLE

pISSN 2383-7837 · eISSN 2383-7845

Journal of Pathology and Translational Medicine 2026; 60: 20-46
https://doi.org/10.4132/jptm.2025.10.08

Solitary fibrous tumor: an updated review

Joon Hyuk Choi

Department of Pathology, Yeungnam University College of Medicine, Daegu, Korea

Solitary fibrous tumor (SFT) is a fibroblastic neoplasm characterized by a branching, thin-walled dilated staghorn-shaped (hemangiopericytoma-like) vasculature and a *NAB2*::*STAT6* gene fusion. SFTs can occur in almost any anatomical location, including superficial and deep soft tissues, visceral organs, and bone. They most commonly occur in extrapleural locations, equally affect both sexes, and are typically present in adults. Although metastasis is rare, SFTs frequently show local recurrence. The diagnosis of SFTs is difficult because of their broad histological and morphological overlap with other neoplasms. An accurate diagnosis is important for guiding disease management and prognosis. Despite advances in molecular diagnostics and therapeutic strategies, the biological complexity and unpredictable clinical behavior of SFTs present significant challenges. This review provides an updated overview of SFT, with a focus on its molecular genetics, histopathological features, and diagnostic considerations.

Keywords: Solitary fibrous tumors; Hemangiopericytoma; Diagnosis, differential; Neoplasms, fibrous tissue; Gene rearrangement

INTRODUCTION

Solitary fibrous tumor (SFT) is a rare fibroblastic neoplasm defined by a distinctive network of thin-walled, branching staghorn-shaped (hemangiopericytoma-like) vessels [1]. It may occur in almost any anatomical location, such as superficial and deep soft tissue, visceral organs, and bone, although it most often arises in extrapleural sites. SFT affects both sexes equally and is typically diagnosed in adults.

Many tumors previously classified as hemangiopericytomas are now recognized as SFTs and reflect fibroblastic rather than true pericytic differentiation [2]. Histologically, SFTs exhibit a wide morphological spectrum, usually consisting of spindle to ovoid cells arranged haphazardly within a collagen-rich stroma and associated with prominent staghorn-shaped vasculature [3]. However, its biological behavior is often unpredictable and cannot be reliably inferred from morphology alone [4].

Recent advances in molecular pathology, particularly the discovery of the *NAB2*::*STAT6* gene fusion and its downstream effects, have provided considerable insight into the biology, classification, and potential therapeutic targets of SFT [5-7]. Nonetheless, diagnosis remains difficult because of marked histological heterogeneity and overlap with other spindle cell neoplasms.

Most SFTs pursue an indolent course; however, a clinically important subset shows aggressive behavior, including local recurrence or distant metastasis. Therefore, accurate pathological classification, integrated with molecular findings, is essential for guiding management and prognostication.

In this review, the clinicopathological and molecular features of SFT are summarized, including the histological subtypes, diagnostic approaches, and key differential diagnoses.

HISTORICAL ASPECTS

The term hemangiopericytoma was first introduced in the 1940s by Stout and Murray [8] and Stout [9,10] to describe tumors thought to originate from pericytes, which are specialized contractile cells surrounding capillaries and venules; however, their original definition lacked specificity and encompassed a heterogeneous group of neoplasms, including entities now classified as

---

Received: September 1, 2025 **Revised:** October 5, 2025 **Accepted:** October 8, 2025

Corresponding Author: Joon Hyuk Choi, MD, PhD
Department of Pathology, Yeungnam University College of Medicine, 170 Hyeonchung-ro, Nam-gu, Daegu 42415, Korea
Tel: +82-53-640-6754, Fax: +82-53-640-6769, E-mail: joonhyukchoi@ynu.ac.kr

This is an Open Access article distributed under the terms of the Creative Commons Attribution Non-Commercial License (https://creativecommons.org/licenses/by-nc/4.0/) which permits unrestricted non-commercial use, distribution, and reproduction in any medium, provided the original work is properly cited.
© 2026 The Korean Society of Pathologists/The Korean Society for Cytopathology

myofibromas. In 1976, Enzinger and Smith [11] refined the concept, characterizing these tumors by their undifferentiated small round-to-spindle cells and the presence of prominent, branching staghorn-shaped vessels. Despite this refinement, its classification remains problematic because of inconsistent ultrastructural evidence of pericytic differentiation [12-15], infrequent actin expression [16-19], and poor diagnostic reproducibility [20], which has resulted in a gradual decline in the use of the term.

The entity known as SFT subsequently emerged. First described by Klemperer and Rabin [21] as a pleural-based lesion designated "fibrous mesothelioma" or "benign fibrous tumor of the pleura," it was more clearly defined by England in 1989 [22], who proposed the term "localized fibrous tumor of the pleura." By the late 1980s and early 1990s, histologically indistinguishable tumors were increasingly recognized at extrapleural sites, which supported the concept of a broader, site-independent lesion.

Extrapleural tumors with a hemangiopericytoma-like morphology frequently express CD34, similar to SFTs, which suggests a shared lineage. This was confirmed by the discovery of the recurrent *NAB2*::*STAT6* gene fusion and its corresponding nuclear signal transducer and activator of transcription 6 (STAT6) expression in SFTs and tumors, which were previously diagnosed as hemangiopericytomas, regardless of anatomical site [23-26].

Based on this evidence, the 2002 WHO classification of tumors of soft tissue and bone (3rd edition) [27] revised the definition of hemangiopericytoma. It was recognized that most remaining cases closely resemble the cell variant of SFT morphologically and clinically. In 2013, the 4th edition of the WHO classification [28] eliminated the term hemangiopericytoma, reclassifying nearly all such tumors under the unified diagnosis of SFT. Table 1 lists the conceptual changes in hemangiopericytoma classification.

EPIDEMIOLOGY

SFTs affect both sexes equally and predominantly occur in adults, with a peak incidence between 40 and 70 years of age [29-31]. Although SFTs may arise anywhere in the body, extrapleural locations are more common. Approximately 30%–40% occur in the extremities, 30%–40% in the deep soft tissues of the abdomen, pelvis, or retroperitoneum, 10%–15% in the head and neck, and 10%–15% in the trunk [30,32].

In the gastrointestinal system, SFTs typically develop in adults aged 20–70 years, but are rare in children and adolescents. The liver, pancreas, mesentery, or serosal surfaces of the gastrointestinal tract are considered common sites. A slight male predominance was reported in the lipomatous (fat-forming) subtype [33-35]. In the female genital tract, SFTs primarily affect women aged 22–75 years, with a peak incidence during the fifth decade. Common sites include the vulva, vagina, and cervix [36].

In the thorax, SFTs primarily occur from the visceral pleura and typically present in the sixth decade. They may also arise in the lung or pericardium, whereas mediastinal involvement is rare. No sex predilection is evident [22,37]. In the central nervous system (CNS), SFTs are extremely rare and account for less than 1% of all CNS tumors. They often present in middle-aged to older adults. Most are dural-based and are often located in the supratentorial region, with occasional cases reported in the skull base, spinal cord, or pineal region [38-40].

In the urinary and male genital tracts, SFTs generally occur in adults between 20 and 70 years of age, with no clear sex predilection. Reported locations include the kidney, bladder, prostate, seminal vesicles, and penis [41,42]. In the endocrine system, SFTs most commonly involve the thyroid gland or pituitary fossa, whereas other endocrine organs are rare. These tumors typically occur between ages of 50 and 60, with no sex predilection [43,44].

In the head and neck, a marked male predominance is observed in the larynx (male-to-female ratio ~6:1), whereas tumors arising in the orbit, nasal cavity, or paranasal sinuses occur across a broad age range in both sexes [45,46]. Orbital SFTs are most common in individuals in their mid-40s and are rare in children. These tumors may occur in the intraconal and extraconal compartments, with occasional involvement of the lacrimal

Table 1. Conceptual changes in hemangiopericytoma classification

Tumor type	Updated concept	Line of differentiation
Adult hemangiopericytoma	Reclassified as solitary fibrous tumor (cellular subtype)	Fibroblastic differentiation
Infantile hemangiopericytoma	Considered within the spectrum of infantile myofibromatosis	Pericytic (perivascular myoid) differentiation
Meningeal hemangiopericytoma	Reclassified as cellular/malignant solitary fibrous tumor	Fibroblastic differentiation
Sinonasal hemangiopericytoma	Reclassified as sinonasal glomangiopericytoma	Pericytic (perivascular myoid) differentiation

gland, conjunctiva, or eyelid [47-49].

CLINICAL FEATURES

The clinical presentation of SFTs varies by anatomical site, but they most commonly manifest as a slow-growing, painless mass. Abdominopelvic SFTs may cause symptoms, such as abdominal distention, constipation, urinary retention, or early satiety [50,51], whereas head and neck lesions result in nasal obstruction, hoarseness, or epistaxis [52,53]. Orbital SFTs typically present with periorbital fullness, proptosis, globe displacement, and diplopia, whereas deeper lesions may compromise the optic nerve [47,49,54].

Thoracic SFTs are often asymptomatic and incidentally detected; however, larger tumors can result in cough, dyspnea, or chest pain [55]. CNS SFTs generally present with mass effect symptoms or increased intracranial pressure [56]. In the digestive, urinary, and endocrine systems, tumors are usually painless but may produce compressive symptoms depending on their size and anatomical relationships [41,43,57].

A subset of large or aggressive SFTs secretes insulin-like growth factor 2 (IGF2), which results in paraneoplastic hypoglycemia (Doege-Potter syndrome) and, rarely, acromegaloid features [58,59].

RADIOLOGICAL FEATURES

Upon imaging, SFTs typically show nonspecific radiographic features [60,61], whereas computed tomography (CT) usually yields a well-defined, occasionally lobulated, isodense mass relative to the skeletal muscle (Fig. 1). They exhibit heterogeneous contrast enhancement because of their rich vascularity [62,63]. Magnetic resonance imaging (MRI) typically shows intermediate T1 signal intensity and variable T2 signals, which correspond to fibrous (low T2) and cellular or myxoid (high T2) components [63-65]. Larger or more aggressive tumors may display heterogeneity because of fibrosis, necrosis, hemorrhage, or cystic changes [63].

In the thorax, SFTs are usually present as sharply marginated, pleural-based masses without chest wall invasion. Malignant lesions may exhibit increased fluorodeoxyglucose uptake on positron emission tomography; however, overlap with benign tumors may occur [66,67]. In the CNS, SFTs often mimic meningiomas on imaging. The lesions exhibit isointensity on T1-weighted MRI, variable T2 signals, and peripheral dural enhancement (dural tail); however, no specific CT or MRI features reliably distinguish them from other dural-based tumors [68,69].

In the head and neck region, SFTs typically appear as well-circumscribed, contrast-enhanced masses by CT and MRI [70,71]. In the orbit, MRI typically exhibits iso-intense signals on T1-weighted images, whereas CT demonstrates contrast enhancement and is valuable for assessing bone involvement [47,72].

MOLECULAR CHARACTERISTICS

Most SFTs harbor a recurrent paracentric inversion on chromosome 12q13. This inversion results in the fusion of the *NAB2* and *STAT6* genes [26,73,74]. This fusion replaces the C-terminal repression domain of NAB2 with the transcriptional activation domain of STAT6, thereby converting NAB2 from a transcriptional repressor into a constitutive activator of *EGR1*. Consequently, *EGR1* drives the expression of downstream targets, such as *IGF2* and *FGFR1*, as well as other genes that promote growth and survival [73].

Multiple *NAB2*::*STAT6* gene fusion variants have been discovered, with the length of the retained STAT6 portion correlating with tumor morphology and clinical behavior. For example, fusions involving *NAB2* exon 4 and *STAT6* exon 2 or 3 are associated with a reduced cellular and more indolent course. In contrast, fusions involving *NAB2* exons 6–7 and *STAT6* exons 16–17 more commonly occur in cellular or clinically aggressive

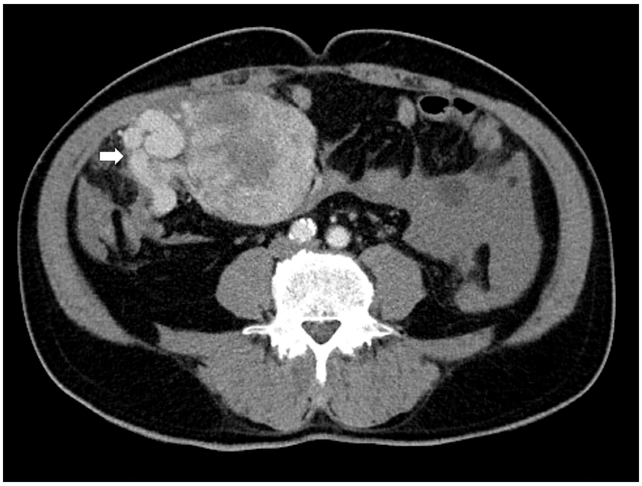

Fig. 1. Radiological findings of solitary fibrous tumor. Axial contrast-enhanced abdominal computed tomography demonstrates a large central abdominal mass. Prominent feeding vessels (arrow) are visible along the anterior aspect of the lesion.

variants [75,76].

No distinct molecular features have been identified that can reliably distinguish benign from malignant SFTs; however, other genetic alterations linked to high-grade transformation or aggressive behavior have been identified, including *TERT* promoter mutations [55,77], *TP53* mutations, and p16 overexpression [78-81]. Moreover, *IGF2*, a key mediator of Doege-Potter syndrome in SFTs, is a target gene of *EGR1* and may be dysregulated by the *NAB2*::*STAT6* fusion, which may account for the relatively high frequency of this paraneoplastic syndrome [26].

The *NAB2*::*STAT6* gene fusion is definitively diagnostic; however, its detection by molecular methods is challenging because of the close proximity of the genes on chromosome 12q and the heterogeneity of the fusion breakpoints. Thus, STAT6 immunohistochemistry demonstrating strong, diffuse nuclear staining, serves as a sensitive and specific surrogate marker for all fusion variants and is widely used in routine diagnostic practice [23,25,82].

HISTOPATHOLOGICAL FEATURES

Macroscopic features

SFTs are usually well-circumscribed, solid masses ranging in size from 1 cm to greater than 25 cm, with most measuring between 5–10 cm in diameter [83,84]. The cut surface varies from firm and white in more fibrous tumors to tan and fleshy in highly cellular lesions (Fig. 2). Hemorrhage, calcification, or necrosis may occur, particularly in the larger tumors [85-88]. Benign SFTs are typically well-circumscribed, but unencapsulated, whereas malignant tumors often exhibit infiltrative borders and areas of necrosis [89].

Tumors arising from serosal surfaces often exhibit an exophytic appearance, whereas those within body cavities may be present as polypoid, stalk-attached fibrous masses [3]. Pleural SFTs are often large (>10 cm) and pedunculated, with a pedicle containing prominent feeder vessels. Some cases lack direct pleural attachment and can appear enclosed within the lung parenchyma [37].

In the CNS, SFTs are usually dural-based, well-circumscribed, firm, white to reddish-brown masses; however, they may occasionally exhibit infiltrative growth or lack dural attachment [90-92]. In the head and neck region, tumor size varies by anatomical site, including approximately 2.5 cm in the larynx, 4 cm in the salivary glands, and 5 cm in the sinonasal tract [46,52,53,89].

Histopathology

Histologically, classic SFTs display the so-called patternless pattern, characterized by alternating hypocellular and hypercellular areas, with tumor cells frequently interposed between collagen bundles (Fig. 3A). The tumor cells are ovoid to spindle-shaped, with vesicular nuclei, pale eosinophilic cytoplasm, and indistinct cell borders, and are embedded in a variably collagenous stroma (Fig. 3B). A characteristic feature is the presence of thin-walled, branching, staghorn-shaped vessels (Fig. 3C). Perivascular hyalinization may also be observed (Fig. 3D). The degree of cellularity varies considerably, ranging from sparsely scattered

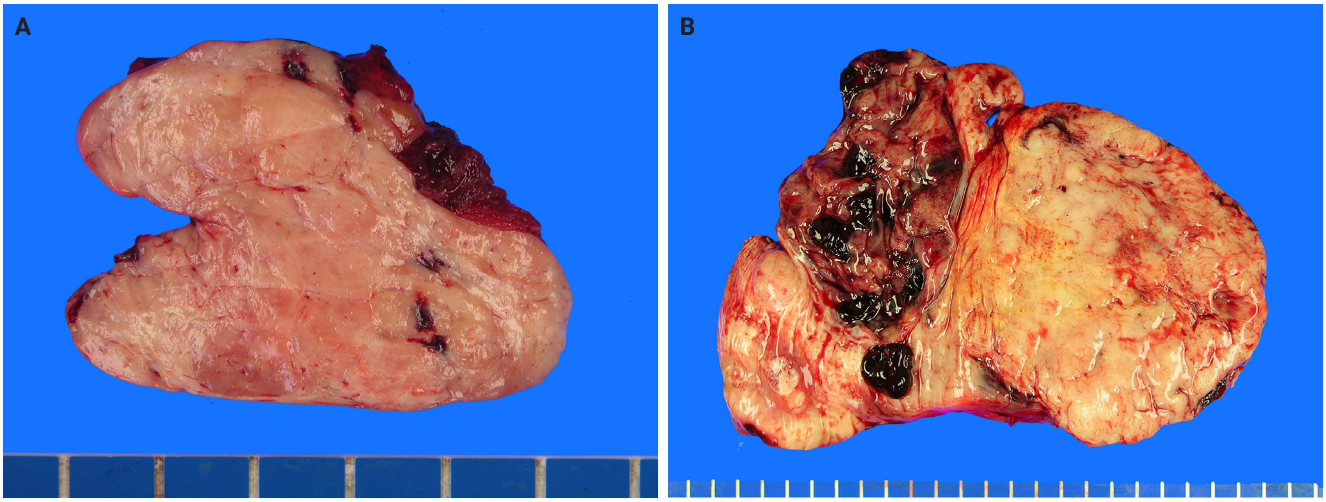

Fig. 2. Macroscopic findings of solitary fibrous tumor. (A) The cut surface of the tumor is well-circumscribed, with a pinkish-gray, fleshy, and solid appearance. (B) The tumor is multilobulated, with yellow-tan to gray coloration and prominent areas of hemorrhage.

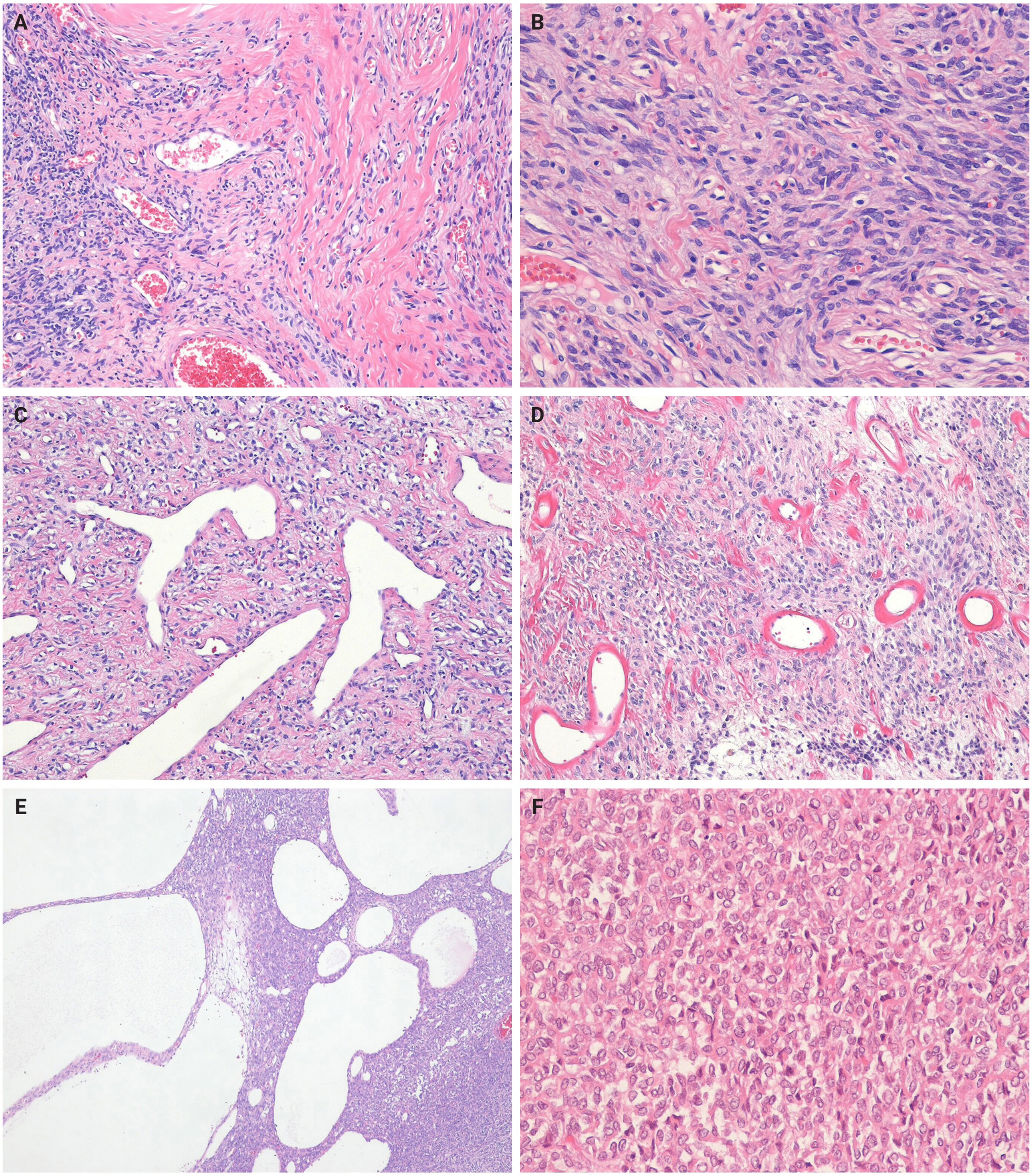

Fig. 3. Histological findings of classic solitary fibrous tumor. (A) The tumor shows variation in cellularity, with prominent stromal collagen deposition in the hypocellular regions. (B) The tumor cells are relatively uniform and spindle-shaped, with vesicular nuclei and scant pale eosinophilic cytoplasm, arranged in a patternless architecture. (C) Branching, staghorn-shaped vessels are present. (D) Perivascular hyalinization is present. (E) Cystic changes are present. (F) Epithelioid tumor cells are observed.

individual cells or linear clusters to highly cellular areas, even within the same tumor. The tumor cells are haphazardly arranged within the stroma, often in a storiform configuration or as randomly oriented fascicles. Mitoses are typically infrequent, and significant nuclear pleomorphism or necrosis is absent in conventional cases. Additional histological features may include multinucleated giant cells, myxoid or cystic changes, and hemorrhage (Fig. 3E). Rarely, the foci of epithelioid or rhabdoid tumor cells may also be present (Fig. 3F).

Subtypes of solitary fibrous tumor

SFT subtypes share clinical, histological, and immunohistochemical characteristics that support their close relationship.

Cellular solitary fibrous tumor

Cellular SFT is characterized by densely packed tumor cells with indistinct cytoplasmic borders and prominent thin-walled, branching staghorn-shaped vessels, with little or no intervening stroma. This subtype corresponds to the originally described hemangiopericytoma. The tumor cells are typically monotonous, showing loss of spindled morphology and transition to a more ovoid or rounded shape (Fig. 4A). Hemorrhage is common in cellular SFT, whereas necrosis may also be present.

Lipomatous (fat-forming) solitary fibrous tumor

Lipomatous (fat-forming) SFT is a rare histological subtype characterized by mature adipose tissue forming an integral component of the tumor. Histologically, it displays the typical features of SFT mixed with a variable amount of mature fat (Fig. 4B) [35,93-95]. An immature lipoblastic component may also be present. Although the majority of lipomatous SFTs are benign, cases with malignant histological features have also been reported [96].

Giant cell-rich solitary fibrous tumor

Giant cell-rich SFT (formerly known as giant cell angiofibroma) is a rare SFT subtype that retains the typical morphological features of conventional SFT, but contains a mixed population of multinucleated giant cells scattered within the stroma and lining pseudovascular spaces [97,98]. The tumor is composed of bland, round-to-spindle cells and multinucleated giant cells (Fig. 4C). It exhibits alternating hypocellular/sclerotic and hypercellular areas, often associated with staghorn-shaped vasculature.

Myxoid solitary fibrous tumor

Focal myxoid change is a common finding in SFTs and may result from an increase in mucin production by neoplastic cells within the connective tissue. Myxoid SFT is a rare SFT subtype characterized by diffuse and prominent myxoid changes involving most of the tumor and exhibit a hypocellular, bland histological appearance (Fig. 4D) [99].

Malignant solitary fibrous tumor

Malignant SFT is defined by one or more adverse histological features, including hypercellularity, increased mitotic activity (>4 mitoses per 10 high-power fields [HPFs]), cytological atypia, tumor necrosis, and/or infiltrative margins (Fig. 4E, F) [84,100,101]. Of these, a high mitotic count is considered the most reliable predictor of aggressive behavior and poor clinical outcome [30,102]. In accordance with the College of American Pathologists (CAP) and WHO guidelines, it is currently recommended that mitotic activity be reported as the number of mitoses per mm^2. With older models of microscopes, 10 HPFs are equivalent to 1 mm^2. With a modern microscope featuring a 0.5 mm field diameter, 5 HPFs correspond to an area of approximately 1 mm^2. Risk-stratification models, such as that of Demicco et al. [103], integrate clinical and pathological parameters to improve prognostic accuracy.

Dedifferentiated solitary fibrous tumor

Dedifferentiated SFT accounts for less than 1% of all cases and is characterized by an abrupt transition from conventional SFT morphology to high-grade spindle or pleomorphic sarcoma features (Fig. 4G, H) [104-112]. It may occur in various anatomical sites, including the meninges and orbit. Heterologous elements, such as rhabdomyosarcoma or osteosarcoma, have also been described. Dedifferentiated SFT has a high risk of recurrence and metastasis and portends a poor prognosis.

IMMUNOHISTOCHEMICAL FEATURES

Immunohistochemical studies have shown that SFTs typically exhibit strong, diffuse nuclear expression of STAT6 and CD34 (Fig. 5) [23,25,73,84,113]. The nuclear localization of STAT6 reflects the presence of the *NAB2*::*STAT6* fusion and serves as a sensitive and specific diagnostic marker that distinguishes SFT from histological mimics [114-117]. However, STAT6 expression has also been reported in dedifferentiated liposarcoma (DDLPS) [118] and *GLI1*-altered soft tissue tumor [119]. CD34 is expressed in approximately 81%–95% of cases, particularly in low-grade tumors; however, its expression may be decreased or lost in high-grade or dedifferentiated SFTs [120-123]. Similarly, loss of STAT6 expression has been observed in dedifferentiated or embolized tumors [121].

Gene expression profiling identified other markers that can distinguish SFTs from their histological mimics. Among these, glutamate ionotropic receptor AMPA type subunit 2 (GRIA2) shows 80%–93% sensitivity for SFT [124]. Cytoplasmic aldehyde

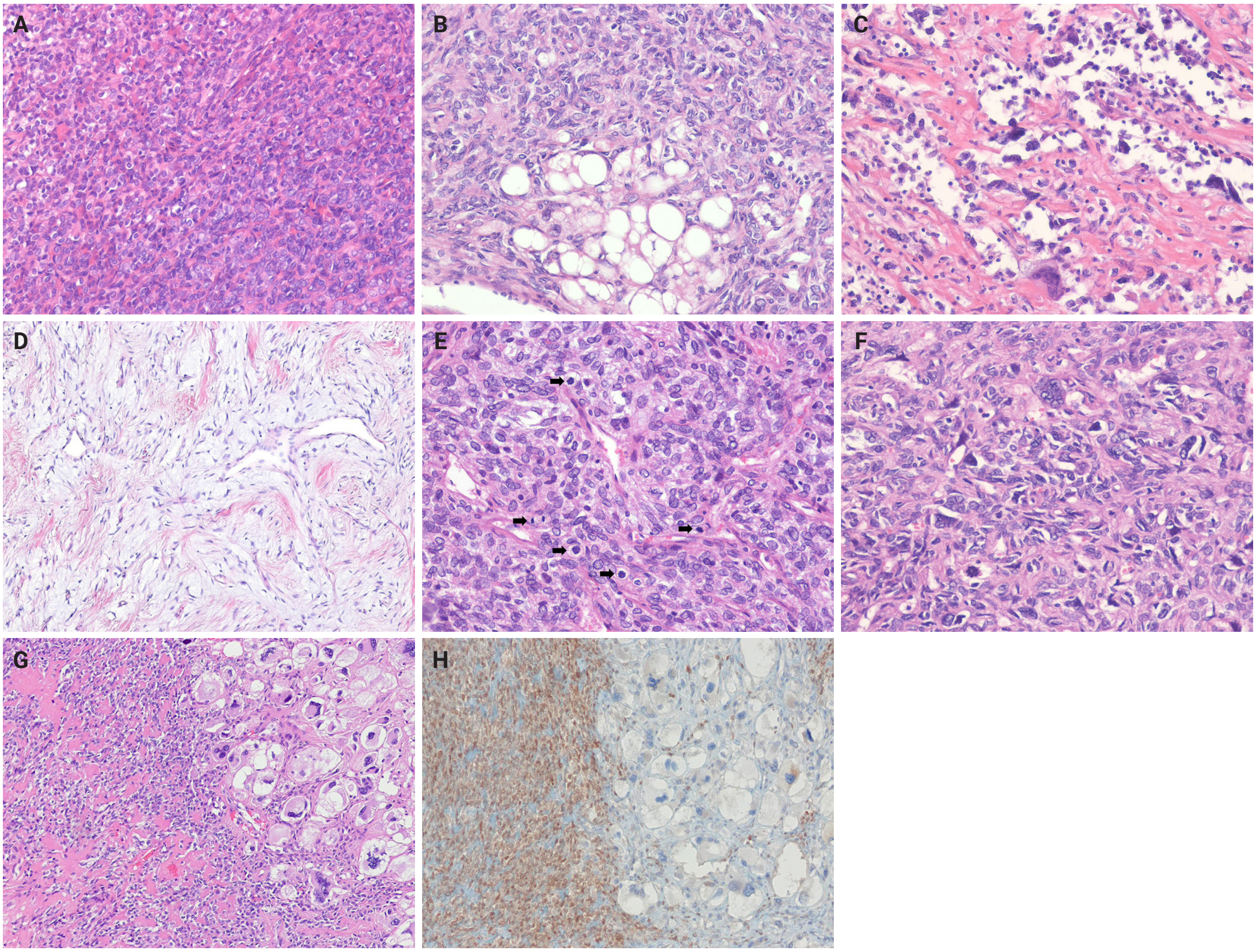

Fig. 4. Histological findings of solitary fibrous tumor subtypes. (A) Cellular subtypes. The tumor shows predominantly increased cellularity, and the tumor cells exhibit a more ovoid or rounded cytomorphology. (B) Lipomatous (fat-forming) subtypes. The tumor shows areas of mature adipose tissue. (C) Giant cell-rich subtypes. There are abundant multinucleated tumor giant cells, which frequently line pseudovascular spaces. (D) Myxoid subtype. The tumor shows prominent myxoid stroma with hypocellularity. Dilated, thin-walled vessels are present. (E) Malignant subtype (high-risk solitary fibrous tumor). Mitotic figures (arrows) are frequently observed. (F) Malignant subtype (high-risk solitary fibrous tumor). The tumor cells exhibit marked nuclear pleomorphism and cytological atypia. (G) Dedifferentiated subtype. The tumor shows an abrupt transition from solitary fibrous tumor (left) to high-grade dedifferentiated area (right). (H) Dedifferentiated subtype. Classic solitary fibrous tumor shows strong, diffuse nuclear expression of STAT6, whereas the dedifferentiated area demonstrates loss of STAT6 expression.

dehydrogenase 1 (ALDH1) demonstrates 84% sensitivity and 99% specificity in differentiating SFT from meningioma and synovial sarcoma (SS) [125]. Subsequent studies indicate that ALDH1 sensitivity ranges from 76% to 97% and GRIA2 sensitivity ranges from 64% to 84%, with GRIA2 exhibiting lower specificity compared with ALDH1 and STAT6 [111,112,126].

Other immunohistochemical markers, such as BCL2 and CD99, are frequently positive. Epithelial membrane antigen (EMA) and smooth muscle actin (SMA) show variable expression, whereas desmin, S100 protein, SOX10, actins, cytokeratins, and the progesterone receptor are typically negative or only focally expressed [83,127,128]. Transducin-like enhancer of split 1 (TLE1) may show weak positivity [129]. Occasional PAX8 expression has also been reported, which may cause diagnostic confusion with renal cell carcinoma [130]. Table 2 summarizes the immunohistochemistry profiles for SFT.

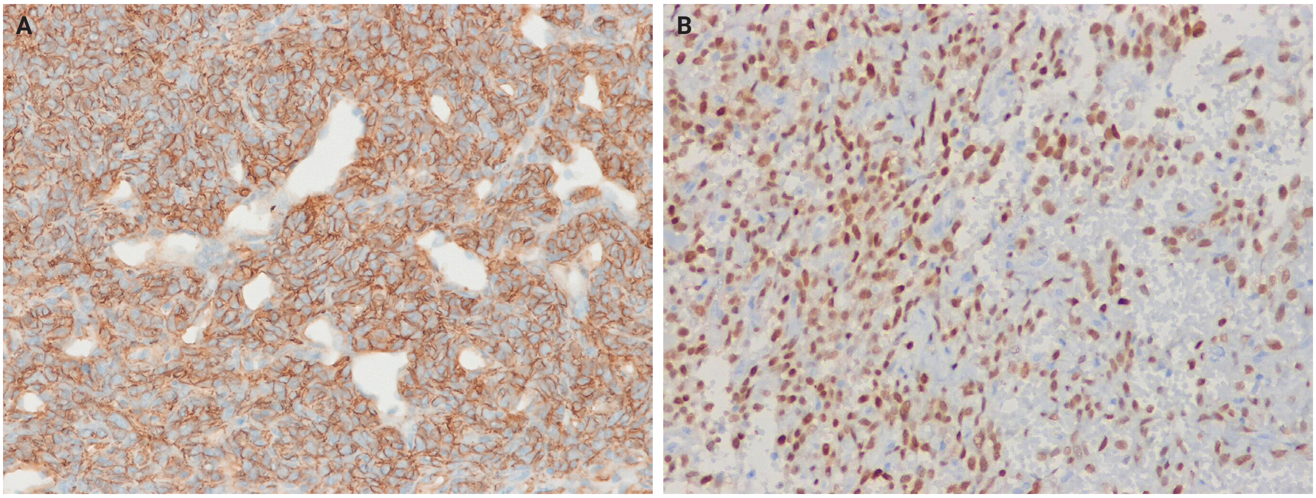

Fig. 5. Immunohistochemical findings of solitary fibrous tumor. (A) The tumor cells demonstrate strong, diffuse cytoplasmic and membranous expression of CD34. (B) The tumor cells show strong, diffuse nuclear expression of STAT6.

DIAGNOSTIC APPROACH

A systematic and integrated approach is required to accurately diagnose SFTs. The process begins with a thorough histopathological evaluation of hematoxylin and eosin sections, particularly at low magnification, to assess tumor borders, cellular uniformity, and overall architecture. Key histological features include bland spindle cell morphology, patternless or short fascicular architecture, and stromal characteristics, such as hyalinization, myxoid change, and the distinctive staghorn-shaped vascular pattern. Recognizing these features is critical for distinguishing SFTs from other spindle cell neoplasms with overlapping morphologies.

The clinical context, including patient age, tumor location, and symptomatology, together with radiological findings, provides valuable complementary information. For example, a well-circumscribed, hypervascular mass on imaging in a middle-aged or older adult supports the presumptive diagnosis of SFT. These clinical-radiological correlations are particularly helpful when histological findings are equivocal.

Immunohistochemistry plays an essential role in the diagnostic algorithm and has largely replaced electron microscopy due to its accessibility and diagnostic utility. It is necessary not only for establishing the line of differentiation but also for identifying molecular surrogates of specific genetic alterations. For SFTs, strong, diffuse nuclear STAT6 expression, which serves as a surrogate marker for the *NAB2*::*STAT6* gene fusion, together with CD34 positivity, constitutes a highly sensitive and specific marker combination. These two markers are routinely used and are generally sufficient to confirm an SFT diagnosis in most cases. However, they are not entirely specific, as focal STAT6 expression may also occur in other mesenchymal tumors, creating potential diagnostic pitfalls. Moreover, additional diagnostic confusion may arise, particularly in tumors occurring in visceral organs, such as the lung, salivary gland, or prostate [32,131]. For example, entrapment of normal glandular epithelium should not be misinterpreted as a biphasic neoplasm, such as phyllodes tumor, pleomorphic adenoma, or sarcomatoid carcinoma (Fig. 6). If STAT6 is negative, second-line antibodies, such as GRIA2 and ALDH1, may be used.

For diagnostically challenging or histologically atypical cases, fluorescence in situ hybridization (FISH) or next-generation sequencing may provide additional diagnostic clarity. These approaches are also helpful for detecting fusion genes or mutations associated with dedifferentiation. They have been incorporated into routine diagnostic workflows to enhance diagnostic precision and enable prognostic stratification, particularly in high-grade or dedifferentiated subtypes. In summary, a comprehensive diagnostic approach that integrates morphologic, immunophenotypic, clinical, and molecular data is essential for achieving diagnostic accuracy, refining risk stratification, and guiding appropriate patient management.

HISTOLOGICAL DIFFERENTIAL DIAGNOSIS

The histological differential diagnosis of SFT depends on the

Table 2. Immunohistochemical profile of solitary fibrous tumors

Immunostain	Approximate frequency (%)	Comment
Fusion-related marker		
STAT6	>95	Strong, diffuse nuclear staining; highly sensitive and specific surrogate for *NAB2::STAT6* gene fusion, although rare exceptions have been reported in other tumors[a]
Markers discovered by gene expression profiling		
ALDH1	75–95	Stem cell marker; not entirely specific
GRIA2	60–80	Relatively specific; limited commercial availability
TLE1	<10	Rarely positive; not diagnostically useful
Endothelial marker		
CD34	90–95	Commonly positive; may be lost in dedifferentiated SFT
Neuroectodermal marker		
CD99	~70	Nonspecific; also positive in other tumors
Muscle markers		
SMA	20–35	Nonspecific; focal expression
Desmin	<5	Usually negative
Nerve sheath marker		
S100 protein	~15	Focal expression; may mimic nerve sheath tumors; potential diagnostic pitfall
Epithelial markers		
EMA	20–35	Focal expression; potential diagnostic pitfall
Cytokeratins	<10	Rare focal expression; may be confused with carcinoma
PAX8	~40	Relatively frequent expression; not a specific marker of SFT; potential diagnostic pitfall
Prognostic markers		
p53	Variable	Aberrant expression associated with malignant/dedifferentiated SFT[b]
p16	Variable	Overexpression may be associated with aggressive behavior
Others		
BCL2	~30	Frequently expressed but nonspecific; limited diagnostic value

STAT6, signal transducer and activator of transcription 6; ALDH1, aldehyde dehydrogenase 1; GRIA2, glutamate ionotropic receptor AMPA type subunit 2; TLE1, transducin-like enhancer of split 1; SMA, smooth muscle actin; EMA, epithelial membrane antigen; PAX8, paired box gene 8; SFT, solitary fibrous tumor; BCL2, B-cell lymphoma 2.

[a]STAT6 is rarely expressed in dedifferentiated liposarcoma and GLI1-altered soft tissue tumor; [b]*TP53* mutation in approximately 40% of malignant SFTs.

location and morphology of the tumor; however, it may be substantially improved by immunohistochemical detection of nuclear STAT6 expression. Accurate diagnosis requires a combination of clinical context, anatomic site, histopathological features, and a focused immunohistochemical panel.

Spindle cell lipoma

Spindle cell lipoma (SCL) is a benign adipocytic tumor consisting of variable amounts of mature adipocytes, bland spindle cells, and ropy collagen [132]. It occurs most commonly in men aged 45–60 years and typically arises in the subcutaneous tissue of the posterior neck, back, and shoulders. SCL is histologically characterized by bland spindle cells arranged in small, aligned clusters within a myxoid matrix, accompanied by mature adipose tissue and ropy collagen. The spindle cells are typically CD34-positive [133,134] and show loss of nuclear RB1 protein expression [135]. SFTs with hyalinized stroma and admixed adipose tissue may resemble SCL; however, SCLs rarely exhibit a staghorn-shaped vasculature and lack nuclear STAT6 expression.

Nodular fasciitis

Nodular fasciitis (NF) is a benign, self-limited fibroblastic/myofibroblastic neoplasm that frequently exhibits a recurrent *USP6* rearrangement [136]. It is usually found in the subcutaneous tissue of the extremities and is typically <3 cm in size. NF is relatively common and can present at any age, although it most

https://doi.org/10.4132/jptm.2025.10.08

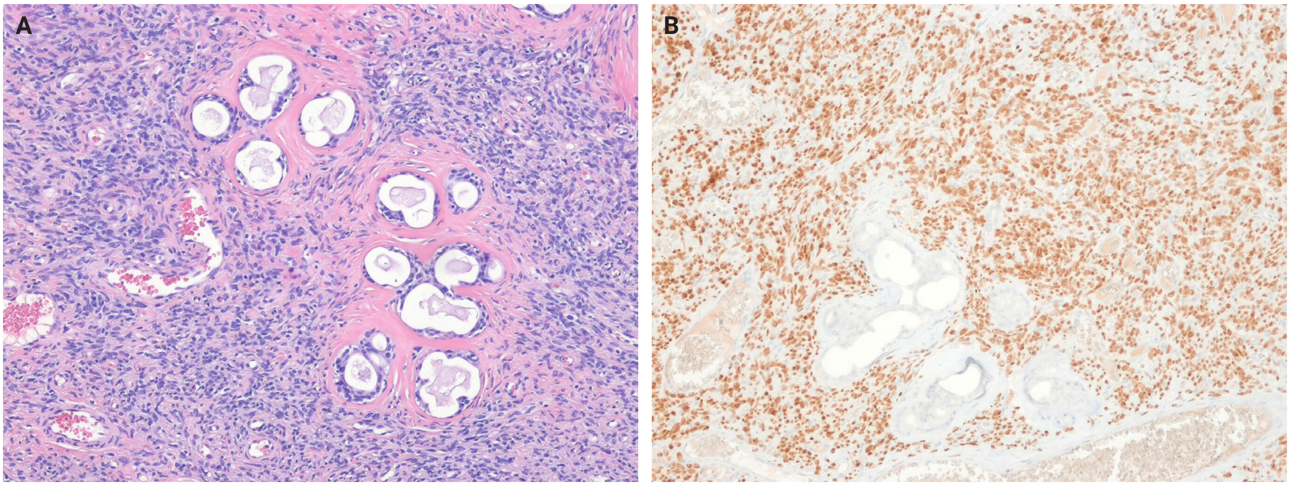

Fig. 6. Solitary fibrous tumor of the oral cavity. (A) Entrapped benign glandular inclusions are present within the tumor, mimicking pleomorphic adenoma. (B) The spindled tumor cells show strong, diffuse nuclear STAT6 expression, supporting the diagnosis of solitary fibrous tumor.

frequently occurs in young adults. Histologically, NF consists of plump, uniform fibroblasts and myofibroblasts arranged in a tissue culture-like pattern, within a variably myxoid stroma that often contains microcystic changes and extravasated erythrocytes. The tumor cells are positive for SMA and muscle-specific actin (MSA), with occasional desmin expression, but consistently negative for STAT6. The identification of a *USP6* rearrangement can assist in diagnostically challenging cases [137-139].

Desmoid fibromatosis

Desmoid fibromatosis (DFM) is a locally aggressive, non-metastasizing myofibroblastic neoplasm that is characterized by infiltrative growth and a high propensity for local recurrence [140]. It frequently arises in the extremities, abdominal cavity, retroperitoneum, abdominal wall, and chest wall, and predominantly affects young female adults, with a median age of 37–39 years. DFM is driven by somatic *CTNNB1* mutations or inactivating germline *APC* mutations [141-144]. Histologically, it consists of uniform fibroblastic cells arranged in long, sweeping fascicles with collagen deposition. Small-caliber vessels with perivascular edema are also present. Immunohistochemically, DFM is positive for SMA and MSA, and nuclear β-catenin expression is observed in most cases. STAT6 negativity helps distinguish DFM from SFT.

Cellular angiofibroma

Cellular angiofibroma (CAF) is a benign, cellular, and richly vascular fibroblastic neoplasm that typically arises in the vulvar or inguinoscrotal region [145]. It affects both sexes with a similar frequency, with peak incidence in women during the fifth decade and in men during the seventh decade. Loss of 13q14, including *RB1*, is a characteristic genetic alterations in CAFs [146,147]. Histologically, it consists of bland spindle cells arranged in short fascicles among delicate collagen fibers, accompanied by numerous small- to medium-sized thick-walled vessels, and may contain intermixed adipose tissue. Immunohistochemically, CD34 is expressed in 30%–60% of cases, whereas SMA and desmin are variably expressed in a minority of cases [145,148]. Loss of nuclear RB1 expression is frequently observed. CAF can mimic SFT morphologically; however, the vessels are generally smaller, more hyalinized, and fibrotic. STAT6 expression is consistently negative.

Angiofibroma of soft tissue

Angiofibroma of soft tissue (AFST) is a benign fibroblastic neoplasm characterized by a prominent, arborizing network of numerous branching, thin-walled blood vessels [149]. It primarily affects middle-aged adults, with a peak incidence in the sixth decade of life [150-152]. AFSTs typically arise in the extremities, particularly the legs. A recurrent t(5;8)(p15;q13) translocation, resulting in an *AHRR*::*NCOA2* gene fusion, occurs in approximately 60%–80% of cases [151-153]. Histologically, AFST is composed of bland, uniform short spindle cells embedded in a variable myxoid or collagenous stroma with innumerable small, thin-walled, branching blood vessels (Fig. 7). Immunohistochemically, the tumor cells variably express EMA and CD34, whereas desmin positivity may be observed in scattered dendritic cells [150,152]. AFST often exhibits morphologic overlap with SFT; however, STAT6 expression is consistently absent.

Dermatofibrosarcoma protuberans

Dermatofibrosarcoma protuberans (DFSP) is a superficial, locally aggressive fibroblastic neoplasm. It is characterized by a storiform arrangement of uniform spindle cells and is typically associated with a *COL1A1*::*PDGFB* or related gene [154]. DFSP usually occurs on the trunk and proximal extremities, followed by the head and neck region. It predominantly affects young to middle-aged adults with a slight male predominance. Histologically, DFSP shows diffusely infiltrative growth into surrounding tissues, often producing a characteristic honeycomb pattern within the subcutaneous fat. Immunohistochemically, the tumor cells are diffusely positive for CD34 and negative for STAT6. In contrast, SFTs are usually well-circumscribed and show nuclear STAT6 expression, which serves as a distinguishing feature.

Deep fibrous histiocytoma

Deep fibrous histiocytoma (DFH) is a benign morphological variant of fibrous histiocytoma that arises entirely within the subcutaneous or deep soft tissue [155]. It occurs over a wide age range (6–84 years old, with a median age of 37 years) with a slight male predominance. The extremities are the most commonly affected sites, followed by the head and neck region. Approximately 10% of cases occur in visceral soft tissues, such as the retroperitoneum, mediastinum, and pelvis [156]. Rearrangements of either *PRKCB* or *PRKCD* have been identified [157,158]. Histologically, DFH is a well-circumscribed lesion that exhibits monomorphic spindle-shaped or histiocytoid cells arranged in a mixed fascicular and storiform pattern, which is often accompanied by prominent branching vessels. Approximately 40% of DFHs express CD34 [156]. These cases may be challenging to distinguish from SFTs; however, they are characteristically negative for STAT6.

Myopericytoma

Myopericytoma is a distinctive perivascular myoid neoplasm that forms part of a morphological spectrum with myofibroma [159]. It occurs at any age but is most commonly observed in adults. It usually involves the distal extremities, followed by the proximal extremities, neck, trunk, and oral cavity. Mutations in the *PDGFRB* gene may underlie a shared pathogenesis among myopericytoma, myopericytomatosis, and myofibroma [160,161]. In addition, cellular or atypical myofibromas are associated with *SRF*::*RELA* gene fusions [162]. Histologically, myopericytoma consists of bland, myoid-appearing spindled cells arranged in a concentric perivascular pattern around numerous small vessels (Fig. 8A). Immunohistochemically, myopericytomas express SMA and caldesmon, with focal positivity for desmin and/or CD34 (Fig. 8B). In contrast, SFTs do not show concentric perivascular architecture but instead demonstrate diffuse CD34 and STAT6 positivity.

Sinonasal glomangiopericytoma

Sinonasal glomangiopericytoma is a distinctive soft tissue tumor

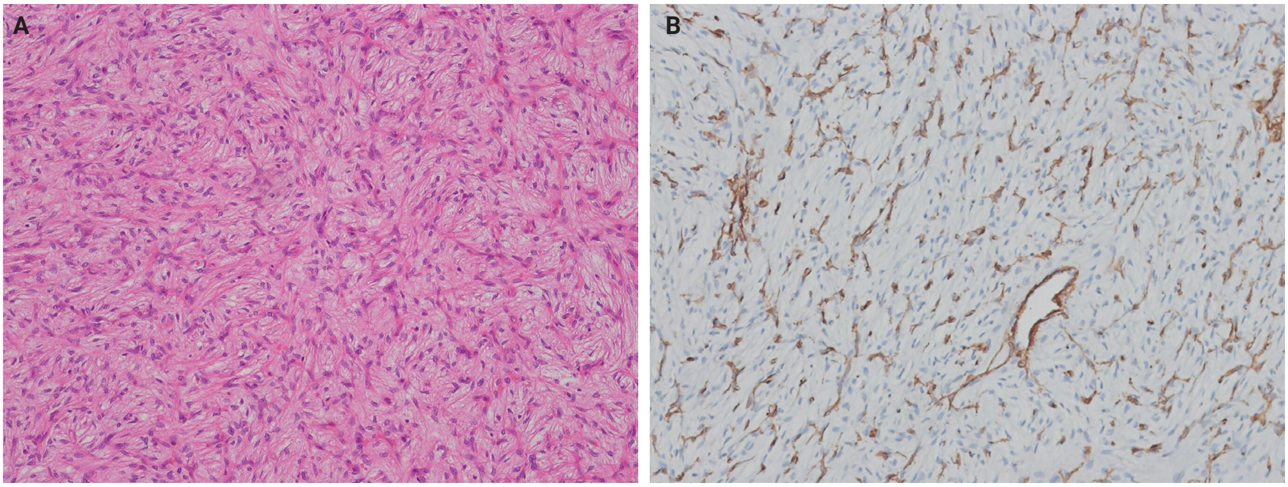

Fig. 7. Angiofibroma of soft tissue. (A) The tumor is composed of uniform, spindle-shaped tumor cells with prominent, thin-walled, branching blood vessels. (B) CD34 immunostaining highlights thin-walled, branching blood vessels.

of the sinonasal tract characterized by perivascular myoid differentiation [163]. It occurs at any age, but most commonly presents in the sixth or seventh decade of life, with a slight female predilection. Unilateral involvement of the nasal cavity, particularly the turbinates and septum, is typical, whereas bilateral disease is rare and occurs in fewer than 5% of cases. Molecular alterations include recurrent missense mutations in exon 3 of *CTNNB1*. Histologically, the tumor appears as an ovoid to spindled syncytium of myoid-type cells within a richly vascularized stroma (Fig. 9A). Perivascular hyalinization with extravasated erythrocytes, mast cells, and eosinophils is commonly observed. The tumor cells exhibit strong SMA and nuclear β-catenin expression, with variable CD34 positivity (Fig. 9B) [164,165]. In contrast, SFTs are positive for CD34 and STAT6, but negative for SMA.

Dedifferentiated liposarcoma

DDLPS arises through progression from an atypical lipomatous tumor (ALT) or well-differentiated liposarcoma (WDLPS) into a non-lipogenic sarcoma of variable histologic grade [166]. It most frequently occurs in the retroperitoneum, followed by the spermatic cord and, more rarely, the mediastinum, head and neck, and trunk. DDLPS predominantly affects middle-aged

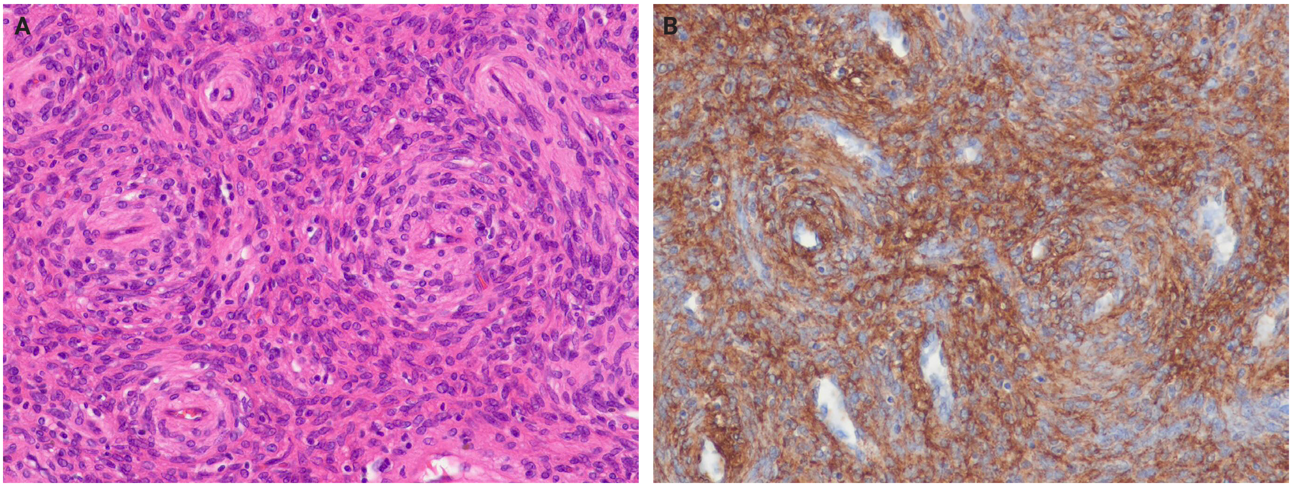

Fig. 8. Myopericytoma. (A) The ovoid tumor cells are arranged in a concentric perivascular growth pattern. (B) The tumor cells show homogeneous expression of smooth muscle actin.

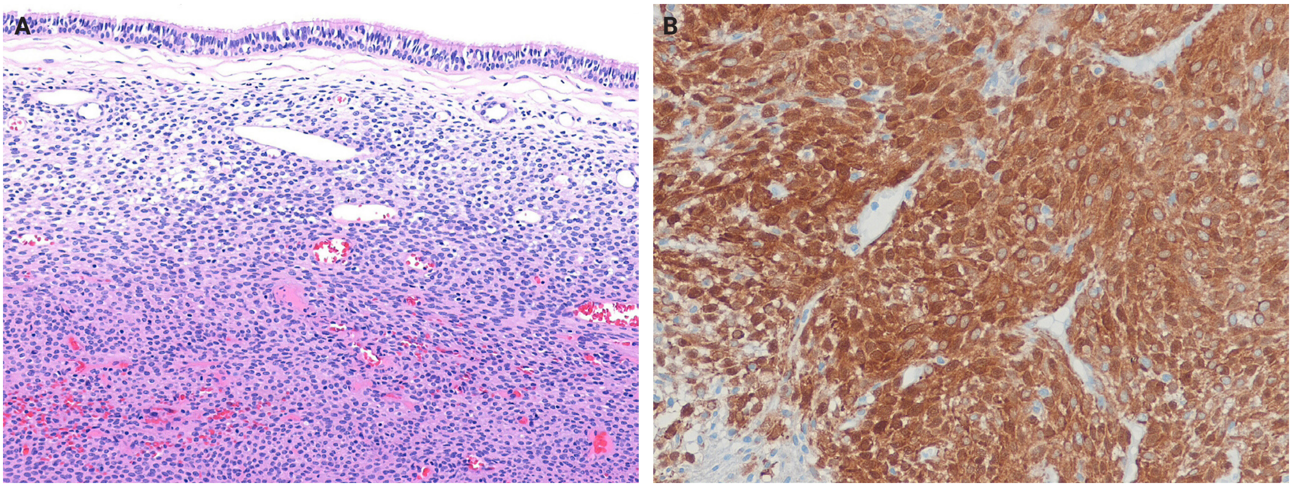

Fig. 9. Sinonasal glomangiopericytoma. (A) The tumor cells have ovoid nuclei, eosinophilic cytoplasm, and indistinct cell borders, with dilated, thin-walled blood vessels. Extravasated red blood cells are also observed. (B) The tumor cells show strong, diffuse nuclear expression of β-catenin.

adults, with a peak incidence in the fourth to fifth decade of life, and show no significant sex predilection. Approximately 90% of cases develop de novo, whereas about 10% arise from recurrent ALT/WDLPS [167]. DDLPS shares molecular features with ALT/WDLPS, as both harbor amplification of *MDM2* (mouse double minute 2 homolog) and *CDK4* (cyclin-dependent kinase 4) on chromosome 12q14-q15 [168,169]. Histologically, DDLPS shows an abrupt or gradual transition from a WDLPS to a spindle cell or pleomorphic non-lipogenic tumor (rarely lipogenic), which may be low or high grade. Immunohistochemically, nuclear positivity for MDM2 and CDK4 is observed in most cases. Lipomatous SFTs may be mistaken for WDLPS or DDLPS because of their fat-containing appearance, particularly in limited biopsy samples or imaging studies. Rarely, DDLPS may display an SFT-like morphology and even show STAT6 positivity [118], whereas SFTs are typically negative for MDM2 and CDK4. Myxoid SFT may resemble myxoid liposarcoma; however, *DDIT3* FISH is negative, and STAT6 expression is diffusely positive in SFTs.

Gastrointestinal stromal tumor

Gastrointestinal stromal tumors (GISTs) are mesenchymal neoplasms with variable biological behavior and are characterized by differentiation toward the interstitial cells of Cajal [170]. GISTs can occur at any site within the gastrointestinal tract, whereas extragastrointestinal GISTs most commonly develop in the mesentery, omentum, and retroperitoneum. Sporadic GISTs occur at any age, but most cases appear in the sixth decade of life (median age, 60 to 65 years), with a slight male predominance [171]. Most GISTs have activating mutations in *KIT* or *PDGFRA*. Histologically, GISTs display a broad morphological spectrum and typically consist of relatively monomorphic spindle cells, epithelioid cells, or a mixture of both. Immunohistochemically, GISTs positively express CD34, CD117 (KIT), and DOG1. They may closely resemble SFTs, but can be distinguished by their positive CD117 (KIT) and DOG1 expression, and negative STAT6 expression.

Malignant peripheral nerve sheath tumor

Malignant peripheral nerve sheath tumor (MPNST) is a malignant spindle cell neoplasm with Schwannian differentiation [172]. It most commonly arises in older adults during the seventh decade of life, although it can occur across a wide age range [173]. Approximately 50% of cases occur in association with neurofibromatosis type 1 (NF1), 10% are associated with prior radiation exposure, and the remainder are sporadic [174]. MPNST most frequently involves the trunk and extremities, followed by the head and neck region. At the molecular level, MPNSTs exhibit complex structural and numerical chromosomal abnormalities, and biallelic inactivation of the *NF1* gene is commonly observed in MPNST [175,176]. Histologically, conventional MPNST displays fascicular growth of relatively uniform spindle cells, alternating hypercellular and hypocellular areas, perivascular accentuation, and geographical necrosis (Fig. 10A). The tumor cells show focal positivity for S100 protein and SOX10 expression, along with loss of H3K27me3 expression (Fig. 10B) [177]. MPNST may resemble cellular SFT; however, it is usually negative for CD34 and STAT6, while showing focal expression of S100 protein and SOX10.

Synovial sarcoma

SS is a monomorphic spindle cell sarcoma with variable epithelial differentiation. It is defined by *SS18*::*SSX1*, *SS18*::*SSX2*, or *SS18*::*SSX4* gene fusions [178]. Approximately 70% of the cases occur in the deep soft tissue of the extremities, often near joints, with 15% in the trunk and 7% in the head and neck. SS can occur at any age, with no sex predilection, although half of the patients are adolescents or young adults [179]. Histologically, SS may be classified into three subtypes: monophasic (dense fascicles of monomorphic spindle cells with staghorn-shaped vasculature), biphasic (containing epithelial and spindle components), and poorly differentiated (high cellularity, nuclear atypia, and brisk mitotic activity) (Fig. 11A) [180]. TLE1 shows nuclear positivity in up to 95% of cases, with patchy to focal cytokeratin and EMA staining. *SS18*::SSX fusion–specific and SSX-specific C-terminal antibodies have recently been developed that yield strong, diffuse nuclear staining with >95% sensitivity and specificity (Fig. 11B) [181]. Cellular SFT can mimic SS; however, SSs are typically negative for CD34 and *STAT6*.

Phosphaturic mesenchymal tumor

Phosphaturic mesenchymal tumors (PMTs) are morphologically distinct neoplasms that cause tumor-induced osteomalacia, most often through overproduction of fibroblast growth factor 23 (FGF23) [182]. PMTs may arise in almost any soft tissue or bone, but are uncommon in the retroperitoneum, viscera, and mediastinum. They frequently affect middle-aged adults with no sex predilection, although they can also develop in pediatric and elderly patients. Approximately half of all PMTs harbor *FN1*::*FGFR1* fusions and, rarely, *FN1*::*FGF1* fusions [183,184]. Histologically, PMT consists of bland spindle-shaped cells with charac-

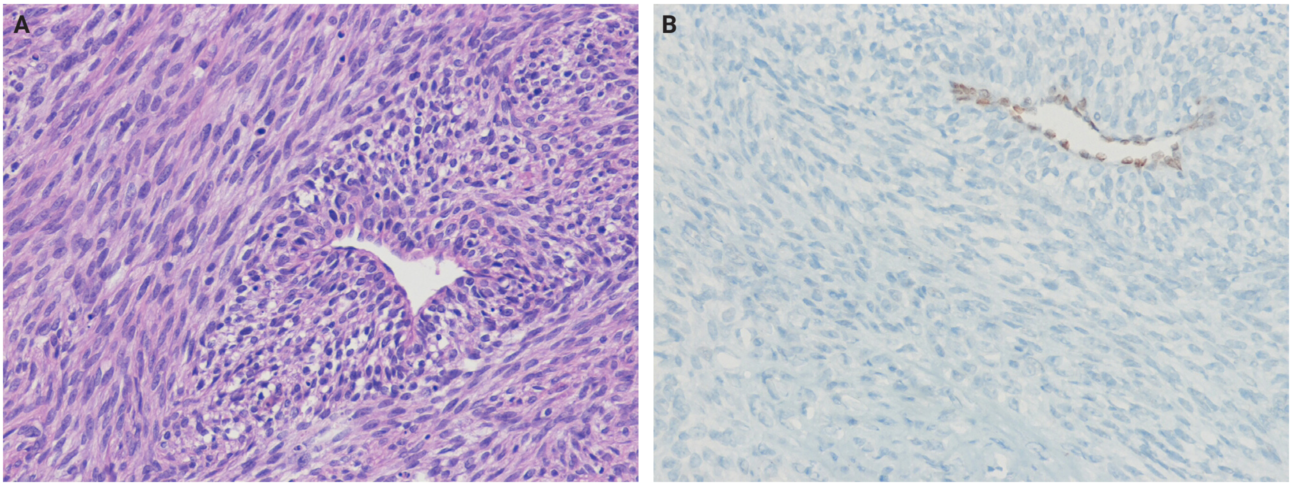

Fig. 10. Malignant peripheral nerve sheath tumor. (A) The spindle tumor cells are arranged in a fascicular pattern with perivascular accentuation. (B) The tumor cells show loss of H3K27me3 expression. Vascular endothelial cells serve as positive internal controls.

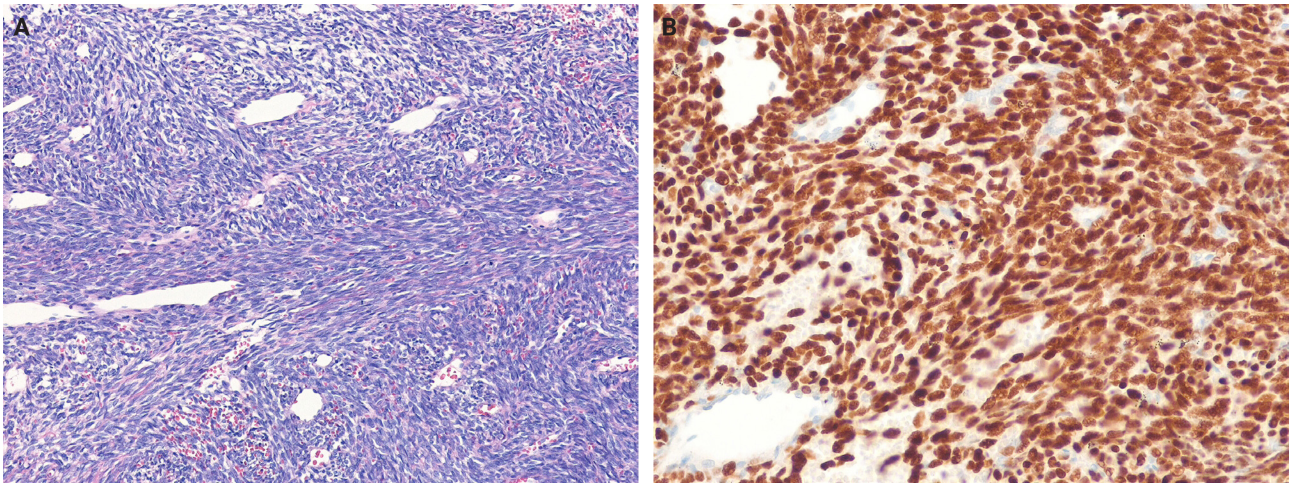

Fig. 11. Monophasic synovial sarcoma. (A) The tumor is composed of dense fascicles of monomorphic spindle cells with staghorn-shaped vasculature. (B) The tumor cells demonstrate strong, diffuse nuclear staining for SS18-SSX fusion-specific antibody.

teristic grungy calcification and a prominent capillary network, with occasional staghorn-shaped vessels. PMT exhibits variable ERG, SATB2, and CD56 expression. FGF23 expression has been reported in some cases, but currently available antibodies lack specificity, which limits their diagnostic utility [185,186]. PMTs may mimic SFTs; however, SFTs lack the grungy calcified matrix typical of PMTs and usually show CD34 and STAT6 positivity.

Mesenchymal chondrosarcoma

Mesenchymal chondrosarcoma (MCS) is a high-grade malignant tumor with a distinct biphasic pattern. It consists of primitive undifferentiated mesenchymal cells and well-differentiated hyaline cartilage [187]. MCS most commonly arises in the second or third decade of life, with a median age of approximately 30 years and a slight male predominance. MCS exhibits a broad anatomical distribution, involving bone, soft tissue, and intracranial locations. Approximately 40% of cases occur in somatic soft tissues, and the meninges are a common extra-skeletal site [188]. At a molecular level, MCS harbors a specific and recurrent *HEY1*::*NCOA2* fusion, which has been identified in nearly all cases [189]. Histologically, MCS exhibits undifferentiated tumor cells, cartilage islands, and a staghorn-shaped vascular pattern. The undifferentiated tumor cells often express CD99, SOX9, and NKX2.2 [190], and may occasionally show aberrant expression of desmin, myogenin, and MYOD1. Because the cartilage foci may be scant or absent in limited biopsies, MCS may be mistaken for malignant SFT; however, SFTs are distinguished by nuclear STAT6 positivity, which is absent in MCSs.

Table 3 provides an overview of the differential diagnosis of SFTs, summarizing the clinical, histological, immunohistochemical, and molecular features of morphologically similar entities.

Fig. 12 shows diagnostic algorithm and differential diagnosis of SFT.

PROGNOSIS

SFTs exhibit a broad spectrum of clinical behavior, with local or distant recurrence occurring in 10%–30% of cases and, occasionally, >15 years after treatment [30,31,101,191]. To improve prognosis, multivariate risk models have been developed and validated across various anatomical sites. The most commonly used model includes mitotic count, tumor size (≥5 cm), and patient age (≥55 years), with some modifications that also include necrosis as a fourth parameter [31,103,192]. Table 4 presents three-variable and modified four-variable risk models for predicting metastatic risk in SFTs [31,103]. These models are superior to the traditional benign versus malignant classification and may be applied to thoracic, extra-thoracic, and gynecologic SFTs.

At the molecular level, *TERT* promoter mutations and *TP53* loss are more frequently observed in high-grade or dedifferentiated tumors [77,193]. Positive p53 expression and elevated Ki-67 index (>5%) are associated with poorer prognosis in some studies [54].

In the CNS, SFTs exhibit higher rates of long-term recurrence and metastasis, even in WHO grade 1 cases. Mitotic activity and necrosis, rather than tumor size or patient age, are the strongest predictors of progression. A three-tiered histologic grading scheme was recommended for CNS SFTs [39,76]. In the head and neck region, most SFTs behave indolently, with recurrence rates <10%; however, ocular adnexal SFTs exhibit a higher local recurrence rate (~25%) with a low metastatic potential (~2%) [46,194]. Positive surgical margins and dedifferentiation are independent risk factors of relapse. If metastasis occurs, it most often involves the lungs, bones, and liver [55].

TREATMENT

The management of SFT should be done in specialized sarcoma centers with a multidisciplinary team experienced in this rare entity [7]. Treatment response is generally assessed using Response Evaluation Criteria in Solid Tumors (RECIST); however, because of the hypervascular nature of SFT, some studies also use the Choi criteria, which is defined as a ≥10% decrease in tumor size or a >15% decrease in tumor density [195-197].

Localized lesions

Complete en bloc surgical resection with negative margins (R0) is the gold standard for treatment. The 10-year overall survival rate following R0 resection ranges from 54% to 89% [198-200]. If margins are positive (R1/R2), re-resection should be considered where feasible. Adjuvant radiotherapy (RT) can achieve >80% 5-year local control for high-risk or margin-positive cases, although no survival benefit has been demonstrated [68,201-204]. Preoperative RT may be considered in selected cases to increase resectability; however, there is no proven role for neoadjuvant or adjuvant chemotherapy [205-207]. SFTs generally do not respond well to conventional sarcoma regimens. Thus, systemic therapy should be reserved for clinical trials or in very high-risk situations.

Advanced or metastatic lesions

Isolated, resectable metastases (e.g., lung) can be treated with surgery or ablative methods. RT is an option for local control in selected cases. Conventional chemotherapy demonstrates low overall response rates (0%–20%) [208,209]. Anthracycline-based regimens are used as first-line therapy. Ifosfamide, dacarbazine, or trabectedin may be administered in later lines [210-212]. Median progression-free survival is generally limited to 4–5 months. Because SFTs are highly vascular, antiangiogenic therapy has shown promising results. Pazopanib, sunitinib, sorafenib, and temozolomide plus bevacizumab have achieved partial responses and significant disease control [213-218]. In prospective trials, pazopanib produced partial responses in >50% of patients by Choi criteria, supporting its role as a potential first-line therapy for advanced SFT. IGF-1 is frequently overexpressed in SFTs. Figitumumab, an anti–IGF-1 receptor monoclonal antibody, has shown efficacy in some advanced cases [218,219]. Data on immunotherapy are limited, although anecdotal durable responses have been reported with programmed death-1 inhibitors (e.g., pembrolizumab) [220,221]. Ongoing studies are evaluating

Table 3. Differential diagnosis of solitary fibrous tumor by clinical, histological, immunohistochemical, and molecular features

Tumor type	Clinical feature	Histological feature	Immunohistochemistry	Molecular feature
Spindle cell lipoma	Men aged 45–60 years; posterior neck, back, shoulders	Bland spindle cells, mature adipose tissue, myxoid stroma, ropy collagen	CD34 (+); loss of RB1 protein expression	Loss of chromosome 13q14, including *RB1*
Nodular fasciitis	Young adults; subcutaneous tissue of extremities; usually <3 cm in size	Fibroblasts and myofibroblasts in tissue culture-like growth pattern, myxoid, microcystic changes	SMA (+), often diffuse; desmin (±)	*USP6* rearrangement
Desmoid fibromatosis	Young to middle-aged adult; female predominance; abdominal wall, extremities, mesentery	Uniform fibroblasts arranged in long sweeping fascicles, collagen deposition	SMA (+); desmin (±); nuclear β-catenin (+) in the majority of cases	Somatic mutations in *CTNNB1*; inactivating germline mutations in *APC*
Cellular angiofibroma	Women (5th decade) and men (7th decade); vulvar and inguinoscrotal sites	Bland spindle cells with delicate collagen fibers, small- to medium-sized thick-walled vessels	CD34 (+); SMA (±); desmin (±); loss of RB1 protein expression	Loss of chromosome 13q14, including *RB1*
Angiofibroma of soft tissue	Middle-aged adults (6th decade); extremities, most commonly legs	Bland spindle cells in myxoid or collagenous stroma with small thin-walled branching blood vessels	SMA (+); desmin (±)	t(5;8)(p15;q13); *AHRR::NCOA2*
Dermatofibrosarcoma protuberans	Young to middle-aged adults; trunk, proximal extremities, head and neck region	Uniform spindle cells arranged in a storiform pattern with fat infiltration showing a honeycomb pattern	CD34 (+)	*COL1A1::PDGFB*
Deep fibrous histiocytoma	Broad age range (median 37 years); most commonly subcutaneous; extremities, head and neck	Monomorphic spindle or histiocytoid cells in storiform or fascicular pattern	CD34 (+) in approximately 40% of cases	*PRKCB* or *PRKCD* rearrangements
Myopericytoma	Any age, most often adults; extremities, neck, trunk, oral cavity	Bland, myoid-appearing spindle cells in a concentric perivascular growth pattern	SMA (+); caldesmon (+); desmin (±); CD34 (±)	*PDGFRB* mutations; *SRF::RELA* (cellular/atypical myofibromas)
Sinonasal glomangiopericytoma	Any age, most common in adults; sinonasal tract, particularly turbinate and septum	Ovoid to spindle cells, syncytial arrangement, thin-walled staghorn-shaped vessels	SMA (+); nuclear β-catenin (+)	Mutations in *CTNNB1* exon 3
Dedifferentiated liposarcoma	Middle-aged adults; retroperitoneum, spermatic cord, mediastinum	Abrupt transition from WDLPS to spindle cell or pleomorphic non-lipogenic sarcoma	MDM2 (+); CDK4 (+)	*MDM2* and *CDK4* amplification
Gastrointestinal stromal tumor	Any age (peak in the 6th decade); gastrointestinal tract, mesentery, omentum	Relatively monomorphic spindle cells, epithelioid cells, or mixture of both	CD117 (+), DOG1 (+); PDGFRA (+)[a]; loss of SDHB expression[b]	*KIT* or *PDGFRA* mutations
Malignant peripheral nerve sheath tumor	Older adults, but can occur across a wide age range; trunk, extremities, head and neck	Spindle cells arranged in fascicles with alternating hypocellular and hypercellular areas, often with necrosis	S100 protein (+)[c], SOX10 (+); loss of H3K27me3 expression	Mutations in *NF1*, *CDKN2A/CDKN2B*, *PRC2* core components (*EED* or *SUZ12*)
Synovial sarcoma	Adolescents and young adults; extremities, trunk, head and neck	Monophasic (monomorphic spindle cells), biphasic, poorly differentiated patterns	*SS18::SSX* fusion–specific antibody (+), SSX-specific antibody (+); TLE1 (+)	*SS18::SSX1*, *SS18::SSX2*, or *SS18::SSX4*
Phosphaturic mesenchymal tumor	Middle-aged adults; any site; typically associated with hypophosphatemia and osteomalacia	Bland spindle-shaped cells with grungy calcification and a prominent vascular network	ERG (+); SATB2 (+); CD56 (+); FGF23 (+)	*FN1::FGFR1*, *FN1::FGF*
Mesenchymal chondrosarcoma	Adolescents and young adults; bone, soft tissue, and meninges	Undifferentiated round tumor cells with islands of cartilage and staghorn-shaped vascular pattern	CD99 (+); SOX9 (+); NKX2.2 (+); desmin (±); myogenin (±)	*HEY1::NCOA2*

+, positive staining; RB1, retinoblastoma 1; SMA, smooth muscle actin; ±, variable staining; WDLPS, well-differentiated liposarcoma; MDM2, mouse double minute 2; CDK4, cyclin-dependent kinase 4; DOG1, discovered on GIST-1; PDGFRA, platelet-derived growth factor receptor alpha; SDHB, succinate dehydrogenase subunit B; SOX10, SRY-box transcription factor 10; PRC2, polycomb repressive complex 2; H3K27me3, trimethylation of histone H3 at lysine 27; TLE1, transducin-like enhancer of split 1; ERG, ETS-related gene; SATB2, special AT-rich sequence-binding protein 2; FGF23, fibroblast growth factor 23; NKX2.2, NK2 homeobox 2.

[a] *PDGFRA*-mutant gastrointestinal stromal tumors typically demonstrate strong, diffuse expression of PDGFRA; [b] Succinate dehydrogenase-deficient gastrointestinal stromal tumors show complete loss of SDHB staining; [c] S100 protein is focally positive in 50%–60% of cases.

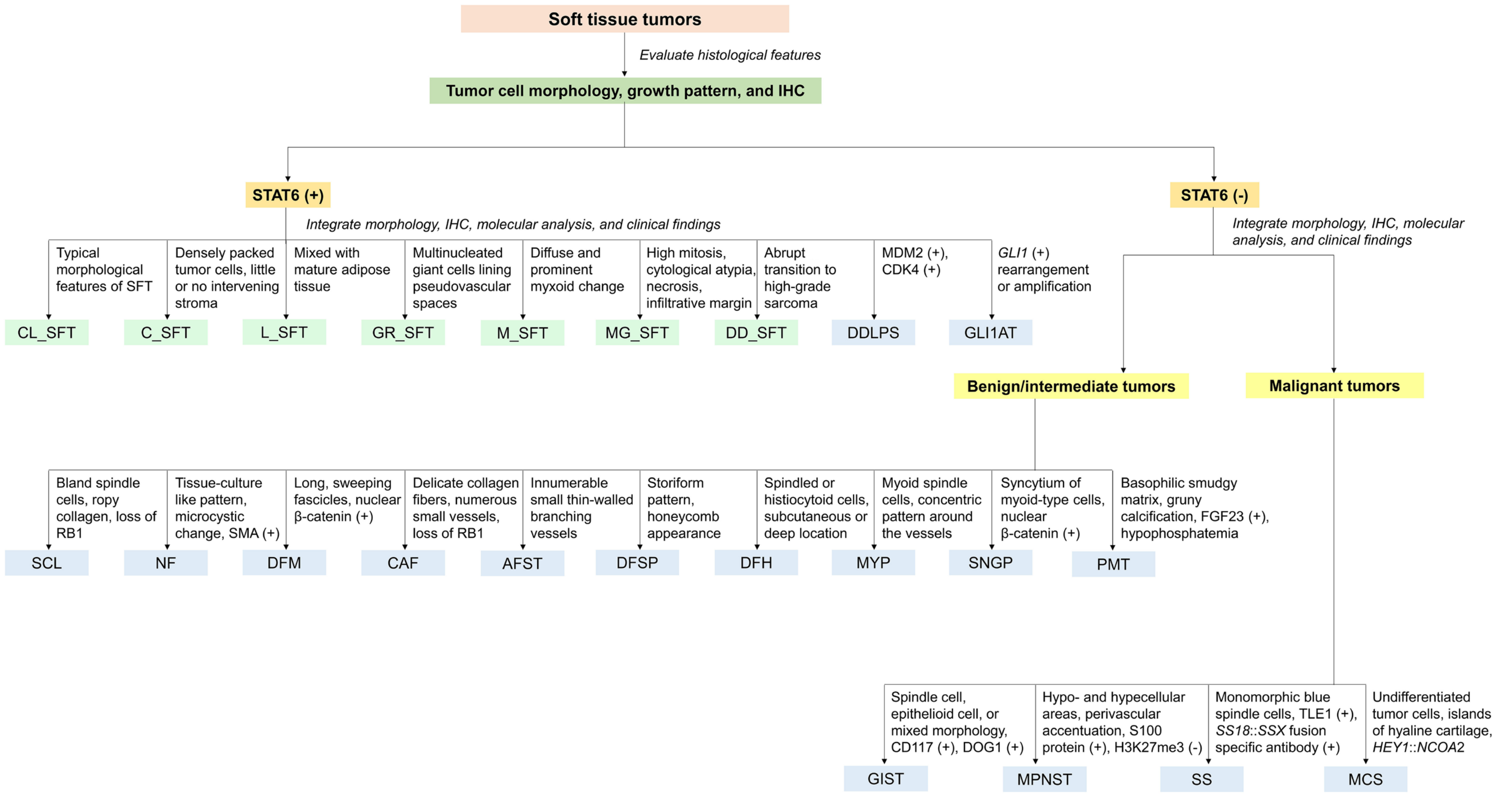

Fig. 12. Diagnostic algorithm and differential diagnosis of solitary fibrous tumor (SFT). This flowchart illustrates a systematic approach to diagnosing soft tissue tumors with spindle cell morphology, emphasizing the importance of histological assessment, immunohistochemistry (IHC), and molecular analysis. The algorithm distinguishes between STAT6-positive tumors, encompassing the SFT subtypes and mimickers, and STAT6-negative tumors. STAT6, signal transducer and activator of transcription 6; CL_SFT, classic SFT; C_SFT, cellular SFT; L_SFT, lipomatous SFT; GR_SFT, giant cell-rich SFT; M_SFT, myxoid SFT; MG_SFT, malignant SFT; DD_SFT, dedifferentiated SFT; DDLPS, dedifferentiated liposarcoma; GLI1AT, GLI1-altered soft tissue tumor; SCL, spindle cell lipoma; NF, nodular fasciitis; SMA, smooth muscle actin; DFM, desmoid fibromatosis; CAF, cellular angiofibroma; AFST, angiofibroma of soft tissue; DFSP, dermatofibrosarcoma protuberans; DFH, deep fibrous histiocytoma; MYP, myopericytoma; SNGP, sinonasal glomangiopericytoma; FGF23, fibroblast growth factor 23; PMT, phosphaturic mesenchymal tumor; DOG1, discovered on GIST-1; GIST, gastrointestinal stromal tumor; H3K27me3, histone H3 lysine 27 trimethylation; MPNST, malignant peripheral nerve sheath tumor; TLE1, transducin-like enhancer of split 1; SS, synovial sarcoma; MCS, mesenchymal chondrosarcoma.

Table 4. Three-variable and four-variable risk models for predicting metastatic risk in solitary fibrous tumors

Risk factor	Cut-off	Points (3-variable model)	Points (4-variable model)
Patient age (yr)	<55	0	0
	≥55	1	1
Mitoses per mm^2 (mitoses per 10 HPFs)	0 (0)	0	0
	0.5–1.5 (1–3)	1	1
	≥2 (≥4)	2	2
Tumor size (cm)	0–4.9	0	0
	5–9.9	1	1
	10–14.9	2	2
	≥15	3	3
Tumor necrosis	<10%	N/A	0
	≥10%	N/A	1
Risk category (total points)[a]	Low risk	0–2	0–3
	Intermediate risk	3–4	4–5
	High risk	5–6	6–7

HPF, high-power field; N/A, not applicable.
[a] Point ranges indicate cumulative risk scores.

combinatorial approaches with immune checkpoint inhibitors and antiangiogenic agents.

FUTURE PERSPECTIVES

The current understanding of SFTs is primarily based on retrospective case series and preclinical studies, which limits the generalizability and robustness of existing diagnostic and therapeutic strategies [222]. Consequently, substantial gaps remain in the areas of tumor biology, prognostication, and optimal treatment pathways.

A critical area of investigation is the prognostic relevance of the specific *NAB2*::*STAT6* gene fusion variants. Although the *NAB2*::*STAT6* fusion is a molecular hallmark of SFTs, its transcript variants and their effects on tumor behavior, metastatic potential, and treatment response remain unclear. Prospective studies integrating molecular and clinicopathological data are essential for developing reliable, fusion-based risk stratification models.

The development of advanced molecular platforms, such as NGS, offers the ability not only to detect *NAB2*::*STAT6* gene fusions but also to identify additional genetic alterations with prognostic or therapeutic significance. In addition, ongoing research into the immunologic profile of SFTs warrants further study of immune checkpoint inhibitors and other immunotherapeutic strategies.

Ultimately, progress in SFT management will depend on coordinated efforts to refine molecular classification, improve diagnostic accuracy, and develop targeted therapies tailored to individual patient risk profiles.

Recent advances in artificial intelligence and digital pathology suggest new opportunities for prognostic assessment in SFTs. By enabling quantitative and reproducible evaluation of histomorphological features, AI-based image analysis may complement existing clinicopathological models. Although data are still limited, future integration of these technologies could enhance risk stratification and individualized patient management.

CONCLUSION

SFT is a rare fibroblastic neoplasm that poses significant diagnostic and therapeutic challenges. Its broad histological spectrum and frequent morphological overlap with other soft tissue tumors make accurate diagnosis difficult, often requiring an integrated approach that combines immunohistochemistry and molecular testing. A comprehensive understanding of SFT, including its histological variants, molecular subtypes, and variable clinical behavior, is essential for optimizing surgical management, identifying patients requiring systemic therapy, and establishing effective long-term surveillance protocols. As the molecular mechanisms underlying SFT are further elucidated, it will be critical to incorporate these advances into clinical practice to enhance diagnostic precision, refine risk stratification, and enable the development of personalized treatment strategies.

Ethics Statement
Not applicable.

Availability of Data and Material
Data sharing not applicable to this article as no datasets were generated or analyzed during the study.

Code Availability
Not applicable.

ORCID
Joon Hyuk Choi https://orcid.org/0000-0002-8638-0360

Conflicts of Interest
J.H.C., a contributing editor of the *Journal of Pathology and Translational Medicine*, was not involved in the editorial evaluation or decision to publish this article.

Funding Statement
No funding to declare.

REFERENCES

1. Demicco EG, Han A. Solitary fibrous tumour. In: The WHO Classification Editorial Board, ed. WHO classification of tumours: soft tissue and bone tumours. 5th ed. Lyon: IARC Press, 2020; 104-8.
2. Fletcher CD. The evolving classification of soft tissue tumours: an update based on the new WHO classification. Histopathology 2006; 48: 3-12.
3. Kallen ME, Hornick JL. The 2020 WHO classification: what's new in soft tissue tumor pathology? Am J Surg Pathol 2021; 45: e1-23.
4. Thway K, Ng W, Noujaim J, Jones RL, Fisher C. The current status of solitary fibrous tumor: diagnostic features, variants, and genetics. Int J Surg Pathol 2016; 24: 281-92.
5. Martin-Broto J, Mondaza-Hernandez JL, Moura DS, Hindi N. A comprehensive review on solitary fibrous tumor: new insights for new horizons. Cancers (Basel) 2021; 13: 2913.
6. Bianchi G, Lana D, Gambarotti M, et al. Clinical, histological, and molecular features of solitary fibrous tumor of bone: a single institution retrospective review. Cancers (Basel) 2021; 13: 2470.
7. de Bernardi A, Dufresne A, Mishellany F, Blay JY, Ray-Coquard I, Brahmi M. Novel therapeutic options for solitary fibrous tumor: antiangiogenic therapy and beyond. Cancers (Basel) 2022; 14: 1064.
8. Stout AP, Murray MR. Hemangiopericytoma: a vascular tumor featuring Zimmermann's pericytes. Ann Surg 1942; 116: 26-33.
9. Stout AP. Hemangiopericytoma: a study of 25 cases. Cancer 1949; 2: 1027-54.
10. Stout AP. Tumors featuring pericytes: glomus tumor and hemangiopericytoma. Lab Invest 1956; 5: 217-23.
11. Enzinger FM, Smith BH. Hemangiopericytoma: an analysis of 106 cases. Hum Pathol 1976; 7: 61-82.
12. Battifora H. Hemangiopericytoma: ultrastructural study of five cases. Cancer 1973; 31: 1418-32.
13. Erlandson RA, Woodruff JM. Role of electron microscopy in the evaluation of soft tissue neoplasms, with emphasis on spindle cell and pleomorphic tumors. Hum Pathol 1998; 29: 1372-81.
14. Dardick I, Hammar SP, Scheithauer BW. Ultrastructural spectrum of hemangiopericytoma: a comparative study of fetal, adult, and neoplastic pericytes. Ultrastruct Pathol 1989; 13: 111-54.
15. Gengler C, Guillou L. Solitary fibrous tumour and haemangiopericytoma: evolution of a concept. Histopathology 2006; 48: 63-74.
16. Schurch W, Skalli O, Lagace R, Seemayer TA, Gabbiani G. Intermediate filament proteins and actin isoforms as markers for soft-tissue tumor differentiation and origin. III. Hemangiopericytomas and glomus tumors. Am J Pathol 1990; 136: 771-86.
17. Nemes Z. Differentiation markers in hemangiopericytoma. Cancer 1992; 69: 133-40.
18. Middleton LP, Duray PH, Merino MJ. The histological spectrum of hemangiopericytoma: application of immunohistochemical analysis including proliferative markers to facilitate diagnosis and predict prognosis. Hum Pathol 1998; 29: 636-40.
19. D'Amore ES, Manivel JC, Sung JH. Soft-tissue and meningeal hemangiopericytomas: an immunohistochemical and ultrastructural study. Hum Pathol 1990; 21: 414-23.
20. Fletcher CD. Haemangiopericytoma: a dying breed? Reappraisal of an ‘entity’ and its variants: a hypothesis. Curr Diagn Pathol 1994; 1: 19-23.
21. Klemperer P, Rabin CB. Primary neoplasms of the pleura: a report of five cases. Arch Pathol 1931; 11: 385-412.
22. England DM, Hochholzer L, McCarthy MJ. Localized benign and malignant fibrous tumors of the pleura: a clinicopathologic review of 223 cases. Am J Surg Pathol 1989; 13: 640-58.
23. Doyle LA, Vivero M, Fletcher CD, Mertens F, Hornick JL. Nuclear expression of STAT6 distinguishes solitary fibrous tumor from histologic mimics. Mod Pathol 2014; 27: 390-5.
24. Barthelmess S, Geddert H, Boltze C, et al. Solitary fibrous tu-

mors/hemangiopericytomas with different variants of the *NAB2-STAT6* gene fusion are characterized by specific histomorphology and distinct clinicopathological features. Am J Pathol 2014; 184: 1209-18.
25. Schweizer L, Koelsche C, Sahm F, et al. Meningeal hemangiopericytoma and solitary fibrous tumors carry the *NAB2-STAT6* fusion and can be diagnosed by nuclear expression of STAT6 protein. Acta Neuropathol 2013; 125: 651-8.
26. Robinson DR, Wu YM, Kalyana-Sundaram S, et al. Identification of recurrent *NAB2-STAT6* gene fusions in solitary fibrous tumor by integrative sequencing. Nat Genet 2013; 45: 180-5.
27. Guillou L, Fletcher JA, Fletcher CD, Mandahl N. Extrapleural solitary fibrous tumour and haemangiopericytoma. In: Fletcher CD, Unni KK, Mertens F, eds. World Health Organization classification of tumours: pathology and genetics of tumours of soft tissue and bone. 3rd ed. Lyon: IARC Press, 2002; 86-90.
28. Fletcher CD, Bridge JA, Lee JC. Extrapleural solitary fibrous tumour. In: Fletcher CD, Bridge JA, Hogendoorn CW, Mertens F, eds. WHO classification of tumours of soft tissue and bone. 4th ed. Lyon: IARC Press, 2013; 80-2.
29. Salas S, Resseguier N, Blay JY, et al. Prediction of local and metastatic recurrence in solitary fibrous tumor: construction of a risk calculator in a multicenter cohort from the French Sarcoma Group (FSG) database. Ann Oncol 2017; 28: 1979-87.
30. Gholami S, Cassidy MR, Kirane A, et al. Size and location are the most important risk factors for malignant behavior in resected solitary fibrous tumors. Ann Surg Oncol 2017; 24: 3865-71.
31. Demicco EG, Park MS, Araujo DM, et al. Solitary fibrous tumor: a clinicopathological study of 110 cases and proposed risk assessment model. Mod Pathol 2012; 25: 1298-306.
32. Pasquali S, Gronchi A, Strauss D, et al. Resectable extra-pleural and extra-meningeal solitary fibrous tumours: a multi-centre prognostic study. Eur J Surg Oncol 2016; 42: 1064-70.
33. Makino H, Miyashita M, Nomura T, et al. Solitary fibrous tumor of the cervical esophagus. Dig Dis Sci 2007; 52: 2195-200.
34. Bratton L, Salloum R, Cao W, Huber AR. Solitary fibrous tumor of the sigmoid colon masquerading as an adnexal neoplasm. Case Rep Pathol 2016; 2016: 4182026.
35. Nielsen GP, Dickersin GR, Provenzal JM, Rosenberg AE. Lipomatous hemangiopericytoma: a histologic, ultrastructural and immunohistochemical study of a unique variant of hemangiopericytoma. Am J Surg Pathol 1995; 19: 748-56.
36. Yang EJ, Howitt BE, Fletcher CD, Nucci MR. Solitary fibrous tumour of the female genital tract: a clinicopathological analysis of 25 cases. Histopathology 2018; 72: 749-59.
37. Rao N, Colby TV, Falconieri G, Cohen H, Moran CA, Suster S. Intrapulmonary solitary fibrous tumors: clinicopathologic and immunohistochemical study of 24 cases. Am J Surg Pathol 2013; 37: 155-66.
38. Mena H, Ribas JL, Pezeshkpour GH, Cowan DN, Parisi JE. Hemangiopericytoma of the central nervous system: a review of 94 cases. Hum Pathol 1991; 22: 84-91.
39. Macagno N, Vogels R, Appay R, et al. Grading of meningeal solitary fibrous tumors/hemangiopericytomas: analysis of the prognostic value of the Marseille grading system in a cohort of 132 patients. Brain Pathol 2019; 29: 18-27.
40. Ostrom QT, Cioffi G, Gittleman H, et al. CBTRUS statistical report: primary brain and other central nervous system tumors diagnosed in the United States in 2012-2016. Neuro Oncol 2019; 21: v1-100.
41. Kouba E, Simper NB, Chen S, et al. Solitary fibrous tumour of the genitourinary tract: a clinicopathological study of 11 cases and their association with the *NAB2-STAT6* fusion gene. J Clin Pathol 2017; 70: 508-14.
42. Sun S, Tang M, Dong H, et al. Solitary fibrous tumor involving urinary bladder: a case report and literature review. Transl Androl Urol 2020; 9: 766-75.
43. Thompson LD, Wei C, Rooper LM, Lau SK. Thyroid gland solitary fibrous tumor: report of 3 cases and a comprehensive review of the literature. Head Neck Pathol 2019; 13: 597-605.
44. Suh YJ, Park JH, Jeon JH, Bilegsaikhan SE. Extrapleural solitary fibrous tumor of the thyroid gland: a case report and review of literature. World J Clin Cases 2020; 8: 782-9.
45. Demicco EG, Griffin AM, Gladdy RA, et al. Comparison of published risk models for prediction of outcome in patients with extrameningeal solitary fibrous tumour. Histopathology 2019; 75: 723-37.
46. Thompson LD, Liou SS, Feldman KA. Orbit solitary fibrous tumor: a proposed risk prediction model based on a case series and comprehensive literature review. Head Neck Pathol 2021; 15: 138-52.
47. Alkatan HM, Alsalamah AK, Almizel A, et al. Orbital solitary fibrous tumors: a multi-centered histopathological and immunohistochemical analysis with radiological description. Ann Saudi Med 2020; 40: 227-33.
48. Krishnakumar S, Subramanian N, Mohan ER, Mahesh L, Biswas J, Rao NA. Solitary fibrous tumor of the orbit: a clinicopathologic study of six cases with review of the literature. Surv Ophthalmol 2003; 48: 544-54.
49. Kim HJ, Kim HJ, Kim YD, et al. Solitary fibrous tumor of the or-

bit: CT and MR imaging findings. AJNR Am J Neuroradiol 2008; 29: 857-62.
50. Ng DW, Tan GH, Soon JJ, et al. The approach to solitary fibrous tumors: are clinicopathological features and nomograms accurate in the prediction of prognosis? Int J Surg Pathol 2018; 26: 600-8.
51. Kayani B, Sharma A, Sewell MD, et al. A review of the surgical management of extrathoracic solitary fibrous tumors. Am J Clin Oncol 2018; 41: 687-94.
52. Thompson LD, Karamurzin Y, Wu ML, Kim JH. Solitary fibrous tumor of the larynx. Head Neck Pathol 2008; 2: 67-74.
53. Thompson LD, Lau SK. Sinonasal tract solitary fibrous tumor: a clinicopathologic study of six cases with a comprehensive review of the literature. Head Neck Pathol 2018; 12: 471-80.
54. Furusato E, Valenzuela IA, Fanburg-Smith JC, et al. Orbital solitary fibrous tumor: encompassing terminology for hemangiopericytoma, giant cell angiofibroma, and fibrous histiocytoma of the orbit: reappraisal of 41 cases. Hum Pathol 2011; 42: 120-8.
55. Bahrami A, Lee S, Schaefer IM, et al. TERT promoter mutations and prognosis in solitary fibrous tumor. Mod Pathol 2016; 29: 1511-22.
56. Goellner JR, Laws ER, Soule EH, Okazaki H. Hemangiopericytoma of the meninges. Mayo Clinic experience. Am J Clin Pathol 1978; 70: 375-80.
57. Fukasawa Y, Takada A, Tateno M, et al. Solitary fibrous tumor of the pleura causing recurrent hypoglycemia by secretion of insulin-like growth factor II. Pathol Int 1998; 48: 47-52.
58. De Los Santos-Aguilar RG, Chavez-Villa M, Contreras AG, et al. Successful multimodal treatment of an *IGF2*-producing solitary fibrous tumor with acromegaloid changes and hypoglycemia. J Endocr Soc 2019; 3: 537-43.
59. Chen S, Zheng Y, Chen L, Yi Q. A broad ligament solitary fibrous tumor with Doege-Potter syndrome. Medicine (Baltimore) 2018; 97: e12564.
60. Denewar FA, Takeuchi M, Khedr D, et al. Solitary fibrous tumors from A to Z: a pictorial review with radiologic-pathologic correlation. Insights Imaging 2025; 16: 112.
61. Xiao Y, Chen J, Yang W, Yan H, Chen R, Li Y. Solitary fibrous tumors: radiologic features with clinical and histopathologic correlation. Front Oncol 2025; 15: 1510059.
62. Yi X, Wang J, Zhang Y, et al. Renal solitary fibrous tumor/hemangiopericytoma: computed tomography findings and clinicopathologic features. Abdom Radiol (NY) 2019; 44: 642-51.
63. Keraliya AR, Tirumani SH, Shinagare AB, Zaheer A, Ramaiya NH. Solitary fibrous tumors: 2016 imaging update. Radiol Clin North Am 2016; 54: 565-79.
64. Bhat A, Layfield LJ, Tewari SO, Gaballah AH, Davis R, Wu Z. Solitary fibrous tumor of the ischioanal fossa: a multidisciplinary approach to management with radiologic-pathologic correlation. Radiol Case Rep 2018; 13: 468-74.
65. Fernandez A, Conrad M, Gill RM, Choi WT, Kumar V, Behr S. Solitary fibrous tumor in the abdomen and pelvis: a case series with radiological findings and treatment recommendations. Clin Imaging 2018; 48: 48-54.
66. Lococo F, Cafarotti S, Treglia G. Is 18F-FDG-PET/CT really able to differentiate between malignant and benign solitary fibrous tumor of the pleura? Clin Imaging 2013; 37: 976.
67. Lococo F, Rapicetta C, Filice A, et al. The role of 68Ga-DOTATOC PET/CT in the detection of relapsed malignant solitary fibrous tumor of the pleura. Rev Esp Med Nucl Imagen Mol (Engl Ed) 2018; 37: 257-8.
68. Wang X, Qian J, Bi Y, Ping B, Zhang R. Malignant transformation of orbital solitary fibrous tumor. Int Ophthalmol 2013; 33: 299-303.
69. Chen T, Jiang B, Zheng Y, et al. Differentiating intracranial solitary fibrous tumor/hemangiopericytoma from meningioma using diffusion-weighted imaging and susceptibility-weighted imaging. Neuroradiology 2020; 62: 175-84.
70. Stomeo F, Padovani D, Bozzo C, Pastore A. Laryngeal solitary fibrous tumour. Auris Nasus Larynx 2007; 34: 405-8.
71. Yang BT, Song ZL, Wang YZ, Dong JY, Wang ZC. Solitary fibrous tumor of the sinonasal cavity: CT and MR imaging findings. AJNR Am J Neuroradiol 2013; 34: 1248-51.
72. Yang BT, Wang YZ, Dong JY, Wang XY, Wang ZC. MRI study of solitary fibrous tumor in the orbit. AJR Am J Roentgenol 2012; 199: W506-11.
73. Chmielecki J, Crago AM, Rosenberg M, et al. Whole-exome sequencing identifies a recurrent *NAB2-STAT6* fusion in solitary fibrous tumors. Nat Genet 2013; 45: 131-2.
74. Mohajeri A, Tayebwa J, Collin A, et al. Comprehensive genetic analysis identifies a pathognomonic *NAB2/STAT6* fusion gene, nonrandom secondary genomic imbalances, and a characteristic gene expression profile in solitary fibrous tumor. Genes Chromosomes Cancer 2013; 52: 873-86.
75. Fritchie KJ, Jin L, Rubin BP, et al. *NAB2-STAT6* gene fusion in meningeal hemangiopericytoma and solitary fibrous tumor. J Neuropathol Exp Neurol 2016; 75: 263-71.
76. Fritchie K, Jensch K, Moskalev EA, et al. The impact of histopathology and *NAB2-STAT6* fusion subtype in classification and grading of meningeal solitary fibrous tumor/hemangiopericytoma. Acta Neuropathol 2019; 137: 307-19.

77. Demicco EG, Wani K, Ingram D, et al. *TERT* promoter mutations in solitary fibrous tumour. Histopathology 2018; 73: 843-51.
78. Kurisaki-Arakawa A, Akaike K, Hara K, et al. A case of dedifferentiated solitary fibrous tumor in the pelvis with *TP53* mutation. Virchows Arch 2014; 465: 615-21.
79. Park HK, Yu DB, Sung M, et al. Molecular changes in solitary fibrous tumor progression. J Mol Med (Berl) 2019; 97: 1413-25.
80. Liang Y, Heller RS, Wu JK, et al. High p16 expression is associated with malignancy and shorter disease-free survival time in solitary fibrous tumor/hemangiopericytoma. J Neurol Surg B Skull Base 2019; 80: 232-8.
81. Adachi S, Kondo A, Ogino I, et al. The significance of cytoplasmic STAT6 positivity and high p53/p16 expression as a novel predictor of histological/clinical malignancy in *NAB2*::*STAT6* fusion-positive orbital solitary fibrous tumors. Pathol Int 2025; 75: 513-22.
82. Koelsche C, Schweizer L, Renner M, et al. Nuclear relocation of *STAT6* reliably predicts *NAB2-STAT6* fusion for the diagnosis of solitary fibrous tumour. Histopathology 2014; 65: 613-22.
83. Fukunaga M, Naganuma H, Nikaido T, Harada T, Ushigome S. Extrapleural solitary fibrous tumor: a report of seven cases. Mod Pathol 1997; 10: 443-50.
84. Hasegawa T, Hirose T, Seki K, Yang P, Sano T. Solitary fibrous tumor of the soft tissue: an immunohistochemical and ultrastructural study. Am J Clin Pathol 1996; 106: 325-31.
85. Bakhshwin A, Berry RS, Cox RM, et al. Malignant solitary fibrous tumour of the prostate: four cases emphasising significant histological and immunophenotypical overlap with sarcomatoid carcinoma. Pathology 2020; 52: 643-8.
86. Westra WH, Grenko RT, Epstein J. Solitary fibrous tumor of the lower urogenital tract: a report of five cases involving the seminal vesicles, urinary bladder, and prostate. Hum Pathol 2000; 31: 63-8.
87. Smith SC, Gooding WE, Elkins M, et al. Solitary fibrous tumors of the head and neck: a multi-institutional clinicopathologic study. Am J Surg Pathol 2017; 41: 1642-56.
88. Tariq MU, Din NU, Abdul-Ghafar J, Park YK. The many faces of solitary fibrous tumor: diversity of histological features, differential diagnosis and role of molecular studies and surrogate markers in avoiding misdiagnosis and predicting the behavior. Diagn Pathol 2021; 16: 32.
89. Bauer JL, Miklos AZ, Thompson LD. Parotid gland solitary fibrous tumor: a case report and clinicopathologic review of 22 cases from the literature. Head Neck Pathol 2012; 6: 21-31.
90. Carneiro SS, Scheithauer BW, Nascimento AG, Hirose T, Davis DH. Solitary fibrous tumor of the meninges: a lesion distinct from fibrous meningioma: a clinicopathologic and immunohistochemical study. Am J Clin Pathol 1996; 106: 217-24.
91. Cassarino DS, Auerbach A, Rushing EJ. Widely invasive solitary fibrous tumor of the sphenoid sinus, cavernous sinus, and pituitary fossa. Ann Diagn Pathol 2003; 7: 169-73.
92. Metellus P, Bouvier C, Guyotat J, et al. Solitary fibrous tumors of the central nervous system: clinicopathological and therapeutic considerations of 18 cases. Neurosurgery 2007; 60: 715-22.
93. Folpe AL, Devaney K, Weiss SW. Lipomatous hemangiopericytoma: a rare variant of hemangiopericytoma that may be confused with liposarcoma. Am J Surg Pathol 1999; 23: 1201-7.
94. Guillou L, Gebhard S, Coindre JM. Lipomatous hemangiopericytoma: a fat-containing variant of solitary fibrous tumor? Clinicopathologic, immunohistochemical, and ultrastructural analysis of a series in favor of a unifying concept. Hum Pathol 2000; 31: 1108-15.
95. Chen Y, Wang F, Han A. Fat-forming solitary fibrous tumor of the kidney: a case report and literature review. Int J Clin Exp Pathol 2015; 8: 8632-5.
96. Lee JC, Fletcher CD. Malignant fat-forming solitary fibrous tumor (so-called "lipomatous hemangiopericytoma"): clinicopathologic analysis of 14 cases. Am J Surg Pathol 2011; 35: 1177-85.
97. Dei Tos AP, Seregard S, Calonje E, Chan JK, Fletcher CD. Giant cell angiofibroma: a distinctive orbital tumor in adults. Am J Surg Pathol 1995; 19: 1286-93.
98. Guillou L, Gebhard S, Coindre JM. Orbital and extraorbital giant cell angiofibroma: a giant cell-rich variant of solitary fibrous tumor? Clinicopathologic and immunohistochemical analysis of a series in favor of a unifying concept. Am J Surg Pathol 2000; 24: 971-9.
99. de Saint Aubain Somerhausen N, Rubin BP, Fletcher CD. Myxoid solitary fibrous tumor: a study of seven cases with emphasis on differential diagnosis. Mod Pathol 1999; 12: 463-71.
100. Fukunaga M, Naganuma H, Ushigome S, Endo Y, Ishikawa E. Malignant solitary fibrous tumour of the peritoneum. Histopathology 1996; 28: 463-6.
101. Vallat-Decouvelaere AV, Dry SM, Fletcher CD. Atypical and malignant solitary fibrous tumors in extrathoracic locations: evidence of their comparability to intra-thoracic tumors. Am J Surg Pathol 1998; 22: 1501-11.
102. Gold JS, Antonescu CR, Hajdu C, et al. Clinicopathologic correlates of solitary fibrous tumors. Cancer 2002; 94: 1057-68.
103. Demicco EG, Wagner MJ, Maki RG, et al. Risk assessment in solitary fibrous tumors: validation and refinement of a risk strat-

ification model. Mod Pathol 2017; 30: 1433-42.

104. Magro G, Emmanuele C, Lopes M, Vallone G, Greco P. Solitary fibrous tumour of the kidney with sarcomatous overgrowth: case report and review of the literature. APMIS 2008; 116: 1020-5.
105. Masuda Y, Kurisaki-Arakawa A, Hara K, et al. A case of dedifferentiated solitary fibrous tumor of the thoracic cavity. Int J Clin Exp Pathol 2014; 7: 386-93.
106. Subramaniam MM, Lim XY, Venkateswaran K, Shuen CS, Soong R, Petersson F. Dedifferentiated solitary fibrous tumour of the nasal cavity: the first case reported with molecular characterization of a *TP53* mutation. Histopathology 2011; 59: 1269-74.
107. Akaike K, Kurisaki-Arakawa A, Hara K, et al. Distinct clinicopathological features of *NAB2-STAT6* fusion gene variants in solitary fibrous tumor with emphasis on the acquisition of highly malignant potential. Hum Pathol 2015; 46: 347-56.
108. Thway K, Hayes A, Ieremia E, Fisher C. Heterologous osteosarcomatous and rhabdomyosarcomatous elements in dedifferentiated solitary fibrous tumor: further support for the concept of dedifferentiation in solitary fibrous tumor. Ann Diagn Pathol 2013; 17: 457-63.
109. Mosquera JM, Fletcher CD. Expanding the spectrum of malignant progression in solitary fibrous tumors: a study of 8 cases with a discrete anaplastic component: is this dedifferentiated SFT? Am J Surg Pathol 2009; 33: 1314-21.
110. Collini P, Negri T, Barisella M, et al. High-grade sarcomatous overgrowth in solitary fibrous tumors: a clinicopathologic study of 10 cases. Am J Surg Pathol 2012; 36: 1202-15.
111. Tardio JC, Machado I, Alemany I, Lopez-Soto MV, Nieto MG, Llombart-Bosch A. Solitary fibrous tumor of the vulva: report of 2 cases, including a de novo dedifferentiated solitary fibrous tumor diagnosed after molecular demonstration of *NAB2-STAT6* gene fusion. Int J Gynecol Pathol 2018; 37: 547-53.
112. Olson NJ, Linos K. Dedifferentiated solitary fibrous tumor: a concise review. Arch Pathol Lab Med 2018; 142: 761-6.
113. Demicco EG, Harms PW, Patel RM, et al. Extensive survey of STAT6 expression in a large series of mesenchymal tumors. Am J Clin Pathol 2015; 143: 672-82.
114. Ouladan S, Trautmann M, Orouji E, et al. Differential diagnosis of solitary fibrous tumors: a study of 454 soft tissue tumors indicating the diagnostic value of nuclear *STAT6* relocation and ALDH1 expression combined with in situ proximity ligation assay. Int J Oncol 2015; 46: 2595-605.
115. Macagno N, Figarella-Branger D, Mokthari K, et al. Differential diagnosis of meningeal SFT-HPC and meningioma: which immunohistochemical markers should be used? Am J Surg Pathol 2016; 40: 270-8.
116. Cheah AL, Billings SD, Goldblum JR, Carver P, Tanas MZ, Rubin BP. STAT6 rabbit monoclonal antibody is a robust diagnostic tool for the distinction of solitary fibrous tumour from its mimics. Pathology 2014; 46: 389-95.
117. Yoshida A, Tsuta K, Ohno M, et al. STAT6 immunohistochemistry is helpful in the diagnosis of solitary fibrous tumors. Am J Surg Pathol 2014; 38: 552-9.
118. Doyle LA, Tao D, Marino-Enriquez A. STAT6 is amplified in a subset of dedifferentiated liposarcoma. Mod Pathol 2014; 27: 1231-7.
119. Xu B, Chang K, Folpe AL, et al. Head and neck mesenchymal neoplasms with *GLI1* gene alterations: a pathologic entity with distinct histologic features and potential for distant metastasis. Am J Surg Pathol 2020; 44: 729-37.
120. Perry A, Scheithauer BW, Nascimento AG. The immunophenotypic spectrum of meningeal hemangiopericytoma: a comparison with fibrous meningioma and solitary fibrous tumor of meninges. Am J Surg Pathol 1997; 21: 1354-60.
121. Schneider N, Hallin M, Thway K. STAT6 loss in dedifferentiated solitary fibrous tumor. Int J Surg Pathol 2017; 25: 58-60.
122. Kakkar A, Sakthivel P, Rajeshwari M, Kairo A, Sharma MC. Recurrent sinonasal CD34-negative malignant solitary fibrous tumor diagnosed on STAT6 immunohistochemistry and *NAB2-STAT6* fusion. Head Neck Pathol 2020; 14: 250-6.
123. Dagrada GP, Spagnuolo RD, Mauro V, et al. Solitary fibrous tumors: loss of chimeric protein expression and genomic instability mark dedifferentiation. Mod Pathol 2015; 28: 1074-83.
124. Vivero M, Doyle LA, Fletcher CD, Mertens F, Hornick JL. GRIA2 is a novel diagnostic marker for solitary fibrous tumour identified through gene expression profiling. Histopathology 2014; 65: 71-80.
125. Bouvier C, Bertucci F, Metellus P, et al. ALDH1 is an immunohistochemical diagnostic marker for solitary fibrous tumours and haemangiopericytomas of the meninges emerging from gene profiling study. Acta Neuropathol Commun 2013; 1: 10.
126. Yamashita D, Suehiro S, Kohno S, et al. Intracranial anaplastic solitary fibrous tumor/hemangiopericytoma: immunohistochemical markers for definitive diagnosis. Neurosurg Rev 2021; 44: 1591-600.
127. Hanau CA, Miettinen M. Solitary fibrous tumor: histological and immunohistochemical spectrum of benign and malignant variants presenting at different sites. Hum Pathol 1995; 26: 440-9.
128. Barak S, Wang Z, Miettinen M. Immunoreactivity for calretinin

https://doi.org/10.4132/jptm.2025.10.08

and keratins in desmoid fibromatosis and other myofibroblastic tumors: a diagnostic pitfall. Am J Surg Pathol 2012; 36: 1404-9.

129. Foo WC, Cruise MW, Wick MR, Hornick JL. Immunohistochemical staining for TLE1 distinguishes synovial sarcoma from histologic mimics. Am J Clin Pathol 2011; 135: 839-44.
130. Ullman D, Gordetsky J, Siegal GP, Prieto-Granada CN, Wei S, Stevens TM. PAX8 expression in solitary fibrous tumor: a potential diagnostic pitfall. Appl Immunohistochem Mol Morphol 2019; 27: 195-202.
131. Huang SC, Huang HY. Solitary fibrous tumor: an evolving and unifying entity with unsettled issues. Histol Histopathol 2019; 34: 313-34.
132. Billings SD, Ud Din N. Spindle cell lipoma and pleomorphic lipoma. In: WHO Classification of Tumours Editorial Board, ed. WHO classification of tumours: soft tissue and bone tumours. 5th ed. Lyon: IARC Press, 2020; 29-30.
133. Templeton SF, Solomon AR. Spindle cell lipoma is strongly CD34 positive: an immunohistochemical study. J Cutan Pathol 1996; 23: 546-50.
134. Suster S, Fisher C. Immunoreactivity for the human hematopoietic progenitor cell antigen (CD34) in lipomatous tumors. Am J Surg Pathol 1997; 21: 195-200.
135. Chen BJ, Marino-Enriquez A, Fletcher CD, Hornick JL. Loss of retinoblastoma protein expression in spindle cell/pleomorphic lipomas and cytogenetically related tumors: an immunohistochemical study with diagnostic implications. Am J Surg Pathol 2012; 36: 1119-28.
136. Oliveira AM, Wang J, Wang WL. Nodular fasciitis. In: WHO Classification of Tumours Editorial Board, ed. WHO classification of tumours: soft tissue and bone tumours. 5th ed. Lyon: IARC Press, 2020; 49-50.
137. Patel NR, Chrisinger JS, Demicco EG, et al. USP6 activation in nodular fasciitis by promoter-swapping gene fusions. Mod Pathol 2017; 30: 1577-88.
138. Erber R, Agaimy A. Misses and near misses in diagnosing nodular fasciitis and morphologically related reactive myofibroblastic proliferations: experience of a referral center with emphasis on frequency of *USP6* gene rearrangements. Virchows Arch 2018; 473: 351-60.
139. Lam SW, Cleton-Jansen AM, Cleven AH, et al. Molecular analysis of gene fusions in bone and soft tissue tumors by anchored multiplex PCR-based targeted next-generation sequencing. J Mol Diagn 2018; 20: 653-63.
140. Fritchie KJ, Crago AM, van de Rijin M. Desmoid fibromatosis. In: WHO Classification of Tumours Editorial Board, ed. WHO classification of tumours: soft tissue and bone tumours. 5th ed. Lyon: IARC Press, 2020; 93-5.
141. Amary MF, Pauwels P, Meulemans E, et al. Detection of beta-catenin mutations in paraffin-embedded sporadic desmoid-type fibromatosis by mutation-specific restriction enzyme digestion (MSRED): an ancillary diagnostic tool. Am J Surg Pathol 2007; 31: 1299-309.
142. Lazar AJ, Tuvin D, Hajibashi S, et al. Specific mutations in the beta-catenin gene (*CTNNB1*) correlate with local recurrence in sporadic desmoid tumors. Am J Pathol 2008; 173: 1518-27.
143. Sturt NJ, Gallagher MC, Bassett P, et al. Evidence for genetic predisposition to desmoid tumours in familial adenomatous polyposis independent of the germline *APC* mutation. Gut 2004; 53: 1832-6.
144. Wang L, Motoi T, Khanin R, et al. Identification of a novel, recurrent *HEY1-NCOA2* fusion in mesenchymal chondrosarcoma based on a genome-wide screen of exon-level expression data. Genes Chromosomes Cancer 2012; 51: 127-39.
145. Iwasa Y, Fletcher CD. Cellular angiofibroma: clinicopathologic and immunohistochemical analysis of 51 cases. Am J Surg Pathol 2004; 28: 1426-35.
146. Maggiani F, Debiec-Rychter M, Vanbockrijck M, Sciot R. Cellular angiofibroma: another mesenchymal tumour with 13q14 involvement, suggesting a link with spindle cell lipoma and (extra)-mammary myofibroblastoma. Histopathology 2007; 51: 410-2.
147. Flucke U, van Krieken JH, Mentzel T. Cellular angiofibroma: analysis of 25 cases emphasizing its relationship to spindle cell lipoma and mammary-type myofibroblastoma. Mod Pathol 2011; 24: 82-9.
148. Laskin WB, Fetsch JF, Mostofi FK. Angiomyofibroblastomalike tumor of the male genital tract: analysis of 11 cases with comparison to female angiomyofibroblastoma and spindle cell lipoma. Am J Surg Pathol 1998; 22: 6-16.
149. Marino-Enriquez A, Mertens F, Wang J, Yamada Y. Angiofibroma of soft tissue. In: WHO Classification of Tumours Editorial Board, ed. WHO classification of tumours: soft tissue and bone tumours. 5th ed. Lyon: IARC Press, 2020; 80-1.
150. Mariño-Enríquez A, Fletcher CD. Angiofibroma of soft tissue: clinicopathologic characterization of a distinctive benign fibrovascular neoplasm in a series of 37 cases. Am J Surg Pathol 2012; 36: 500-8.
151. Yamada Y, Yamamoto H, Kohashi K, et al. Histological spectrum of angiofibroma of soft tissue: histological and genetic analysis of 13 cases. Histopathology 2016; 69: 459-69.

152. Bekers EM, Groenen PJ, Verdijk MA, et al. Soft tissue angiofibroma: clinicopathologic, immunohistochemical and molecular analysis of 14 cases. Genes Chromosomes Cancer 2017; 56: 750-7.
153. Jin Y, Moller E, Nord KH, et al. Fusion of the *AHRR* and *NCOA2* genes through a recurrent translocation t(5;8)(p15;q13) in soft tissue angiofibroma results in upregulation of aryl hydrocarbon receptor target genes. Genes Chromosomes Cancer 2012; 51: 510-20.
154. Mentzel TD, Pedeutour F. Dermatofibrosarcoma protuberans. In: WHO Classification of Tumours Editorial Board, ed. WHO classification of tumours: soft tissue and bone tumours. 5th ed. Lyon: IARC Press, 2020; 100-3.
155. Jo VY. Deep fibrous histiocytoma. In: WHO Classification of Tumours Editorial Board, ed. WHO classification of tumours: soft tissue and bone tumours. 5th ed. Lyon: IARC Press, 2020; 137-8.
156. Gleason BC, Fletcher CD. Deep "benign" fibrous histiocytoma: clinicopathologic analysis of 69 cases of a rare tumor indicating occasional metastatic potential. Am J Surg Pathol 2008; 32: 354-62.
157. Plaszczyca A, Nilsson J, Magnusson L, et al. Fusions involving protein kinase C and membrane-associated proteins in benign fibrous histiocytoma. Int J Biochem Cell Biol 2014; 53: 475-81.
158. Walther C, Hofvander J, Nilsson J, et al. Gene fusion detection in formalin-fixed paraffin-embedded benign fibrous histiocytomas using fluorescence in situ hybridization and RNA sequencing. Lab Invest 2015; 95: 1071-6.
159. Mentzel TD, Agaram NP. Myopericytoma, including myofibroma. In: WHO Classification of Tumours Editorial Board, ed. WHO classification of tumours: soft tissue and bone tumours. 5th ed. Lyon: IARC Press, 2020; 182-5.
160. Hung YP, Fletcher CD. Myopericytomatosis: clinicopathologic analysis of 11 cases with molecular identification of recurrent *PDGFRB* alterations in myopericytomatosis and myopericytoma. Am J Surg Pathol 2017; 41: 1034-44.
161. Agaimy A, Bieg M, Michal M, et al. Recurrent somatic *PDGFRB* mutations in sporadic infantile/solitary adult myofibromas but not in angioleiomyomas and myopericytomas. Am J Surg Pathol 2017; 41: 195-203.
162. Antonescu CR, Sung YS, Zhang L, Agaram NP, Fletcher CD. Recurrent *SRF-RELA* fusions define a novel subset of cellular myofibroma/myopericytoma: a potential diagnostic pitfall with sarcomas with myogenic differentiation. Am J Surg Pathol 2017; 41: 677-84.
163. Thompson LD, Jun SY, Lai CK. Sinonasal glomangiopericytoma. In: WHO Classification of Tumours Editorial Board, ed. WHO classification of tumours: head and neck tumours. 5th ed. Lyon: IARC Press, 2024; 90-2.
164. Thompson LD, Miettinen M, Wenig BM. Sinonasal-type hemangiopericytoma: a clinicopathologic and immunophenotypic analysis of 104 cases showing perivascular myoid differentiation. Am J Surg Pathol 2003; 27: 737-49.
165. Sangoi AR, Bishop JA. Variability of CD34 expression in sinonasal glomangiopericytoma: a potential diagnostic pitfall. Head Neck Pathol 2020; 14: 459-64.
166. Dei Tos AP, Marino-Enriquez A, Pedeutour F. Dedifferentiated liposarcoma. In: WHO Classification of Tumours Editorial Board, ed. WHO classification of tumours: soft tissue and bone tumours. 5th ed. Lyon: IARC Press, 2020; 39-41.
167. Dei Tos AP. Liposarcomas: diagnostic pitfalls and new insights. Histopathology 2014; 64: 38-52.
168. Saada-Bouzid E, Burel-Vandenbos F, Ranchere-Vince D, et al. Prognostic value of *HMGA2, CDK4,* and *JUN* amplification in well-differentiated and dedifferentiated liposarcomas. Mod Pathol 2015; 28: 1404-14.
169. Italiano A, Bianchini L, Gjernes E, et al. Clinical and biological significance of *CDK4* amplification in well-differentiated and dedifferentiated liposarcomas. Clin Cancer Res 2009; 15: 5696-703.
170. Dei Tos AP, Hornick JL, Miettinen M, Wanless IR, Wardelmann E. Gastrointestinal stromal tumour. In: WHO Classification of Tumours Editorial Board, ed. WHO classification of tumours: soft tissue and bone tumours. 5th ed. Lyon: IARC Press, 2020; 216-21.
171. Miettinen M, Sobin LH, Lasota J. Gastrointestinal stromal tumors of the stomach: a clinicopathologic, immunohistochemical, and molecular genetic study of 1765 cases with long-term follow-up. Am J Surg Pathol 2005; 29: 52-68.
172. Nielsen GP, Chi P. Malignant peripheral nerve sheath tumour. In: WHO Classification of Tumours Editorial Board, ed. WHO classification of tumours: soft tissue and bone tumours. 5th ed. Lyon: IARC Press, 2020; 254-7.
173. Boland JM, Colby TV, Folpe AL. Intrathoracic peripheral nerve sheath tumors-a clinicopathological study of 75 cases. Hum Pathol 2015; 46: 419-25.
174. Ducatman BS, Scheithauer BW, Piepgras DG, Reiman HM, Ilstrup DM. Malignant peripheral nerve sheath tumors: a clinicopathologic study of 120 cases. Cancer 1986; 57: 2006-21.
175. Mechtersheimer G, Otano-Joos M, Ohl S, et al. Analysis of chromosomal imbalances in sporadic and NF1-associated peripheral

nerve sheath tumors by comparative genomic hybridization. Genes Chromosomes Cancer 1999; 25: 362-9.

176. Bottillo I, Ahlquist T, Brekke H, et al. Germline and somatic NF1 mutations in sporadic and NF1-associated malignant peripheral nerve sheath tumours. J Pathol 2009; 217: 693-701.

177. Schaefer IM, Fletcher CD, Hornick JL. Loss of H3K27 trimethylation distinguishes malignant peripheral nerve sheath tumors from histologic mimics. Mod Pathol 2016; 29: 4-13.

178. Suurmeijer AJ, Ladanyi M, Nielsen TO. Synovial sarcoma. In: WHO Classification of Tumours Editorial Board, ed. WHO classification of tumours: soft tissue and bone tumours. 5th ed. Lyon: IARC Press, 2020; 290-3.

179. Sultan I, Rodriguez-Galindo C, Saab R, Yasir S, Casanova M, Ferrari A. Comparing children and adults with synovial sarcoma in the Surveillance, Epidemiology, and End Results program, 1983 to 2005: an analysis of 1268 patients. Cancer 2009; 115: 3537-47.

180. van de Rijn M, Barr FG, Xiong QB, Hedges M, Shipley J, Fisher C. Poorly differentiated synovial sarcoma: an analysis of clinical, pathologic, and molecular genetic features. Am J Surg Pathol 1999; 23: 106-12.

181. Baranov E, McBride MJ, Bellizzi AM, et al. A novel SS18-SSX fusion-specific antibody for the diagnosis of synovial sarcoma. Am J Surg Pathol 2020; 44: 922-33.

182. Lee JC, Folpe AL. Phosphaturic mesenchymal tumour. In: WHO Classification of Tumours Editorial Board, ed. WHO classification of tumours: soft tissue and bone tumours. 5th ed. Lyon: IARC Press, 2020; 284-6.

183. Lee JC, Su SY, Changou CA, et al. Characterization of *FN1-FGFR1* and novel *FN1-FGF1* fusion genes in a large series of phosphaturic mesenchymal tumors. Mod Pathol 2016; 29: 1335-46.

184. Lee JC, Jeng YM, Su SY, et al. Identification of a novel *FN1-FGFR1* genetic fusion as a frequent event in phosphaturic mesenchymal tumour. J Pathol 2015; 235: 539-45.

185. Folpe AL, Fanburg-Smith JC, Billings SD, et al. Most osteomalacia-associated mesenchymal tumors are a single histopathologic entity: an analysis of 32 cases and a comprehensive review of the literature. Am J Surg Pathol 2004; 28: 1-30.

186. Bahrami A, Weiss SW, Montgomery E, et al. RT-PCR analysis for FGF23 using paraffin sections in the diagnosis of phosphaturic mesenchymal tumors with and without known tumor induced osteomalacia. Am J Surg Pathol 2009; 33: 1348-54.

187. Fanburg-Smith JC, de Pinieux G, Ladanyi M. Mesenchymal chondrosarcoma. In: WHO Classification of Tumours Editorial Board, ed. WHO classification of tumours: soft tissue and bone tumours. 5th ed. Lyon: IARC Press, 2020; 385-7.

188. Fanburg-Smith JC, Auerbach A, Marwaha JS, et al. Immunoprofile of mesenchymal chondrosarcoma: aberrant desmin and EMA expression, retention of INI1, and negative estrogen receptor in 22 female-predominant central nervous system and musculoskeletal cases. Ann Diagn Pathol 2010; 14: 8-14.

189. Wang WL, Nero C, Pappo A, et al. CTNNB1 genotyping and APC screening in pediatric desmoid tumors: a proposed algorithm. Pediatr Dev Pathol 2012; 15: 361-7.

190. Fanburg-Smith JC, Auerbach A, Marwaha JS, Wang Z, Rushing EJ. Reappraisal of mesenchymal chondrosarcoma: novel morphologic observations of the hyaline cartilage and endochondral ossification and beta-catenin, Sox9, and osteocalcin immunostaining of 22 cases. Hum Pathol 2010; 41: 653-62.

191. McMaster MJ, Soule EH, Ivins JC. Hemangiopericytoma: a clinicopathologic study and long-term followup of 60 patients. Cancer 1975; 36: 2232-44.

192. Reisenauer JS, Mneimneh W, Jenkins S, et al. Comparison of risk stratification models to predict recurrence and survival in pleuropulmonary solitary fibrous tumor. J Thorac Oncol 2018; 13: 1349-62.

193. Vogels R, Macagno N, Griewank K, et al. Prognostic significance of *NAB2-STAT6* fusion variants and *TERT* promotor mutations in solitary fibrous tumors/hemangiopericytomas of the CNS: not (yet) clear. Acta Neuropathol 2019; 137: 679-82.

194. Yang P, Liu HC, Qiu E, et al. Factors for postoperative recurrence of orbital solitary fibrous tumor: an analysis of long-term clinical follow-up results from a Chinese tertiary hospital. BMC Ophthalmol 2021; 21: 61.

195. Benjamin RS, Choi H, Macapinlac HA, et al. We should desist using RECIST, at least in GIST. J Clin Oncol 2007; 25: 1760-4.

196. Choi H, Charnsangavej C, Faria SC, et al. Correlation of computed tomography and positron emission tomography in patients with metastatic gastrointestinal stromal tumor treated at a single institution with imatinib mesylate: proposal of new computed tomography response criteria. J Clin Oncol 2007; 25: 1753-9.

197. Stacchiotti S, Verderio P, Messina A, et al. Tumor response assessment by modified Choi criteria in localized high-risk soft tissue sarcoma treated with chemotherapy. Cancer 2012; 118: 5857-66.

198. Espat NJ, Lewis JJ, Leung D, et al. Conventional hemangiopericytoma: modern analysis of outcome. Cancer 2002; 95: 1746-51.

199. Robinson LA. Solitary fibrous tumor of the pleura. Cancer Control 2006; 13: 264-9.

200. Spitz FR, Bouvet M, Pisters PW, Pollock RE, Feig BW. Heman-

giopericytoma: a 20-year single-institution experience. Ann Surg Oncol 1998; 5: 350-5.
201. Bowe SN, Wakely PE, Ozer E. Head and neck solitary fibrous tumors: diagnostic and therapeutic challenges. Laryngoscope 2012; 122: 1748-55.
202. Yang XJ, Zheng JW, Ye WM, et al. Malignant solitary fibrous tumors of the head and neck: a clinicopathological study of nine consecutive patients. Oral Oncol 2009; 45: 678-82.
203. Wushou A, Jiang YZ, Liu YR, Shao ZM. The demographic features, clinicopathologic characteristics, treatment outcome and disease-specific prognostic factors of solitary fibrous tumor: a population-based analysis. Oncotarget 2015; 6: 41875-83.
204. Bishop AJ, Zagars GK, Demicco EG, Wang WL, Feig BW, Guadagnolo BA. Soft tissue solitary fibrous tumor: combined surgery and radiation therapy results in excellent local control. Am J Clin Oncol 2018; 41: 81-5.
205. Oike N, Kawashima H, Ogose A, et al. A malignant solitary fibrous tumour arising from the first lumbar vertebra and mimicking an osteosarcoma: a case report. World J Surg Oncol 2017; 15: 100.
206. de Boer J, Jager PL, Wiggers T, et al. The therapeutic challenge of a nonresectable solitary fibrous tumor in a hypoglycemic patient. Int J Clin Oncol 2006; 11: 478-81.
207. Han G, Zhang Z, Shen X, et al. Doege-Potter syndrome: a review of the literature including a new case report. Medicine (Baltimore) 2017; 96: e7417.
208. Constantinidou A, Jones RL, Olmos D, et al. Conventional anthracycline-based chemotherapy has limited efficacy in solitary fibrous tumour. Acta Oncol 2012; 51: 550-4.
209. Levard A, Derbel O, Meeus P, et al. Outcome of patients with advanced solitary fibrous tumors: the Centre Léon Bérard experience. BMC Cancer 2013; 13: 109.
210. Stacchiotti S, Tortoreto M, Bozzi F, et al. Dacarbazine in solitary fibrous tumor: a case series analysis and preclinical evidence vis-a-vis temozolomide and antiangiogenics. Clin Cancer Res 2013; 19: 5192-201.
211. Khalifa J, Ouali M, Chaltiel L, et al. Efficacy of trabectedin in malignant solitary fibrous tumors: a retrospective analysis from the French Sarcoma Group. BMC Cancer 2015; 15: 700.
212. Le Cesne A, Ray-Coquard I, Duffaud F, et al. Trabectedin in patients with advanced soft tissue sarcoma: a retrospective national analysis of the French Sarcoma Group. Eur J Cancer 2015; 51: 742-50.
213. Mulamalla K, Truskinovsky AM, Dudek AZ. Rare case of hemangiopericytoma responds to sunitinib. Transl Res 2008; 151: 129-33.
214. De Pas T, Toffalorio F, Colombo P, et al. Brief report: activity of imatinib in a patient with platelet-derived-growth-factor receptor positive malignant solitary fibrous tumor of the pleura. J Thorac Oncol 2008; 3: 938-41.
215. George S, Merriam P, Maki RG, et al. Multicenter phase II trial of sunitinib in the treatment of nongastrointestinal stromal tumor sarcomas. J Clin Oncol 2009; 27: 3154-60.
216. Domont J, Massard C, Lassau N, Armand JP, Le Cesne A, Soria JC. Hemangiopericytoma and antiangiogenic therapy: clinical benefit of antiangiogenic therapy (sorafenib and sunitinib) in relapsed malignant haemangioperyctoma/solitary fibrous tumour. Invest New Drugs 2010; 28: 199-202.
217. Valentin T, Fournier C, Penel N, et al. Sorafenib in patients with progressive malignant solitary fibrous tumors: a subgroup analysis from a phase II study of the French Sarcoma Group (GSF/GETO). Invest New Drugs 2013; 31: 1626-7.
218. Stacchiotti S, Negri T, Palassini E, et al. Sunitinib malate and figitumumab in solitary fibrous tumor: patterns and molecular bases of tumor response. Mol Cancer Ther 2010; 9: 1286-97.
219. Quek R, Wang Q, Morgan JA, et al. Combination mTOR and IGF-1R inhibition: phase I trial of everolimus and figitumumab in patients with advanced sarcomas and other solid tumors. Clin Cancer Res 2011; 17: 871-9.
220. Boothe JT, Budd GT, Smolkin MB, Ma PC. Durable near-complete response to anti-PD-1 checkpoint immunotherapy in a refractory malignant solitary fibrous tumor of the pleura. Case Rep Oncol 2017; 10: 998-1005.
221. Toulmonde M, Penel N, Adam J, et al. Use of PD-1 targeting, macrophage infiltration, and IDO pathway activation in sarcomas: a phase 2 clinical trial. JAMA Oncol 2018; 4: 93-7.
222. Ren C, D'Amato G, Hornicek FJ, Tao H, Duan Z. Advances in the molecular biology of the solitary fibrous tumor and potential impact on clinical applications. Cancer Metastasis Rev 2024; 43: 1337-52.

https://doi.org/10.4132/jptm.2025.10.08

JPTM

ORIGINAL ARTICLE

pISSN 2383-7837 · eISSN 2383-7845

Journal of Pathology and Translational Medicine 2026; 60: 47-57
https://doi.org/10.4132/jptm.2025.09.11

Clinicopathological and molecular mechanisms of CLDN18.2 in gastric cancer aggressiveness: a high-risk population study with multi-omics profiling

Hengquan Wu[1,2,3,4*], Mei Li[1,3,4*], Gang Wang[2,3,4,5], Peiqing Liao[1,2,3,4], Peng Zhang[1,3,4], Luxi Yang[1,2,3,4], Yumin Li[1,2,3,4], Tao Liu[1,2,3,4,5], Wenting He[1,2,3,4,5]

[1]The Second Hospital & Clinical Medical School, Lanzhou University, Lanzhou, China
[2]Gansu Provincial Key Laboratory of Environmental Oncology, Lanzhou, China
[3]Digestive System Tumor Prevention and Treatment and Translational Medicine Engineering Innovation Center of Lanzhou University, Lanzhou, China
[4]Digestive System Tumor Translational Medicine Engineering Research Center of Gansu Province, Lanzhou, China
[5]School of Basic Medical Sciences, Lanzhou University, Lanzhou, China

Graphical abstract

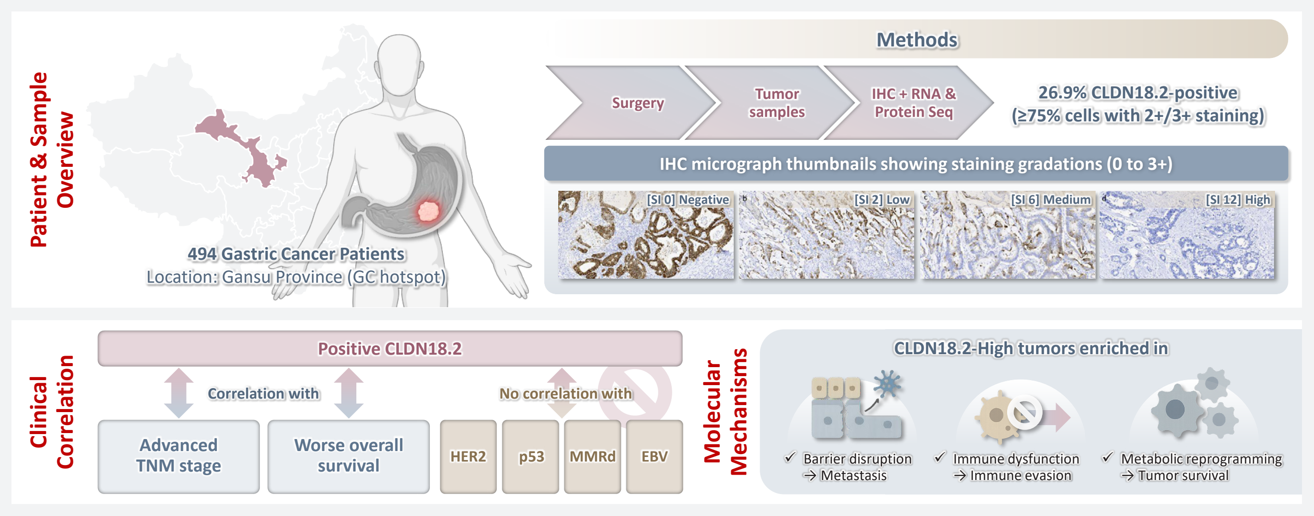

CONCLUSION CLDN18.2 overexpression is associated with poor prognosis in gastric cancer patients. Transcriptomic and proteomic analyses demonstrate that CLDN18.2 promotes tumor progression and metastasis, underscoring its potential as an independent prognostic factor in high-incidence regions.

Wu HQ et al. Journal of pathology and translational medicine

JPTM

ORIGINAL ARTICLE

pISSN 2383-7837 · eISSN 2383-7845

Journal of Pathology and Translational Medicine 2026; 60: 47-57
https://doi.org/10.4132/jptm.2025.09.11

Clinicopathological and molecular mechanisms of CLDN18.2 in gastric cancer aggressiveness: a high-risk population study with multi-omics profiling

Hengquan Wu[1,2,3,4*], Mei Li[1,3,4*], Gang Wang[2,3,4,5], Peiqing Liao[1,2,3,4], Peng Zhang[1,3,4], Luxi Yang[1,2,3,4], Yumin Li[1,2,3,4], Tao Liu[1,2,3,4,5], Wenting He[1,2,3,4,5]

[1]The Second Hospital & Clinical Medical School, Lanzhou University, Lanzhou, China
[2]Gansu Provincial Key Laboratory of Environmental Oncology, Lanzhou, China
[3]Digestive System Tumor Prevention and Treatment and Translational Medicine Engineering Innovation Center of Lanzhou University, Lanzhou, China
[4]Digestive System Tumor Translational Medicine Engineering Research Center of Gansu Province, Lanzhou, China
[5]School of Basic Medical Sciences, Lanzhou University, Lanzhou, China

Background: The tight junction protein claudin18.2 (CLDN18.2) has been implicated in poor prognosis and suboptimal immunotherapy response in gastric cancer (GC). This study investigates the clinicopathological relevance of CLDN18.2 expression and its association with molecular subtypes in GC patients from a high-incidence region, combining transcriptomic and proteomic approaches to explore how CLDN18.2 contributes to progression and metastasis. **Methods:** A retrospective cohort of 494 GC patients (2019–2024) underwent immunohistochemical analysis for CLDN18.2, Epstein-Barr virus (Epstein–Barr virus–encoded RNA), p53, human epidermal growth factor receptor 2 (HER2), and mismatch repair proteins (MLH1, MSH2, PMS2, and MSH6). CLDN18.2 positivity was defined as moderate to strong (2+/3+) membranous staining in ≥75% of tumor cells. Clinicopathological correlations, biomarker associations, and survival outcomes were evaluated. Transcriptomic and proteomic sequencing was performed to explore molecular mechanisms. **Results:** CLDN18.2 positivity was observed in 26.9% (133/494) of gastric adenocarcinomas. CLDN18.2-positive tumors correlated with TNM stage ($p = .003$) and shorter overall survival ($p = .018$). No associations were identified with age, sex, HER2 status, microsatellite instability, or Epstein-Barr virus infection. Transcriptomic profiling revealed CLDN18.2-high tumors enriched in pathways involving cell junction disruption, signaling regulation, and immune modulation. Proteomic profiling showed that tumors with high CLDN18.2 were enriched in multiple mechanism-related pathways such as integrated metabolic reprogramming, cytoskeletal recombination, immune microenvironment dysregulation, and pro-survival signaling. These mechanisms may collectively contribute to tumor progression and metastasis. **Conclusions:** CLDN18.2 overexpression is associated with poor prognosis in GC patients. Transcriptomic and proteomic analyses demonstrate that CLDN18.2 promotes tumor progression and metastasis, underscoring its potential as an independent prognostic factor in regions with a high incidence of GC.

Keywords: CLDN18.2; Gastric adenocarcinoma; Immunohistochemistry; RNA sequencing; Protein sequencing

---

Received: June 30, 2025 **Revised:** September 7, 2025 **Accepted:** September 11, 2025
Corresponding Author: Wenting He, PhD
The Second Hospital & Clinical Medical School, Lanzhou University, Lanzhou 730030, China
Tel: +86-09315190901, E-mail: hewt@lzu.edu.cn

Tao Liu, PhD
The Second Hospital & Clinical Medical School, Lanzhou University, Lanzhou 730030, China
Tel: +86-09318943240, Fax: +86-09318458109, E-mail: liut@lzu.edu.cn

*Hengquan Wu and Mei Li contributed equally to this work.

This is an Open Access article distributed under the terms of the Creative Commons Attribution Non-Commercial License (https://creativecommons.org/licenses/by-nc/4.0/) which permits unrestricted non-commercial use, distribution, and reproduction in any medium, provided the original work is properly cited.
© 2026 The Korean Society of Pathologists/The Korean Society for Cytopathology

INTRODUCTION

Gastric cancer (GC) is the fifth most common malignancy and cause of cancer mortality globally, with approximately one million new cases diagnosed annually [1]. Despite advances in diagnostic and therapeutic strategies, clinical outcomes for advanced GC remain dismal, with limited patient eligibility for targeted therapies and a 5-year survival rate less than 30% [2-4]. This underscores the urgent need to elucidate molecular drivers of tumor progression and identify biomarkers for precision medicine.

Gastric adenocarcinoma is characterized by profound molecular heterogeneity, complicating efforts to standardize treatment paradigms [5]. While the Lauren classification has historically guided clinical management, its utility in predicting therapeutic responses remains constrained [6]. Landmark work by The Cancer Genome Atlas (TCGA) redefined GC into four molecular subtypes of chromosomally unstable, microsatellite unstable, genomically stable, and Epstein-Barr virus–positive (EBV+) tumors, providing a framework for molecularly stratified therapies [7]. However, the clinical translation of these subtypes remains uncertain, necessitating the discovery of actionable biomarkers to refine patient stratification.

Claudin18.2 (CLDN18.2), a splice variant of the tight junction protein claudin18, has emerged as a promising therapeutic target [8]. It is confined to gastric mucosal tight junctions in normal tissues but is exposed on the surface upon malignant transformation [9,10]. In addition to GC, aberrant CLDN18.2 expression is observed in pancreatic, biliary, ovarian, and lung adenocarcinomas, positioning it as a selective biomarker [11].

Preclinical and clinical studies, including trials of the monoclonal antibody zolbetuximab (formerly IMAB362) and antibody-drug conjugates (ADCs) targeting CLDN18.2, have demonstrated significant antitumor efficacy in CLDN18.2-high GC subsets [12,13]. For instance, the phase III SPOTLIGHT and GLOW trials validated zolbetuximab combined with chemotherapy as a first-line regimen for CLDN18.2-positive/human epidermal growth factor receptor 2 (HER2)–negative advanced GC, achieving median overall survival (OS) of 18.23 months and 14.39 months, respectively [9,14]. Additionally, novel ADCs such as CMG901 (AZD0901) demonstrated an objective response rate of 28%–29% and median OS of 10.1 months in a phase I trial for refractory GC [15].

Despite advances in CLDN18.2-targeted therapies, its expression exhibits heterogeneity across geographical regions and ethnic groups. In Gansu Province, a global GC hotspot with elevated incidence linked to the arid climate and high dietary nitrosamines, our prior analysis of 75,522 GC patients (2013–2021) identified climatic factors as key contributors to GC risk [16]. To address the research gap of CLDN18.2 in this region, we conducted a comprehensive multi-omics investigation encompassing immunohistochemistry (IHC), transcriptomic profiling, and proteomic analysis in 494 GC patients from this region. This study evaluated the relationships between CLDN18.2 expression and molecular subtype, clinicopathological features, and survival outcomes and further explored its potential mechanisms in GC progression and metastasis.

MATERIALS AND METHODS

Case selection

During the period 2019–2024, we conducted a retrospective cohort study of 510 patients with gastric adenocarcinoma who underwent radical surgical resection in the Second Hospital of Lanzhou University. All specimens were obtained surgically in patients who had not undergone neoadjuvant chemotherapy.

Patient inclusion criteria were (1) preoperative endoscopic biopsy-confirmed GC; (2) indications for GC surgery; (3) eligible for curative resection; (4) adequate function of other organ systems to tolerate surgery, without comorbidities (such as severe cardiac, cerebral, pulmonary, or metabolic diseases) significantly impacting surgical risk; (5) informed consent by both the patient and their family for curative GC resection; and (6) availability of complete medical records. Patient exclusion criteria were (1) unsuitable for curative GC surgery (defined as R0 resection with D2 lymphadenectomy) due to invasion of adjacent organs or concurrent other tumors; (2) significant comorbidities potentially impacting the surgery; (3) presentation as a surgical emergency; (4) refusal of the surgical plan by either the patient or their family; and (5) incomplete medical records or patient withdrawal from the study.

After excluding 16 ineligible samples, the final cohort comprised 494 patients. Clinicopathological data were systematically collected, including demographic variables (sex, age), diagnosis schedule (date of initial diagnosis), tumor characteristics (grade, location, histotype, Lauren classification), biomarker profiles (HER2, p53, Epstein–Barr virus–encoded RNA [EBER], MSH2, MSH6, MLH1, and PMS2), and OS outcomes. Tissue specimens were fixed in formalin within 48 hours post-resection and processed according to standardized histopathological protocols.

Immunohistochemistry

IHC analyses on fresh-frozen paraffin-embedded specimens were conducted using a fully automatic slide stainer, the Ventana Benchmark Ultra automated staining platform (Roche Diagnostics, Basel, Switzerland), with the Ultra View DAB detection kit. HER2 (Kit-0043, MXB), p53 (MAB-0674, MXB), PMS2 (RMA-0775, MXB), MSH2 (MAB-0836, MXB), MSH6 (MAB-0831, MXB), MLH1 (MAB-0838, MXB), EBER, and all immunoreagents were obtained from Ventana Medical Systems (Roche Diagnostics).

CLDN18.2 expression was assessed using a polyclonal antibody (1:500 dilution, ab222513, Immunoway, San Jose, CA, USA) through immunohistochemical analysis. Two experienced pathologists independently evaluated the cytoplasmic staining patterns based on established criteria. Staining intensity was graded as strong (3+), moderate (2+), weak (1+), or absent (0), and the percentage of stained tumor cells was recorded. A staining index (SI) ranging from 0 to 12 was calculated by multiplying the intensity score by the percentage score. Based on predefined clinical thresholds, cases were categorized by expression intensity as absent (SI 0), weak (SI 1–2), moderate (SI 3–6), or strong (SI 8–12). Cases were classified according to a cutoff of ≥75% tumor cell 2+ or 3+ intensity, which is the eligible IHC cut-off for an ongoing zolbetuximab study [17]. In samples undergoing RNA and protein sequencing, high CLDN18.2 expression is defined as immunohistochemical staining intensity ≥2+ in ≥75% of tumor cells, while low CLDN18.2 expression is defined as staining intensity <2+ in ≥40% of tumor cells.

Mismatch repair deficiency (MMRd) was determined by loss of MLH1, MSH2, MSH6, or PMS2 on IHC [18]. p53 status was defined as wild-type (patchy nuclear staining) or aberrant (diffuse or complete loss) [19]. HER2 status assessment for gastric adenocarcinoma requires IHC testing, with specimens classified as negative (IHC 0/1+: no/faint reactivity), equivocal (IHC 2+: weak-moderate membranous reactivity in ≥10% tumor cells), or positive (IHC 3+: strong membranous reactivity in ≥10% tumor cells). Equivocal cases require confirmation via in situ hybridization (ISH), where positivity is defined as HER2:CEP17 ratio ≥2 or *HER2* copy number ≥6.0 signals/cell; IHC 0/1+ or 3+ results preclude additional ISH testing [20].

EBER in situ hybridization

EBV infection was detected using the ISH EBER Probe (MC-3003, MXB) on the Ventana platform per manufacturer guidelines.

RNA and protein sequencing

Paired tumor and adjacent normal tissues from eight gastric adenocarcinoma patients were collected as fresh-frozen samples, snap-frozen in liquid nitrogen, and stored at −80°C until processing. For RNA extraction, tissues were homogenized in TRIzol reagent (Invitrogen, Carlsbad, CA, USA). After chloroform phase separation, RNA was precipitated with isopropanol, washed with 75% ethanol, air-dried, and dissolved in RNase-free water. RNA integrity was verified via agarose gel electrophoresis (1% gel; 120 V, 20 minutes), confirming distinct 18S/28S ribosomal RNA bands without degradation. Only high-quality RNA (RNA integrity number > 7.0 implied by gel assessment) was used for cDNA synthesis.

For protein extraction, tissues were mechanically disrupted in lysis buffer (8 M urea, 2% sodium dodecyl sulfate) using a glass homogenizer, followed by centrifugation (14,000 ×g, 20 minutes, 4°C). The supernatant was collected, and total protein was quantified via BCA assay (Pierce, Rockford, IL, USA). Quality control was performed using sodium dodecyl sulfate polyacrylamide gel electrophoresis (12% gel; 80 V, 2 hours), ensuring intact protein bands without smearing.

Subsequent RNA sequencing included reverse transcription polymerase chain reaction–based cDNA amplification, Illumina-compatible paired-end library preparation, and sequencing on the HiSeq platform. For proteomics, proteins were denatured, reduced (10 mM dithiothreitol), alkylated (50 mM iodoacetamide), and digested with trypsin (2 hours, 37°C). Peptides were desalted (C18 SPE), fractionated (high-pH reverse-phase high-performance liquid chromatography), lyophilized, reconstituted, separated via nano-LC (C18 column), and analyzed by tandem mass spectrometry. A data-dependent acquisition spectral library was generated; differential proteins were identified using Spectronaut (v16.1), with functional enrichment (Gene Ontology [GO]/Kyoto Encyclopedia of Genes and Genomes [KEGG]) and subcellular localization analyses.

Statistical analysis

Associations between CLDN18.2 and clinicopathological variables were assessed using χ^2 or Fisher's exact test (significance threshold: $p < .05$). The Kaplan-Meier method and log-rank test were used to calculate the survival curve. Statistical analysis was performed using SPSS software ver. 26.0 (IBM Corp., Armonk, NY, USA). The statistical results were plotted using GraphPad Prism 9.1.0 (GraphPad Software Inc., San Diego, CA, USA).

RESULTS

Clinicopathological correlates and prognostic significance of CLDN18.2 expression in primarily resected gastric adenocarcinomas

The study cohort comprised 494 gastric adenocarcinoma patients, comprising 380 males (76.9%) and 114 females (23.1%), with a mean age of 58.54 ± 9.66 years (median, 59 years; range, 22 to 85 years) (Table 1). All patients underwent surgical resection of the primary tumor with an R0 margin. Tumor localization analysis revealed that nearly half of the cases originated in the gastric antrum, while 23.1% and 22.9% were located in the gastric fundus and body, respectively. Pathological staging demonstrated distinct distributions: pT4a and pT4b tumors predominated in pathological tumor (pT) staging (n = 276, 55.8%), whereas pathological nodal (pN) staging showed a higher frequency of pN0 (n = 171, 34.6%). TNM staging classified 22.3% (n = 110) as stage I, 20. 9% (n= 103) as stage II, and 56.8% (n = 281) as stage III–IV. Among them, 200 cases received postoperative chemotherapy, while 81 cases did not (Supplementary Fig. S1). Histologically, 8.5% (n = 42) of tumors were graded as G1, 55.3% (n = 273) as G2, and 36.2% (n = 179) as G3. Lauren classification categorized 31.8% (n = 157) as intestinal type, 40.9% (n=202) as diffuse type, and 27.3% (n = 135) as mixed type. The results demonstrated significant associations of CLDN18.2-positive status with pT category (p = .046), pN category (p = .013), and TNM stage (p = .003). No significant correlations were observed with age, sex, tumor location, histological grade, or Lauren subtype (Table 1). Representative immunohistochemical staining patterns of CLDN18.2 expression are presented in Fig. 1. Our survival analysis revealed that CLDN18.2-positive expression was associated with significantly shorter OS (p = .018) (Fig. 2).

Characteristics of molecular biomarkers

MMRd was identified in 6.3% (n = 31) of cases, with 93.7% (n = 463) demonstrating mismatch repair proficiency. EBV infection was detected in 2.0% (n=10) of tumors, while 98.0% (n = 484) tested negative. HER2 overexpression or amplification was observed in 16.2% (n = 80) of cases, while 83.8% (n = 414) lacked *HER2* alterations. *TP53* abnormalities were present in 46.8% (n=231) of cases, accounting for approximately half of the total cohort (Table 2). No correlation between the expression of CLDN18.2 and MMRd, HER2, TP53, or EBER-ISH was found.

Analysis of the biological function of genes significantly related to CLDN18.2 by RNA sequencing

We divided the eight pairs of tissue samples after sequencing into high CLDN18.2 expression (n = 4) and low expression (n = 4) groups. Compared with the low-expression group, the high-expression group showed 183 genes that were significantly differentially expressed and strongly correlated with CLDN18.2, including 133 upregulated and 50 downregulated genes (Fig. 3A, B). This indicates that broad transcriptional reprogramming is associated with CLDN18.2 overexpression. GO enrichment analysis across cellular components, molecular function, and biological processes identified functional clusters in CLDN18.2-high tumors (Fig. 3C, D). Cellular component enrichment predominantly comprised terms related to membrane integrity, including cell periphery, intrinsic membrane component, and integral plasma membrane component. Molecular function analysis highlighted steroid binding, flavonol 3-sulfotransferase activity, and inorganic anion transmembrane transporter activity. Biological process terms were enriched in pathways governing organic hydroxy compound transport, cholesterol transport, and vitamin E metabolism. KEGG pathway analysis further identified significant enrichment in phagosomes, cytokine-cytokine receptor interactions, and chemical carcinogenesis (Fig. 3E, F). These results suggest that CLDN18.2 may influence tumor progression and metastasis via mechanisms involving cell junction disruption, signaling pathway regulation, and immune regulation.

Analysis of the biological functions of genes significantly associated with CLDN18.2 on proteome sequencing

Based on proteome sequencing analysis, the CLDN18.2 high-expression group was mainly enriched in choline transport, adenylyl cyclase-G-protein-coupled receptor signal regulation, and regulation of actomyosin structure organization in biological processes (Fig. 4A). Cellular component analysis highlighted dysregulation of the Golgi apparatus, membrane, and endomembrane system, suggesting roles in secretory pathway activation and cell polarity disruption (Fig. 4B). In terms of molecular function, choline transmembrane transporter activity, TAP binding, peptide antigen binding, T-cell receptor binding, and chloride channel inhibitor activity were abnormal (Fig. 4C). KEGG pathway analysis showed that endocytosis, FcγR-mediated phagocytosis, choline metabolism in tumors, and the pentose phosphate pathway jointly regulated metabolic

Table 1. Clinicopathological features of GC according to CLDN18.2 status

Characteristic	Total (n = 494)	CLDN18-negative	CLDN18-positive	p-value
Age (yr) (median, 59 yr)				
Mean ± SD	58.54 ± 9.66			
<59	246 (49.8)	175 (71.1)	71 (28.9)	.333
≥59	248 (50.2)	186 (75.0)	62 (25.0)	
Sex				
Male	380 (76.9)	272 (71.6)	108 (28.4)	.171
Female	114 (23.1)	89 (78.1)	25 (21.9)	
Gastric localization				
Fundus	114 (23.1)	85 (74.6)	29 (25.4)	.802
Body	113 (22.9)	80 (70.8)	33 (29.2)	
Antrum	267 (54.0)	196 (73.4)	71 (26.6)	
pT				
1a–1b	79 (16.0)	67 (84.8)	12 (15.2)	.046
2	64 (13.0)	49 (76.6)	15 (23.4)	
3	75 (15.2)	51 (68.0)	24 (32.0)	
4a–4b	276 (55.8)	194 (70.3)	82 (29.7)	
pN				
0	171 (34.6)	137 (80.1)	34 (19.9)	.013
1	63 (12.8)	50 (79.4)	13 (20.6)	
2	120 (24.3)	79 (65.8)	41 (34.2)	
3a-3b	140 (28.3)	95 (67.9)	45 (32.1)	
TNM staging				
I	110 (22.3)	90 (81.9)	20 (18.1)	.003
II	103 (20.9)	82 (79.6)	21 (20.4)	
III–IV	281 (56.8)	189 (67.3)	92 (32.7)	
Tumor grading				
G1	42 (8.5)	33 (78.6)	9 (21.4)	.638
G2	273 (55.3)	196 (71.8)	77 (28.2)	
G3	179 (36.2)	132 (73.7)	47 (26.3)	
Lauren				
Intestinal	157 (31.8)	125 (79.6)	32 (20.4)	.077
Diffuse	202 (40.9)	140 (69.3)	62 (30.7)	
Mixed	135 (27.3)	96 (71.1)	39 (28.9)	

Values are presented as number (%).
GC, gastric cancer; CLDN18.2, claudin18.2; SD, standard deviation.

reprogramming, immune microenvironment dysregulation, and pro-survival signaling, promoting the progression and metastasis of GC (Fig. 4D).

DISCUSSION

CLDN18.2, a gastric system–specific tight junction protein, is normally localized to differentiated epithelial cells, maintaining mucosal barrier integrity via cell-cell adhesion. However, malignant transformation disrupts cell adhesion and polarity, leading to aberrant CLDN18.2 surface exposure, which may promote metastatic dissemination by compromising epithelial cohesion [9]. In this study, we analyzed CLDN18.2 expression in a high-incidence GC cohort, combining clinicopathological correlations, survival data, and multi-omics profiling to explore its role in tumor progression.

While our findings demonstrate that CLDN18.2 positivity (26.9%, 133/494) was significantly associated with advanced

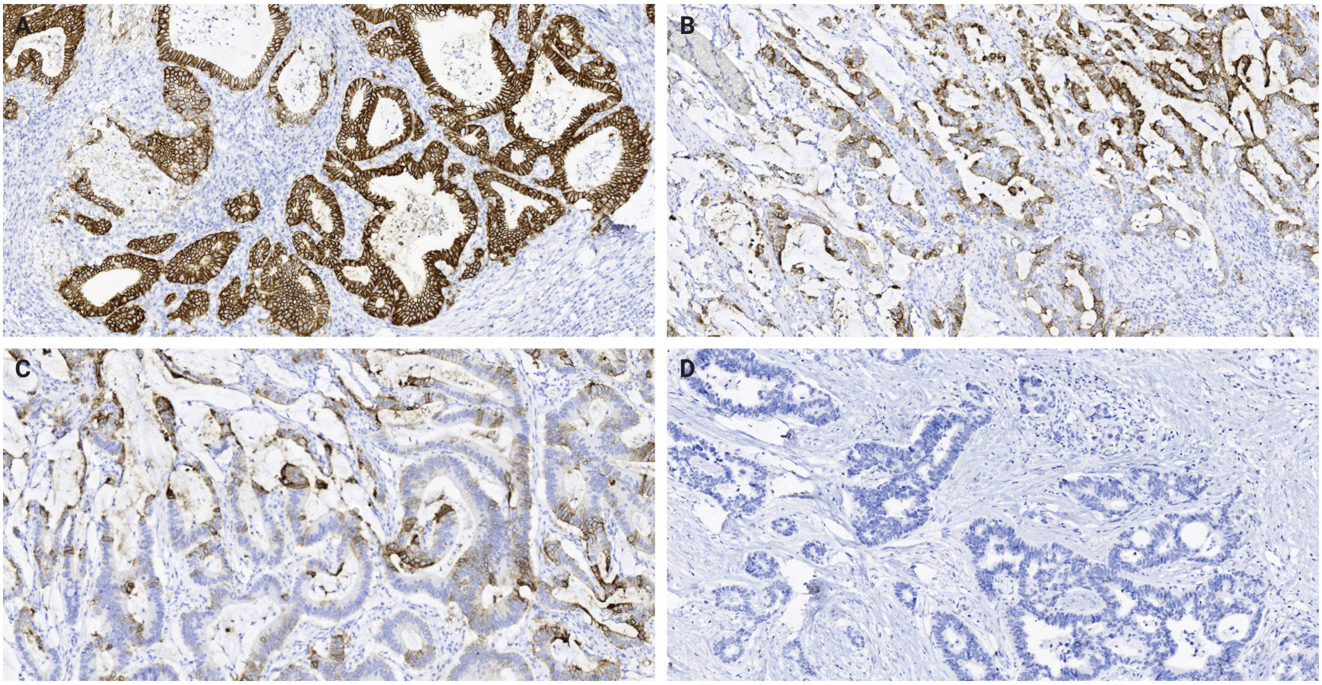

Fig. 1. Immunohistochemical staining of claudin18.2 (CLDN18.2) (A–D) in a primary resected gastric adenocarcinoma specimen. (A) Cytoplasmic staining intensity was high (staining index [SI] 12). (B) Cytoplasmic staining intensity was medium (SI 6). (C) Cytoplasmic staining intensity was low (SI 2). (D) Cytoplasmic staining of CLDN18.2 was negative (SI 0).

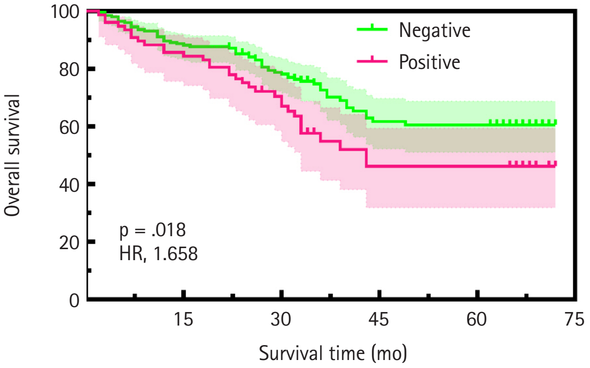

Fig. 2. Overall survival time in patients with claudin18.2 (CLDN18.2) expression, CLDN18.2 positive is defined as strong (2+/3+) membrane staining ≥75% of tumor cells. Median follow-up: 34 months. HR, hazard ratio.

TNM stage (p = .003) and shorter survival time (p = .018), underscoring its role in aggressive disease biology in our cohort, it is important to acknowledge conflicting evidence in the literature regarding its prognostic value. Recent meta-analyses, including studies by Park et al. [21] and Ungureanu et al. [22], as well as individual studies of comparable scale and population focus [23], have reported no significant association between CLDN18.2 expression and survival outcomes in GC [21-23]. Notably, we found no association between CLDN18.2 and molecular subtypes defined by EBER, HER2, MMRd, p53, or TCGA classification, suggesting that its prognostic value may transcend conventional molecular stratification in our dataset. These findings align with prior studies reporting CLDN18.2 as a stage-dependent biomarker [24]. While our cohort showed no association between CLDN18.2 and age, gender, Lauren classification, tumor grade, or tumor location, Kwak et al. [25] observed a significant correlation between CLDN18.2-positive GC and tumor location in the upper third of the stomach. This difference, along with the prognostic discrepancies highlighted above, may stem from variations in immunohistochemical scoring protocols or regional epidemiological factors, emphasizing the need for standardized CLDN18.2 assessment criteria.

RNA sequencing revealed enriched genes regulating membrane integrity (e.g., cell periphery and plasma membrane components) in CLDN18.2-high tumors. This molecular signature suggests compromised tight junction function, likely resulting from malignant transformation that disrupts cellular polarity

Table 2. Immunohistochemical profiles according to CLDN18.2 status

Characteristic	Total (n = 494)	CLDN18-negative	CLDN18-positive	p-value
MMRd				
Yes	31 (6.3)	23 (74.2)	8 (25.8)	.885
No	463 (93.7)	338 (73.0)	125 (27.0)	
HER2				
Positive	80 (16.2)	53 (66.3)	27 (33.8)	.133
Negative	414 (83.8)	308 (74.4)	106 (25.6)	
p53				
Altered	231 (46.8)	168 (72.8)	63 (27.2)	.870
Wild type	263 (53.2)	193 (73.4)	70 (26.6)	
EBER				
Positive	10 (2.0)	5 (50.0)	5 (50.0)	.193
Negative	484 (98.0)	356 (73.6)	128 (26.4)	

Values are presented as number (%).
CLDN18.2, claudin18.2; MMRd, mismatch repair deficiency; HER2, human epidermal growth factor receptor 2; EBER, Epstein–Barr virus–encoded RNA.

and exposes CLDN18.2 on the cell surface. Preclinical data indicate that aberrant CLDN18.2 expression may contribute to cancer progression, but its direct role in the epithelial-mesenchymal transition remains unconfirmed in clinical studies [26]. Molecular function indicated that CLDN18.2 is linked to steroid binding and inorganic anion transport, implicating roles in lipid metabolism and ion homeostasis. Studies show that CLDN18 loss disrupts transcellular chloride flux and activates YAP/TEAD signaling, which can drive lipid and sterol biosynthesis. The steroid-binding signal likely reflects indirect effects via lipid-handling or steroid-responsive pathways rather than direct ligand binding, suggesting that altered ion transport and lipid metabolism are mechanistically coupled in the CLDN18.2-deficient gastric epithelium [27-29]. Biological processes such as organic hydroxy compound transport and vitamin E metabolism further highlighted metabolic reprogramming toward redox balance and biosynthetic support [30]. KEGG pathway analysis revealed enrichment in phagosomes, cytokine-cytokine receptor interaction, and chemical carcinogenesis, suggesting that CLDN18.2 synergizes with immune dysregulation and pro-carcinogenic signaling to drive cancer progression [24,31].

Proteomic profiling corroborated the role of CLDN18.2 in cytoskeletal remodeling and metabolic adaptation. Notably, KEGG analysis identified aberrant endocytosis as a central mechanism, wherein CLDN18.2 may enhance nutrient internalization to sustain proliferation in nutrient-scarce microenvironments [23,32,33]. Concurrent dysregulation of FcγR-mediated phagocytosis and T-cell receptor binding implies that CLDN18.2 fosters immune evasion by perturbing antigen presentation or sequestering immunostimulatory molecules [34]. These perturbations collectively establish an immunosuppressive niche conducive to metastatic outgrowth.

The relationship between CLDN18.2 and programmed death-ligand 1 (PD-L1) expression in GC remains uncertain, with studies reporting conflicting findings. Several groups have found no significant correlation between these biomarkers, suggesting they may independently inform treatment strategies; for example, Ogawa et al. [35] reported that CLDN18.2 expression did not correlate with PD-L1, indicating that anti–programmed death-1 (PD-1)/PD-L1 therapy might not benefit CLDN18.2-positive patients. However, other studies suggest a potential interaction, such as Wang et al. [36], who observed a positive correlation between CLDN18.2 and PD-L1 expression, and Tao et al. [23], whose GSEA revealed significant enrichment of PD-1 signaling in CLDN18.2-high tumors. Clinically, the presence or absence of this overlap is highly relevant, particularly with the recent approval of the anti-CLDN18.2 agent zolbetuximab. Divergent reports regarding co-expression rates underscore the necessity for further research to correlate expression patterns with therapeutic outcomes [37].

A limitation of this study is that the patients included in the analysis are from a single institution and underwent a relatively short follow-up period, which may introduce selection bias. The small proteomic subset limits mechanistic generalizability, warranting validation in larger cohorts.

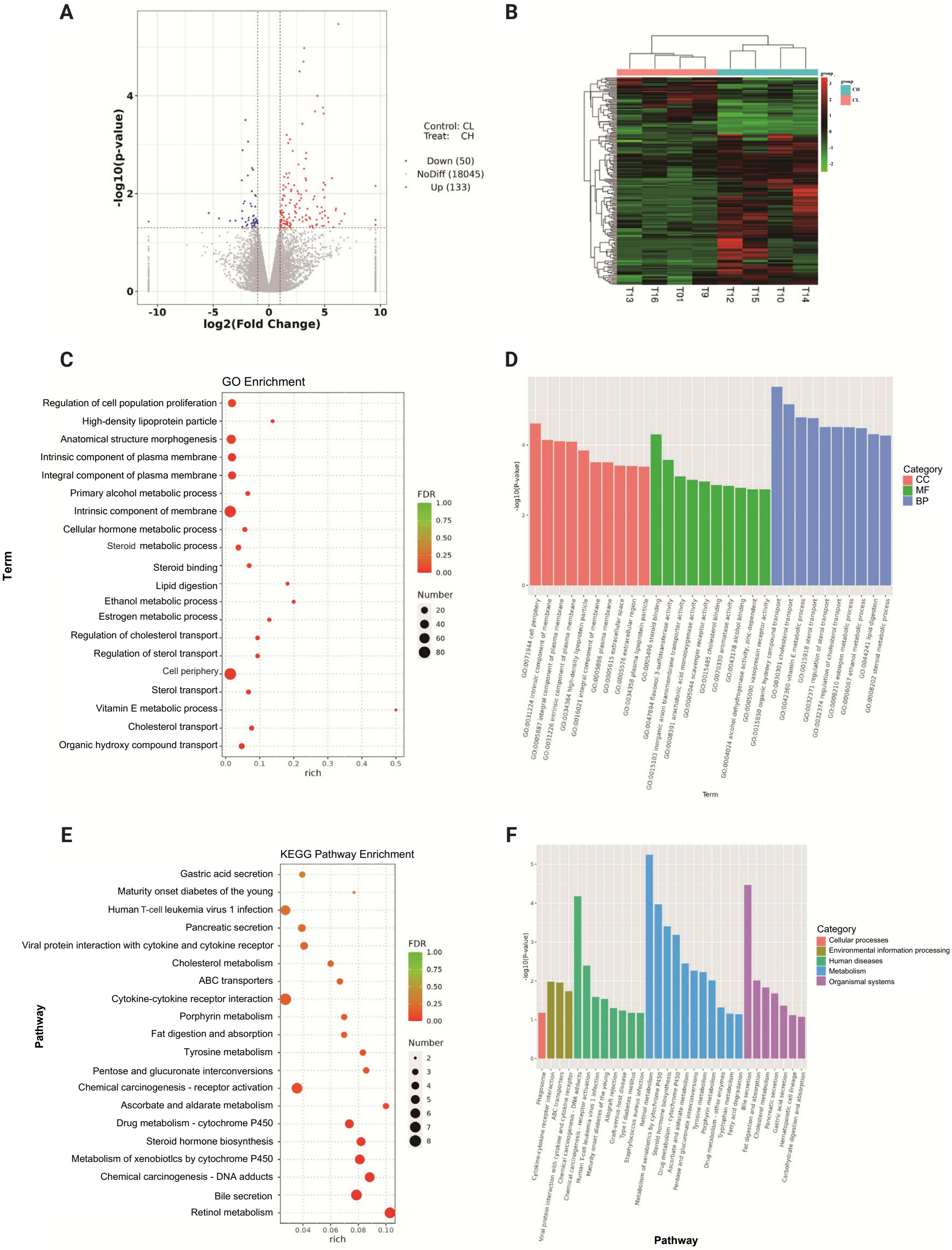

Fig. 3. Results of transcriptome functional enrichment analysis. (A) Differentially expressed gene (DEG) volcano plot. Vertical axis: –log10 p-value (significance); horizontal axis: log2 fold change (high vs. low expression). Upregulated (red)/downregulated (blue) genes marked by threshold (gray dashed line). (B) DEG heatmap. Left axis: gene clustering; horizontal axis: samples; right axis: gene names. Color gradient: red (high expression), green (low). (C) Gene ontology (GO)-rich factor of the claudin18.2 (CLDN18.2) gene. (D) Three GO terms. (E, F) Kyoto Encyclopedia of Genes and Genomes (KEGG) pathways. BP, biological process; CC, cellular component; CH, CLDN18.2-high expression; CL, CLDN18.2-low expression; ECM, extracellular matrix; FDR, false discovery rate; MF, molecular function.

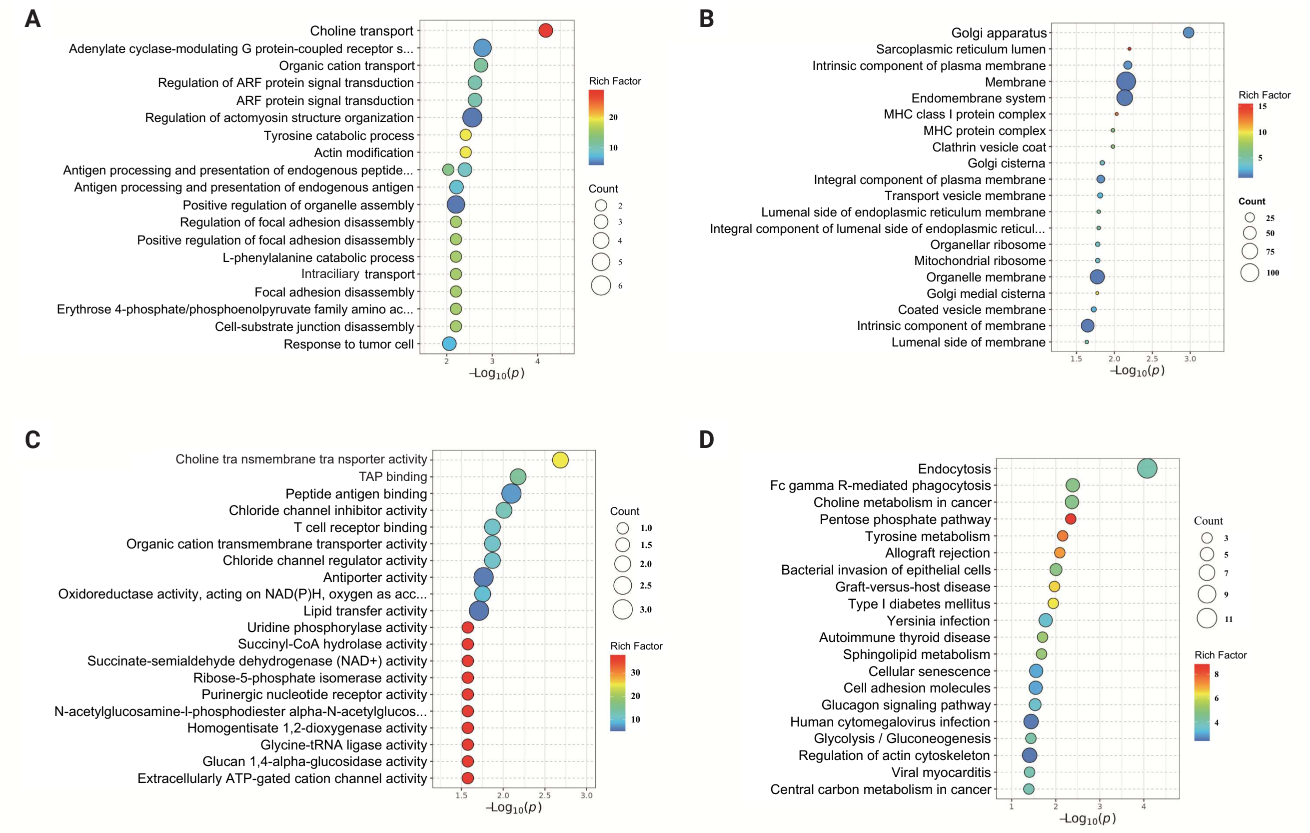

Fig. 4. Results of proteome functional enrichment analysis. (A) Biological process enrichment term bubble plots of differentially expressed proteins. (B) Cellular component enrichment term bubble plot of differentially expressed proteins. (C) Molecular function enrichment term bubble plot of differentially expressed proteins. (D) Kyoto Encyclopedia of Genes and Genomes pathway enrichment bubble diagram of differentially regulated proteins (top 20), enrichment term of differentially beneficial proteins with top 20 enrichment significance, abscissa is the negative log transformation of enrichment significance p-value, and the ordinate is the corresponding enrichment term.

In this study, we demonstrate that elevated CLDN18.2 expression is significantly associated with TNM stage and OS in GC patients from high-incidence regions. Integrated transcriptomic and proteomic analyses revealed that CLDN18.2 drives progression via metabolic reprogramming, cytoskeletal remodeling, and immune dysregulation, establishing it as a key metastasis regulator and potential target for high-risk GC. The prognostic value of CLDN18.2 is pronounced in environmentally high-risk populations, with identified pathways (e.g., endocytosis, FcγR-mediated immune suppression) informing the suitability of combination therapies targeting CLDN18.2 and downstream effectors.

Supplementary Information

The Data Supplement is available with this article at https://doi.org/10.4132/jptm.2025.09.11.

Ethics Statement

Ethical approval for the use of tissue samples in this research was granted by the Ethical Review Committee of Lanzhou University Second Hospital (IRB No. 2021A-153), and written informed consent was obtained from all participants.

Availability of Data and Material

The original contributions presented in the study are included in the article; further inquiries can be directed to the corresponding authors.

Code Availability

Not applicable.

ORCID

Hengquan Wu https://orcid.org/0009-0002-8680-4925

Mei Li	https://orcid.org/0009-0004-3331-8426
Gang Wang	https://orcid.org/0009-0006-6673-368X
Peiqing Liao	https://orcid.org/0009-0001-9788-6674
Peng Zhang	https://orcid.org/0009-0007-6470-978X
Luxi Yang	https://orcid.org/0000-0002-5242-7642
Yumin Li	https://orcid.org/0000-0002-9267-1412
Tao Liu	https://orcid.org/0000-0003-1573-6777
Wenting He	https://orcid.org/0009-0008-4718-4114

Author Contributions

Conceptualization: WH, TL. Data curation: WH, ML, HW, PZ, GW, LY, YL. Formal analysis: HW. Funding acquisition: WH, TL. Investigation: WH, ML, HW, GW, PL. Methodology: WH, TL. Project administration: WH, TL. Resources: WH, TL, ML. Supervision: WH, TL. Validation: WH, ML, HW. Visualization: HW. Writing—original draft: HW. Writing—review & editing: TL, WH. Approval of final manuscript: all authors.

Conflicts of Interest

The authors declare that they have no potential conflicts of interest.

Funding Statement

This work was supported by The Fundamental Research Funds for The Science and Technology Program of Gansu Province (No. 23JRRA1015); International science and technology cooperation project of Gansu Provincial Science and Technology Department (No. 2023YFWA0009).

REFERENCES

1. Bray F, Laversanne M, Sung H, et al. Global cancer statistics 2022: GLOBOCAN estimates of incidence and mortality worldwide for 36 cancers in 185 countries. CA Cancer J Clin 2024; 74: 229-63.
2. Shi D, Yang Z, Cai Y, et al. Research advances in the molecular classification of gastric cancer. Cell Oncol (Dordr) 2024; 47: 1523-36.
3. Matsuoka T, Yashiro M. Molecular insight into gastric cancer invasion: current status and future directions. Cancers (Basel) 2023; 16: 54.
4. Kahraman S, Yalcin S. Recent advances in systemic treatments for HER-2 positive advanced gastric cancer. Onco Targets Ther 2021; 14: 4149-62.
5. Zhang M, Hu S, Min M, et al. Dissecting transcriptional heterogeneity in primary gastric adenocarcinoma by single cell RNA sequencing. Gut 2021; 70: 464-75.
6. Ye Y, Yang W, Ruan X, et al. Metabolism-associated molecular classification of gastric adenocarcinoma. Front Oncol 2022; 12: 1024985.
7. Cancer Genome Atlas Research Network. Comprehensive molecular characterization of gastric adenocarcinoma. Nature 2014; 513: 202-9.
8. Sahin U, Koslowski M, Dhaene K, et al. Claudin-18 splice variant 2 is a pan-cancer target suitable for therapeutic antibody development. Clin Cancer Res 2008; 14: 7624-34.
9. Shitara K, Lordick F, Bang YJ, et al. Zolbetuximab plus mFOLFOX6 in patients with CLDN18.2-positive, HER2-negative, untreated, locally advanced unresectable or metastatic gastric or gastro-oesophageal junction adenocarcinoma (SPOTLIGHT): a multicentre, randomised, double-blind, phase 3 trial. Lancet 2023; 401: 1655-68.
10. Sahin U, Schuler M, Richly H, et al. A phase I dose-escalation study of IMAB362 (Zolbetuximab) in patients with advanced gastric and gastro-oesophageal junction cancer. Eur J Cancer 2018; 100: 17-26.
11. Zhou KI, Strickler JH, Chen H. Targeting claudin-18.2 for cancer therapy: updates from 2024 ASCO annual meeting. J Hematol Oncol 2024; 17: 73.
12. Qi C, Gong J, Li J, et al. Claudin18.2-specific CAR T cells in gastrointestinal cancers: phase 1 trial interim results. Nat Med 2022; 28: 1189-98.
13. Qi C, Liu C, Gong J, et al. Claudin18.2-specific CAR T cells in gastrointestinal cancers: phase 1 trial final results. Nat Med 2024; 30: 2224-34.
14. Shah MA, Shitara K, Ajani JA, et al. Zolbetuximab plus CAPOX in CLDN18.2-positive gastric or gastroesophageal junction adenocarcinoma: the randomized, phase 3 GLOW trial. Nat Med 2023; 29: 2133-41.
15. Ruan DY, Liu FR, Wei XL, et al. Claudin 18.2-targeting antibody-drug conjugate CMG901 in patients with advanced gastric or gastro-oesophageal junction cancer (KYM901): a multicentre, open-label, single-arm, phase 1 trial. Lancet Oncol 2025; 26: 227-38.
16. Huang B, Liu J, Ding F, Li Y. Epidemiology, risk areas and macro determinants of gastric cancer: a study based on geospatial analysis. Int J Health Geogr 2023; 22: 32.
17. Klempner SJ, Lee KW, Shitara K, et al. ILUSTRO: Phase II multicohort trial of zolbetuximab in patients with advanced or metastatic Claudin 18.2-positive gastric or gastroesophageal junction adenocarcinoma. Clin Cancer Res 2023; 29: 3882-91.

18. de la Fouchardiere C, Cammarota A, Svrcek M, et al. How do I treat dMMR/MSI gastro-oesophageal adenocarcinoma in 2025? A position paper from the EORTC-GITCG gastro-esophageal task force. Cancer Treat Rev 2025; 134: 102890.
19. Coati I, Lotz G, Fanelli GN, et al. Claudin-18 expression in oesophagogastric adenocarcinomas: a tissue microarray study of 523 molecularly profiled cases. Br J Cancer 2019; 121: 257-63.
20. Ajani JA, D'Amico TA, Bentrem DJ, et al. Gastric cancer, version 2.2025, NCCN clinical practice guidelines in oncology. J Natl Compr Canc Netw 2025; 23: 169-91.
21. Park G, Park SJ, Kim Y. Clinicopathological significance and prognostic values of claudin18.2 expression in solid tumors: a systematic review and meta-analysis. Front Oncol 2024; 14: 1453906.
22. Ungureanu BS, Lungulescu CV, Pirici D, et al. Clinicopathologic relevance of Claudin 18.2 expression in gastric cancer: a meta-analysis. Front Oncol 2021; 11: 643872.
23. Tao D, Guan B, Li Z, Jiao M, Zhou C, Li H. Correlation of Claudin18.2 expression with clinicopathological characteristics and prognosis in gastric cancer. Pathol Res Pract 2023; 248: 154699.
24. Liu S, Zhang Z, Jiang L, Zhang M, Zhang C, Shen L. Claudin-18.2 mediated interaction of gastric cancer cells and cancer-associated fibroblasts drives tumor progression. Cell Commun Signal 2024; 22: 27.
25. Kwak Y, Kim TY, Nam SK, et al. Clinicopathologic and molecular characterization of stages II-IV gastric cancer with Claudin 18.2 expression. Oncologist 2025; 30: oyae238.
26. Kubota Y, Shitara K. Zolbetuximab for claudin18.2-positive gastric or gastroesophageal junction cancer. Ther Adv Med Oncol 2024; 16: 17588359231217967.
27. Gaitan-Penas H, Apaja PM, Arnedo T, et al. Leukoencephalopathy-causing *CLCN2* mutations are associated with impaired Cl(-) channel function and trafficking. J Physiol 2017; 595: 6993-7008.
28. Caron TJ, Scott KE, Sinha N, et al. Claudin-18 loss alters transcellular chloride flux but not tight junction ion selectivity in gastric epithelial cells. Cell Mol Gastroenterol Hepatol 2021; 11: 783-801.
29. Hagen SJ, Ang LH, Zheng Y, et al. Loss of tight junction protein Claudin 18 promotes progressive neoplasia development in mouse stomach. Gastroenterology 2018; 155: 1852-67.
30. Chiaramonte R, Sauro G, Giannandrea D, Limonta P, Casati L. Molecular insights in the anticancer activity of natural tocotrienols: targeting mitochondrial metabolism and cellular redox homeostasis. Antioxidants (Basel) 2025; 14: 115.
31. Wu J, Lu J, Chen Q, Chen H, Zheng Y, Cheng M. Pan-cancer analysis of CLDN18.2 shed new insights on the targeted therapy of upper gastrointestinal tract cancers. Front Pharmacol 2024; 15: 1494131.
32. Banushi B, Joseph SR, Lum B, Lee JJ, Simpson F. Endocytosis in cancer and cancer therapy. Nat Rev Cancer 2023; 23: 450-73.
33. Basagiannis D, Zografou S, Murphy C, et al. VEGF induces signalling and angiogenesis by directing VEGFR2 internalisation through macropinocytosis. J Cell Sci 2016; 129: 4091-104.
34. Wu B, Wang Q, Li B, Jiang M. LAMTOR1 degrades MHC-II via the endocytic in hepatocellular carcinoma. Carcinogenesis 2022; 43: 1059-70.
35. Ogawa H, Abe H, Yagi K, Seto Y, Ushiku T. Claudin-18 status and its correlation with HER2 and PD-L1 expression in gastric cancer with peritoneal dissemination. Gastric Cancer 2024; 27: 802-10.
36. Wang C, Wang Y, Chen J, et al. CLDN18.2 expression and its impact on prognosis and the immune microenvironment in gastric cancer. BMC Gastroenterol 2023; 23: 283.
37. Cho Y, Ahn S, Kim KM. PD-L1 as a biomarker in gastric cancer immunotherapy. J Gastric Cancer 2025; 25: 177-91.

JPTM
ORIGINAL ARTICLE
pISSN 2383-7837 · eISSN 2383-7845
Journal of Pathology and Translational Medicine 2026; 60: 58-68
https://doi.org/10.4132/jptm.2025.09.12

The significance of papillary architecture in the follow-up biopsies of patients with progestin-treated atypical endometrial hyperplasia

Wangpan J. Shi, Oluwole Fadare

Department of Pathology, University of California San Diego, San Diego, CA, USA

Graphical abstract

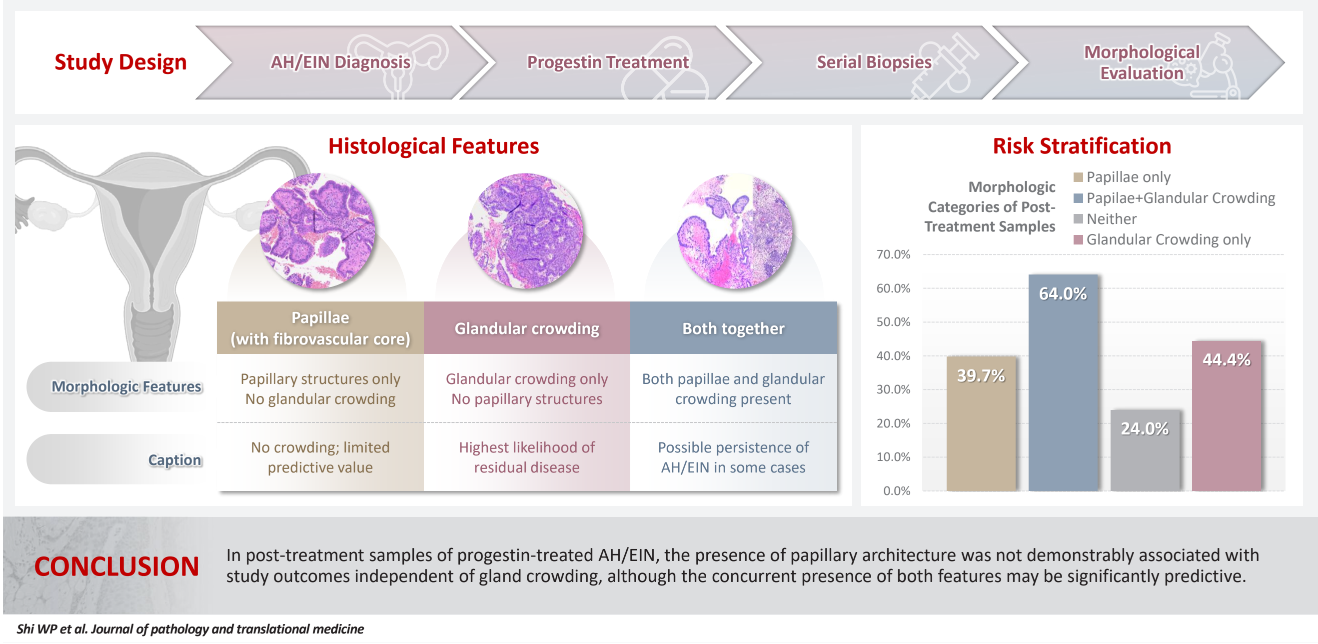

	Papillae (with fibrovascular core)	Glandular crowding	Both together
Morphologic Features	Papillary structures only No glandular crowding	Glandular crowding only No papillary structures	Both papillae and glandular crowding present
Caption	No crowding; limited predictive value	Highest likelihood of residual disease	Possible persistence of AH/EIN in some cases

CONCLUSION In post-treatment samples of progestin-treated AH/EIN, the presence of papillary architecture was not demonstrably associated with study outcomes independent of gland crowding, although the concurrent presence of both features may be significantly predictive.

Shi WP et al. Journal of pathology and translational medicine

JPTM

ORIGINAL ARTICLE

pISSN 2383-7837 · eISSN 2383-7845

Journal of Pathology and Translational Medicine 2026; 60: 58-68
https://doi.org/10.4132/jptm.2025.09.12

The significance of papillary architecture in the follow-up biopsies of patients with progestin-treated atypical endometrial hyperplasia

Wangpan J. Shi, Oluwole Fadare

Department of Pathology, University of California San Diego, San Diego, CA, USA

Background: Follow-up biopsies in patients with progestin-treated atypical endometrial hyperplasia/endometrioid intraepithelial neoplasia (AH/EIN) may show papillary structures, the significance of which is unclear. **Methods:** The authors reviewed 253 serial specimens of 84 consecutive patients diagnosed with AH/EIN, inclusive of each patient's pre-progestin treatment sample and all post-treatment specimens. We assessed the predictive relationship between papillary architecture in a post-treatment biopsy and two study outcomes: AH/EIN or carcinoma in at least one sample subsequent to the one in which papillae were identified, and/or the last specimen received for that patient. **Results:** Papillae were identified in only 51.5% of pre-treatment samples but were present in at least one subsequent post-treatment sample for all patients. Post-treatment samples that exhibited papillae and no glandular crowding were associated with AH/EIN in at least one subsequent specimen in 39.7% (29/73) of cases, compared to 24.0% (6/25) in samples with neither papillae nor glandular crowding ($p = .227$) and 64.0% (16/25) in samples with concurrent gland crowding and papillae ($p = .048$). Univariate logistic regression analyses showed that the presence of papillae was not associated with study outcomes (odds ratio [OR], 0.99; 95% confidence interval [CI], 0.49 to 1.99; $p = .985$), as compared with gland crowding (OR, 1.54; 95% CI, 1.04 to 2.27; $p = .031$), or concurrent papillae and gland crowding (OR, 2.36; 95% CI, 1.01 to 5.52; $p = .048$). **Conclusions:** In post-treatment samples of progestin-treated AH/EIN, the presence of papillary architecture was not demonstrably associated with study outcomes independent of gland crowding, although the concurrent presence of both features may be significantly predictive.

Keywords: Endometrium; Progestins; Atypical endometrial hyperplasia

INTRODUCTION

Atypical endometrial hyperplasia/endometrioid intraepithelial neoplasia (AH/EIN) is generally considered to be the immediate precursor lesion to endometrial endometrioid carcinoma, one that confers a substantial risk of concurrent carcinoma or if left untreated, progression [1-7]. Surgical resection of the uterus is widely recognized as definitive treatment for AH/EIN [8]. However, for women who desire fertility, are poor surgical candidates due to medical comorbidities, or who decline surgical intervention for other reasons, progestin therapies have gained widespread use in recent decades [8-10]. Progestin-based therapies may include medroxyprogesterone acetate, depot medroxyprogesterone, micronized vaginal progesterone, megestrol acetate, and a levonorgestrel intrauterine system, among others [3,9,10]. Patients on progestin-based therapies require close surveillance and follow-up biopsies to assess for efficacy of treatments, as inferred from the persistence, regression or

---

Received: June 10, 2025 **Revised:** September 9, 2025 **Accepted:** September 12, 2025

Corresponding Author: Oluwole Fadare, MD
Department of Pathology, Anatomic Pathology Division, University of California San Diego Health, 9300 Campus Point Drive, Suite 1-200, MC 7723, La Jolla, CA 92037, USA
Tel: +1-858-657-6772, Fax: +1-858-657-5495, E-mail: Oluwole.fadare@gmail.com

*A preliminary version of this work was presented at the Annual Meeting of the United States and Canadian Academy of Pathologists Annual Meeting, Boston, MA, USA, March 2025.

This is an Open Access article distributed under the terms of the Creative Commons Attribution Non-Commercial License (https://creativecommons.org/licenses/by-nc/4.0/) which permits unrestricted non-commercial use, distribution, and reproduction in any medium, provided the original work is properly cited.
© 2026 The Korean Society of Pathologists/The Korean Society for Cytopathology

progression of disease [1,9-11]. The pathologist's determination is arguably central to this process, which highlights the importance of accuracy, reproducibility, and consistency of reporting in the evaluation of those follow-up biopsies [11-14]. However, although the diagnostic criteria for AH/EIN are relatively well established, progestin treatments may induce cytoarchitectural changes therein that render those derangements more difficult to recognize, criteria more challenging to apply, and that overall may engender significant uncertainty about the presence or absence of residual disease in a given sample [11,12,15,16]. One particular architectural alteration that may be encountered in the follow-up endometrial samples of a patient on progestin treatment is papillary change, especially when devoid of concurrent glandular crowding. The significance of these structures, and whether they truly denote residual hyperplasia, has never been fully defined. This study aims to comprehensively characterize the significance of papillary structures in this setting.

MATERIALS AND METHODS

Case selection

The laboratory information system at an academic medical center was queried for all diagnosed cases of AH/EIN during a 10-year period. From an initial dataset, we excluded cases in which the diagnosis of AH/EIN was not made in a sampling specimen, duplications, patients with no follow-up samples subsequent to the index biopsy, patients with index diagnoses of non-atypical hyperplasia, and patients with a diagnosis of AH/EIN concurrent with carcinoma. Various subsidiary analyses called for analysis-specific exclusions, as detailed in Fig. 1. For this report, a "sample" refers to tissue from an endometrial biopsy or curettage, whereas "specimen" refers to tissue from an endometrial biopsy, endometrial curettage, or uterus resection. The sample on which the original diagnosis of AH/EIN was rendered is the "index" or "pre-treatment" sample, whereas samples obtained on follow-up (i.e., after the initiation of treatment) are referred to as "post-treatment" or "follow-up" samples.

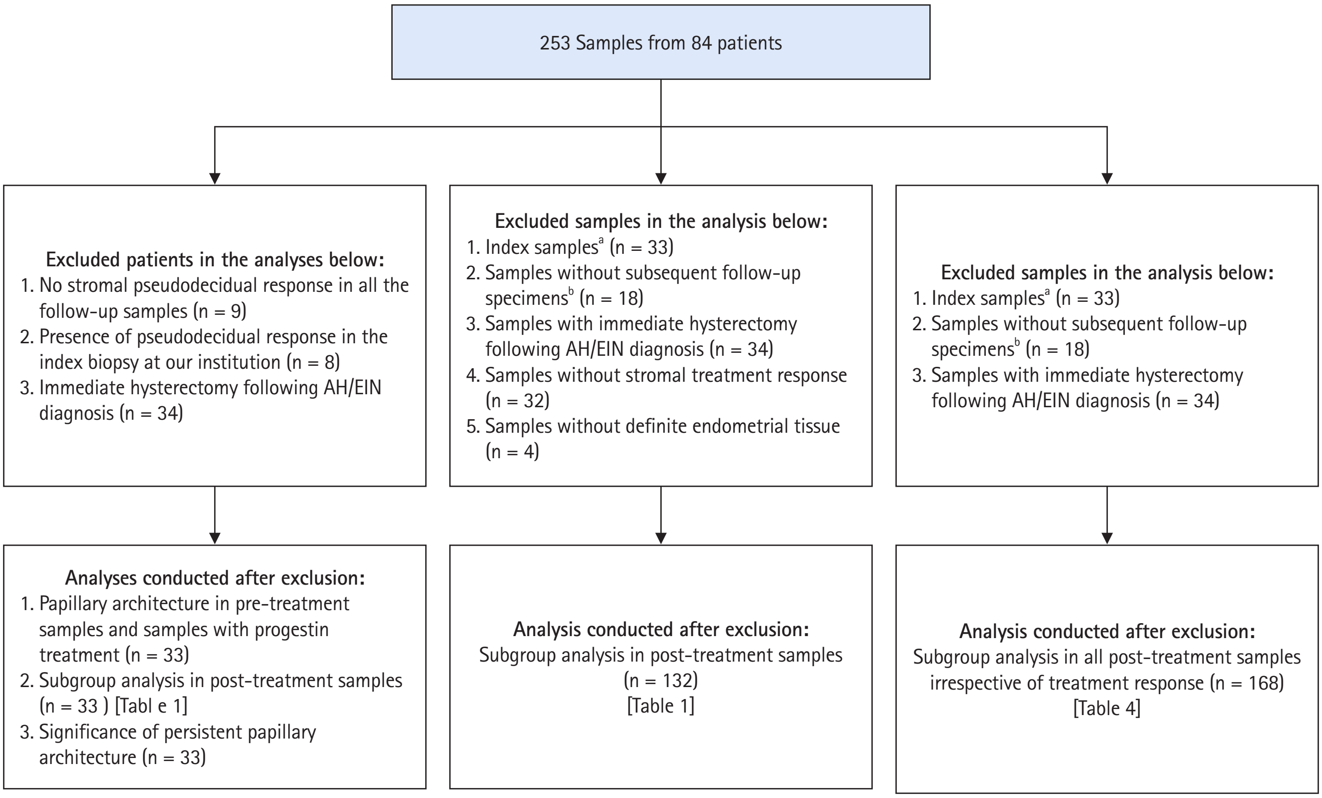

Fig. 1. Analysis-specific exclusion diagram based on patients and samples. AH/EIN, atypical endometrial hyperplasia/endometrioid intraepithelial neoplasia. [a]Pretreatment samples; [b]Significance of papillae cannot be determined given the absence of follow-up specimens.

Morphologic review

Slides for all samples (mean, 3.0 ± 2.5 slides/patient) were retrieved and reviewed jointly by the authors, inclusive of the index and all follow-up samples, with the aim of identifying the presence of papillary architecture of any type, describing their morphologic spectrum, and any concurrent pathological processes that may be present. For every case, we documented the presence of papillary structures and estimated the proportion of the specimen that they represented. A papillary structure was defined as a round, oval or filigree structure, at least 75% covered by epithelium, and harboring a stromal or fibrovascular core (Fig. 2). Large bulbous, polypoid structures

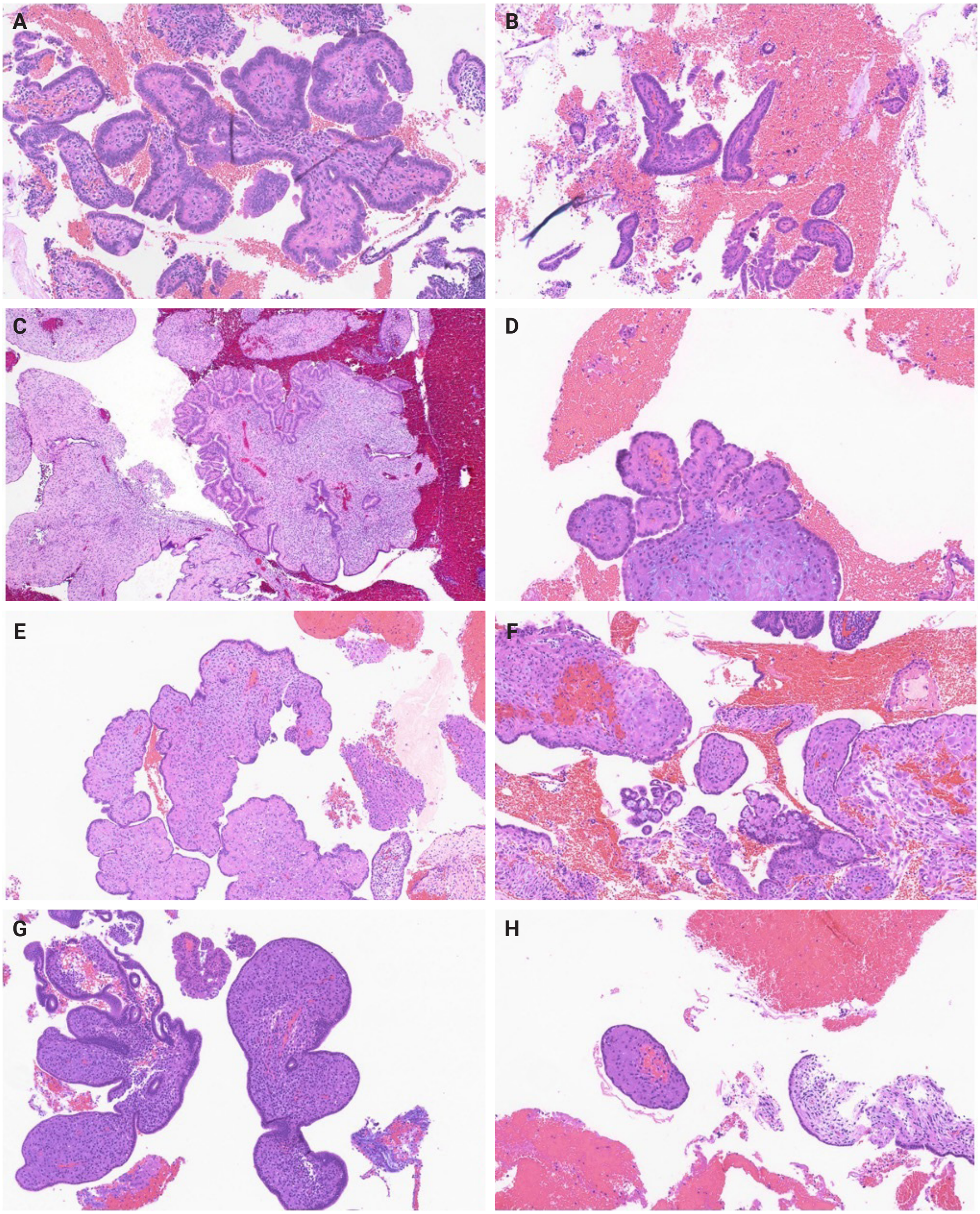

Fig. 2. Morphologic spectrum of papillae with morphologic variations (A–H).

with prominently pseudodecidualized stroma were not included, given that it is well recognized that such structures are common endometrial alterations associated with exogenous progestins in non-hyperplastic endometrium (Fig. 3) [17,18]. Additionally, we documented for each sample the presence of papillae branching as a surrogate indicator of architectural complexity, with subcategorization to no branching, simple (one level) branching off a central stalk irrespective of the number of such branches, and complex (≥two level) branching (i.e. the presence in the sample of at least one central stalk that gives rise to a primary branch, from which a secondary and possibly tertiary branch originate). We also evaluated other morphologic features that are relevant to the diagnoses of AH/EIN, including glandular crowding, cytologic demarcation/atypia, intraglandular architectural complexity, squamous morules, metaplastic changes, cystic structures (presence, whether they are crowded, and whether they are lined by atrophic-appearing or non-atrophic appearing epithelium), and pseudodecidual stromal change.

Follow-up and analytic outcomes

The central study questions were (1) whether the presence of papillary architecture in any sample was significantly associated with an increased likelihood of residual AH/EIN or carcinoma in subsequent specimens for that patient; (2) whether papillae characteristics: complexity of papillae, volume of papillae were similarly associated with an increased likelihood of residual AH/EIN or carcinoma in subsequent specimens for that patient. Accordingly, papillary architecture was not used in our analytic definition of AH/EIN. Rather, AH/EIN in post-treatment samples was defined primarily by criteria outlined in the 5th edition of the World Health Organization Classification, i.e., cytologically-demarcated glandular confluence/crowding (i.e., area of glands exceeds the stroma) [19]. We utilized two outcomes to assess for the significance of papillary architecture in post-treatment specimens. Outcome-1 was defined by the presence of AH/EIN or carcinoma in at least one sample subsequent to the sample in which the papillary structures were identified. Outcome-2 was defined by the presence of AH/EIN or carcinoma in the last specimen that was received for that patient. The dualistic outcomes facilitated a more robust assessment of any AH/EIN or carcinoma that were subsequent to the identification of papillary structures in a post-treatment sample, inclusive of those from patients that went to hysterectomy after the sample in which papillae were identified, as well as those from patients that continued to receive follow-up samplings and that never underwent a resection.

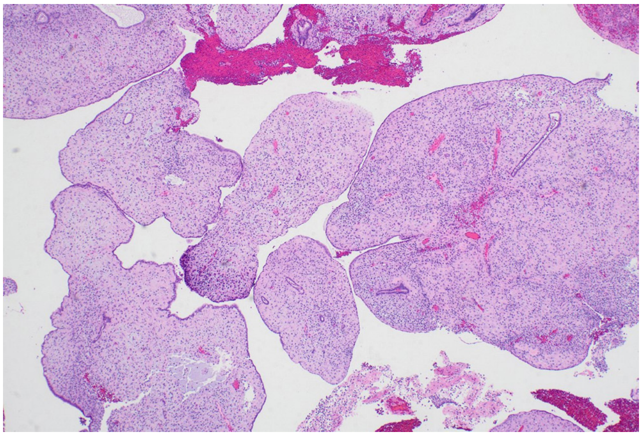

Fig. 3. Large bulbous, polypoid structures with prominently pseudodecidualized stroma were not classified as displaying papillary architecture for the purposes of this study, given that it is well recognized that such structures are common endometrial alterations associated with exogenous progestins in non-hyperplastic endometrium.

Statistics

SPSS ver. 29.0.2.0 software (IBM Corp., Armonk, NY, USA) was used for statistical analyses. Categorical and continuous variables were assessed using Chi-square tests and independent T-tests, respectively. For analysis that included small numbers, the Fisher exact test was used. A univariate logistic regression analysis was conducted to further evaluate any association between papillae, gland crowding, and the concurrent presence of both with study outcomes. $p < .05$ was considered statistically significant in all analyses.

RESULTS

General description of the cohort

In total, we studied 253 specimens from 84 patients with a diagnosis of AH/EIN in a sampling specimen. The average age of these patients was 52.4 years (± 14.7). Thirty-four of the 84 patients (40.5%) underwent a hysterectomy immediately after their index biopsies, whereas the remaining 50 (59.5%) were treated with various oral and intrauterine progestins, followed by follow-up biopsies. Among the latter group, 14.3% ultimately underwent a hysterectomy.

Papillary architecture in pre-treatment samples and samples with progestin treatment

Among the 33 index endometrial samples, 17 (51.5%) had at least focal papillary architecture. The average percentage of index samples displaying papillary architecture was 11.2% (± 12.1) when present. Papillary architecture was present in at least one post-treatment sample of every patient irrespective of the presence or absence of such architecture in their pre-treatment samples. Group analysis of the 33 patients showed that as a group, papillary architecture was observed more frequently in post-treatment samples than in pretreatment samples (89.2% vs. 51.5%, p = .001). Furthermore, the average percentage of the sample comprised of papillae was substantially higher in the post-treatment than in the pretreatment samples (23.8 ± 19.0 vs. 11.2 ± 12.1, p = .001).

Subgroup analysis in post-treatment samples

In this subgroup analysis, we sought to determine the significance of papillary architecture (separate from gland crowding) in post-treatment samples by evaluating their association with AH/EIN or carcinoma in at least one subsequent specimen. Accordingly, in addition to the sample in which the papillae were identified, the index/pretreatment samples and the last biopsy sample for each patient were excluded as the former were irrelevant and the latter constituted an analytic end point for patients that never underwent a resection. The post-treatment samples were categorized into four groups in Table 1. Briefly, the percentage of samples with AH/EIN or carcinoma in at least one sample subsequent to the one in which papillae were initially identified, were 39.7%, 64.0%, 24.0%, and 44.4% respectively for group 1 (papillae present, gland crowding absent), group 2 (papillae and gland crowding both present), group 3 (gland crowding and papillae were both absent) and group 4 (gland crowding present, papillae absent). When the 4 groups were compared to each other regarding the frequency of outcome-1 (i.e. AH/EIN or carcinoma in at least one subsequent sample), the group 2 versus group 3 comparison showed a statistically significant difference (64.0% vs. 24.0% respectively; p = .010); Concurrent gland crowding and papillae (group 2) was associated with a significantly higher rate of outcome results compared to papillae alone (group 1) (64.0% vs. 39.7%, p = .040). Also notable was the absence of any significant difference between group 1 and group 3 regarding the frequency of the study outcomes. Results from a univariate logistic regression analysis showed that the presence of papillary architecture was not significantly associated with study outcomes (odds ratio [OR], 0.99; 95% confidence interval [CI], 0.49 to 1.99; p =.985), in contrast with glandular crowding (OR, 1.54; 95% CI, 1.04 to 2.27; p = .031), and the concurrent presence of papillae and glandular crowding (OR, 2.36; 95% CI, 1.01 to 5.52; p = .048). In a subsidiary analysis in which the cohort were grouped based only on the first post-treatment sample, concurrent gland crowding and papillae (group 2) was associated with a significantly higher rate of outcome results compared to papillae alone (group 1) (91.6% vs. 42.8%, p = .009) (Table 2).

Analysis of post-treatment samples from group 1 patients

Group 1 cases (papillary architecture and no gland crowding in a post-treatment sample) were more expansively assessed, since their significance constituted a central study question. There were 73 post-treatment samples from 21 patients in this group. We assessed the association of various papillae features (percentage of sample with papillary architecture, complexity of papillae) with two outcome measures (outcome-1, outcome-2) compared to controls (absence of AH/EIN or carcinoma in any follow-up specimen). Findings are detailed in Table 3, and show that (1) the proportion of the sample with papillary architecture

Table 1. Categorization of follow-up samples based on papillary architecture and/or gland crowding, and their association with the finding of AH or carcinoma in at least one subsequent specimen

Study groupings of selected post-treatment samples	Samples with residual atypical hyperplasia or carcinoma in at least one subsequent specimen
Group 1: Follow up biopsies with papillary architecture and no gland crowding (n = 73)	29/73 (39.7)
Group 2: Follow up biopsies with concurrent papillary architecture and gland crowding (n = 25)	16/25 (64.0)
Group 3: Follow up biopsies with no papillary architecture or gland crowding (n = 25)	6/25 (24.0)
Group 4: Follow up biopsies with gland crowding and no papillary architecture (n = 9)	4/9 (44.4)

Values in parentheses indicate percentages.
Group 1 vs. 2 (p = .040); group 1 vs. 3 (p = .227); group 2 vs. 3 (p = .010); group 1 vs. 4 (p > .99); group 2 vs. 4 (p = .435); group 3 vs. 4 (p = .395).
AH, atypical endometrial hyperplasia.

Table 2. Categorization of patients based on papillary architecture and/or gland crowding on the first post-treatment sample, and their association with the finding of AH or carcinoma in at least one subsequent specimen

Study groupings of patients based on the first post-treatment sample	Samples with residual atypical hyperplasia or carcinoma in at least one subsequent specimen
Group 1: Follow up biopsies with papillary architecture and no gland crowding (n = 21)	9/21 (42.8)
Group 2: Follow up biopsies with concurrent papillary architecture and gland crowding (n = 12)	11/12 (91.6)
Group 3: Follow up biopsies with no papillary architecture or gland crowding (n = 10)	6/10 (60.0)
Group 4: Follow up biopsies with gland crowding and no papillary architecture (n = 7)	2/7 (28.5)

Values in parentheses indicate percentages.
Group 1 vs. 2 (p = .009); group 1 vs. 3 (p = .458); group 2 vs. 3 (p = .135); group 1 vs. 4 (p = .668); group 2 vs. 4 (p = .010); group 3 vs. 4 (p = .335).
AH, atypical endometrial hyperplasia.

Table 3. Analysis of the significance of papillae in group 1 post-treatment specimens

(Group 1, "primary sample") Post-treatment samples with papillary architecture and no gland crowding	Residual AH/carcinoma in the last specimen, outcome-2 (n = 13)	Residual AH/carcinoma in any specimen subsequent to primary sample, outcome-1 (n = 28)	No residual AH or carcinoma in any specimen subsequent to the primary sample (n = 44)	p-value
Mean percentage of papillary architecture in the sample	37.5 ± 20.4	30.9 ± 18.9	19.8 ± 17.2	.003
Papillae with any branching present	8/13 (61.5)	20/28 (71.4)	29/44 (65.9)	.799
Surface micropapillae present	3/13 (23.1)	5/28 (17.8)	4/44 (9.1)	.350
Surface micropapillae with any branching	2/13 (15.4)	3/28 (10.7)	3/44 (6.8)	.623
Complex papillae (>1 branching) present	0/13 (0)	4/28 (14.3)	2/44 (4.5)	.162

Values are presented as mean ± standard deviation and values in parentheses indicate percentages. AH, atypical endometrial hyperplasia.

was significantly higher than controls for those group 1 patients that were found to have AH/EIN or carcinoma in a subsequent sample; (2) neither the presence nor degree of papillae branching significantly distinguished cases that were ultimately associated with outcome-1 and 2 from those that were not.

Significance of papillary architecture "persistence"

For current analytic purposes, persistence of papillary architecture was defined as the scenario wherein at least two post-treatment biopsies showed papillary architecture in the absence of concurrent glandular crowding. Among the 33 patients who had index biopsies with post-treatment samples, 20/33 (60.7%) had more than two follow-up samples taken (not inclusive of the final sample or resection specimen). Among these patients, 16/20 (80.0%) had persistent papillary architecture, 11/33 (33.3%) had one follow-up sample with papillary architecture, and 6/33 (18.2%) had follow-up samples without persistent papillary architecture. The frequency of outcomes-1 or -2 in these three groups were 43.7%, 36.4%, and 33.3%, respectively (p > .99). A representative case in which there was persistent papillary architecture in nine post-treatment samples over time is shown in Fig. 4.

Microscopic findings in post-treatment samples associated with residual AH/EIN or carcinoma

Table 4 outlines findings from a subsidiary analysis that was designed to identify morphologic findings that were significantly more prevalent in the group of samples for which there was a diagnosis of AH/EIN or carcinoma in a subsequent specimen (i.e., outcomes-1 and –2) irrespective of progestin-treatment response. Sixty-seven post-treatment samples for which there was a subsequent diagnosis of AH/EIN or carcinoma (in a post-treatment biopsy or resection specimen, study group) were compared with 101 post-treatment samples for which there were no subsequent diagnoses of AH/EIN or carcinoma (control group), regarding a variety of morphologic findings. Features that were significantly more prevalent in the study group include glandular crowding, glandular crowding concurrent with papillae, and cytologic demarcation. Table 4 also shows that there was no linear association between the percentage of the sample with papillary architecture and the likelihood of residual AH/EIN or carcinoma in subsequent specimens. Briefly, papillae in >10% and >20% (but not >30% or >40%) of the sample were more significantly more frequent in the study group than the control group. However, even at the >10% or >20% levels,

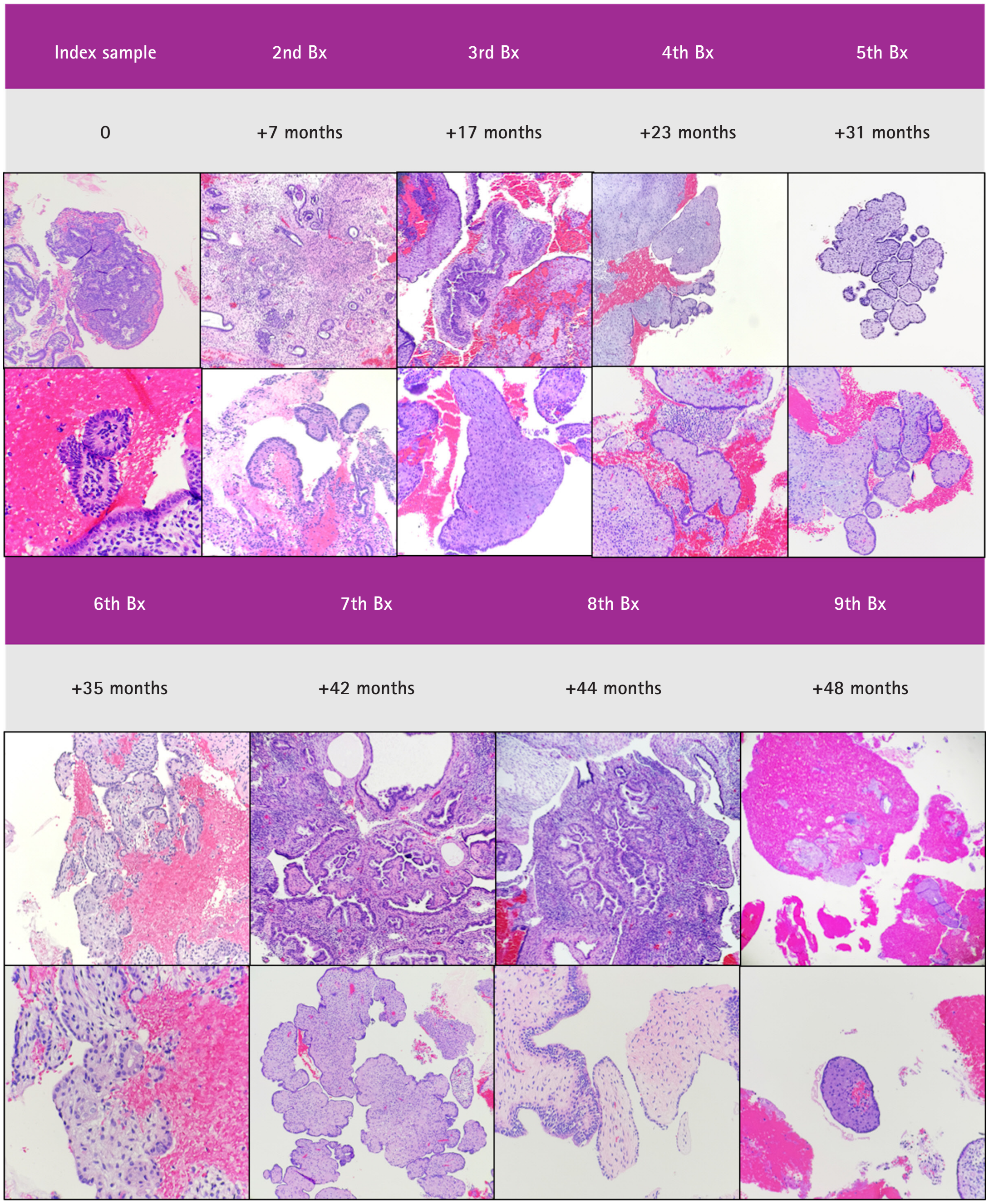

Fig. 4. A representative patient whose follow-up biopsies (Bx) showed persistence of papillary architecture of various types over an extended period.

the addition of concurrent glandular crowding eliminates the statistical significance of the difference between the study and control groups. The presence of squamous morules, crowded cysts, mucinous metaplasia, degree of papillary branching, or surface micropapillae showed no statistically significant difference in frequency between the two groups.

DISCUSSION

A wide variety of cytoarchitectural alterations may be observed in samples of progestin-treated AH/EIN, including a relative decrease in gland-to-stroma ratio, nuclear size, mitotic index, and nucleus-to-cytoplasm ratio, “acquisition” of various meta-

Table 4. Analysis of all post-treatment specimens irrespective of progestin-treatment response

All post-treatment samples (n = 168)	AH or carcinoma present in any subsequent specimen (n = 67)	Absence of AH or carcinoma in any subsequent specimen (n = 101)	p-value
Presence of papillae	48/67 (71.6)	71/101 (70.3)	.851
Gland crowding	28/67 (41.8)	24/101 (23.8)	.013
Percentage of sample with papillae	21.3 ± 22.3	13.8 ± 21.3	.031
Gland crowding and papillae	15/67 (22.4)	10/101 (10.0)	.045
Papillae in >40% of the sample	15/67 (22.4)	15/101 (14.9)	.212
Papillae in >40% of the sample and no gland crowding	11/67 (16.4)	11/101 (10.9)	.298
Papillae in >30% of the sample	21/67 (31.3)	22/101 (21.8)	.164
Papillae in >30% of the sample and no gland crowding	15/67 (22.4)	17/101 (16.8)	.369
Papillae in >20% of the sample	27/67 (40.3)	22/101 (21.8)	.010
Papillae in >20% of the sample and no gland crowding	18/67 (26.8)	17/101 (16.8)	.117
Papillae in >10% of the sample	37/67 (55.2)	29/101 (28.7)	.001
Papillae in >10% of the sample and no gland crowding	25/67 (37.3)	33/101 (32.6)	.700
Number of branching papillae	30/67 (44.8)	33/101 (32.6)	.113
Complex branching	5/67 (7.5)	2/101 (2.0)	.082
Simple branching	25/67 (37.3)	31/101 (30.7)	.373
No branching	37/67 (55.2)	68/101 (67.3)	.113
Surface micropapillae	9/67 (13.4)	5/101 (5.0)	.084
Surface micropapillae with any branching papillae	9/67 (13.4)	4/101 (3.9)	.037
Cytological demarcation	27/67 (40.3)	13/101 (12.9)	.001
Morules	15/67 (22.4)	12/101 (11.9)	.597
Crowded cysts	8/67 (11.9)	9/101 (8.9)	.246
Mucinous/columnar metaplasia	21/67 (31.3)	19/101 (18.8)	.062

Values in parentheses indicate percentages and values are presented as mean ± standard deviation.
AH, atypical endometrial hyperplasia.

plasias (including increase in cytoplasmic eosinophilia), changes in chromatin pattern and prominence of nucleoli, surface micropapillary architecture, glandular cystic dilatation, and in some cases, an apparent "increase" in architectural complexity relative to the pre-treatment sample [15,16]. The diagnostic challenge for the pathologist is in the identification and "interpretation" of individual features or combinations of features, and how well such interpretations predict the likelihood that disease is present. A 2022 survey suggests that there remains significant interobserver variability amongst practitioners in these interpretations [12].

In the current study, the authors evaluate the significance of a specific architectural alteration that in our experience, is not uncommonly observed in this setting: papillary change. A few studies have previously addressed the issue, albeit peripherally: In one study of progestin-treated AH/EIN and carcinoma, "cribriform/papillary changes" were noted to be present in 59.1% of the patient samples associated with eventual complete response to treatment, as compared with 40.9% of those without complete response, and the presence of "cribriform or papillary glandular pattern" was not associated with complete response on univariate analyses [20]. In another study, "cribriform and/or papillary pattern" were presumed to be indicative of glandular confluency for analytic purposes [15]. Mentrikoski et al. [16] noted that prominent papillae may be observed in this setting after several months of treatment. Finally, the authors of the aforementioned survey on the issue considered "foci of crowded glands and/or papillary architecture" to be indicative of residual hyperplasia [12]. None of the above studies, however, specifically assessed papillary change as an individual variable. In the current study, we made no baseline assumptions about the significance of papillary architecture, but sought to determine what the presence, qualitative, and quantitative features of such architecture might indicate in a post-treatment sample regarding the likelihood of residual hyperplasia (defined by glandular crowding/confluency) or carcinoma in subsequent samples and specimens.

We highlight a few central findings: First, although papillae were present in only 51.5% of index (pre-treatment) samples, they were present in at least one post-treatment sample for every patient independent of their presence or absence in the corresponding pre-treatment sample. This finding suggests that papillary architecture in the studied setting is a change that develops, or becomes more apparent with progestin-treatment. When index and post-treatment biopsies were compared, the latter showed a significantly higher frequency of papillary architecture. Findings from our analysis of the four post-treatment groups, including the most study-germane group 1, addresses the central study questions. Our study showed that in group 1 samples (papillae and no gland crowding), 39.7% showed AH/EIN or carcinoma in at least one subsequent specimen. However, corresponding proportions in samples without any abnormalities (group 3) and samples with glandular crowding only (group 4) were 24.0% and 44.4% respectively. Notably, group 1 was not associated with a significantly higher frequency of the AH/EIN or carcinoma end points than group 3, casting doubt on the significance of papillae as an isolated variable in a post-treatment sample (i.e., in the absence of concurrent glandular crowding). More extensive analysis of group 1 cases highlighted the significance of the various papillae types. This analysis showed that the average percentage of samples with papillae was significantly higher in samples that were associated with outcomes-1 and -2 than those that were not (Table 3). Therefore, we considered the possibility that it is the “extensiveness” of papillary architecture that is significant, rather than the mere “presence” of papillary architecture. Our group analysis of all post-treatment samples, as outlined in Table 4, compared the frequencies of various pathologic features in patients with and without the analytic end-point (AH/EIN or carcinoma in a subsequent specimen). The frequency of papillary architecture was not significantly different between the two groups. Although more extensive papillary growth was seen in patient with a diagnosis of AH/EIN or carcinoma in a subsequent sample than in patients without such diagnoses, this was not independent of glandular crowding. Moreover, incrementally extensive presence of papillary growth was not clearly associated with residual AH/EIN or carcinoma. The practical implication of these findings may be that a post-treatment sample that displays papillary architecture as the only abnormal finding simply raises the possibility of unsampled glandular crowding but is not in and of itself diagnostic of residual hyperplasia. In the current analysis, the OR for study outcomes in the papillae + glandular crowding group was higher than the OR for the glandular crowding group, raising the possibility that the addition to papillae to glandular crowding increases the risk of study outcomes than would otherwise be associated with glandular crowding alone. However, the margin of error for that subsidiary analysis was estimated to be high given the wide confidence interval. As such, analyses with larger datasets will be required to conclusively settle the question.

The present study has some additional limitations that should be considered when assessing the significance of the findings. Although we evaluated a large number of samples, the overall cohort size is relatively small, which limited consideration of potentially relevant variables such as highly complex papillae or necrotic papillae, both of which had a low prevalence in our cohort. Second, our outcome measures may be distorted if papillae are indeed a manifestation of hyperplasia, since we excluded papillae in our definition of AH/EIN to allow for an analysis of its significance. A follow-up sample inherently only gives a partial portrait of the disease in the uterus when the biopsy was taken, and it is unclear whether a longer follow-up timeline than was present in our cohort is required to identify the significance of papillary structures. Molecular and immunohistochemical biomarkers of potential utility were not considered due to the intentional emphasis on morphologic features and the current inability of aberrant phenotypes to serve as a diagnostic gold standard. Duration of treatment and biopsy sample intervals were not specifically analyzed given the size of our sample as well as the fact the decision faced by the diagnostic pathologist on the significance of a papillary structure in a given sample is not significantly influenced by these factors. The key strength of the study is that it is the first to comprehensively analyze this group of patients and that specifically assessed the significance of papillary architecture in the setting of progestin-treatment surveillance.

In summary, in post-treatment samples of AH/EIN, the presence of papillary architecture in and of itself was not associated with a significantly higher likelihood of AH/EIN or carcinoma in a subsequent specimen, compared to specimens without any abnormalities. Glandular crowding, as well as glandular crowding concurrent with papillae, were found to be predictors of subsequent residual AH/EIN or carcinoma in this setting.

Ethics Statement

Research involving Human Participants and/or Animals: This work was approved by the Human Research and Protection Program at the University of California San Diego (IRB#190068 and #191204), along with a waiver of consent.

Availability of Data and Material

The datasets generated or analyzed during the study are available from the corresponding author on reasonable request.

Code Availability

Not applicable.

ORCID

Wangpan J. Shi	https://orcid.org/0000-0002-9538-9535
Oluwole Fadare	https://orcid.org/0000-0001-8017-2854

Author Contributions

Conceptualization: WJS, OF. Data curation: WJS, OF. Formal analysis: WJS, OF. Investigation: WJS, OF. Funding acquisition: WJS, OF. Methodology: WJS, OF. Project administration: WJS, OF. Resources: WJS, OF. Software: WJS, OF. Supervision: OF. Validation: WJS, OF. Visualization: WJS. Writing—original draft: WJS, OF. Writing—review & editing: WJS, OF. Approval of final manuscript: all authors.

Conflicts of Interest

The authors declare that they have no potential conflicts of interest.

Funding Statement

No funding to declare.

REFERENCES

1. Lacey JV Jr, Sherman ME, Rush BB, et al. Absolute risk of endometrial carcinoma during 20-year follow-up among women with endometrial hyperplasia. J Clin Oncol 2010; 28: 788-92.
2. Giannella L, Grelloni C, Bernardi M, et al. Atypical endometrial hyperplasia and concurrent cancer: a comprehensive overview on a challenging clinical condition. Cancers (Basel) 2024; 16: 914.
3. Ring KL, Mills AM, Modesitt SC. Endometrial hyperplasia. Obstet Gynecol 2022; 140: 1061-75.
4. Doherty MT, Sanni OB, Coleman HG, et al. Concurrent and future risk of endometrial cancer in women with endometrial hyperplasia: a systematic review and meta-analysis. PLoS One 2020; 15: e0232231.
5. Pennant S, Manek S, Kehoe S. Endometrial atypical hyperplasia and subsequent diagnosis of endometrial cancer: a retrospective audit and literature review. J Obstet Gynaecol 2008; 28: 632-3.
6. Rakha E, Wong SC, Soomro I, et al. Clinical outcome of atypical endometrial hyperplasia diagnosed on an endometrial biopsy: institutional experience and review of literature. Am J Surg Pathol 2012; 36: 1683-90.
7. Trimble CL, Kauderer J, Zaino R, et al. Concurrent endometrial carcinoma in women with a biopsy diagnosis of atypical endometrial hyperplasia: a Gynecologic Oncology Group study. Cancer 2006; 106: 812-9.
8. Management of endometrial intraepithelial neoplasia or atypical endometrial hyperplasia: ACOG clinical consensus No. 5. Obstet Gynecol 2023; 142: 735-44.
9. Chandra V, Kim JJ, Benbrook DM, Dwivedi A, Rai R. Therapeutic options for management of endometrial hyperplasia. J Gynecol Oncol 2016; 27: e8.
10. Kim MK, Seong SJ. Conservative treatment for atypical endometrial hyperplasia: what is the most effective therapeutic method? J Gynecol Oncol 2014; 25: 164-5.
11. Zheng W, Fadare O, Quick CM. Unveiling residual diseases of endometrial precancer/cancer after progestin therapy. In: Zheng W, Fadare O, Quick CM, eds. Gynecologic and obstetric pathology. Singapore: Springer, 2024; 1-34.
12. Ganesan R, Gilks CB, Soslow RA, McCluggage WG. Survey on reporting of endometrial biopsies from women on progestogen therapy for endometrial atypical hyperplasia/endometrioid carcinoma. Int J Gynecol Pathol 2022; 41: 142-50.
13. Williams AT, Ganesan R. Role of the pathologist in assessing response to treatment of ovarian and endometrial cancers. Histopathology 2020; 76: 93-101.
14. Chang RJ, Rivera-Colon G, Chen H, et al. Navigating through perplex morphologic changes after exogenous hormone usage. Semin Diagn Pathol 2022; 39: 148-58.
15. Wheeler DT, Bristow RE, Kurman RJ. Histologic alterations in endometrial hyperplasia and well-differentiated carcinoma treated with progestins. Am J Surg Pathol 2007; 31: 988-98.
16. Mentrikoski MJ, Shah AA, Hanley KZ, Atkins KA. Assessing endometrial hyperplasia and carcinoma treated with progestin therapy. Am J Clin Pathol 2012; 138: 524-34.
17. Phillips V, Graham CT, Manek S, McCluggage WG. The effects of the levonorgestrel intrauterine system (Mirena coil) on endometrial morphology. J Clin Pathol 2003; 56: 305-7.
18. Hejmadi RK, Chaudhri S, Ganesan R, Rollason TP. Morphologic changes in the endometrium associated with the use of the mirena coil: a retrospective study of 106 cases. Int J Surg Pathol 2007; 15: 148-54.

19. Lax SF, Mutter GL. Endometrial atypical hyperplasia/endometrioid intraepithelial neoplasia. In: WHO Classification of Tumours Editorial Board, ed. WHO classification of tumours: female genital tumours. 5th ed. Vol. 4. Lyon: International Agency for Research on Cancer, 2020; 250-1.
20. Gunderson CC, Dutta S, Fader AN, et al. Pathologic features associated with resolution of complex atypical hyperplasia and grade 1 endometrial adenocarcinoma after progestin therapy. Gynecol Oncol 2014; 132: 33-7.

JPTM
ORIGINAL ARTICLE
pISSN 2383-7837 · eISSN 2383-7845
Journal of Pathology and Translational Medicine 2026; 60: 69-82
https://doi.org/10.4132/jptm.2025.09.17

Significance of KM55 immunohistochemical staining in the diagnosis and prognosis of IgA nephropathy

Hoe In Jeong, Beom Jin Lim, Minsun Jung

Departments of Pathology, Yonsei University College of Medicine, Seoul, Korea

Graphical abstract

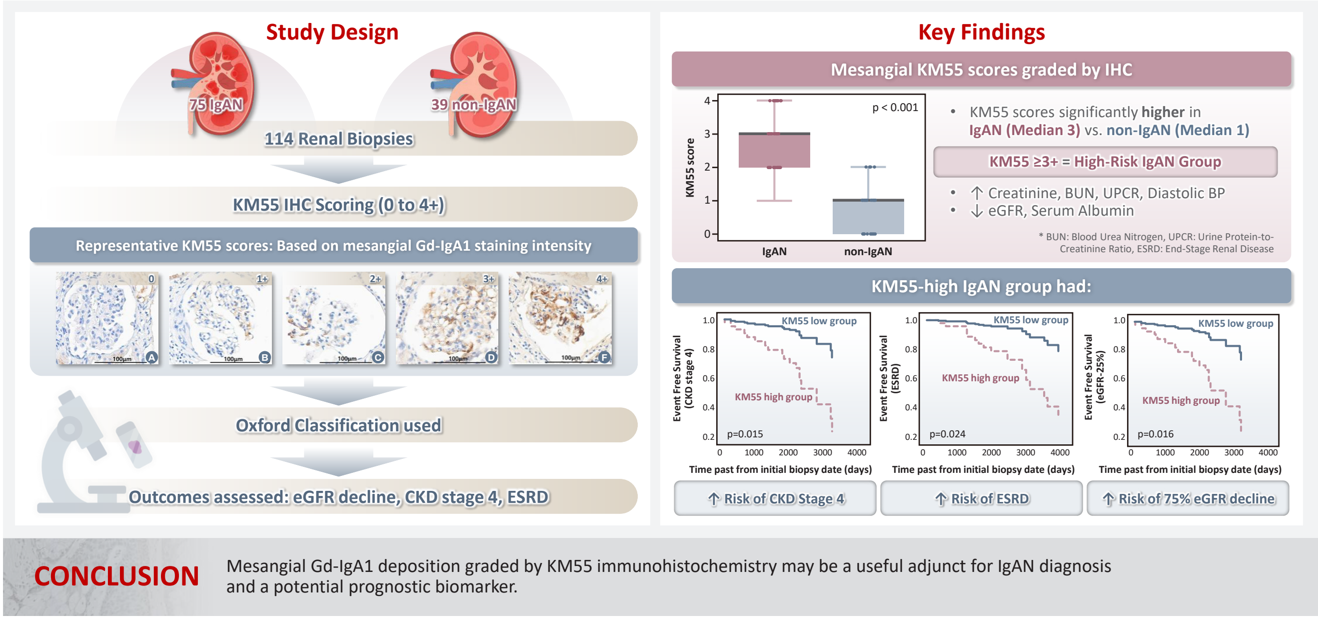

Study Design

75 IgAN · 39 non-IgAN

114 Renal Biopsies

KM55 IHC Scoring (0 to 4+)

Representative KM55 scores: Based on mesangial Gd-IgA1 staining intensity

Oxford Classification used

Outcomes assessed: eGFR decline, CKD stage 4, ESRD

Key Findings

Mesangial KM55 scores graded by IHC

- KM55 scores significantly **higher** in **IgAN (Median 3)** vs. **non-IgAN (Median 1)**

KM55 ≥3+ = High-Risk IgAN Group

- ↑ Creatinine, BUN, UPCR, Diastolic BP
- ↓ eGFR, Serum Albumin

* BUN: Blood Urea Nitrogen, UPCR: Urine Protein-to-Creatinine Ratio, ESRD: End-Stage Renal Disease

KM55-high IgAN group had:

↑ Risk of CKD Stage 4 · ↑ Risk of ESRD · ↑ Risk of 75% eGFR decline

CONCLUSION Mesangial Gd-IgA1 deposition graded by KM55 immunohistochemistry may be a useful adjunct for IgAN diagnosis and a potential prognostic biomarker.

Jeong HI et al. Journal of pathology and translational medicine

JPTM

ORIGINAL ARTICLE

pISSN 2383-7837 · eISSN 2383-7845

Journal of Pathology and Translational Medicine 2026; 60: 69-82
https://doi.org/10.4132/jptm.2025.09.17

Significance of KM55 immunohistochemical staining in the diagnosis and prognosis of IgA nephropathy

Hoe In Jeong, Beom Jin Lim, Minsun Jung

Departments of Pathology, Yonsei University College of Medicine, Seoul, Korea

Background: Galactose-deficient IgA1 (Gd-IgA1) plays a crucial role in IgA nephropathy (IgAN). The monoclonal antibody KM55 has emerged as a simplified method for detecting Gd-IgA1; however, the clinicopathological significance of immunohistochemistry for Gd-IgA1 remains underexplored. This study evaluated the prognostic and clinicopathological significance of KM55 immunohistochemistry in IgAN. **Methods:** A total of 114 native kidney biopsies showing at least mild mesangial IgA positivity on immunofluorescence were retrospectively analyzed. Patients were categorized as having IgAN or non-IgAN diseases. The KM55 immunohistochemical staining was graded as 0, 1+, 2+, 3+, or 4+. Data on Oxford classification, laboratory parameters, and renal outcomes were collected. **Results:** The IgAN group showed significantly higher KM55 scores than the non-IgAN group (median: 3 vs. 1; $p < .001$). IgAN cases were further stratified into KM55-high (≥3+, n = 38) and -low groups (≤2+, n = 37). The KM55-high group had significantly higher diastolic blood pressure, blood urea nitrogen, creatinine, urine protein/creatinine ratio, and Oxford mesangial hypercellularity scores, along with lower estimated glomerular filtration rate (eGFR) and serum albumin. Cox analysis revealed significantly poorer outcomes in the KM55-high group for chronic kidney disease stage 4 ($p = .015$), end-stage renal disease ($p = .024$), and 75% eGFR decline ($p = .016$). **Conclusions:** Mesangial Gd-IgA1 deposition graded by KM55 immunohistochemistry may be a useful adjunct for IgAN diagnosis and a potential prognostic biomarker.

Keywords: Glomerulonephritis, IGA; Galactosyl-deficient IgA1; Immunohistochemistry

INTRODUCTION

IgA nephropathy (IgAN) is the most common glomerular disease worldwide, affecting individuals across all age groups. Its clinical course is highly variable, ranging from asymptomatic spontaneous remission to slow progression, or end-stage renal disease (ESRD) requiring renal replacement therapy. Approximately 30%–40% of adults with IgAN progress to renal failure within 20–30 years of follow-up [1,2]. Current understanding of IgAN pathophysiology highlights a central role for galactose-deficient IgA1 (Gd-IgA1) in disease development [2-4]. Among the two mucosal plasma cell-derived isoforms of IgA, IgA1 and IgA2, IgA1 typically undergoes galactosylation of O-linked N-acetylgalactosamine residues. Defects in this process result in Gd-IgA1 formation. When autoantibodies bind to Gd-IgA1 polymers, immune complexes can deposit in the mesangial matrix, triggering complement activation, mesangial expansion, and cellular proliferation [2,4]. This mechanism has prompted efforts to incorporate serum levels or histologic Gd-IgA1 expression into IgAN diagnosis, emphasizing the need for efficient and specific measuring methods. Yasutake et al. [5] developed a highly specific monoclonal antibody, KM55, which has been successfully used to quantify serum Gd-IgA1 via enzyme-linked immunosorbent assay (ELISA). Unlike traditional lectin-based assays or mass spectroscopy, KM55 is now recognized as a reliable tool for quantitatively detecting Gd-IgA1 in biopsied kidney tissue or serum, independent of bioactivity and stability [3]. In a study by Zhang et al. [3], immunohistochemical (IHC) staining with KM55 showed greater mesangial KM55 deposition in IgAN cases than in controls.

Received: May 7, 2025 **Revised:** September 14, 2025 **Accepted:** September 17, 2025

Corresponding Author: Minsun Jung, MD, PhD
Department of Pathology, Yonsei University College of Medicine, 50-1 Yonsei-ro, Seodaemun-gu, Seoul 03722, Korea
Tel: +82-2-2228-1771, Fax: +82-2-362-0860, E-mail: jjunglammy@yuhs.ac

This is an Open Access article distributed under the terms of the Creative Commons Attribution Non-Commercial License (https://creativecommons.org/licenses/by-nc/4.0/) which permits unrestricted non-commercial use, distribution, and reproduction in any medium, provided the original work is properly cited.
© 2026 The Korean Society of Pathologists/The Korean Society for Cytopathology

However, the comparison lacked systematic numeric scoring and statistical validation. Moreover, a standardized KM55 IHC scoring system and the optimal diagnostic cutoff for IgAN have yet to be established [3]. Martin-Penagos et al. [6] reported that serum Gd-IgA1 levels, measured using KM55, correlated with the risk of progression to chronic kidney disease (CKD) stage 5, suggesting KM55's potential utility in prognostic assessment of IgAN. However, most clinicopathological studies have focused solely on plasma levels. To the best of our knowledge, no robust quantitative study has examined the relationship between mesangium-specific Gd-IgA1 deposition, as measured by KM55 IHC, and clinical or pathological features, such as those defined by the Oxford classification. Furthermore, the correlation between long-term prognosis and the extent of mesangial Gd-IgA1 deposition remains insufficiently explored.

This study employed the KM55 monoclonal antibody to assess the correlation between mesangial Gd-IgA1 deposition and clinicopathologic characteristics in IgAN. Its predictive value for long-term outcomes, particularly progression to ESRD, was evaluated, and the mesangial KM55 staining was compared between IgAN and non-IgAN glomerular diseases.

MATERIALS AND METHODS

Patient selection and grouping

Patients who underwent renal biopsy and received a pathological diagnosis at Severance Hospital (Seoul, Korea) between January 2010 and June 2024 were retrospectively analyzed (n = 114). Inclusion criteria were as follows: (1) renal biopsy specimen containing more than three viable glomeruli per section, (2) immunofluorescence (IF) test demonstrating at least mild mesangial IgA staining (IgA ≥1+), and (3) no prior history of kidney transplantation. IgA intensity in IF was graded on a scale of 0 (negative), 0.5+ (trace), 1+ (mild), 2+ (moderate), and 3+ (strong).

Patients diagnosed with IgAN (n = 75) demonstrated mesangial electron-dense deposits (EDD) on electron microscopy (EM) when glomeruli were available for evaluation. The IF showed a C3 intensity of 1+ or greater in cases lacking EDD. All IgAN cases exhibited IgA dominance or co-dominance on IF. None of the IgAN cases met the diagnostic criteria for systemic lupus nephritis as per the 2019 European League Against Rheumatism (EULAR)/American College of Rheumatology (ACR) guidelines [7]. A subset of patients with IgAN (n = 9), whose symptoms began within 50 days of coronavirus disease 2019 (COVID-19) vaccination or infection, as previously reported [8], were subclassified as the COVID-19–related IgAN group. All IgAN cases had a clinical follow-up duration (the interval between the first and last laboratory tests) exceeding 3 months. Patients who did not meet the criteria for IgAN were assigned to the non-IgAN group (n = 39). Pathological diagnoses in this group included lupus nephritis (n = 27), post-infectious glomerulonephritis (n = 3), pauci-immune crescentic glomerulonephritis (n = 2), focal segmental glomerulosclerosis (FSGS), not otherwise specified (n = 1), IgA-dominant infection-related glomerulonephritis (n = 1), IgM nephropathy (n = 1), immune complex-associated crescentic glomerulonephritis (n = 1), membranous nephropathy (n = 1), membranoproliferative glomerulonephritis (n = 1), and subacute bacterial endocarditis-associated immune complex-mediated glomerulonephritis (n = 1). A summary of the recruitment process is illustrated in Fig. 1.

Pathologic diagnosis

Biopsy specimens were processed into formalin-fixed paraffin-embedded (FFPE) blocks and IF samples at collection. Tissue sections were stained with hematoxylin-eosin, acid fuchsin orange G, periodic acid methenamine silver, and periodic acid-Schiff stains. IgAN was diagnosed based on the dominance or co-dominance of IgA in IF. For each case, IF staining was performed for IgG, IgA, IgM, C3, C4, C1q, fibrinogen, kappa light chain, and lambda light chain.

The Oxford classification was applied to each IgAN case [9,10]. Mesangial hypercellularity (M) was classified as M0 (less than half of glomeruli exhibit mesangial expansion and cell proliferation) or M1 (more than half of glomeruli exhibit mesangial expansion and cell proliferation). Endocapillary hypercellularity (E) was scored as E0 (no endocapillary hypercellularity) or E1 (presence of endocapillary hypercellularity). Segmental sclerosis (S) was classified as S0 (absence of segmental sclerosis or adhesion of capillary tuft) or S1 (presence). Tubular atrophy and interstitial fibrosis (T) were classified as T0 (<25% cortical involvement), T1 (25%–50% cortical involvement), and T2 (>50% cortical involvement). Crescent formation (C) score was classified as C0 (no crescent), C1 (0%–25% of glomeruli with crescent formation), and C2 (>25% of glomeruli with crescent formation). Moreover, each IgAN case was evaluated according to the Haas classification system: grade I (minimal change), II (focal segmental glomerulosclerosis), III (focal mesangioendocapillary proliferation), IV (diffuse proliferation), and V (advanced chronic, >40% of glomeruli are globally scle-

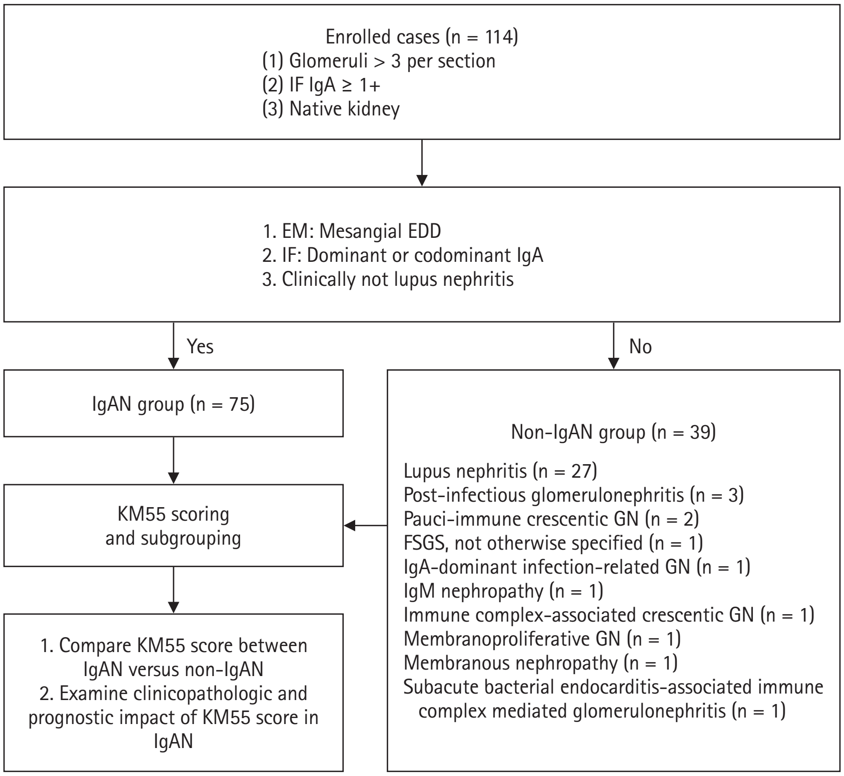

Fig. 1. Overview of study design. IF, immunofluorescence; EM, electron microscopy; EDD, electron-dense deposit; IgAN, IgA nephropathy; GN, glomerulonephritis; FSGS, focal segmental glomerulosclerosis.

rotic) [11].

Each case underwent an EM examination. The researcher reviewed digitalized images of glomeruli. Among the IgAN group, 71 cases had examinable glomeruli, all exhibiting EDD in the mesangium. In the non-IgAN group, all cases had examinable glomeruli, with 29 showing mesangial EDD, while the remaining 10 cases showed no EDD in the mesangium.

IHC staining and evaluation of KM55

The IHC staining was performed using an automated IHC stainer (BOND-III, Leica Biosystems, Nussloch, Germany). The FFPE sections (3 μm thick) were dewaxed using BOND Dewax Solution (Leica Biosystems) and 100% alcohol. Heat-induced epitope retrieval was performed with BOND Epitope Retrieval Solution 2 (Leica Biosystems) for 20 minutes. Antigen retrieval was carried out using protease 1 (Ventana Medical Systems, Tucson, AZ, USA) at a concentration of 0.38 mg/mL for 30 minutes. Peroxidation was processed for 10 minutes. The KM55 primary antibody (rat IgG monoclonal antibody against human Gd-IgA1, Immuno-Biological Laboratories, Fujioka, Japan) at a 10 μg/mL concentration was applied for 15 minutes. The secondary antibody (conjugated goat anti-rat IgG antibody) was automatically added for 15 minutes. Then, the Bond Polymer Refine Detection Kit (Leica Biosystems) was used for the polymer, 3,3'-diaminobenzidine (DAB), and hematoxylin staining in an automated process: polymer for 8 minutes, mixed DAB for 8 minutes, and hematoxylin for 3 minutes. The protocol was validated using positive controls (several IgAN cases) and negative controls (nephrectomy specimens from patients without medical kidney disease). In each case, mesangial KM55 expression was assessed via IHC and graded on a scale of 0 (negative), 1+ (faint), 2+ (weak), 3+ (moderate), and 4+ (strong). Representative images for each grade are represented in Fig. 2.

Clinical information

Clinical information, including age at diagnosis, sex, presenting complaint, date of initial presentation, and laboratory results at the time of initial biopsy, was obtained from electronic medical records. Laboratory parameters included blood pressure, serum creatinine, albumin, estimated glomerular filtration rate (eGFR), calculated using the CKD-epidemiology collaboration (CKD-

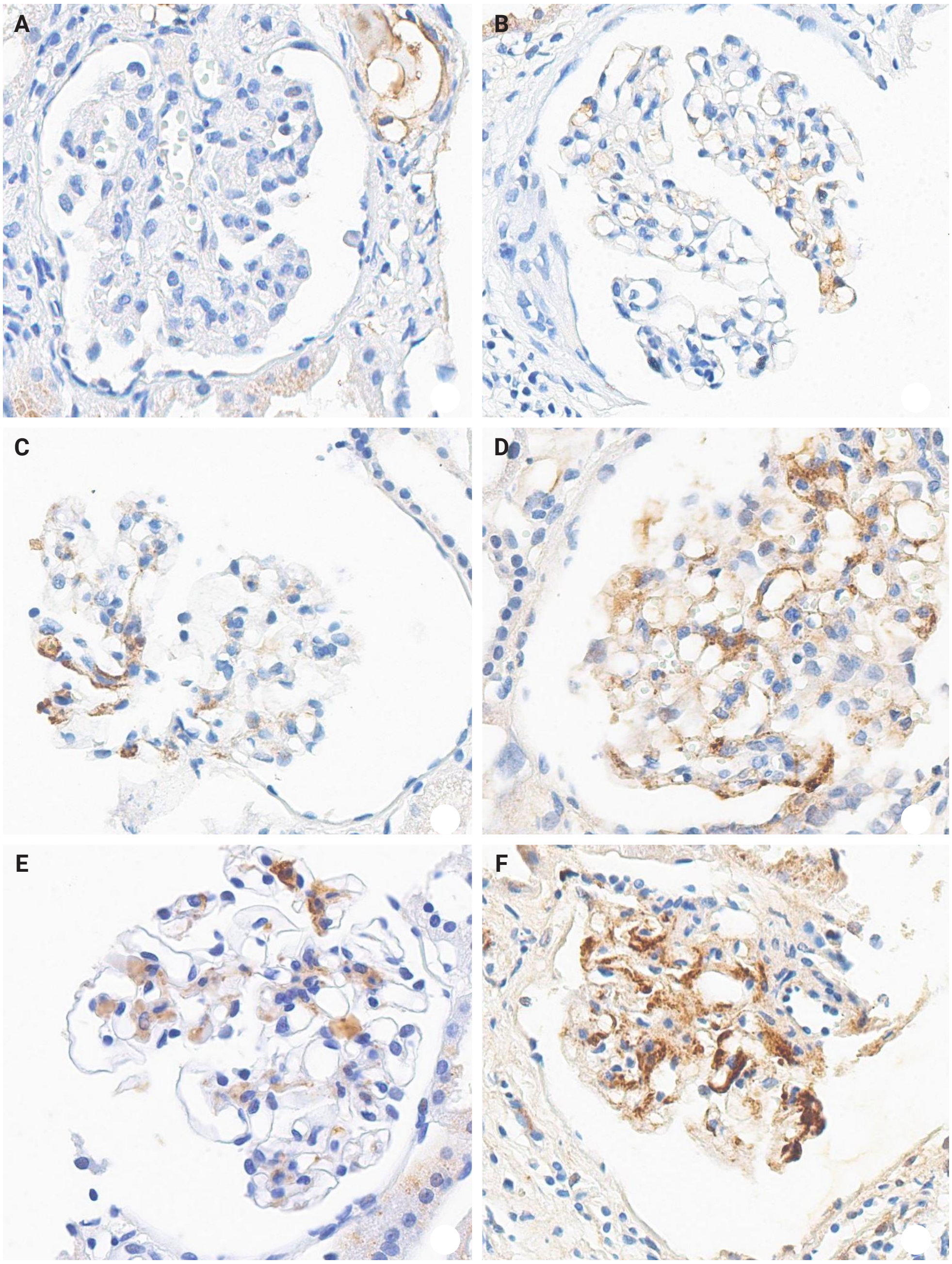

Fig. 2. Representative KM55 scores. (A) 0. (B) 1+. (C) 2+. (D, E) 3+. (F) 4+.

EPI) method, urine protein-creatinine ratio, 24-hour urine protein excretion, microscopic red blood cell count in urine, and complete blood count. Follow-up medical records to May 2024 were reviewed for the IgAN group to gather prognostic information. The ESRD state was defined as an eGFR <15 mL/min/1.73 m^2 along with a clinical plan for renal replacement therapy (dialysis or transplant). CKD stage 4 was defined as an eGFR of 15–29 mL/min/1.73 m^2. For IgAN cases, the dates of ESRD onset, CKD stage 4 progression, and a ≥75% reduction from baseline eGFR (eGFR-25%) were recorded. Survival time was calculated from the biopsy date to the occurrence of one of these outcomes. In patients with clinical features suggestive of systemic lupus erythematosus (SLE), anti-nuclear antibody (ANA) levels were measured; those with positive ANA results underwent complement testing. Among 17 patients with ANA positivity, six had anti-DNA antibody levels evaluated. At the time of biopsy, serum C3 and C4 levels were measured in 70 IgAN cases, and serum IgA levels were assessed in 65 IgAN cases.

Statistics

Depending on data distribution, either the independent two-tailed t-test or the Mann-Whitney U test was used to compare the two groups. For comparisons across three or more groups, normally distributed variables were analyzed using analysis of variance (ANOVA), followed by Bonferroni post-hoc testing. Conversely, non-normally distributed variables were evaluated using the Kruskal-Wallis test. Categorical variables were compared using the chi-square test or Fisher's exact test, as appropriate. Prognostic analyses for progression to ESRD, CKD stage 4, and eGFR-25% were analyzed using Kaplan-Meier curves, and univariate and multivariate Cox regression models.

RESULTS

Discriminative ability of KM55 IHC in diagnosing IgAN

Seventy-five patients were classified as the IgAN group and 39 as the non-IgAN group. Baseline clinico-epidemiological characteristics are presented in Table 1. For each case, KM55 IHC staining was graded on a five-tier scale based on the intensity and extent of mesangial Gd-IgA1 deposition. The IgAN group exhibited substantially higher KM55 scores than the non-IgAN group (median [interquartile range (IQR)], 3 [2 to 3] vs. 1 [0 to 1]; p < .001) (Fig. 3A). Four patients in the non-IgAN group exhibited a KM55 score of 2+, all diagnosed with lupus nephritis. The receiver operating characteristic curve illustrating the diagnostic performance of KM55 IHC is shown in Fig. 3B. The area under the curve was 0.907 (95% confidence interval [CI], 0.855 to 0.959). The optimal KM55 score cutoff for diagnosing IgAN was 2+, yielding a sensitivity of 0.760 and a specificity of 0.897. Eighteen patients in the IgAN group had a KM55 score of 1+, falling below this cutoff. Further clinical data were analyzed to compare these KM55 1+ IgAN cases with those scoring ≥2+. The serum IgA levels at the time of initial biopsy were available for 16 patients with KM55 1+ and 49 with KM55 ≥2+. The KM55 1+ group had significantly lower IgA levels (mean ± standard deviation, 237.23 ± 78.91 vs. 317.66 ± 136.87; p = .025). However, no considerable differences were found between the groups in IF IgA intensity (p = .327) or the interval between clinical presentation and biopsy (p = .651).

Relationship between pathologic variables and KM55 score in IgAN

Among IgAN patients, 21 had an M1 score, 30 had E1, 48 had S1, 11 had T1 or T2, and 29 had C1 or C2 scores. The distribution by Haas classification was as follows: two (grade I), seven (II), 42 (III), 18 (IV), and 6 (V). The M and T scores of the Oxford classification were significantly associated with the KM55 mesangial scores (Table 2). Patients with an M1 score had higher KM55 scores (median [IQR], 3 [2.5 to 3]) than those with an

Table 1. Clinical characteristics and initial laboratory data profile of study groups

Characteristic	IgAN group (n = 75)	Non-IgAN group (n = 39)	p-value
Male sex	24 (32.0)	12 (31.0)	>.99
Age (yr)	38.6 ± 15.7	41.2 ± 12.1	.226
Microscopic hematuria (≥3 RBC/HPF)	70 (93.3)	34 (87.2)	.451
Proteinuria (UPCR, g/g Cr)	1.33 (0.72–2.50)	2.81 (1.46–6.78)	<.001
Serum creatinine (mg/dL)	0.95 (0.71–1.21)	0.79 (0.55–0.97)	.212
Serum albumin (g/dL)	4.2 (3.7–4.3)	2.8 (2.2–3.5)	<.001
eGFR (mL/min/1.73 m^2)	84.0 (60.0–113.0)	103.0 (78.5–119.5)	.467
Hemoglobin (g/dL)	13.1 ± 1.7	10.4 ± 2.5	<.001
WBC count (/μL)	6,740 (5,420–7,960)	5,570 (2,500–8,540)	.022
Platelet (×10^3/μL)	265 (217–310)	220 (121–300)	.003
EDD in mesangium	71/71[a] (100)	29/39 (74.4)	<.001
IF IgA intensity (1+, 2+, 3+)	5, 30, 40	20, 15, 4	<.001

Values are presented as number (%), mean ± SD, or median (IQR).
IgAN, IgA nephropathy; RBC, red blood cell; HPF, high-power field; UPCR, urine protein/creatinine ratio; eGFR, estimated glomerular filtration rate; WBC, white blood cell; EDD, electron-dense deposit; IF, immunofluorescence; SD, standard deviation; IQR, interquartile range.
[a] Case without identifiable glomeruli in electron microscopy is excluded.

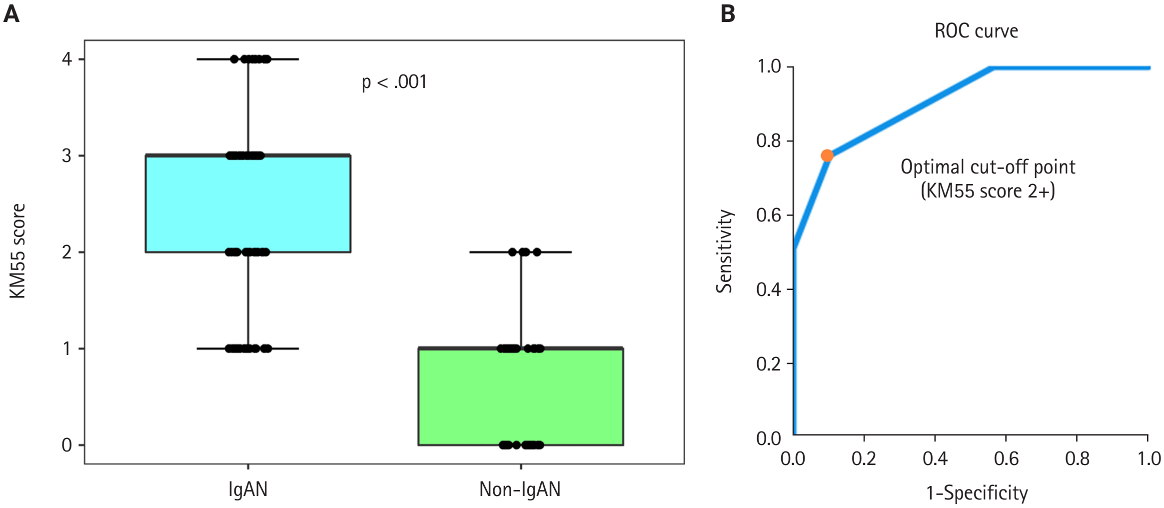

Fig. 3. Mesangial KM55 scores graded by immunohistochemistry. (A) Comparison between IgA nephropathy (IgAN) and control groups. Boxes represent the interquartile range; bold horizontal lines indicate median KM55 scores. (B) Receiver operating characteristic (ROC) curve for IgAN differentiation using mesangial KM55 scores. The dot indicates sensitivity and 1-specificity at optimal cutoff (2+).

M0 score (2 [1 to 3]) (p = .017). Patients with a T1–2 score had significantly higher KM55 scores (3 [3 to 3]) compared to those scored with a T0 score (2 [1 to 3]) (p = .049). However, E, S, and C scores from the Oxford classification showed no substantial association with mesangial KM55 scores. Similarly, differences in KM55 scores across Haas classification grades were insignificant (p = .233) (Table 2).

Clinicopathological and prognostic implications of the KM55 score in IgAN

Given the significant association between the KM55 score and Oxford classification, patients with IgAN were further stratified by mesangial KM55 score. All patients scored 1+, 2+, 3+, or 4+, allowing categorization into four groups. Comparison across these groups revealed significant differences in serum creatinine (p = .015), eGFR (p = .020), and serum albumin (p = .008) (Table 3). Pairwise comparisons showed significant differences in serum creatinine between KM55 2+ vs. KM55 3+ (p = .003), and KM55 2+ vs. KM55 4+ (p = .018); in eGFR between KM55 2+ vs. KM55 4+ (p = .045) and in serum albumin between KM55 1+ vs. KM55 2+ (p = .031), KM55 1+ vs. KM55 3+ (p = .003), and KM55 1+ vs. KM55 4+ (p = .004). Moreover, serum creatinine, uric acid, blood urea nitrogen (BUN), and systolic blood pressure showed a rising trend from KM55 2+ to 4+, though this trend was not observed between 1+ and 2+ (Table 3). The interval from initial clinical presentation to biopsy did

Table 2. Comparison of mesangial KM55 score among different histologic grade group scored according to Oxford classification of IgAN

	Mesangial KM55 score, median (range)	p-value[a]
M score		.017
M0	2 (1–3)	
M1	3 (2.5–3)	
E score		.434
E0	2 (1–3)	
E1	3 (2–3)	
S score		.080
S0	2 (1–3)	
S1	3 (2–3)	
T score		.049
T0	2 (1–3)	
T1 and T2	3 (3–3)	
C score		.881
C0	3 (1–3)	
C1 and C2	2 (2–3)	
Haas classification		.233
I	2 (1–3)	
II	3 (1–3)	
III	2 (1–3)	
IV	3 (2–3)	
V	3 (1.75–4)	

IgAN, IgA nephropathy.
[a] Mann-Whitney U test for MEST-C score, Kruskal-Wallis test for Haas classification score.

not differ substantially across groups (p = .935). Complement levels (C3 and C4) showed no significant differences between the two groups (p = .324 and p = .486) (Table 3). Serum albumin consistently decreased from KM55 1+ to 4+ (Table 3). The urine protein/creatinine ratio (UPCR) and diastolic blood pressure showed a consistent increasing trend as the KM55 score rose from 1+ to 4+, although this change was insignificant (Table 3). Serum IgA levels increased as the KM55 score progressed from 1+ to 3+, while no such trend was observed between 3+ and 4+ (Table 3), with a significant difference in IgA levels (p = .050) (Table 3). Among the Oxford classification variables, only the M score demonstrated a significant difference across the four groups (p = .042), with an increasing trend in the M1 ratio from KM55 1+ to KM55 3+ (Table 3).

Based on these trends, patients with IgAN were categorized into the KM55-high group (≥3+) and the KM55-low group (≤2+). Thirty-eight patients were classified into the KM55-high group, while 37 were placed in the KM55-low group. The KM55-high group had significantly higher serum creatinine (p = .003), lower eGFR (p = .007), higher UPCR (p = .048), higher BUN (p = .041), lower albumin (p = .010), and higher diastolic blood pressure (p = .027) (Table 4). There was no significant difference in the duration between the initial clinical presentation and biopsy date (p = .937). Moreover, complement levels

Table 3. Characteristics comparison of IgAN according to KM55 score

Characteristic	KM55 1+ (n = 18)	KM55 2+ (n = 19)	KM55 3+ (n = 29)	KM55 4+ (n = 9)	p-value
Male sex	5 (27.8)	6 (31.6)	11 (37.9)	2 (22.2)	.808
Age (yr)	37.4 ± 18.1	35.2 ± 15.3	40.0 ± 14.2	50.2 ± 12.8	.111
Microscopic hematuria	17 (94.4)	17 (89.5)	28 (96.6)	8 (88.9)	.855
UPCR (g/g Cr)	1.03 (0.64–1.46)	1.23 (0.45–2.11)	1.58 (0.73–2.77)	2.05 (1.02–2.87)	.172
Serum creatinine (mg/dL)	0.92 (0.75–1.13)	0.72 (0.58–0.97)	1.04 (0.82–1.32)	1.16 (0.81–1.37)	.015
Serum BUN (mg/dL)	14.0 (11.1–18.6)	11.3 (8.5–15.5)	15.8 (11.6–19.5)	16.1 (12.9–19.4)	.078
Serum uric acid (mg/dL)	5.25 (3.98–6.48)	4.90 (3.30–6.40)	5.30 (4.25–7.20)	6.50 (4.70–6.95)	.232
eGFR (mL/min/1.73 m^2)	90.33 ± 42.45	105.68 ± 32.83	78.72 ± 32.45	67.67 ± 20.75	.020
Serum albumin (g/dL)	4.3 (4.2–4.6)	4.2 (3.8–4.3)	4.0 (3.6–4.3)	3.9 (3.7–4.2)	.008
Systolic blood pressure (mmHg)	125.0 (112.8–135.3)	120.0 (105.0–135.0)	124.0 (120.0–130.5)	127.0 (121.0–135.0)	.508
Diastolic blood pressure (mmHg)	73.5 (66.5–79.3)	75.0 (70.0–85.0)	80.0 (70.0–85.5)	80.0 (80.0–87.0)	.083
Hemoglobin (g/dL)	13.51 ± 1.75	12.62 ± 1.34	13.12 ± 1.90	13.00 ± 2.00	.487
White blood cell count (/µL)	7,240 (5,358–7,638)	6,720 (5,090–7,840)	6,650 (5,515–7,710)	9,240 (4,855–10,450)	.774
Platelet count ($\times 10^3$/µL)	283.5 (216.0–318.3)	271.0 (249.0–363.0)	248.0 (214.5–289.0)	261.0 (189.0–346.0)	.396
Immunosuppressant use (%)	3 (16.7)	9 (47.4)	14 (48.3)	5 (55.6)	.113
Serum C3 (mg/dL)	107.00 (99.73–125.28)[a]	108.85 (94.60–133.40)[b]	102.00 (92.95–118.90)[c]	122.10 (98.40–134.05)[d]	.324
Serum C4 (mg/dL)	25.58 (19.18–34.72)[a]	25.47 (21.98–31.01)[b]	25.36 (19.93–29.70)[c]	32.40 (23.25–42.92)[d]	.486
Serum IgA (mg/dL)	237.39 ± 76.72[e]	280.87 ± 130.57[f]	343.42 ± 141.06[g]	312.89 ± 54.37[h]	.050
ESRD progression	1 (5.6)	1 (5.3)	9 (31.0)	5 (55.6)	.003
CKD stage 4 progression	1 (5.6)	2 (10.5)	9 (31.0)	6 (66.7)	.002
eGFR-25% occurrence	0	2 (10.5)	9 (31.0)	5 (55.6)	.002
Days before biopsy	74 (31.75–296.5)	55 (34–238)	80 (29.5–278.5)	59 (53–126.5)	.935
Oxford classification					
M1	2 (11.1)	3 (15.8)	13 (44.8)	3 (33.3)	.042
E1	5 (27.8)	8 (42.1)	14 (48.3)	3 (33.3)	.542
S1	9 (50.0)	12 (63.2)	19 (65.5)	8 (88.9)	.272
T1 and T2	1 (5.6)	1 (5.3)	7 (24.1)	2 (22.2)	.172
C1 and C2	5 (27.8)	11 (57.9)	10 (34.5)	3 (33.3)	.250

Values are presented as number (%), mean ± SD, or median (IQR).

IgAN, IgA nephropathy; UPCR, urine protein/creatinine ratio; BUN, blood urea nitrogen; eGFR, estimated glomerular filtration rate; ESRD, end-stage renal disease; CKD, chronic kidney disease; eGFR-25%, ≥75% reduction from baseline eGFR; SD, standard deviation; IQR, interquartile range.

[a] 18 cases included; [b] 18 cases included; [c] 25 cases included; [d] 9 cases included; [e] 16 cases included; [f] 18 cases included; [g] 22 cases included; [h] 9 cases included.

(C3: p = .522, C4: p =.677) showed no substantial difference between the groups (Table 4). Serum IgA levels were significantly higher in the KM55-high group (p = .012) (Table 4). Among the Oxford classification variables, only the M score, which was higher in the KM55-high group, showed a considerable difference between the two groups (p = .012) (Table 4).

In univariate Cox regression analysis for event-free survival, the KM55 score was revealed as a significant prognostic factor for ESRD (p = .012), CKD stage 4 (p = .005), and eGFR-25% (p = .004). Event-free survival curves comparing the KM55 1+, 2+, 3+, and 4+ subgroups are shown in Fig. 4A, C, and E. A more distinct gap is observed between the KM55 2+ and KM55 3+ subgroups, while survival differences between 1+ and the 2+, 3+, or 4+ subgroups are relatively ambiguous. This pattern suggests that categorizing the IgAN group into KM55-high (≥3+) and KM55-low groups (≤2+) is reasonable. Among the KM55-high group, 14 (37%) progressed to ESRD, 15 (40%) to CKD stage 4, and 14 (37%) to eGFR-25%, while in the KM55-low group, two (5%) progressed to ESRD, three (8%) to CKD stage 4, and two (5%) to eGFR-25% (Table 4). In univariate survival analysis, the KM55-high group revealed a significantly higher risk for progression to ESRD (hazard ratio [HR], 5.54;

Table 4. Characteristics comparison of IgAN between the KM55-high group (KM55 score ≥3+) versus the KM55-low group (KM55 score ≤2+)

Characteristic	KM55-high group (n = 38)	KM55-low group (n = 37)	p-value
Male sex	13 (34.2)	11 (29.7)	.866
Age (yr)	40.9 ± 14.7	36.3 ± 16.6	.207
Microscopic hematuria	36 (94.7)	34 (91.9)	.674
UPCR (g/g Cr)	1.73 (0.81–2.82)	1.13 (0.61–1.79)	.048
Serum creatinine (mg/dL)	1.07 (0.81–1.31)	0.84 (0.60–0.99)	.003
Serum BUN (mg/dL)	15.9 (11.7–19.3)	12.9 (10.2–17.0)	.041
Serum uric acid (mg/dL)	5.86 ± 1.57	5.20 ± 1.65	.083
eGFR (mL/min/1.73 m^2)	76.11 ± 30.21	98.22 ± 38.08	.007
Serum albumin (g/dL)	3.90 (3.68–4.30)	4.20 (4.10–4.45)	.010
SBP (mmHg)	124.5 (120.0–130.3)	120.0 (108.0–135.0)	.279
DBP (mmHg)	80.0 (70.8–85.3)	75.0 (67.5–80.0)	.027
Hemoglobin (g/dL)	13.09 ± 1.90	13.05 ± 1.60	.925
White blood cell count (/µL)	6,665 (5,383–8,948)	7,010 (5,295–7,775)	.990
Platelet count (×10^3/µL)	250.5 (213.8–291.0)	272.0 (233.0–324.5)	.101
Immunosuppressant usage	19 (50.0)	12 (32.4)	.190
Serum C3 (mg/dL)	103.85 (93.63–125.43)[a]	107.00 (97.05–125.63)[b]	.522
Serum C4 (mg/dL)	26.24 (20.93–35.50)[a]	25.47 (20.58–32.14)[b]	.677
Serum IgA (mg/dL)	334.55 ± 122.13[c]	260.41 ± 109.29[d]	.012
ESRD progression	14 (36.8)	2 (5.4)	<.001
CKD stage 4 progression	15 (39.5)	3 (8.1)	<.001
eGFR-25% occurrence	14 (36.8)	2 (5.4)	<.001
Days before biopsy	62 (43.25-223.5)	63 (34-251.5)	.937
Oxford classification			
M1	16 (42.1)	5 (13.5)	.012
E1	17 (44.7)	13 (35.1)	.540
S1	27 (71.1)	21 (56.8)	.294
T1 and T2	9 (23.7)	2 (5.4)	.056
C1 and C2	13 (34.2)	16 (43.2)	.571

Values are presented as number (%), mean ± SD, or median (IQR).

IgAN, IgA nephropathy; UPCR, urine protein/creatinine ratio; BUN, blood urea nitrogen; eGFR, estimated glomerular filtration rate; SBP, systolic blood pressure; DBP, diastolic blood pressure; ESRD, end-stage renal disease; CKD, chronic kidney disease; eGFR-25%, ≥75% reduction from baseline eGFR; SD, standard deviation; IQR, interquartile range.

[a] 34 cases included; [b] 36 cases included; [c] 31 cases included; [d] 34 cases included.

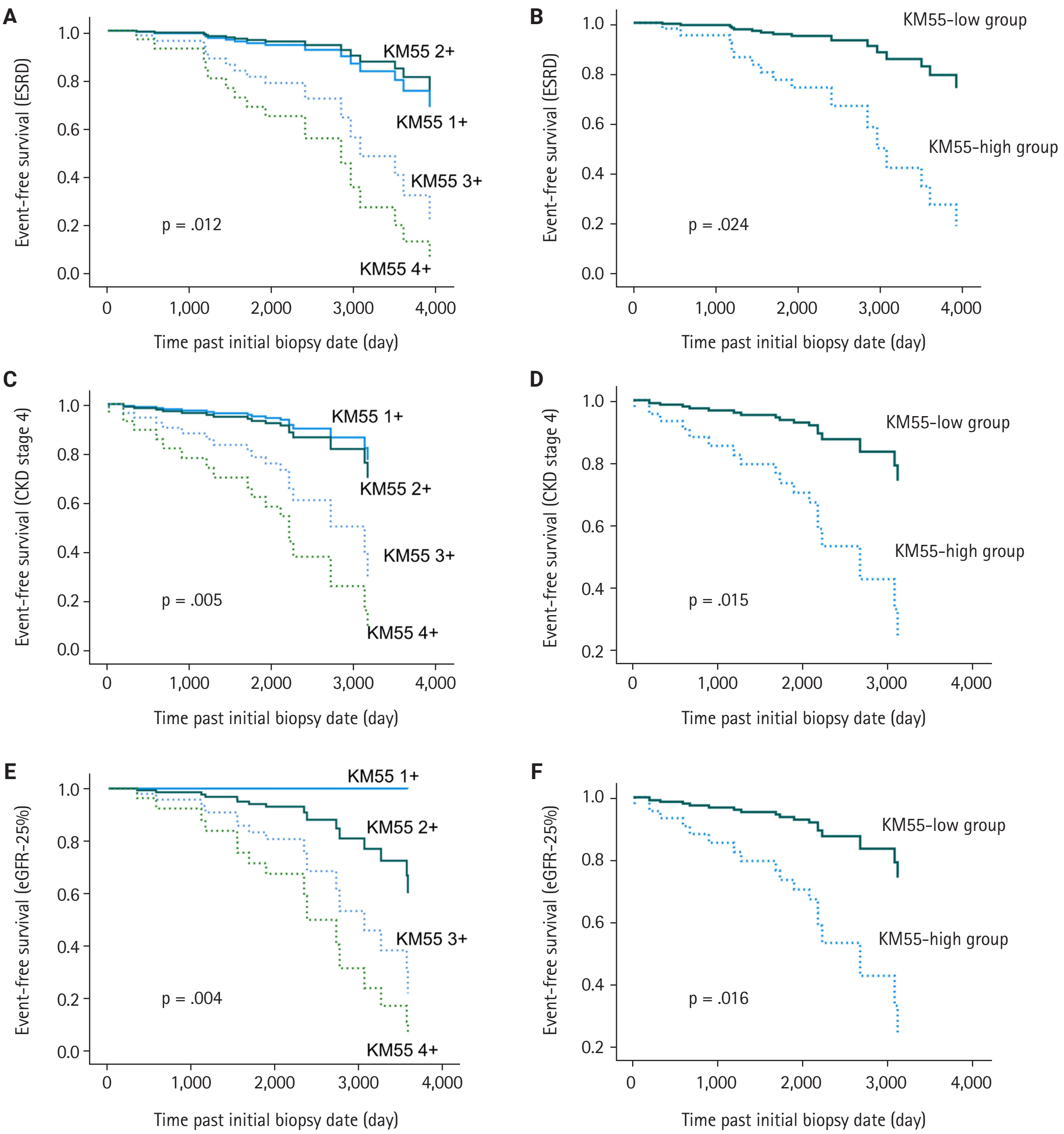

Fig. 4. Survival analysis for renal function decline. (A, B) Event-free survival for end-stage renal disease (ESRD) progression. (C, D) Event-free survival for chronic kidney disease (CKD) stage 4. (E, F) Event-free survival for estimated glomerular filtration rate decline ≥25% (eGFR-25%). (A, C, E) Comparison among KM55 subgroups: 1+, 2+, 3+, and 4+. The blue solid line represents KM55 1+, the green solid line represents 2+, the blue dotted line represents 3+, and the green dotted line represents 4+. (B, D, F) Comparison between KM55-high and KM55-low groups. The solid line represents the KM55-low group; the dotted line represents the KM55-high group.

95% CI, 1.26 to 24.45; p = .024), CKD stage 4 (HR, 4.71; 95% CI, 1.36 to 16.36; p = .015), and eGFR-25% (HR, 6.15; 95% CI, 1.39 to 27.12; p = .016) compared to the KM55 low group (Table 5, Fig. 4B, D, and F). Among the Oxford classification variables, only the T score was significantly associated with ESRD (p < .001) (Table 5) and eGFR-25% progression (p < .001) (Table 5). In contrast, M (p =.021), E (p = .030), and T (p < .001) scores were predictive of CKD stage 4 progression (Table 5). In multi-

Table 5. Survival analysis for risk of progression into ESRD, CKD4, and eGFR-25%

	Univariate analysis		Multivariate analysis	
	HR (95% CI)	p-value	HR (95% CI)	p-value
ESRD progression				
KM55-high vs. KM55-low	5.54 (1.26–24.45)	.024	3.23 (0.67–15.66)	.146
M1 vs. M0	2.71 (0.89–8.22)	.079	-	-
E1 vs. E0	2.46 (0.72–8.41)	.150	-	-
S1 vs. S0	3.42 (0.77–15.19)	.105	-	-
T1 vs. T0	7.04 (2.60–19.08)	<.001	4.73 (1.65–13.58)	.004
C1, 2 vs. C0	1.09 (0.39–3.07)	.876	-	-
CKD4 progression				
KM55-high vs. KM55-low	4.71 (1.36–16.36)	.015	2.34 (0.55–9.91)	.249
M1 vs. M0	3.11 (1.18–8.16)	.021	1.07 (0.27–4.27)	.920
E1 vs. E0	3.25 (1.12–9.43)	.030	2.12 (0.52–8.61)	.291
S1 vs. S0	2.88 (0.83–9.94)	.095	-	-
T1 vs. T0	17.71 (6.09–51.53)	<.001	11.70 (3.55–38.58)	<.001
C1, 2 vs. C0	1.47 (0.58–3.76)	.419	-	-
eGFR-25%				
KM55-high vs. KM55-low	6.15 (1.39–27.12)	.016	4.25 (0.91–19.83)	.066
M1 vs. M0	2.84 (0.95–8.50)	.062	-	-
E1 vs. E0	3.46 (0.90–13.34)	.071	-	-
S1 vs. S0	3.68 (0.84–16.22)	.085	-	-
T1 vs. T0	5.42 (2.00–14.65)	<.001	3.52 (1.25–9.90)	.017
C1, 2 vs. C0	1.10 (0.40–3.02)	.849	-	-

ESRD, end-stage renal disease; CKD4, chronic kidney disease stage 4; eGFR-25%, ≥75% reduction from baseline eGFR; HR, hazard ratio; CI, confidential interval; eGFR, estimated glomerular filtration rate.

variate analysis, after adjusting for significant Oxford classification factors, the KM55 score was not associated with prognosis (ESRD, p = .146; CKD stage 4, p = .249; eGFR-25%, p = .066). However, T score was independently significant for progression to ESRD (HR, 4.73; 95% CI, 1.65 to 13.58; p = .004), CKD stage 4 progression (HR, 11.70; 95% CI, 3.55 to 38.58; p < .001) and eGFR-25% (HR, 3.52; 95% CI, 1.25 to 9.90; p = .017) (Table 5).

Comparison of COVID-19–related and COVID-19–unrelated IgAN groups

Among the patients with IgAN, nine were temporally associated with COVID-19 vaccination or infection (Table 6). In the COVID-19–related group, two (22%) were men, averaging 35.0 years. In the COVID-19–unrelated group, 22 (33%) were men, with an average age of 39.1 years. The serum albumin levels in the COVID-19–related and unrelated groups were 4.30 (4.30–4.55) and 4.10 (3.70–4.30), respectively, showing a significant difference (p = .003). No other clinical variables differed significantly between the two groups. Regarding the Oxford classification scores of MEST-C, only the E score showed a significant difference between the groups (p = .018). The percentage of patients with an E1 score was 77% (n = 7) (COVID-19–related group) compared to 35% (n = 23) (COVID-19–unrelated group). Other clinicopathologic variables are summarized in Table 6. In the COVID-19–related group, no patients progressed to ESRD or CKD stage 4, while in the COVID-19–unrelated group, 16 (24%) patients showed ESRD progression, 18 (27%) showed CKD stage 4 progression, and 16 (24%) showed eGFR-25% progression. In KM55 IHC, the COVID-19–unrelated group had a significantly higher mesangial KM55 score (median, 3; IQR, 2 to 3) than the COVID-19–related group (median, 1; IQR, 1 to 2.5) (p = .022).

DISCUSSION

Recent biological research has emphasized the importance of Gd-IgA1 in the pathophysiology of IgAN [2]. Gd-IgA1 is proposed to form immune complexes that accumulate in the glomerular mesangium, stimulating mesangial cell proliferation and matrix production [2]. In this context, various studies have

Table 6. Baseline characteristics comparison between IgAN patients clinically associated with COVID-19 infection or vaccination, versus COVID-19 unrelated IgAN group

Characteristics	IgAN related to COVID-19 (n = 9)	IgAN unrelated to COVID-19 (n = 66)	p-value
Male sex	2 (22.2)	22 (33.3)	.710
Age (yr)	35.0 ± 16.5	39.1 ± 15.7	.468
Follow up period (day), median (min–max)	452 (98–560)	2,115.5 (245–4,580)	-
Microscopic hematuria	9 (100)	61 (92.4)	>.99
UPCR (g/g Cr), median (IQR)	1.13 (0.86–1.38)	1.49 (0.69–2.65)	.405
Serum creatinine (mg/dL), median (IQR)	0.77 (0.58–0.99)	0.97 (0.72–1.23)	.157
Serum albumin (g/dL), median (IQR)	4.30 (4.30–4.55)	4.10 (3.70–4.30)	.003
eGFR-CKD-EPI (mL/min/1.73 m^2)	101.8 ± 34.8	85.0 ± 35.8	.190
SBP (mmHg)	122.3 ± 19.2	124.7 ± 13.2	.643
DBP (mmHg)	74.0 ± 8.0	77.5 ± 10.7	.352
Uric acid (mg/dL)	5.60 ± 1.47	5.52 ± 1.67	.895
BUN (mg/dL), median (IQR)	12.6 (8.2–15.7)	14.9 (11.2–18.7)	.108
ESRD progression	0	16 (24.2)	<.001
CKD stage 4 progression	0	18 (27.3)	<.001
eGFR-25% occurrence	0	16 (24.2)	<.001
Days before biopsy, median (IQR)	63 (45–118)	62 (33.75–250.75)	.813
Haas classification (I, II, III, IV, V)	0, 1, 7, 1, 0	2, 6, 35, 17, 6	.672
Oxford classification			
M (M0, M1)	9, 0	45, 21	.054
E (E0, E1)	2, 7	43, 23	.018
S (S0, S1)	2, 7	25, 41	.475
T (T0, T1, T2)	9, 0, 0	55, 11, 0	.340
C (C0, C1, C2)	5, 4, 0	41, 23, 2	.485
IF intensity of IgA (1+, 2+, 3+)	0, 4, 5	5, 26, 35	.893
KM55 score, median (IQR)	1 (1–2.5)	3 (2–3)	.022

Values are presented as number (%) or mean ± SD unless otherwise indicated.
IgAN, IgA nephropathy; COVID-19, coronavirus disease 2019; UPCR, urine protein/creatinine ratio; IQR, interquartile range; eGFR; estimated glomerular filtration rate; CKD-EPI, chronic kidney disease Epidemiology Collaboration; SBP, systolic blood pressure; DBP, diastolic blood pressure; BUN, blood urea nitrogen; ESRD, end-stage renal disease; CKD, chronic kidney disease; eGFR-25%, ≥75% reduction from baseline eGFR; IF, immunofluorescence; SD, standard deviation.

focused on measuring Gd-IgA1 levels in the plasma and tissues of patients with IgAN. Earlier methods relied on *Helix aspersa* agglutinin lectin, but these were limited by batch-dependent bioactivity and stability issues [5]. More recently, Yasutake et al. [5] developed a novel monoclonal antibody, KM55, specifically targeting Gd-IgA1. When integrated with ELISA, KM55 enables several studies to measure serum Gd-IgA1 levels without relying on lectin-based assays or mass spectrometry [3,5,6]. This study applied KM55 IHC to detect mesangial deposition of pathogenic Gd-IgA1 in renal biopsy specimens from patients with IgAN. Significantly higher KM55 scores were observed in IgAN cases compared to the non-IgAN group.

Several studies have employed KM55 using different methods to understand IgAN. Zhang et al. [3] reported significantly elevated serum Gd-IgA1 concentration in patients with IgAN using the KM55-based assay; qualitative differences in KM55 IHC staining were noted between the IgAN and non-IgAN groups, though no formal statistical analysis of IHC scores was performed. Additional research utilizing KM55 IF staining identified granular Gd-IgA1 deposits in biopsies from primary and secondary IgAN, as well as Henoch-Schönlein purpura (HSP), whereas other glomerular diseases such as membranoproliferative glomerulonephritis, lupus nephritis, and IgA-related monoclonal gammopathy of renal significance, shows significantly lower KM55 intensity [4,12,13]. Ishiko et al. [14] applied IF staining in pediatric patients, including 17 IgAN cases and various other glomerular diseases, to assess the specificity of KM55. However, the study was limited by a small sample size and insufficient glomeruli per case. Raj et al. [4] reported the specificity of KM55 staining in IgAN and HSP. Meanwhile, Zhao et al. [15] evaluated KM55 IF staining in 40 IgAN cases and other glomerular diseases, demonstrating a significant correlation between Gd-IgA1 deposition scores and the odds of IgAN; however, KM55 expression was not entirely IgAN-specific; however, IF staining has limitations, including poor compatibility with long-term storage or paraffin blocks, and the need for specialized equipment and a darkroom.

In our study, 39 cases were classified as non-IgAN entities. Among them, two were diagnosed with pauci-immune crescentic glomerulonephritis and one with FSGS, not otherwise specified, despite mild IgA expression on IF. The pauci-immune crescentic glomerulonephritis cases were characterized by marked crescent formation on light microscopy and the absence of mesangial EDD on EM. Of those two cases, one demonstrated anti-neutrophil cytoplasmic antibody positivity on serologic testing, presented with rapidly progressive glomerulonephritis, and lacked definite features of mesangial expansion. The diagnosis of the FSGS case was supported by the absence of mesangial hypercellularity on light microscopy and the absence of EDD on EM. Our study assessed the diagnostic utility of KM55 IHC in distinguishing IgAN from other glomerular diseases. The optimal KM55 score cutoff for diagnosing IgAN was determined as ≥2+. Eighteen IgAN cases exhibited only a 1+ score, suggesting the potential for false-negative results. Therefore, KM55 scoring demands a meticulous examination of the mesangial area. Meanwhile, KM55 1+ IgAN cases had significantly lower serum IgA levels than other IgAN cases, implying that serum IgA levels could aid interpretation when KM55 IHC results are borderline. Four non-IgAN cases, all lupus nephritis, showed a KM55 score of 2+, potentially compromising specificity. In these cases, the first patient had IF intensities of IgA, IgG, C3, and C1q at 2+, 3+, 3+, and 3+, respectively. The second patient had ill-defined mesangial EDD, with IF intensities of IgA, IgG, C3, and C1q at 2+, 3+, 1+, and 2+. The third patient exhibited lumpy EDD and IF intensities of IgA, IgG, C3, and C1q at 2+, 3+, 1+, and 1+. The fourth patient showed IF intensities of IgA, IgG, C3, and C1q at 1+, 1+, 2+, and 2+. The EM findings of the first and fourth patients revealed no clear mesangial EDD, though subepithelial and intramembranous deposits were present. These findings underscore the interpretive challenge in distinguishing mesangial from subepithelial regions in glomerular IHC slides. There is a possibility of non-specific staining in IHC, which may lead to overestimation of mesangial Gd-IgA1 deposition in KM55 IHC. In such cases, EM is a useful ancillary tool to exclude false-positives, especially when differential diagnosis is required. All four false-positive cases in our study were lupus nephritis, highlighting the importance of clinical correlation, especially in evaluating for SLE. Although KM55 is a helpful diagnostic adjunct, clinical and serologic data must be carefully considered. Among the patients with KM55 2+ non-IgAN, only one had serum IgA data (247 mg/dL at the time of biopsy), which was comparable to the average in other patients without IgAN (303.0 ± 173.5 mg/dL, $p = .249$). Although serum IgA levels in the IgAN group tended to increase with higher KM55 scores, this correlation was not observed in the non-IgAN group. This finding suggests that false-positive KM55 scores in non-IgAN cases likely result from non-specific staining rather than actual deposition of circulating aberrant IgA.

KM55 IHC likely reflects the extent of Gd-IgA1 deposition, and the observed correlation between the M score and KM55 score in our findings supports existing understanding on IgAN pathogenesis —namely, that mesangial Gd-IgA1 deposition promotes matrix formation and mesangial cell proliferation via complement activation [2]. Moreover, tubular atrophy and interstitial fibrosis, reflecting chronicity of disease, correlated with KM55 scores which might be proportional to disease progression time, reinforcing this relationship. Among clinical characteristics, BUN, UPCR, diastolic blood pressure, eGFR, serum albumin, and serum IgA levels were significantly associated with KM55 score, implying that mesangial Gd-IgA1 deposition may influence renal impairment, hypertension, and proteinuria, in line with prior research. Zhang et al. [3] reported that plasma Gd-IgA1 levels measured via ELISA using KM55 significantly correlated with serum uric acid and IgA levels, while Oxford classification variables did not. In the same study, mesangial KM55 IHC scores showed no significant correlation with plasma Gd-IgA1 levels, and the relationship between KM55 scores and clinical variables was not examined [3]. Conversely, Martin-Penagos et al. [6] found the M and T scores of Oxford classification correlating with plasma Gd-IgA1 levels. Our study demonstrated a similar relationship at the IHC level, supporting the potential of KM55 IHC scoring as a clinical biomarker. Moreover, mesangial Gd-IgA1 deposition, semi-quantified by KM55 IHC, may have prognostic value in IgAN. Although the mesangial KM55 score was not significant in multivariate Cox regression, it emerged as an essential risk factor for progression to CKD stage 4 and ESRD progression in univariate Cox and Kaplan-Meier analyses. This predictive value may partially reflect its association with M and T scores, as noted in multivariate analysis. Whether KM55 scoring can be incorporated into the Oxford classification remains uncertain and requires further validation. Its prognostic utility persisted even after adjusting for initial renal function. While lower eGFR at baseline was correlated with KM55 scores, KM55 retained prognostic significance for eGFR-25%.

Recent reports have documented several new-onset IgAN cases during the COVID-19 pandemic, potentially triggered by vaccines such as BNT162b2 (Pfizer Inc., New York, NY, USA; BioNTech SE, Mainz, Germany) and mRNA-1273 (Moderna, Inc., Cambridge, MA, USA). As of October 2022, at least 52 post-vaccination IgAN cases had been reported, suggesting a possible vaccine-related flare-up [16]. However, the underlying pathophysiologic mechanisms remain unclear. In our cohort, KM55 scores were significantly lower in COVID-19–associated IgAN cases, though the clinical relevance of this result warrants further investigation. The number of COVID-19–related cases was limited. The COVID-19 vaccination may transiently exacerbate renal disease, potentially facilitating earlier detection of IgAN. In our cohort, no patients with COVID-19–related IgAN progressed to ESRD, CKD stage 4, or experienced eGFR-25%. These cases were relatively recent and likely lacked sufficient follow-up duration for renal deterioration. Tang et al. [12] previously reported that primary IgAN cases exhibited significantly higher KM55 intensity and KM55/IgA ratio using IF. Conversely, other studies found no differences in Gd-IgA1 staining intensity [17], plasma Gd-IgA1 levels, IgA1-IgG complexes, or IF features between primary and secondary IgAN [18]. Regarding COVID-19, one cohort study noted significantly lower eGFR in vaccinated individuals with pre-existing IgAN [19]. A case report of post-vaccination IgAN revealed mesangial Gd-IgA1 and C3 co-deposition on IF [20]. Another review of 17 post–COVID-19 infection or vaccination IgAN and IgA vasculitis cases found most had a regressive course [21]. Long-term studies are warranted.

This study has several limitations. More extensive sample sizes are needed to establish the clinical and prognostic relevance of KM55 scoring. Inter-observer variability in mesangial KM55 grading is possible. Implementing more quantitative approaches, such as digital pathology or artificial intelligence-based scoring, may improve consistency. Although KM55 IHC showed prognostic potential in univariate Cox analysis, no significant hazard ratio was observed in the multivariate model.

In conclusion, KM55 IHC can be a practical tool for pathologists in evaluating IgAN. It offers significant utility in distinguishing IgAN from other glomerular diseases. Moreover, this study supports the pathophysiological role of mesangial Gd-IgA1 deposition in IgAN development and subsequent renal dysfunction. Given its prognostic potential demonstrated here, KM55 should be considered for integration into the routine pathological assessment of IgAN, pending further validation.

Ethics Statement

This research received approval from the Institutional Review Board of Severance Hospital, Seoul, Korea (IRB no. 4-2023-0868). Formal written informed consent was not required with a waiver by the appropriate IRB.

Availability of Data and Material

The datasets generated or analyzed during the study are not publicly available due to protect personal information of patients but are available from the corresponding author on reasonable request.

Code Availability

Not applicable.

ORCID

Hoe In Jeong	https://orcid.org/0009-0009-3087-2479
Beom Jin Lim	https://orcid.org/0000-0003-2856-0133
Minsun Jung	https://orcid.org/0000-0002-8701-4282

Author Contributions

Conceptualization: MJ, HIJ. Data curation: HIJ. Formal analysis: HIJ. Investigation: HIJ. Methodology: HIJ, MJ. Resources: MJ, BJL. Supervision: MJ. Writing—original draft: HIJ. Writing—review & editing: MJ, HIJ. Approval of final manuscript: all authors.

Conflicts of Interest

The authors declare that they have no potential conflicts of interest.

Funding Statement

This work was supported by The Korean Society of Pathologist Grant no. KSPG2023-01. This work was also supported by the

National Research Foundation of Korea(NRF) grant funded by the Korea government(MSIT) (RS-2024-00341570).

Acknowledgments

The authors thank the effort of GaYeong Kim from University Industry Foundation, Yonsei University.

REFERENCES

1. Seo KJ, Kim TJ, Lee KY, Shim SI, Choi YJ. IgA nephropathy: correlation of WHO classification and morphologic semi-quantitative scoring system. Korean J Pathol 2009; 43: 244-9.
2. Stamellou E, Seikrit C, Tang SC, et al. IgA nephropathy. Nat Rev Dis Primers 2023; 9: 67.
3. Zhang K, Li Q, Zhang Y, et al. Clinical significance of galactose-deficient IgA1 by KM55 in patients with IgA nephropathy. Kidney Blood Press Res 2019; 44: 1196-206.
4. Raj R, Sharma A, Barwad A, et al. KM55 in the evaluation of IgA-containing glomerular diseases. Glomerular Dis 2022; 2: 59-74.
5. Yasutake J, Suzuki Y, Suzuki H, et al. Novel lectin-independent approach to detect galactose-deficient IgA1 in IgA nephropathy. Nephrol Dial Transplant 2015; 30: 1315-21.
6. Martin-Penagos L, Fernandez-Fresnedo G, Benito-Hernandez A, et al. Measurement of galactosyl-deficient IgA1 by the monoclonal antibody KM55 contributes to predicting patients with IgA nephropathy with high risk of long-term progression. Nefrologia (Engl Ed) 2021; 41: 311-20.
7. Aringer M, Costenbader K, Daikh D, et al. 2019 European League Against Rheumatism/American College of Rheumatology classification criteria for systemic lupus erythematosus. Arthritis Rheumatol 2019; 71: 1400-12.
8. Kim HW, Kim EH, Roh YH, et al. Glomerulonephritis following COVID-19 infection or vaccination: a multicenter study in South Korea. Kidney Res Clin Pract 2024; 43: 165-76.
9. Trimarchi H, Barratt J, Cattran DC, et al. Oxford classification of IgA nephropathy 2016: an update from the IgA Nephropathy Classification Working Group. Kidney Int 2017; 91: 1014-21.
10. Working Group of the International IgA Nephropathy Network and the Renal Pathology Society; Roberts IS, Cook HT, et al. The Oxford classification of IgA nephropathy: pathology definitions, correlations, and reproducibility. Kidney Int 2009; 76: 546-56.
11. Haas M. Histologic subclassification of IgA nephropathy: a clinicopathologic study of 244 cases. Am J Kidney Dis 1997; 29: 829-42.
12. Tang X, Zheng J, Jiang X, et al. The significance of galactose-deficient immunoglobulin A1 staining in kidney diseases with IgA deposition. Int Urol Nephrol 2023; 55: 2119-29.
13. Bu L, Ye B, Kouri AM, Kim Y. Diagnostic utility of galactose-deficient immunoglobulin A1 immunostaining in the differentiation of lupus nephritis and immunoglobulin A nephropathy. Glomerular Dis 2021; 1: 34-9.
14. Ishiko S, Horinouchi T, Fujimaru R, et al. Glomerular galactose-deficient IgA1 expression analysis in pediatric patients with glomerular diseases. Sci Rep 2020; 10: 14026.
15. Zhao L, Peng L, Yang D, et al. Immunostaining of galactose-deficient IgA1 by KM55 is not specific for immunoglobulin A nephropathy. Clin Immunol 2020; 217: 108483.
16. Mima A, Lee S. IgA nephropathy after COVID-19 vaccination and analysis of reported cases. Heliyon 2023; 9: e17206.
17. Cassol CA, Bott C, Nadasdy GM, et al. Immunostaining for galactose-deficient immunoglobulin A is not specific for primary immunoglobulin A nephropathy. Nephrol Dial Transplant 2020; 35: 2123-9.
18. Wang M, Lv J, Zhang X, Chen P, Zhao M, Zhang H. Secondary IgA nephropathy shares the same immune features with primary IgA nephropathy. Kidney Int Rep 2020; 5: 165-72.
19. Chen CH, Wu MJ, Tsai SF. Safety and effectiveness of COVID-19 vaccines in patients with IgA nephropathy: a retrospective cohort study from the TriNetX global collaborative networks. EClinicalMedicine 2023; 65: 102306.
20. Nihei Y, Kishi M, Suzuki H, et al. IgA nephropathy with gross hematuria following COVID-19 mRNA vaccination. Intern Med 2022; 61: 1033-7.
21. Farooq H, Aemaz Ur Rehman M, Asmar A, Asif S, Mushtaq A, Qureshi MA. The pathogenesis of COVID-19-induced IgA nephropathy and IgA vasculitis: a systematic review. J Taibah Univ Med Sci 2022; 17: 1-13.

JPTM
ORIGINAL ARTICLE
pISSN 2383-7837 · eISSN 2383-7845
Journal of Pathology and Translational Medicine 2026; 60: 83-91
https://doi.org/10.4132/jptm.2025.10.14

Revisiting human sparganosis: a pathologic review from a single institution

Jeemin Yim[1], Young A Kim[1], Jeong Hwan Park[1], Hye Eun Park[1], Hyun Beom Song[2], Ji Eun Kim[1]

[1]Department of Pathology, Seoul Metropolitan Government-Seoul National University Boramae Medical Center, Seoul National University College of Medicine, Seoul, Korea
[2]Department of Tropical Medicine and Parasitology, Institute of Endemic Diseases, Seoul National University Medical Research Center, Seoul National University College of Medicine, Seoul, Korea

Graphical abstract

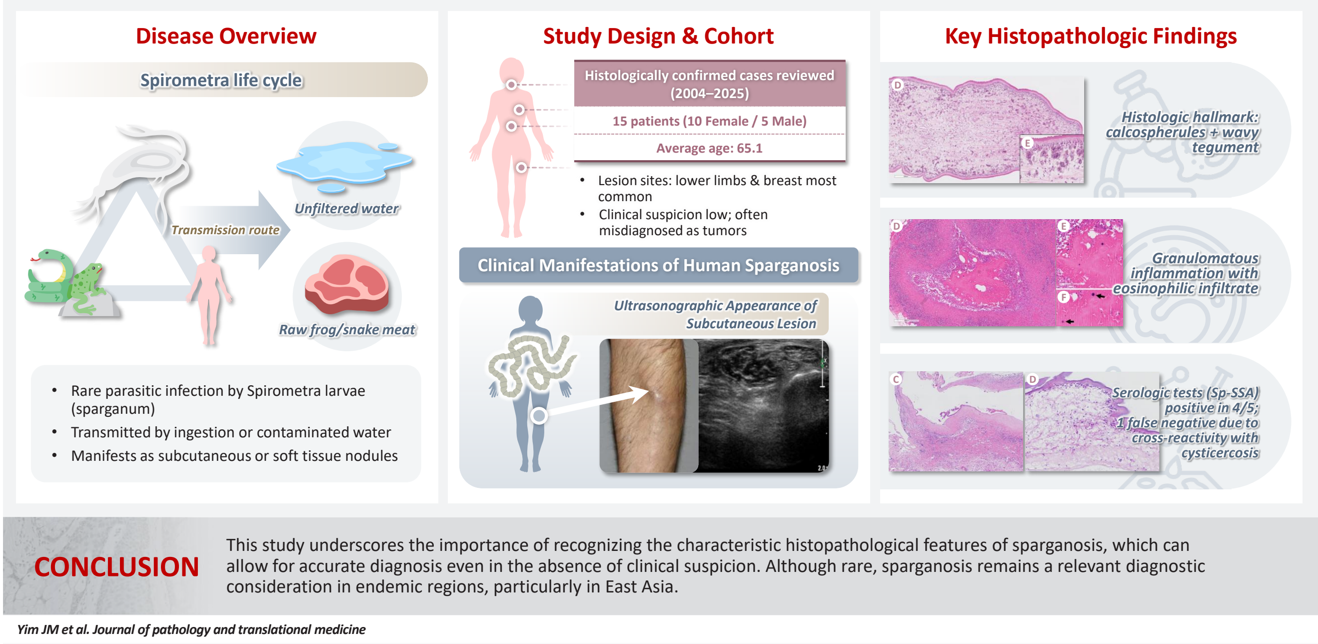

Disease Overview

Spirometra life cycle

- Rare parasitic infection by Spirometra larvae (sparganum)
- Transmitted by ingestion or contaminated water
- Manifests as subcutaneous or soft tissue nodules

Study Design & Cohort

Histologically confirmed cases reviewed (2004–2025)
15 patients (10 Female / 5 Male)
Average age: 65.1

- Lesion sites: lower limbs & breast most common
- Clinical suspicion low; often misdiagnosed as tumors

Clinical Manifestations of Human Sparganosis

Ultrasonographic Appearance of Subcutaneous Lesion

Key Histopathologic Findings

Histologic hallmark: calcospherules + wavy tegument

Granulomatous inflammation with eosinophilic infiltrate

Serologic tests (Sp-SSA) positive in 4/5; 1 false negative due to cross-reactivity with cysticercosis

CONCLUSION This study underscores the importance of recognizing the characteristic histopathological features of sparganosis, which can allow for accurate diagnosis even in the absence of clinical suspicion. Although rare, sparganosis remains a relevant diagnostic consideration in endemic regions, particularly in East Asia.

Yim JM et al. Journal of pathology and translational medicine

JPTM

ORIGINAL ARTICLE

pISSN 2383-7837 · eISSN 2383-7845

Journal of Pathology and Translational Medicine 2026; 60: 83-91
https://doi.org/10.4132/jptm.2025.10.14

Revisiting human sparganosis: a pathologic review from a single institution

Jeemin Yim[1], Young A Kim[1], Jeong Hwan Park[1], Hye Eun Park[1], Hyun Beom Song[2], Ji Eun Kim[1]

[1]Department of Pathology, Seoul Metropolitan Government-Seoul National University Boramae Medical Center, Seoul National University College of Medicine, Seoul, Korea
[2]Department of Tropical Medicine and Parasitology, Institute of Endemic Diseases, Seoul National University Medical Research Center, Seoul National University College of Medicine, Seoul, Korea

Background: Sparganosis is a rare parasitic infection caused by *Spirometra* species. Although it was relatively common in the past, it is now often overlooked. In this study, we review cases diagnosed through histopathological examination at a single institution in recent years to raise awareness of this neglected parasitic disease. **Methods:** We retrospectively analyzed cases of human sparganosis identified in the pathology archives of a single institution in South Korea between 2004 and 2025. A comprehensive review was conducted, including demographic data, clinical features, lesion locations, imaging findings, exposure history (such as dietary habits), and histopathologic findings. **Results:** A total of 15 patients were identified, including 10 females and 5 males, with a mean age of 65.1 years. Lesions were most commonly located in the lower extremities and breast. Imaging findings were largely nonspecific, with ultrasonography being the most frequently used modality. In most cases, clinical suspicion of sparganosis was absent, and excision was performed under the impression of a benign or malignant tumor. Histologically, variably degenerated parasitic structures were identified within granulomatous inflammation. However, preserved features such as calcospherules and tegumental structures facilitated definitive diagnosis. **Conclusions:** This study underscores the importance of recognizing the characteristic histopathological features of sparganosis, which can allow for accurate diagnosis even in the absence of clinical suspicion. Although rare, sparganosis remains a relevant diagnostic consideration in endemic regions, particularly in East Asia.

Keywords: Sparganosis; Infection; Parasite diseases

INTRODUCTION

Sparganosis is a rare parasitic infection in humans caused by the plerocercoid larvae (spargana) of *Spirometra* species, a genus of pseudophyllidean tapeworms [1]. Human infection typically occurs accidentally through the consumption of raw or undercooked amphibians or reptiles, or via drinking water contaminated with procercoid-infected copepods [1]. The life cycle of *Spirometra* involves multiple hosts, with humans serving as secondary or paratenic hosts.

Clinically, sparganosis most commonly presents as a slowly migrating subcutaneous nodule, which may be asymptomatic or mildly tender [2]. Depending on the site of invasion, spargana can involve the orbit, central nervous system, genitourinary tract, or visceral organs, sometimes resulting in significant symptoms. Radiologic studies may provide clues such as calcifications, tubular structures, or peritubular changes; however, these findings are usually nonspecific and rarely diagnostic [3-6]. Consequently, diagnosis is often made histopathologically following surgical excision, frequently in the absence of prior clinical suspicion. This makes diagnosis especially challenging for pathologists unfamiliar with its characteristic features.

Although rare globally, sparganosis is reported more frequently in East and Southeast Asia, particularly in Korea, Chi-

---

Received: September 22, 2025 **Revised:** September 30, 2025 **Accepted:** October 14, 2025

Corresponding Author: Ji Eun Kim, MD, PhD
Department of Pathology, Seoul Metropolitan Government-Seoul National University Boramae Medical Center, Seoul National University College of Medicine, 20 Boramae-ro 5-gil, Dongjak-gu, Seoul 07061, Korea
Tel: +82-2-870-2642, Fax: +82-2-831-0261, E-mail: npol181@snu.ac.kr

This is an Open Access article distributed under the terms of the Creative Commons Attribution Non-Commercial License (https://creativecommons.org/licenses/by-nc/4.0/) which permits unrestricted non-commercial use, distribution, and reproduction in any medium, provided the original work is properly cited.
© 2026 The Korean Society of Pathologists/The Korean Society for Cytopathology

na, Japan, and Thailand. In Korea, over 400 cases have been reported in the literature [7-13], although incidence has declined in recent years, likely due to improvements in public health and hygiene. Nevertheless, sporadic cases continue to be encountered.

Most literature consists of case reports or studies of uncommon anatomical involvement, while comprehensive analyses within defined populations remain limited. In this study, we present a case series of 15 histologically confirmed cases of human sparganosis diagnosed at a single institution in Korea over a 21-year period. This study aims to provide practical diagnostic insights for pathologists and to raise awareness of this neglected parasitic infection.

MATERIALS AND METHODS

A total of 15 cases of human sparganosis diagnosed at Seoul Metropolitan Government-Seoul National University Boramae Medical Center between 2004 and 2025 were included in this study. Two cases previously published as a case report [10] were also included to provide a comprehensive institutional review. Clinical data, imaging findings, exposure history (drinking of unfiltered water or ingestion of raw frog/snakes), and histopathological features were retrospectively reviewed.

RESULTS

Clinical and demographic features

Table 1 summarizes the clinical and histopathologic characteristics of the 15 patients. The cohort comprised 10 women and 5 men, with a mean age of 65.1 years (range, 46 to 83 years). All patients were Korean nationals except for one Chinese individual. Only two patients (13.3%) reported a history of consuming raw snake or frog meat. The remaining patients denied known exposures and were unable to recall any relevant risk factors. Serological testing for sparganum-specific antibody was performed in five patients, of whom four showed positive results (Table 1). In one spinal cord case, however, the sparganum enzyme-linked immunosorbent assay (ELISA) was negative while the cysticercosis antibody was slightly elevated, although histopathology confirmed sparganosis.

Anatomic distribution and imaging characteristics

Lesions were located predominantly in the subcutaneous tissue, most frequently in the lower extremities (n = 6) and breast (n = 4), followed by the trunk (n = 2), neck (n = 1), and pubic region (n = 1). One case involved the spinal canal, and none involved visceral organs. In most cases, sparganosis was not clinically suspected; lesions were often interpreted as benign tu-

Table 1. Summary of clinical profile of patients with sparganosis

No.	Sex	Age (yr)	Nation	Location	Imaging	Recurrences	Sp-SSA	Hx	CC	Clinical diagnosis
1	M	64	Korean	Lower leg	US	Yes	Pos	Yes	Migrating mass	Infection
2	F	58	Korean	Lower leg	US	No	N/A	Yes	Fluctuant mass	Infection
3	F	74	Korean	Trunk	N/A	No	N/A	No	Mass with heating sense	Unknown
4	F	53	Chinese	Neck, SC	US, CT	No	Pos	No	Mass	M. lymphoma
5	F	76	Korean	Lower leg	US, MRI	No	Pos	No	Tender mass	Phlebitis
6	M	79	Korean	Spinal cord	MRI	No	Neg[a]	No	Leg numbness	Neurogenic tumor
7[b]	F	46	Korean	Breast	US, MMG	No	N/A	No	N/A	Fat necrosis
8[b]	F	69	Korean	Breast	US, MMG	No	N/A	No	N/A	Infection
9	M	52	Korean	Trunk	US	No	N/A	No	N/A	Unknown
10	F	57	Korean	Lower leg	N/A	No	N/A	No	Palpable mass	Inflammatory nodule
11	F	60	Korean	Breast	US, MMG	No	N/A	No	Mass	Inflammatory nodule
12	F	70	Korean	Breast	US, MMG	No	N/A	No	Mass	Benign tumor
13	M	62	Korean	Pubic, SC	CT	No	N/A	No	Mass	Benign tumor
14	M	73	Korean	Lower leg	US, MRI	No	N/A	No	Mass	M. lymphoma
15	F	83	Korean	Lower leg	US	Yes	Pos	No	Multiple mass	Infection

Nation, Nationality; Sp-SSA, sparganosis serum specific antibody; Hx, history of drinking unfiltered water or ingestion of raw frog/snakes; CC, chief complaint; US, ultrasonography; Pos, positive; N/A, not assessed; CT, computed tomography; M. lymphoma, malignant lymphoma; MRI, magnetic resonance imaging; Neg, negative; MMG, mammography; SC, subcutis.

[a]Sparganum enzyme-linked immunosorbent assay was negative but cysticercosis antibody was slightly elevated, while histopathology confirmed sparganosis; [b]Cases previously reported [10].

mors, lymphadenopathy, or mesenchymal neoplasms. Ultrasonography was the most commonly used imaging modality, typically revealing nonspecific hypoechoic or tubular structures.

Summary of clinicopathologic findings in representative cases

The patients exhibited diverse clinical manifestations, often leading to diagnostic confusion. In cases 1 and 2, soft tissue masses yielded intact or live spargana during surgical excision (Figs. 1, 2). Case 1 involved a 64-year-old male with a crawling sensation in both legs and a history of consuming raw snake and frog meat. In case 2, a 58-year-old female had a long-standing thigh mass since childhood, with no known exposure history. Case 3 presented with multiple subcutaneous nodules mimicking benign cysts.

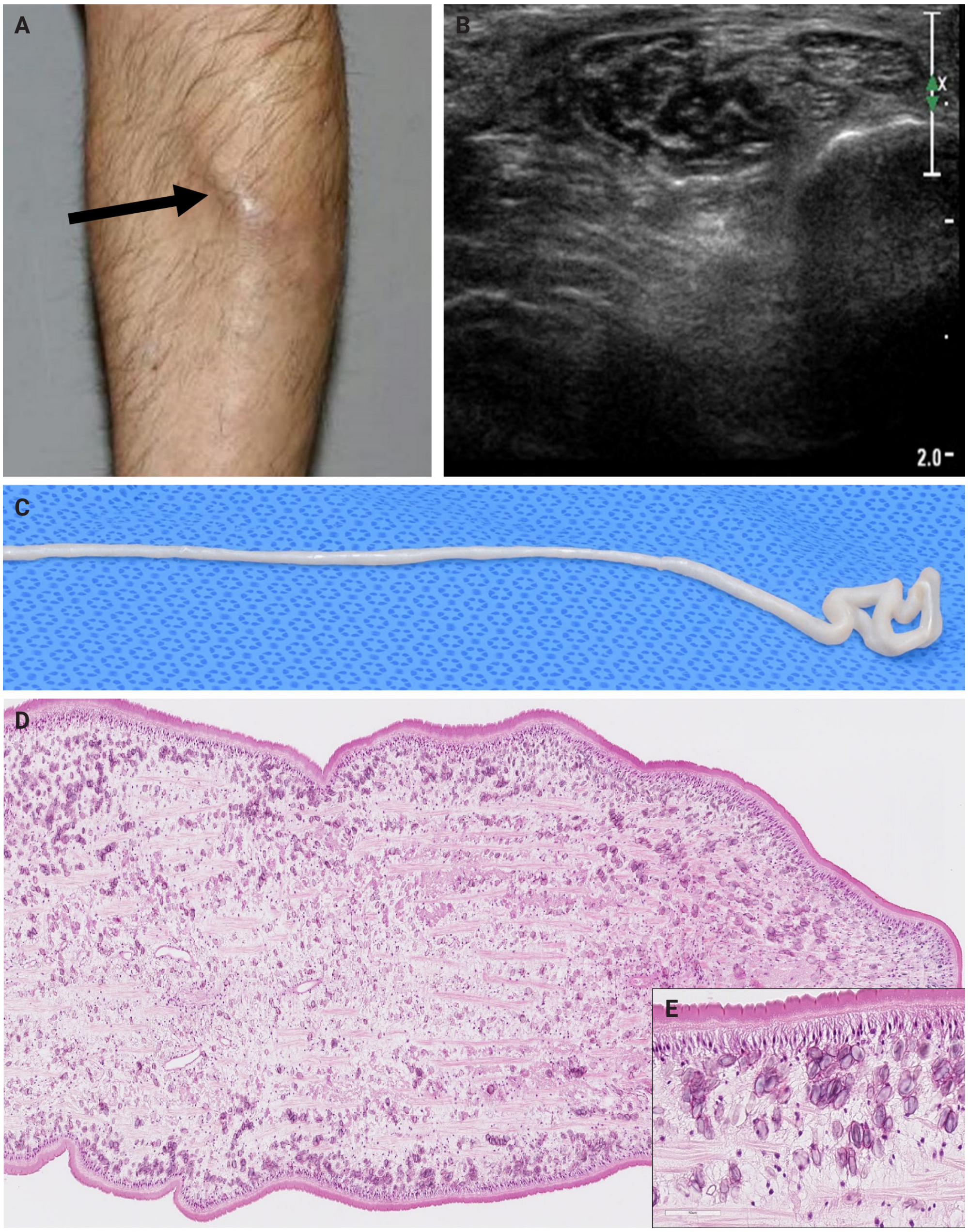

Fig. 1. Case 1. (A) Subcutaneous nodule (arrow). (B) Ultrasonography showing a well-defined serpentine hypoechoic lesion. (C) Gross specimen of an elongated whitish plerocercoid worm. (D, E) Histopathological sections showing a thick eosinophilic tegument, muscle fibers, and calcareous corpuscles.

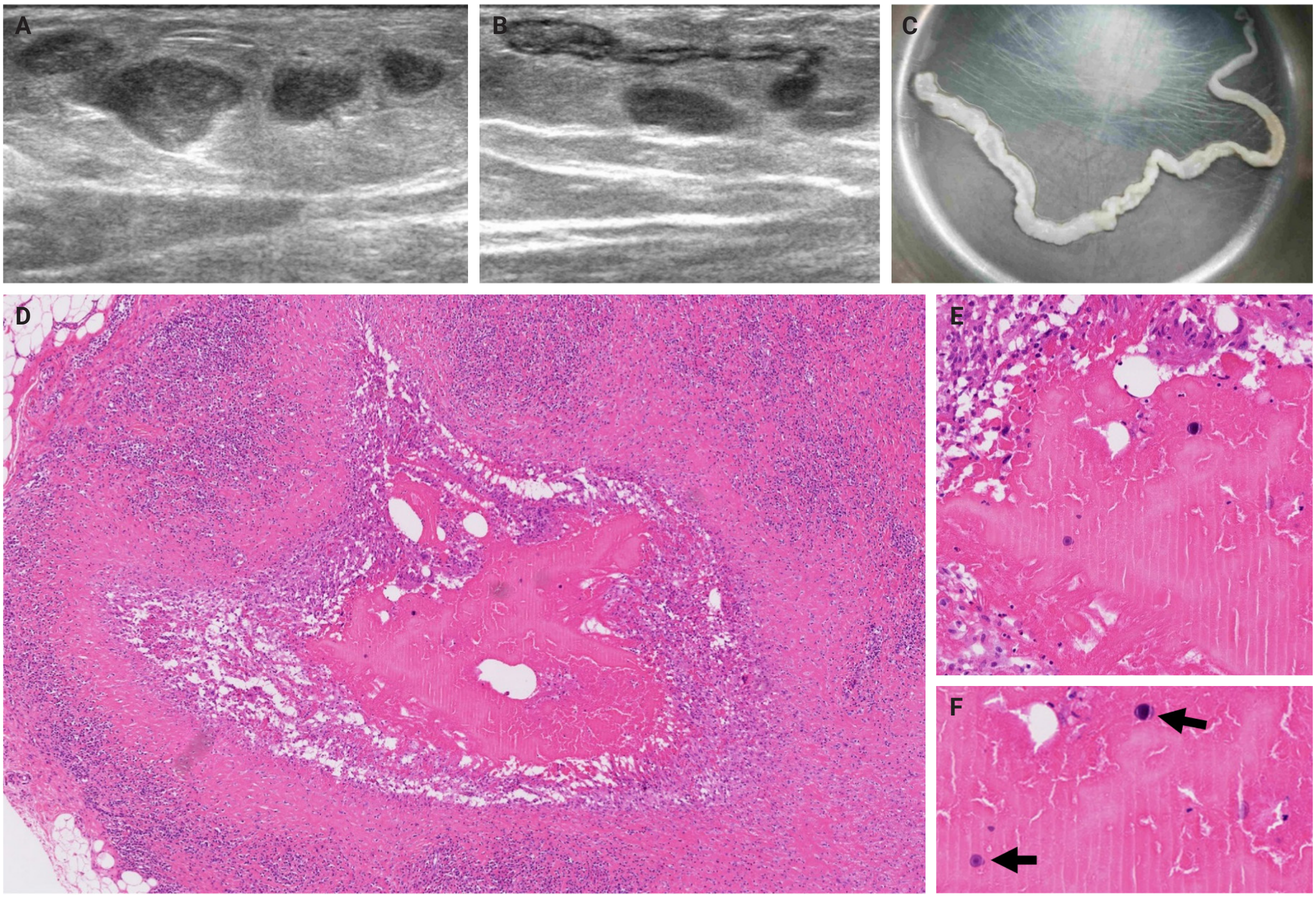

Fig. 2. Case 2. (A, B) Ultrasonography showing elongated structures with perilesional subcutaneous inflammation in the right inner thigh. (C) Gross specimen of an ivory-colored tapeworm, 20 cm in length. (D–F) Fibrotic tissue and granulomatous inflammation surrounding parasitic fragments, with recognizable calcareous corpuscles (arrows, far lower right).

Histologic examination revealed several larval structures embedded in the subcutaneous tissue, surrounded by eosinophilic and giant cell-rich inflammation (Fig. 3). Case 4 involved a neck mass initially suspected to be malignant lymphoma or metastatic carcinoma. Surgical excision revealed necrotic larval fragments with granulomatous inflammation (Fig. 4). Case 5 showed an erythematous, tender, S-shaped linear lesion on the thigh, clinically resembling phlebitis; histology demonstrated a necrotic worm in the dermis with microcalcifications and chronic inflammation (Fig. 5). In case 6, a spinal lesion caused neurologic symptoms and was radiologically interpreted as a nerve sheath tumor. Surgical resection revealed calcified parasite remnants within a yellowish translucent cystic mass (Fig. 6).

DISCUSSION

Despite improvements in hygiene and public health, sporadic cases of sparganosis continue to occur. Pathologists should maintain a high index of suspicion for sparganosis in patients presenting with subcutaneous masses, even in the absence of a relevant exposure history. In our series, most patients were elderly women, and only two reported a history of consuming raw amphibians or reptiles; none had occupations associated with zoonotic exposure. These observations raise the possibility of an alternative, previously unrecognized route of infection, warranting further investigation. Potential routes could include consumption of undercooked fish or untreated drinking water and, although less probable, exposure to companion animals. While domestic dogs and cats are definitive hosts and do not typically transmit spargana to humans, prior studies from Iran, China, and Vietnam have reported Spirometra larvae in up to 40% of domestic animals [14-16]. Further population-based studies are needed to clarify the roles of sex, tissue characteristics, and environmental exposures in sparganosis epidemiology.

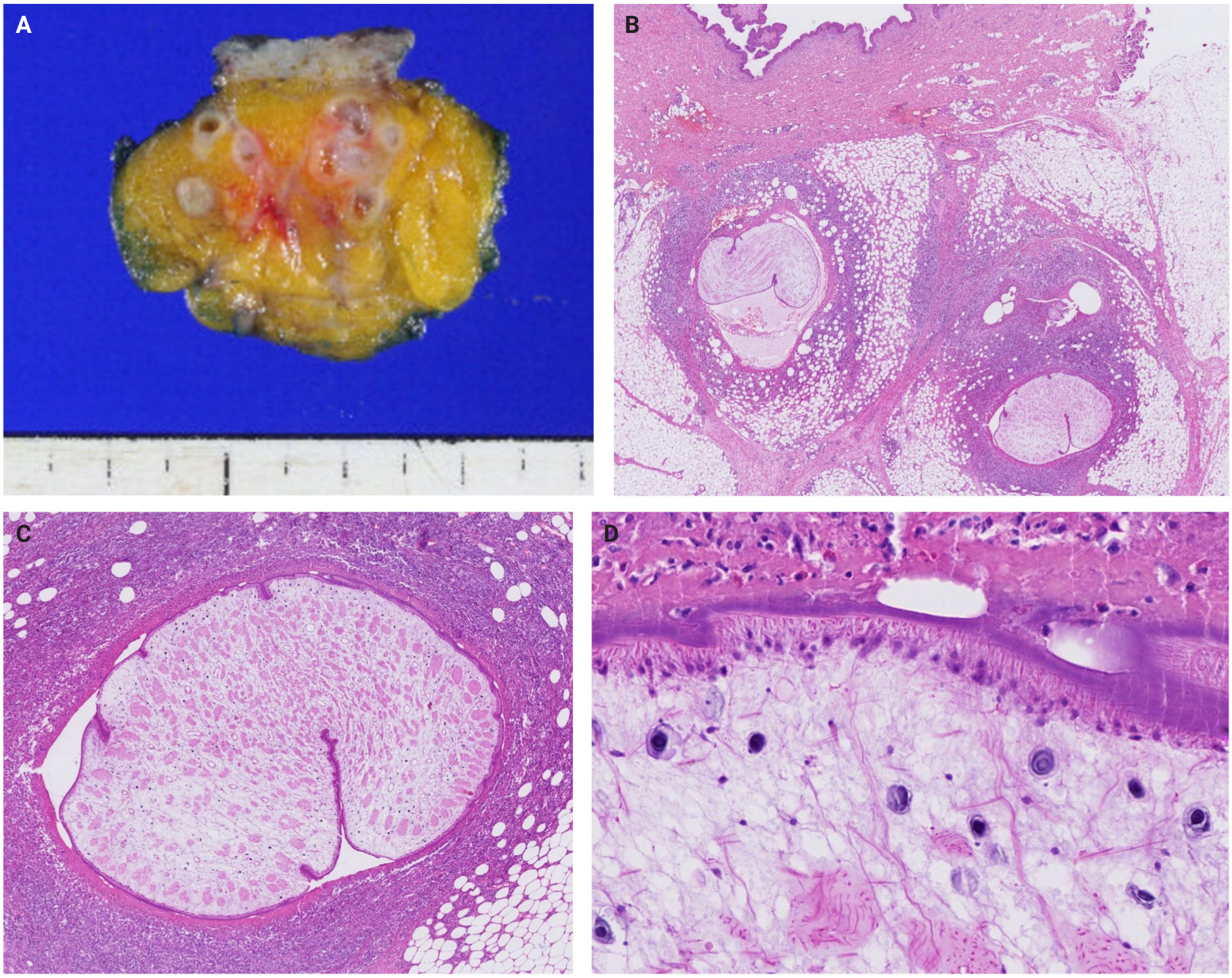

Fig. 3. Case 3. (A) Multiple small circular cavities in the subcutaneous tissue. (B) Larval structures surrounded by dense inflammatory cells. (C, D) Cross-sectioned spargana, readily discernible.

Viable parasites were associated with symptoms such as a crawling sensation or localized warmth. Most diagnoses relied on remnants of the parasite, including calcareous corpuscles or tegumental fragments, rather than intact worms. When residing in human tissues, particularly confined subcutaneous spaces, spargana can cause necrotizing lesions of irregular shape, granulomas, and fibrosis due to tissue damage from parasite movement. Irregular or radiating borders of granulomatous inflammation and abundant eosinophilic infiltration are commonly observed in sparganosis and other forms of cutaneous larva migrans (CLM). However, sparganum larvae display highly characteristic features—including internal calcospherules and an undulating wavy tegument—which are absent in CLM.

Spargana may survive for extended periods, especially in immune-privileged sites such as the brain and eyes [17-20], possibly due to reduced immune surveillance. Experimental studies have demonstrated similar patterns, including variable preservation of parasite structures, granuloma formation, and chronic inflammation [21]. These findings correlate with our human cases, particularly those in which parasites had degenerated significantly.

In our series, serological testing was performed in a few patients. Interestingly, in one case of spinal cord sparganosis, sparganum-specific ELISA yielded a negative result, whereas the cysticercosis antibody level was slightly elevated. Despite this discrepancy, histopathological examination confirmed sparganosis. This case highlights the potential cross-reactivity of ELISA with cysticercosis and underscores the limited reliability of serological testing in isolation. Therefore, serological results should be interpreted with caution, particularly in endemic ar-

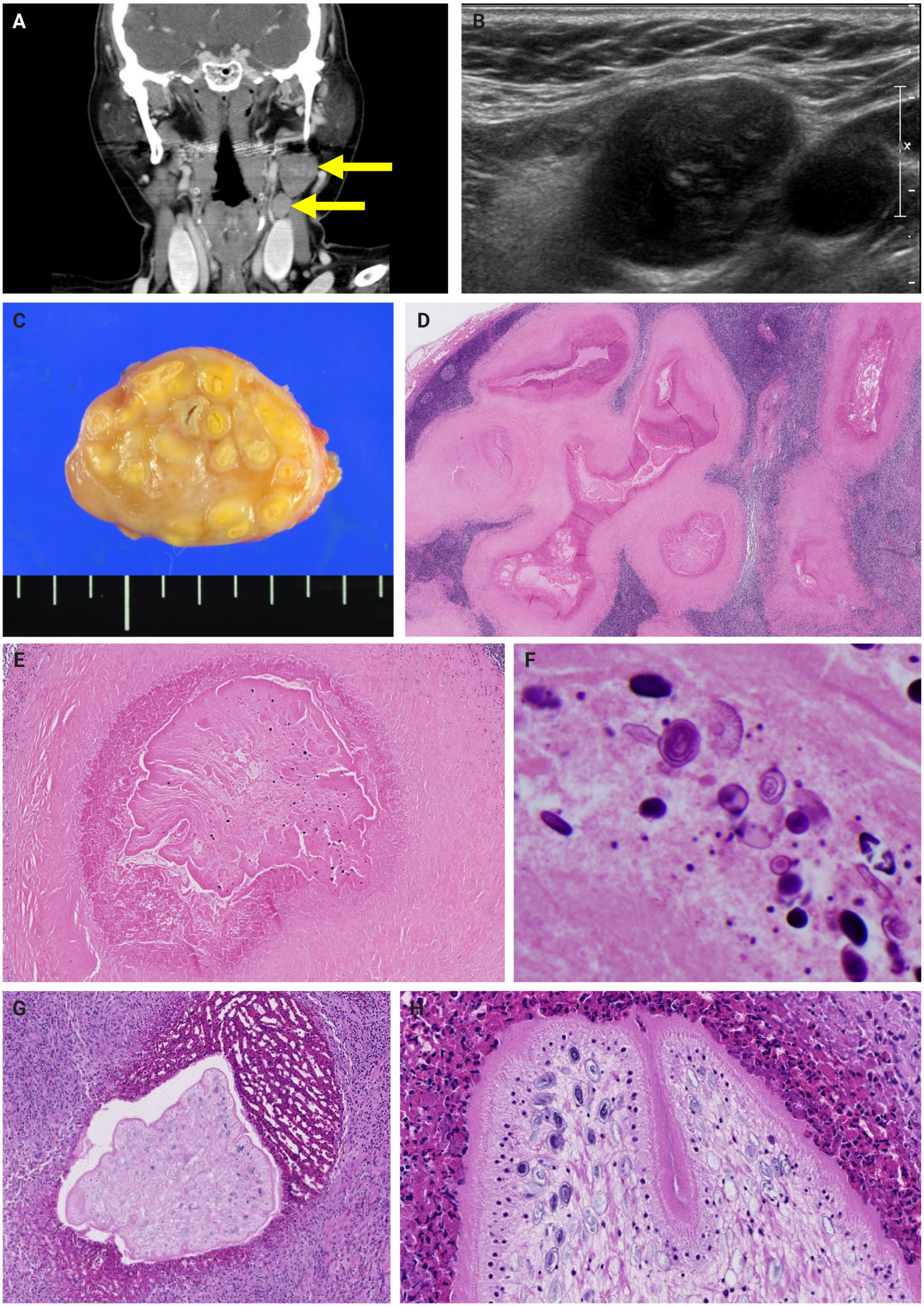

Fig. 4. Case 4. (A) Computed tomography and (B) ultrasonography showing multiple homogeneously enhancing cervical lymph nodes (arrows; enlarged cervical nodes), suspicious for malignant lymphoma or metastasis. (C) Gross specimen with multiple yellowish cystic cavities. (D–H) Necrotic nodules containing degenerated worms with scalloped cuticles and cladophores.

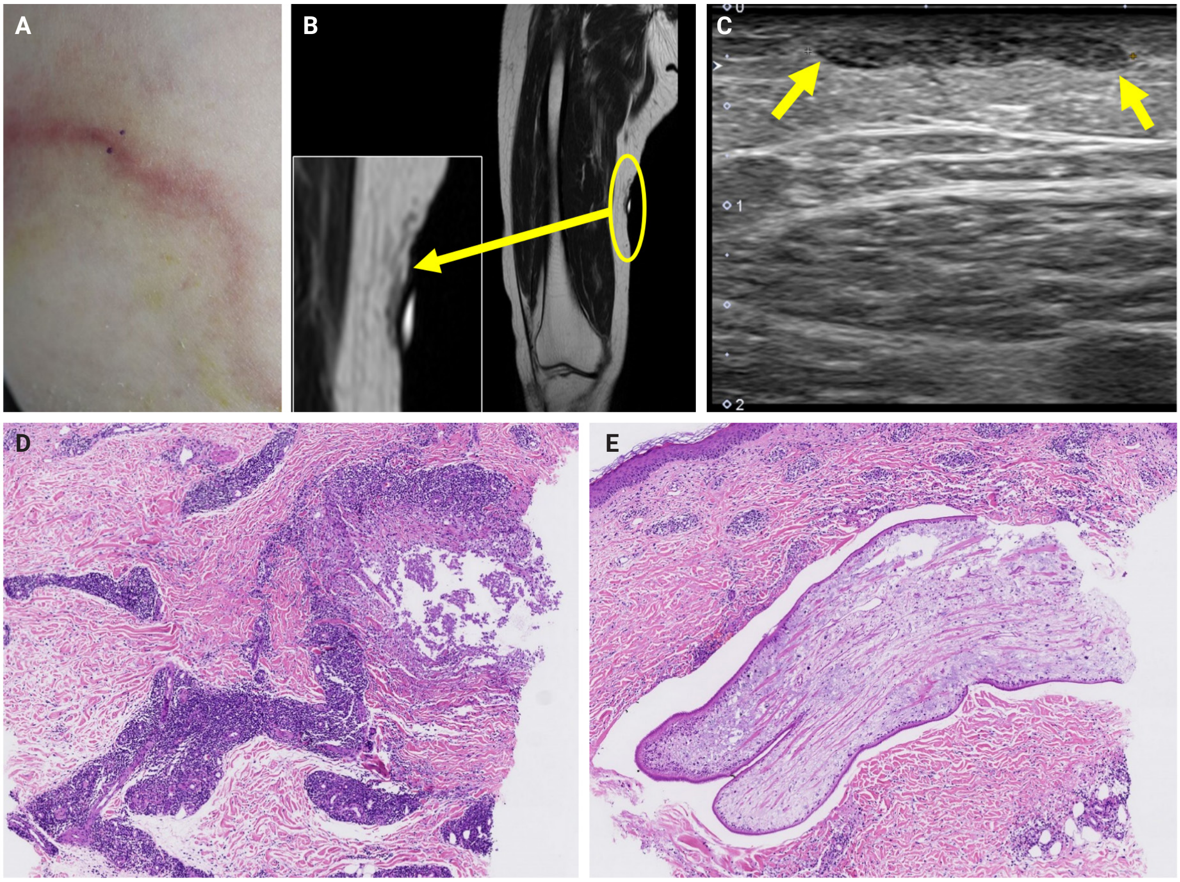

Fig. 5. Case 5. (A) Clinical photograph showing an S-shaped erythematous linear lesion on the inner thigh. (B) Magnetic resonance image showing a low-signal intensity lesion with peripheral enhancement (arrow indicates the lesion). (C) Ultrasonography showing a 2-cm tubular lesion in the subcutis (arrows indicate the lesion). (D) Granulomatous inflammation with a focal necrotic center. (E) Parasite embedded within the cyst.

eas for both sparganosis and cysticercosis, and histopathology remains the gold standard for definitive diagnosis.

Imaging findings vary by site and stage of infection. Early lesions or live worms may appear as mobile tubular structures, whereas older lesions often show nonspecific low-density areas, calcifications, fibrosis, or cystic changes. Such lesions may be misdiagnosed as complicated epidermal cysts, organized abscesses, or post-traumatic pseudocysts. In our series, one patient with a lateral neck mass (case 3) was initially suspected to have metastatic lymph node involvement. The most significant histopathologic diagnostic pitfall is likely confusion with a tuberculous lesion due to an acellular necrotic center surrounded by granulomatous reaction. Histopathological distinction between sparganosis and cysticercosis may also pose challenges, especially when specimens are old, fragmented, or degenerated. In such circumstances, the absence of a bladder wall and fibrillary stroma and the presence of longitudinal smooth muscle bundles and calcareous corpuscles are helpful features favoring sparganosis. Careful recognition of these features is essential to avoid misdiagnosis, particularly in small biopsy samples.

Subcutaneous sparganosis should be distinguished from other conditions presenting with nodular lesions, including Kimura disease. Both entities may appear as slowly enlarging, painless subcutaneous nodules with marked tissue eosinophilia and reactive fibrosis. However, the absence of characteristic histopathologic features of Kimura disease—such as lymphoid follicular hyperplasia, eosinophilic microabscesses, and florid vascular proliferation—together with the presence of larval remnants embedded in granulomatous lesions, are key clues to sparganosis. Awareness of this differential diagnosis is essential for accurate evaluation of subcutaneous nodules in endemic areas.

Although previous reports have consistently documented a

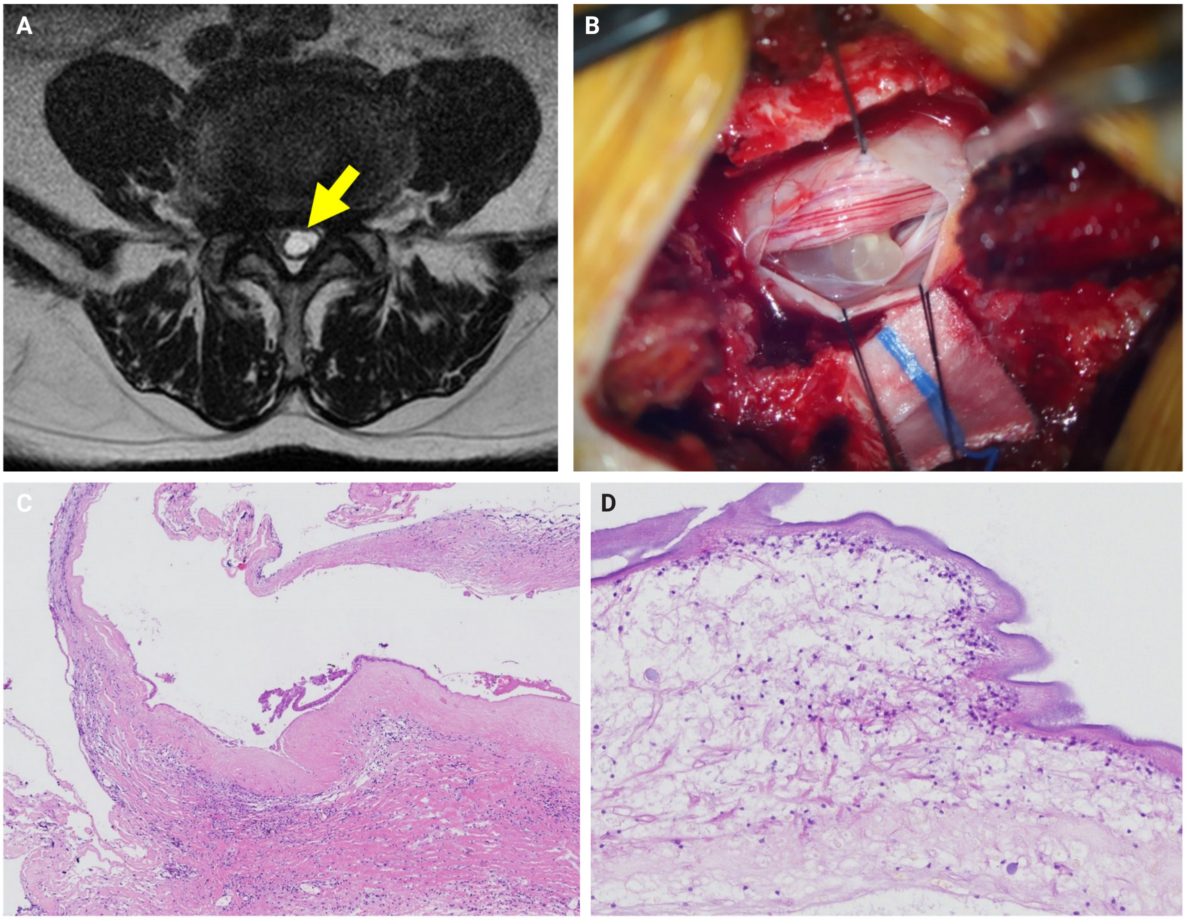

Fig. 6. Case 6. (A) T2-weighted magnetic resonance image showing a 0.9-cm lesion causing central canal compromise (arrow indicates the lesion). (B) Intraoperative photograph of a whitish-yellow cystic mass. (C) Histopathological section showing a cystic lesion filled with necrotic debris, surrounded by dense fibrosis and chronic inflammation. (D) Degenerated parasitic fragments with calcified corpuscles, characteristic of sparganum.

male predominance in sparganosis, our series showed a striking predominance of female patients. This may reflect greater sensitivity in detecting lesions or a higher likelihood of seeking medical attention among women. Additionally, the relatively softer subcutaneous or soft tissue composition in females could provide a more favorable microenvironment for Spirometra larvae.

Although sparganosis has become increasingly rare, it remains an important differential diagnosis for subcutaneous masses, particularly in endemic areas. Most cases are diagnosed histopathologically, often without prior clinical suspicion. Recognizing the characteristic histologic features—even in the absence of intact worms—is essential for accurate diagnosis and appropriate patient management.

Ethics Statement

This study was approved by the Institutional Review Board (IRB) of BRMH (No.10-2025-41) and the requirement for informed consent was waived.

Availability of Data and Material

All data generated or analyzed during the study are included in this published article.

Code Availability

Not applicable.

ORCID

Jeemin Yim	https://orcid.org/0000-0002-8571-7486
Young A Kim	https://orcid.org/0000-0002-8253-2881

Jeong Hwan Park https://orcid.org/0000-0003-4522-9928
Hye Eun Park https://orcid.org/0000-0003-1048-2827
Hyun Beom Song https://orcid.org/0000-0002-3500-2984
Ji Eun Kim https://orcid.org/0000-0002-2156-9875

Author Contributions

Conceptualization: JEK. Data curation: JEK, JY, YAK, JHP, HEP, HBS. Investigation: JEK, JY. Project Administration: JEK, JY. Resources: JEK, JY, YAK, JHP, HEP. Writing—original draft preparation: JEK, JY. Writing—review & editing: all authors. Approval of the final manuscript: all authors.

Conflicts of Interest

J.H.P., a contributing editor of the *Journal of Pathology and Translational Medicine*, was not involved in the editorial evaluation or decision to publish this article. All remaining authors have declared no conflicts of interest.

Funding Statement

No funding to declare.

REFERENCES

1. Liu Q, Li MW, Wang ZD, Zhao GH, Zhu XQ. Human sparganosis, a neglected food borne zoonosis. Lancet Infect Dis 2015; 15: 1226-35.
2. Kim JG, Ahn CS, Sohn WM, Nawa Y, Kong Y. Human sparganosis in Korea. J Korean Med Sci 2018; 33: e273.
3. Cho JH, Lee KB, Yong TS, et al. Subcutaneous and musculoskeletal sparganosis: imaging characteristics and pathologic correlation. Skeletal Radiol 2000; 29: 402-8.
4. Kim HS, Cha ES, Kim HH, Yoo JY. Spectrum of sonographic findings in superficial breast masses. J Ultrasound Med 2005; 24: 663-80.
5. Kim HY, Kang CH, Kim JH, Lee SH, Park SY, Cho SW. Intramuscular and subcutaneous sparganosis: sonographic findings. J Clin Ultrasound 2008; 36: 570-2.
6. Choi SJ, Park SH, Kim MJ, Jung M, Ko BH. Sparganosis of the breast and lower extremities: sonographic appearance. J Clin Ultrasound 2014; 42: 436-8.
7. Wiwanitkit V. A review of human sparganosis in Thailand. Int J Infect Dis 2005; 9: 312-6.
8. Koo M, Kim JH, Kim JS, Lee JE, Nam SJ, Yang JH. Cases and literature review of breast sparganosis. World J Surg 2011; 35: 573-9.
9. Anantaphruti MT, Nawa Y, Vanvanitchai Y. Human sparganosis in Thailand: an overview. Acta Trop 2011; 118: 171-6.
10. Oh MY, Kim KE, Kim MJ, et al. Breast sparganosis presenting with a painless breast lump: report of two cases. Korean J Parasitol 2019; 57: 179-84.
11. Hwang M, Baek HJ, Lee SM. Apparent sparganosis presenting as a palpable neck mass: a case report and review of literature. Taehan Yongsang Uihakhoe Chi 2020; 81: 1210-5.
12. Okino T, Yamasaki H, Yamamoto Y, et al. A case of human breast sparganosis diagnosed as spirometra type I by molecular analysis in Japan. Parasitol Int 2021; 84: 102383.
13. Liu W, Gong T, Chen S, et al. Epidemiology, diagnosis, and prevention of sparganosis in Asia. Animals (Basel) 2022; 12: 1578.
14. Hong Q, Feng J, Liu H, et al. Prevalence of *Spirometra mansoni* in dogs, cats, and frogs and its medical relevance in Guangzhou, China. Int J Infect Dis 2016; 53: 41-5.
15. Beiromvand M, Rafiei A, Razmjou E, Maraghi S. Multiple zoonotic helminth infections in domestic dogs in a rural area of Khuzestan Province in Iran. BMC Vet Res 2018; 14: 224.
16. Nguyen YT, Nguyen LA, Van Dong H, Duong HD, Yoshida A. Molecular identification of sparganum of *Spirometra mansoni* isolated from the abdominal cavity of a domestic cat in Vietnam. J Vet Med Sci 2024; 86: 96-100.
17. Nobayashi M, Hirabayashi H, Sakaki T, et al. Surgical removal of a live worm by stereotactic targeting in cerebral sparganosis: case report. Neurol Med Chir (Tokyo) 2006; 46: 164-7.
18. Yang JW, Lee JH, Kang MS. A case of oular sparganosis in Korea. Korean J Ophthalmol 2007; 21: 48-50.
19. Nkwerem S, Goto T, Ogiwara T, Yamamoto Y, Hongo K, Ohaegbulam S. Ultrasound-assisted neuronavigation-guided removal of a live worm in cerebral sparganosis. World Neurosurg 2017; 102: 696.
20. Hu J, Liao K, Feng X, et al. Surgical treatment of a patient with live intracranial sparganosis for 17 years. BMC Infect Dis 2022; 22: 353.
21. Chang KH, Lee GJ, Han MH, et al. An experimental study on imaging diagnosis of cerebral sparganosis. J Korean Radiol Soc 1995; 33: 171-82.

JPTM

ORIGINAL ARTICLE

pISSN 2383-7837 · eISSN 2383-7845

Journal of Pathology and Translational Medicine 2026; 60: 92-106
https://doi.org/10.4132/jptm.2025.10.15

Correlations and prognostic impacts of tumor spread through airspaces in surgically resected non–small cell lung cancer: a retrospective study from Jordan

Ola Abu Al Karsaneh[1], Amani Al-Rousan[2], Sofian Al Shboul[3], Mohammed El-Sadoni[2], Anas Hayajneh[4], Moath Alrjoub[4], Sura Al-Rawabdeh[2], Tareq Saleh[3,5]

[1]Department of Microbiology, Pathology and Forensic Medicine, Faculty of Medicine, The Hashemite University, Zarqa, Jordan
[2]Princess Iman Center for Research and Laboratory Sciences, King Hussein Medical Center, Royal Medical Services, Amman, Jordan
[3]Department of Pharmacology and Public Health, Faculty of Medicine, The Hashemite University, Zarqa, Jordan
[4]Department of Pathology and Microbiology, Faculty of Medicine, Jordan University of Science and Technology, Irbid, Jordan
[5]Department of Pharmacology & Therapeutics, College of Medicine & Health Sciences, Arabian Gulf University, Manama, Bahrain

Graphical abstract

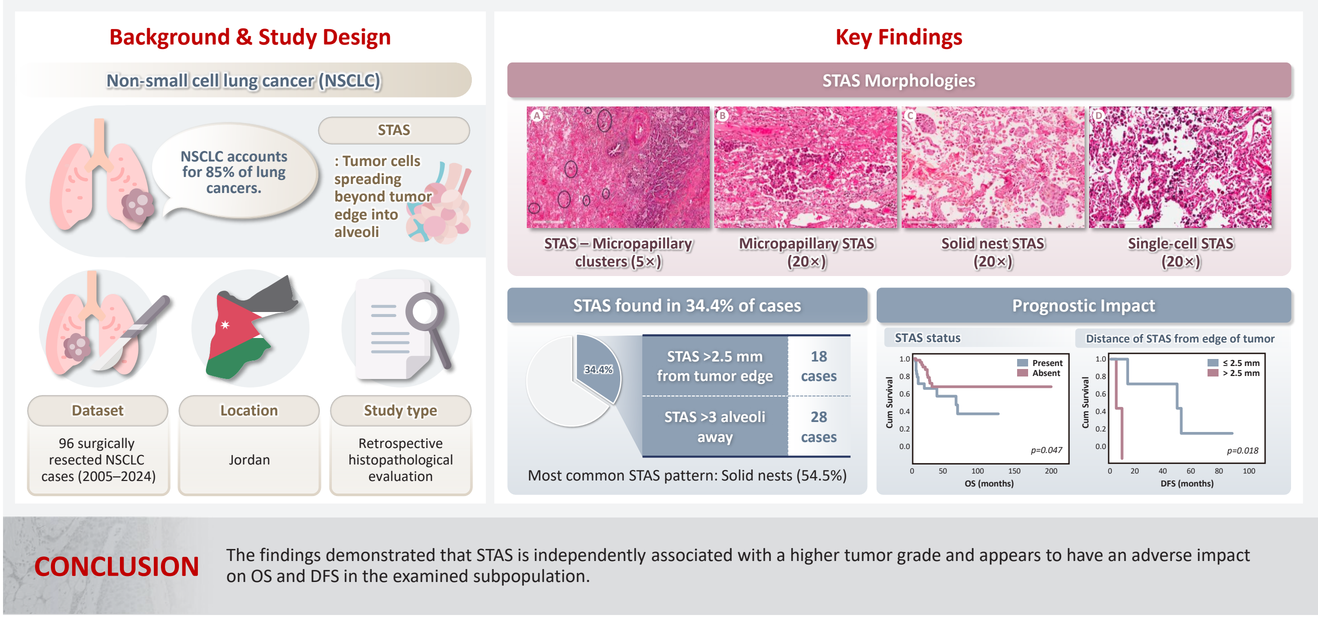

The findings demonstrated that STAS is independently associated with a higher tumor grade and appears to have an adverse impact on OS and DFS in the examined subpopulation.

Abu Al Karsaneh O et al. Journal of pathology and translational medicine

JPTM

ORIGINAL ARTICLE

pISSN 2383-7837 · eISSN 2383-7845

Journal of Pathology and Translational Medicine 2026; 60: 92-106
https://doi.org/10.4132/jptm.2025.10.15

Correlations and prognostic impacts of tumor spread through airspaces in surgically resected non–small cell lung cancer: a retrospective study from Jordan

Ola Abu Al Karsaneh[1], Amani Al-Rousan[2], Sofian Al Shboul[3], Mohammed El-Sadoni[2], Anas Hayajneh[4], Moath Alrjoub[4], Sura Al-Rawabdeh[2], Tareq Saleh[3,5]

[1]Department of Microbiology, Pathology and Forensic Medicine, Faculty of Medicine, The Hashemite University, Zarqa, Jordan
[2]Princess Iman Center for Research and Laboratory Sciences, King Hussein Medical Center, Royal Medical Services, Amman, Jordan
[3]Department of Pharmacology and Public Health, Faculty of Medicine, The Hashemite University, Zarqa, Jordan
[4]Department of Pathology and Microbiology, Faculty of Medicine, Jordan University of Science and Technology, Irbid, Jordan
[5]Department of Pharmacology & Therapeutics, College of Medicine & Health Sciences, Arabian Gulf University, Manama, Bahrain

Background: Spread through air spaces (STAS) has been identified as an invasion pattern in non–small cell lung cancer (NSCLC). This study evaluated the association between tumor STAS and various clinicopathological parameters of NSCLC, with emphasis on the prognostic role of STAS. **Methods:** We evaluated 96 cases of NSCLC for STAS. STAS-positive cases were graded according to the distance between the edge of the primary tumor and the furthest STAS, in millimeters, or the number of alveoli separating STAS from the tumor. **Results:** STAS was observed in 33 patients (34.4%). In 28 cases, STAS was located in airspaces >3 alveoli away from the primary tumor. In 18 cases, STAS was found in airspaces > 2.5 mm away from the edge of the primary tumor. Morphologically, 18 cases of STAS demonstrated a solid nest pattern, eight showed a micropapillary cluster pattern, and seven exhibited a single-cell pattern. In multivariate analysis, only high tumor grade ($p = .001$) was independently associated with STAS in NSCLC. The presence of STAS ($p = .047$), lymphovascular invasion ($p = .001$), positive surgical margin ($p = .021$), adenocarcinoma histology ($p = .020$), and postoperative therapy ($p = .049$) showed a statistically significant lower overall survival (OS). However, multivariate analyses showed that STAS is not an independent predictor of OS in NSCLC. In addition, STAS-positive cases with an extension of >2.5 mm had significantly lower disease-free survival (DFS) ($p = .018$). **Conclusions:** The findings demonstrated that STAS is independently associated with a higher tumor grade and appears to have an adverse impact on OS and DFS in the examined subpopulation.

Keywords: Spread through air spaces; Lung neoplasms; Prognosis; Lymphovascular invasion; Jordan

INTRODUCTION

Lung cancer remains a primary cause of cancer-related mortality worldwide, despite the reported decline in cancer mortality rates, significantly driven by lung cancer due to early detection and advances in treatment [1]. Non–small cell lung cancer (NSCLC) accounts for about 85% of lung cancer cases. In Jordan, lung cancer is the third most common cancer in both sexes and the most common cause of cancer-related mortality in males [2].

Metastasis and invasion are the major prognostic factors in cancer patients. Invasive mechanisms in lung cancer include non-lepidic histological patterns and stromal, vascular, lymphatic, and pleural invasions. Shiono et al. [3] suggested that the presence of 10 or more floating clusters of cancer cells in the airspaces surrounding main tumors in cases of pulmonary metastasis from colorectal cancer was significantly related to local recurrence in these patients. Subsequently, Onozato et al. [4] reported the presence of tumor islands outside the borders

---

Received: June 14, 2025 **Revised:** September 4, 2025 **Accepted:** October 14, 2025

Corresponding Author: Ola Abu Al Karsaneh, MD
Department of Microbiology, Pathology and Forensic Medicine, Faculty of Medicine, The Hashemite University, Zarqa 13133, Jordan
Tel: +962-062-5-390-3333 (5577), Fax: +962-5-3903352, E-mail: olaa@hu.edu.jo

This is an Open Access article distributed under the terms of the Creative Commons Attribution Non-Commercial License (https://creativecommons.org/licenses/by-nc/4.0/) which permits unrestricted non-commercial use, distribution, and reproduction in any medium, provided the original work is properly cited.
© 2026 The Korean Society of Pathologists/The Korean Society for Cytopathology

of the primary tumors in cases of primary lung adenocarcinoma (ADC); these islands were located at least a few alveoli away from the main tumor. Moreover, cases associated with these tumor islands carried a significantly worse prognosis and a higher risk of recurrence compared to those without these tumor islands. In 2015, the concept of spread through air spaces (STAS) was considered by the World Health Organization (WHO) as a mechanism of invasion in lung ADC [5] based on a validation of the concept in two large studies [6,7].

STAS is defined as the spread of single cells, solid nests, or micropapillary clusters of cancer cells into air spaces in the lung parenchyma beyond the edge of the primary tumor. The presence of STAS diagnoses lepidic ADC and excludes a diagnosis of adenocarcinoma in situ (AIS) or minimally invasive adenocarcinoma (MIA) in small tumors [5]. Although most of the studies investigated the characteristics of STAS in conventional lung ADC, it has also been described in other primary lung tumors, including invasive mucinous ADC [8], squamous cell carcinoma (SqCC) [9], and neuroendocrine tumors [10]. The reported incidence of STAS in lung cancer ranges between 15% and 73%, according to different studies and depending on the different stages of the involved tumors [11-17]. Some studies found that the presence of STAS was associated with higher tumor grade, higher tumor stage, lymph node metastasis, high-grade architectural patterns (micropapillary and solid growth patterns), absence of lepidic component, pleural invasion, and lymphovascular and perineural invasion [12-14,16]. More importantly, several reports indicated that STAS is associated with shorter overall survival (OS) and recurrence-free survival (RFS) in patients with lung ADC treated with surgery, suggesting its potential role as a significant risk factor for recurrence [11,18-26]. Different attempts have been made to score STAS according to the number of floating tumor clusters [27] or the distance from the edge of the primary tumor [7,14,28]; however, no consensus has been reached.

Lobectomy has been considered the primary surgical procedure for early-stage lung cancer. However, depending on the overall conditions of the patient, sub-lobar resections, including wedge resection and segmentectomy, are considered an acceptable alternative [29,30]. Although there is no consensus on whether these limited resections increase the risk of regional recurrence compared to lobectomy in patients with STAS, some studies reported that sub-lobar resection was associated with a higher recurrence risk in patients with early-stage lung cancer who have STAS [22,31,32]. Considering this reported adverse effect, it appears that STAS-positive patients who receive sub-lobar resection may benefit from a completion lobectomy or adjuvant therapy to lower the chance of recurrence. However, an undocumented observation in Jordanian hospitals indicated that a majority of surgeons and pathologists do not consider the prognostic effect of STAS. Hence, this study aimed to assess the incidence of STAS in NSCLC, its correlation with various clinicopathological variables, and its prognostic value in a subpopulation of Jordanian patients. This may help in the prognostic stratification of the patients and the determination of the need for any further treatment.

MATERIALS AND METHODS

Study setting and patients' sample

In this work, we retrospectively collected the data and tissue samples of the patients who underwent surgical resection of their primary lung cancer at Jordan Royal Medical Services (JRMS) and King Abdullah University Hospital (KAUH) between 2005 and 2024. The inclusion criteria included patients with a primary lung cancer diagnosis of any stage and any histological subtype who underwent wedge resection, segmentectomy, lobectomy, or pneumonectomy. The exclusion criteria included the following: (1) postoperative diagnosis of AIS or MIA; (2) the utilization of preoperative neoadjuvant therapy; (3) patients with multiple primary lung tumors; (4) lack of tumor slides or tissue for review; and (5) incomplete clinical and follow-up data. After applying these criteria, 96 cases (63 from JRMS and 33 from KAUH) were enrolled. The patients' relevant clinicopathological parameters, including age, sex, smoking history, tumor location, surgical procedure, histological subtypes, margin status, pathological stage, and follow-up data, were obtained from the patients' original medical records and pathological reports.

The surgically resected lung cancer specimens were fixed using the conventional fixation method, where the specimens were immersed and fixed in 10% neutral-buffered formalin within 5 minutes of the resection. Formalin was injected into the bronchi or through the pleura until the lung was dilated, allowing the formalin to permeate the specimen. The fixation duration ranged from 18 to 48 hours. Paraffin-embedded 4-µm sections, hematoxylin and eosin (H&E)–stained slides of all cases were thoroughly reviewed by two pathologists to confirm the histological features and assess other features not included in the pathology report (O.A.A.K. and A.A.R.). Tumor subtypes were determined according to the WHO guidelines [5,33]. Grading of the ADC cases was determined based on the combination of the predominant and the worst architectural patterns [33,34]. Briefly, tumors predominantly having a lepidic architecture with less than 20% of high-grade patterns (solid, micropapillary, cribriform, or complex glands) were classified as well differentiated ADC (grade 1); tumors predominantly having acinar and papillary patterns with less than 20% of high-grade patterns were classified as moderately differentiated ADC (grade 2), and any ADC with more than 20% of high-grade patterns was categorized as poorly differentiated (grade 3). SqCC cases were graded as well differentiated (grade 1), moderately differentiated (grade 2), or poorly differentiated (grade 3), based on the degree of tumor keratinization, histological, and cytomorphological features. For the purposes of disease-free survival (DFS) analysis only, tumor grades were categorized into two groups: low-grade tumors (including grades 1 and 2) and high-grade tumors (grade 3), due to the limited number of patients who experienced recurrence or progression of their disease. Depending on the time of diagnosis, the stages were determined according to the seventh and eighth editions of the American Joint Committee on Cancer (AJCC) TNM classification system [35,36]. Positive pleural invasion was defined as tumor invasion beyond the elastic lamina of the pleura.

Histopathological evaluation of STAS

The H&E-stained tumor sections were independently examined by two expert pathologists (O.A.A.K. and A.A.R.), who were unaware of the clinical data, and a consensus was reached in cases of disagreement. STAS was defined as the presence of tumor cells within the air spaces beyond the edge of the primary tumor, as previously documented in the literature [37,38]. The edge of the primary tumor was defined as the outer border of the tumor, which is clearly appreciated during low-power histological examination. To reliably assess the presence of STAS, all selected cases had a circumferential rim of normal lung tissue surrounding the edge of the tumor in at least one slide. Certain considerations were taken to avoid confusion with artificially detached tumor cells that result from section processing. Tumor cells were considered STAS if they were present continuously in the air spaces from the tumor edge, and individual isolated tumor cells or rare tumor clusters found far away from the tumor without spreading continuously were considered artifacts. Additionally, random tumor clusters scattered across the tissue surface or located at the edge of the tissue section, along with clusters exhibiting jagged edges due to fragmentation or knife cuts during processing, were also classified as artifacts. Linear strips of tumor cells that appeared lifted from the alveolar wall or stroma due to poor preservation, as well as benign-looking ciliated bronchial cells or pneumocytes, and tumor cell clusters mixed with ciliated cell strips were similarly considered artifacts [6,10,14,28]. Furthermore, tumor cells were distinguished from alveolar macrophages based on their morphological features, where tumor cells exhibited nuclear atypia characterized by a high nuclear-to-cytoplasmic ratio, hyperchromasia, and frequent nucleoli. In contrast, macrophages do not show atypical features; they have small, uniform nuclei with inconspicuous or absent nucleoli and foamy cytoplasm in nonsmokers or cytoplasmic brown to black pigments in smokers [28].

Three morphological patterns of STAS were appreciated: (1) single cell pattern composed of discohesive single tumor cells within the alveoli, (2) solid nest pattern, where clusters of tumor cells present in the air spaces, and (3) micropapillary cluster pattern, defined as papillary structures without fibrovascular cores. Initially, the cases were divided into two groups: STAS-positive and STAS-negative. After that, due to a lack of consensus on a grading method, STAS-positive cases were reclassified in various ways to assess the prognostic value of STAS extension. In the first method, the extension of STAS was assessed by measuring the distance between the edge of the primary tumor and the furthest intraalveolar tumor cell clusters in millimeters (mm). Then, the cases were divided into two groups: group I, where all tumor clusters were present ≤2.5 mm away from the tumor, and group II, where any tumor clusters were present >2.5 mm away from the main tumor [14]. In the second approach, the number of alveoli between the edge of the primary tumor and STAS was counted, and cases were categorized into two groups: those with limited spread when ≤3 alveolar spaces separated STAS from the primary tumor, and those with extensive spread when >3 alveoli separated STAS from the primary tumor [7].

Statistical analysis

All statistical analyses were performed using IBM SPSS Statistics ver. 25 (IBM Corp., Armon, NY, USA). OS was determined from the time of surgery to the time of death or the last follow-up visit. DFS was measured from the time of surgery to the time of disease recurrence or progression. OS and DFS were calculated using the Kaplan-Meier method with the log-rank test. Multivariate analysis was conducted using a Cox proportional hazards regression model to identify independent prognostic factors associated with OS. Categorical variables were analyzed using the chi-square test or Fisher's exact test, as appropriate. The association between clinicopathological variables and the presence of STAS was assessed using multivariate logistic regression, with results reported as odds ratios (OR) and 95% confidence intervals (CI). A p-value < .05 was considered statistically significant.

RESULTS

Basic characteristics of patients

The baseline demographic and clinicopathological characteristics of NSCLC patients are summarized in Table 1, categorized by STAS status. A total of 96 patients were included in the study (n = 96). Most patients were males (n = 70, 72.9%), with a median age of 63 years (range, 26 to 80 years). Sixty-one patients (63.5%) were current or former smokers. Most tumors (n = 60, 62.5%) were on the right side, and the right upper lobe was the most common location. Fifty-four patients (56.3%) underwent lobectomy, while the remainder had sublobar resection. A total of 18 patients (18.8%) had positive bronchial or parenchymal margins. Histologically, 61 patients (63.5%) had ADC, 17 patients (17.7%) had SqCC, and 18 patients (18.8%) had other lung cancer subtypes. Regarding the histological grade, 16.7% (n = 16) of the patients had grade 1 tumors, while 47.9% (n = 46) and 35.4% (n = 34) had grades 2 and 3 tumors, respectively. Just more than half of the patients had pathological stage I or

Table 1. Clinicopathological characteristics of the enrolled patients according to STAS status

Variable	Total (n = 96)	STAS status		p-value
		Present	Absent	
Age (yr)				
≤60	36 (37.5)	12 (33.3)	24 (66.7)	.868
>60	60 (62.5)	21 (35.0)	39 (65.0)	
Sex				
Male	70 (72.9)	27 (38.6)	43 (61.4)	.155
Female	26 (27.1)	6 (23.1)	20 (76.9)	
Smoking status				
Former or current smoker	61 (63.5)	24 (39.3)	37 (60.7)	.176
Never-smoker	35 (36.5)	9 (25.7)	26 (74.3)	
Tumor side				
Right	60 (62.5)	22 (36.7)	38 (63.3)	.542
Left	36 (37.5)	11 (30.6)	25 (69.4)	
Tumor site				
RUL	37 (38.5)	13 (35.1)	24 (64.9)	.828
RML	7 (7.3)	2 (28.6)	5 (71.4)	
RLL	16 (16.7)	7 (43.8)	9 (56.2)	
LUL	20 (20.8)	5 (25.0)	15 (75.0)	
LLL	16 (16.7)	6 (37.5)	10 (62.5)	
Surgical procedure				
Lobectomy	54 (56.3)	17 (31.4)	37 (68.6)	.499
Sublobar resection (wedge resection or segmentectomy)	42 (43.7)	16 (38.1)	26 (61.9)	
Margin status				
Positive	18 (18.8)	9 (50.0)	9 (50.0)	.122
Negative	78 (81.3)	24 (30.8)	54 (69.2)	
Histological subtypes				
Adenocarcinoma	61 (63.5)	27 (44.3)	34 (55.7)	.031
Squamous cell carcinoma	17 (17.7)	3 (17.7)	14 (82.3)	
Other	18 (18.8)	3 (16.7)	15 (83.3)	

(Continued to the next page)

Table 1. Continued

Variable	Total (n = 96)	STAS status		p-value
		Present	Absent	
Tumor grade				
Grade 1	16 (16.7)	1 (6.3)	15 (93.7)	<.001
Grade 2	46 (47.9)	11 (23.9)	35 (76.1)	
Grade 3	34 (35.4)	21 (61.8)	13 (38.2)	
pT stage classification				
pT1	48 (50.0)	14 (29.1)	34 (70.9)	.513
pT2	26 (27.1)	12 (46.2)	14 (53.8)	
pT3	16 (16.7)	5 (31.3)	11 (68.7)	
pT4	5 (5.2)	2 (40.0)	3 (60.0)	
Not assessable	1 (1.0)	0	1 (100)	
pN stage classification				
pN0	43 (44.8)	13 (30.2)	30 (69.8)	.801
pN1	15 (15.6)	5 (33.3)	10 (66.7)	
pN2	8 (8.3)	3 (37.5)	5 (62.5)	
pNx	30 (31.3)	12 (40.0)	18 (60.0)	
Pathological stage				
Stage I, II	51 (53.1)	18 (35.3)	33 (64.7)	.313
Stage III, IV	17 (17.7)	8 (47.1)	9 (52.9)	
NA	28 (29.2)	7 (25.0)	21 (75.0)	
Tumor size				
≤3 cm	58 (60.4)	19 (32.8)	39 (67.2)	.545
>3 cm	36 (37.5)	14 (38.9)	22 (61.1)	
Not assessable	2 (2.1)	0	2 (100)	
Visceral pleural invasion				
Present	23 (24.0)	10 (43.5)	13 (56.5)	.291
Absent	70 (72.9)	22 (31.4)	48 (68.6)	
Not assessable	3 (3.1)	1 (33.3)	2 (66.7)	
Lymphovascular invasion				
Present	30 (31.3)	15 (50.0)	15 (50.0)	.03
Absent	66 (68.7)	18 (27.3)	48 (72.7)	
Necrosis				
Present	33 (34.4)	15 (45.5)	18 (54.5)	.098
Absent	63 (65.6)	18 (28.6)	45 (71.4)	
Predominant growth pattern (ADC cases = 61)	61(100)	27 (44.3)	34 (55.7)	.065
Lepidic	9 (14.8)	2 (22.2)	7 (77.8)	
Acinar	34 (55.7)	13 (38.2)	21 (61.8)	
Papillary	5 (8.2)	2 (40.0)	3 (60.0)	
Solid	10 (16.4)	7 (70.0)	3 (30.0)	
Micropapillary	3 (4.9)	3 (100)	0	
Postoperative chemo/radiotherapy				
Yes	38 (39.6)	17 (44.8)	21 (55.2)	.084
No	58 (60.4)	15 (25.9)	43 (74.1)	

Values are presented as number (%). $p < .05$ is considered significant.
STAS, spread through air spaces; RUL, right upper lobe; RML, right middle lobe; RLL, right lower lobe; LUL, left upper lobe; LLL, left lower lobe; ADC, adenocarcinoma.

II (n = 51, 53.1%). The majority of patients (n = 58, 60.4%) had a tumor size of 3 cm or less, and a minority of cases had confirmed lymph node metastasis (24%). Visceral pleural invasion was present in 24% of the cases, lymphovascular invasion (LVI) was identified in 31.3%, and necrosis was found in 34.4% of the cases. The most frequent histological growth pattern in ADC cases was the acinar pattern (n = 34, 55.7%), followed by the solid pattern (n = 10, 16.4%), while the least frequent one was the micropapillary growth pattern (n = 3, 4.9%). Only 39.6% of the patients received postoperative chemo/radiation therapy.

STAS presence and association with the clinicopathological variables in NSCLC

Among the 96 NSCLC samples, STAS was identified in 33 patients (34.4%). Of these, twenty-eight cases showed extensive STAS, with tumor cells presenting in airspaces more than three alveoli away from the primary tumor. In 18 cases, STAS was found in airspaces more than 2.5 mm away from the edge of the primary tumor. Morphologically, eighteen cases of STAS demonstrated a solid nest pattern, eight demonstrated a micropapillary cluster pattern, and seven showed a single-cell pattern. Representative images of STAS with different morphological patterns are shown in Fig. 1A–D.

The presence of STAS was more frequently observed in ADC cases (44.3% vs. 17.7% in SqCC vs. 16.7% in other subtypes) and in patients with a history of smoking (39.3% vs. 25.7% in never-smokers). Moreover, STAS occurrence was more frequent in patients with grade 3 tumors (61.8% vs. 23.9% and 6.3% in grades 2 and 1 tumors, respectively), in patients with stage III or IV, in patients with positive LVI, positive visceral pleural invasion, and in tumor cases with necrosis. ADC cases with predominant solid or micropapillary growth patterns showed the highest frequency of STAS. Interestingly, STAS was slightly more frequent in sublobar resections (wedge resection

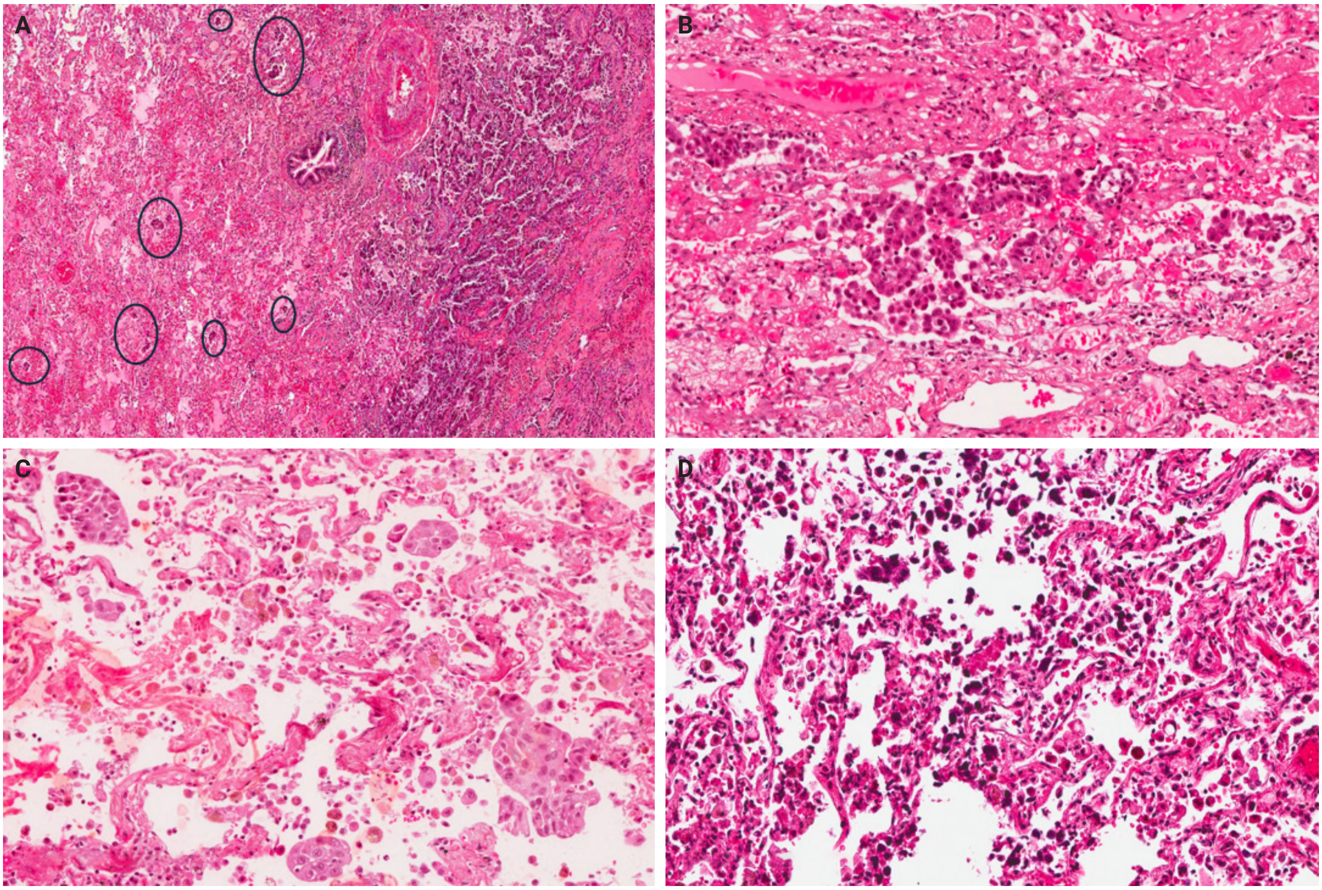

Fig. 1. Representative histopathological images of spread through air spaces (STAS) with different morphological subtypes. (A) STAS in an adenocarcinoma composed of small micropapillary clusters (circles) located beyond the edge of the primary tumor. (B) Micropapillary cluster pattern. (C) Solid nest pattern. (D) Single-cell pattern.

or segmentectomy) than in lobectomy cases (38.1% vs. 31.4%). Among the clinicopathological variables, ADC histological subtype (p = .031), grade 3 tumors (p < .001), and presence of LVI (p = .030) were significantly associated with the presence of STAS; however, no significant association was found with the other parameters in the univariate analysis (Table 1).

Furthermore, we performed multivariate logistic regression analysis on variables that showed a statistically significant association (p < .05) with STAS presence in the univariate analyses. Only tumor grade remained significantly associated with STAS. Specifically, with grade 1 as a reference, patients with grade 3 tumors had higher odds of having STAS (OR, 3.994; 95% CI, 0.434 to 36.709; p = .002). In comparison, histological subtype (using ADC as a reference) and LVI (with absent LVI as a reference) were not independently associated with STAS (Table 2).

Survival analyses of STAS and other clinicopathological variables

The mean OS for the patients was 26 months (range, 0 to 191 months), and the mean DFS was 28 months (range, 0 to 86 months). During the follow-up period, 16 patients (16.7%) experienced recurrence, comprising six with locoregional recurrence, nine with distant metastatic recurrence, and one with both. In NSCLC patients, Kaplan-Meier analysis with a log-rank test demonstrated a statistically significant lower OS with the presence of STAS (p = .047), with the mean OS dropping from 141 months in patients without STAS to 65.4 months in patients with STAS (Fig. 2A). No statistically significant difference in OS was identified among different subgroups of STAS-positive cases, either according to morphology or the distance of extension. Further, positive surgical margin, LVI, ADC tumor histology, and postoperative therapy showed statistically significant associations with lower OS (p = .021, p = .001, p = .020, and p = .049, respectively) (Fig. 2B–E).

In NSCLC patients, the mean DFS rate was slightly lower in patients with STAS than in those without STAS. However, no statistically significant difference was identified (p = .681). Nonetheless, STAS-positive cases with an extension of ≤2.5 mm showed statistically significant (p = .018) higher DFS compared to those with an extension of >2.5 mm (Fig. 2F); however, no statistically significant difference in DFS was identified using three alveoli as a cutoff point for STAS extension (p = .953) (Fig. 2G). Moreover, patients with high-grade tumors and those who underwent sublobar resection had a statistically significant lower DFS (p = .044 and p = .032, respectively) (Fig. 2H, I). Of note, these findings could not be further evaluated in a multivariate analysis due to the limited number of cases that experienced disease recurrence or progression.

When we stratified NSCLC cases by different subgroups of clinicopathological parameters and investigated the impact of STAS on OS, we found a statistically significant negative impact of STAS on OS in subgroups with tumor size ≤3 cm, negative visceral pleural invasion, and pT1 tumor stage (Fig. 3A–C). Regarding the surgical procedure, patients who underwent sublobar resection had lower mean OS and DFS, regardless of whether they had STAS or not, and no significant difference was identified.

In the subsequent step, we examined the impact of STAS and other clinicopathological variables on OS within the cohort of ADC cases (n = 61). Kaplan-Meier curves with a log-rank test revealed no statistically significant difference in OS between STAS-positive and STAS-negative tumors (p > .30). Similarly, neither the morphological subtype of STAS nor its distance of extension (≤2.5 mm vs. >2.5 mm or ≤3 alveoli vs. >3 alveoli) influenced the OS. In contrast, patients whose tumors exhibited LVI experienced markedly poorer OS (p = .033) (Supplementary

Table 2. Multivariate logistic regression analysis for predicting STAS status

Predictor	OR	95% CI	p-value
Histological subtype (reference: ADC)	-	-	.135
SqCC	3.908	0.926–16.493	.064
Other	2.201	0.470–10.317	.566
Tumor grade (reference: grade 1)			.001
Grade 2	0.209	0.076–0.575	.221
Grade 3	3.994	0.434–36.709	.002
LVI (reference: absent)	0.621	0.219–1.760	.370

p < .05 is considered significant.
STAS, spread through air spaces; OR, odds ratio; CI, confidence interval; ADC, adenocarcinoma; SqCC, squamous cell carcinoma; LVI, lymphovascular invasion.

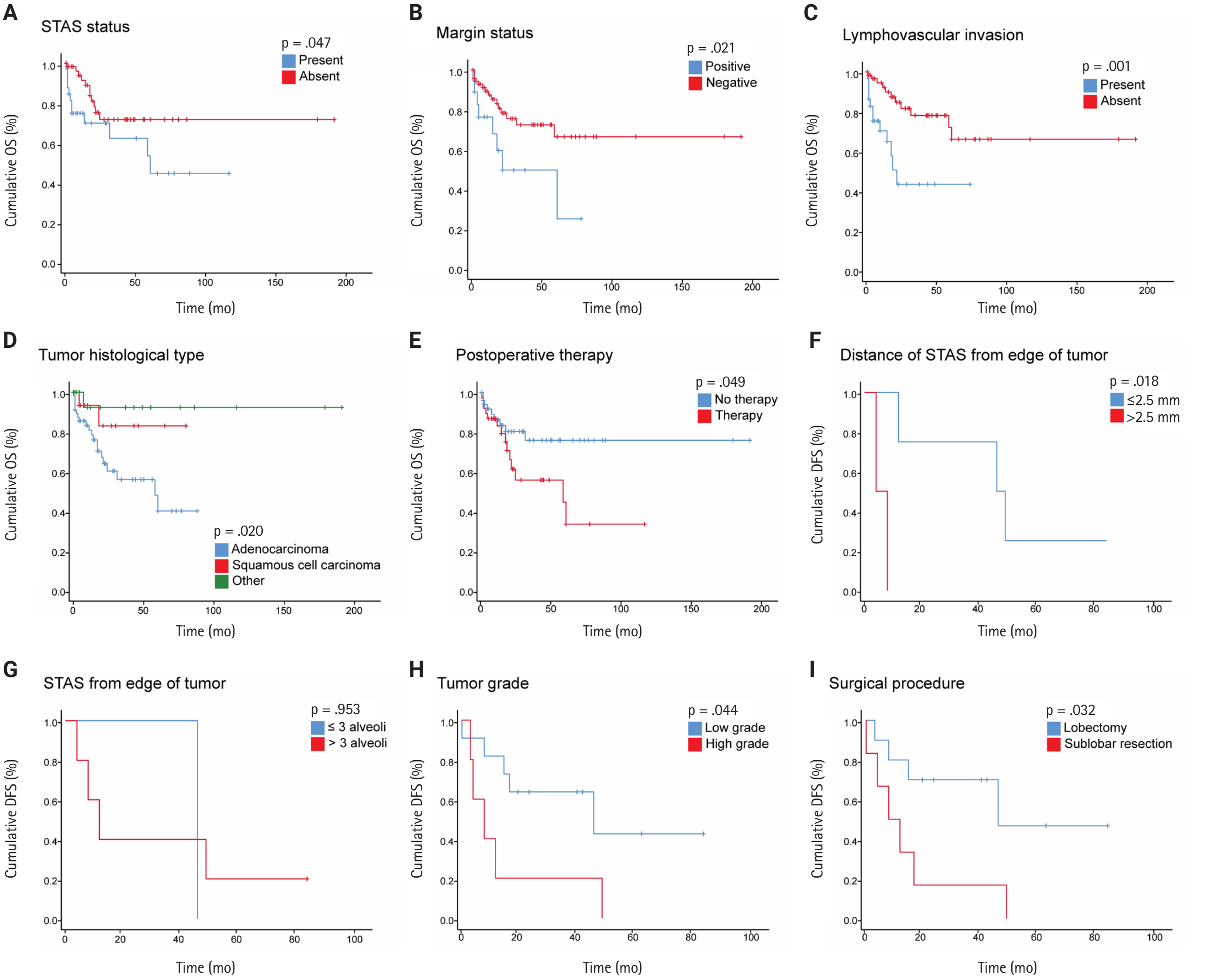

Fig. 2. Kaplan-Meier overall survival (OS) and disease-free survival (DFS) curves according to different clinicopathological parameters in non–small cell lung cancer patients. (A) The correlation between the OS and spread through air spaces (STAS) status. (B) The correlation between the OS and margin status. (C) The correlation between the OS and lymphovascular invasion. (D) The correlation between the OS and tumor histological subtype. (E) The correlation between the OS and postoperative therapy. (F) The correlation between the DFS and the extension of STAS from the tumor edge (≤2.5 mm vs. >2.5 mm). (G) The correlation between the DFS and the extension of STAS from the tumor edge (≤3 alveoli vs. >3 alveoli). (H) The correlation between DFS and tumor grade. (I) The correlation between DFS and surgical procedure. $p < .05$ is considered significant.

Fig. S1) and showed a steeper early mortality slope. Other factors, including tumor grade, pathological stage, and additional clinicopathological variables, did not convincingly stratify survival in ADC cases. Due to the limited number of cases that had disease recurrence or progression in the ADC cohort, no analysis on DFS was performed. Additionally, for SqCC, the cohort size was small (n = 17), and only two deaths occurred during the follow-up period, which rendered the Kaplan-Meier and Cox proportional hazards regression model analyses unreliable.

Prognostic value of clinicopathological variables for OS in NSCLC patients

We performed Cox proportional hazards regression analyses to evaluate the prognostic significance of the clinicopathological variables and to identify potential independent predictors of OS. Univariate analysis identified several clinicopathological variables significantly associated with OS. For example, histological subtype was significantly associated with OS (p = .049); patients with other histological subtypes of lung cancer had

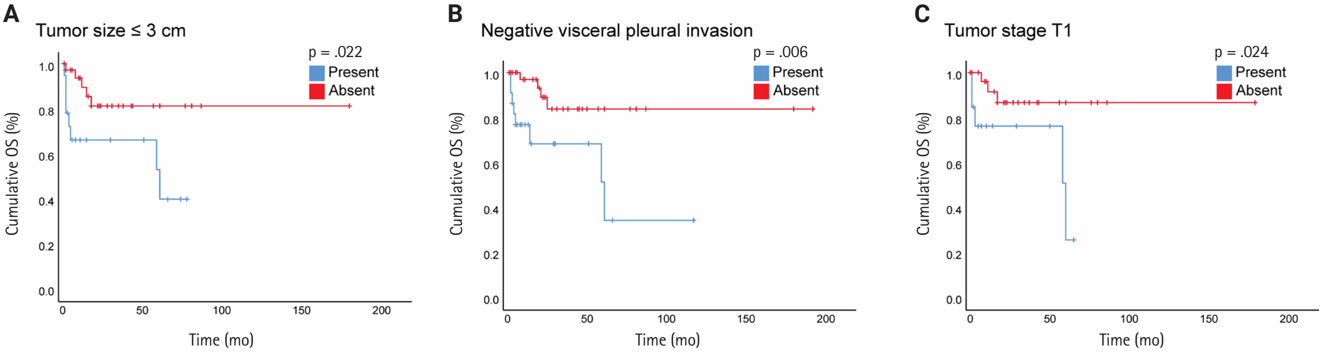

Fig. 3. Survival association of spread through air spaces (STAS) in different clinicopathological subgroups. (A) Overall survival (OS) according to STAS status within the patient population with tumor size ≤ 3 cm, with negative visceral pleural invasion (B), and with pT1 tumor stage (C). $p < .05$ is considered significant.

a significantly lower hazard of death compared to ADC (HR, 0.127; 95% CI, 0.017 to 0.953; p = .045). However, the survival difference between SqCC and ADC was not statistically significant (HR, 0.316; 95% CI, 0.074 to 1.354; p = .121). Additionally, the presence of LVI (HR, 3.743; 95% CI, 1.613 to 8.684; p = .002) and positive margin status (HR, 2.644; 95% CI, 1.119 to 6.251; p = .027) significantly increased the risk of death. Other variables tested in the univariate analysis were not significantly associated with OS (p > .05). Moreover, variables significantly associated with OS in univariate analysis were included in the multivariate Cox regression model. In this analysis, only LVI (HR, 3.143; 95% CI, 1.347 to 7.338; p = .008) and positive margin status (HR, 2.448; 95% CI, 1.033 to 5.801; p = .042) remained significant independent predictors of poorer OS, while the histological subtype was not independently predictive of OS after adjustment for other variables (p = .087) (Table 3).

Prognostic value of clinicopathological variables for OS in ADC patients

Finally, we conducted a Cox proportional hazards regression model to further evaluate the prognostic impact of clinicopathological variables, including STAS, for the ADC cohort but not for SqCC due to an insufficient number of cases and events. In the univariate analysis, LVI was identified as the only significant prognostic factor for OS (HR, 2.559; 95% CI, 1.041 to 6.288; p = .041). Margin positivity showed a strong but non-significant trend towards increased mortality (HR, 2.19; p = .097). In contrast, STAS status—along with its extent, morphological subtypes, tumor grade, tumor stage, smoking history, and other variables—did not show an independent association with mortality (e.g., STAS; HR, 1.474; p = .395) (Table 4). Because only one variable (LVI) reached a statistical significance in the univariate analysis, we did not construct a multivariate model for the ADC cohort.

DISCUSSION

This study found that STAS is significantly associated with high histological tumor grade of lung cancer, where high tumor grade (grade 3) serves as an independent predictor for STAS. STAS presence, positive surgical margin, LVI, ADC histology, and postoperative therapy were associated with statistically significant lower OS in NSCLC cases. However, based on multivariate analysis, only positive surgical margin and LVI were identified as independent predictors of poorer OS. Furthermore, STAS was associated with a statistically significant lower OS in patients with a tumor size of ≤3 cm, pT1 tumor stage, and negative pleural invasion.

In the ADC cohort, only LVI showed a statistically significant lower OS in a univariate analysis, which prevented conducting a multivariate analysis. Although the mean DFS rate was slightly lower in patients with STAS than in those without STAS, no statistically significant difference was identified in NSCLC cases. However, an extension of STAS > 2.5 mm away from the edge of the primary tumor, high tumor grade, and sublobar resection were found to be significantly associated with a lower DFS in a univariate analysis.

The incidence of STAS found in this study was 34.4% across the different histological subtypes, which falls within the range reported by other studies [10,12,13,16,39-42]. The solid nest pattern was the most frequently observed (54.5%). STAS was slightly more frequent in sublobar resections than in lobec-

Table 3. Cox proportional hazards regression model for overall survival in patients with non-small cell lung cancer

Variable	Reference category	Univariate analysis			Multivariate analysis		
		HR	95% CI	p-value	HR	95% CI	p-value
Age	≤60 yr	2.017	0.793–5.128	.141			
Sex	Female	0.679	0.267–1.730	.679			
Histological subtype (overall)	ADC	-	-	.049			.087
SqCC	ADC	0.316	0.074–1.354	.121	0.343	0.080–1.474	.151
Other	ADC	0.127	0.017–0.953	.045	0.162	0.021–1.215	.077
Lymphovascular invasion	Absent	3.743	1.613–8.684	.002	3.143	1.347–7.338	.008
Margin status	Negative	2.644	1.119–6.251	.027	2.448	1.033–5.801	.042
Necrosis	Absent	1.272	0.537–3.016	.584			
Pathological stage	Stage I–II	2.746	0.930–8.107	.067			
pN category (overall)	pN0	-	-	.396			
pN1	pN0	2.162	0.704–6.640	.178			
pN2	pN0	1.108	0.136–9.021	.924			
Predominant growth pattern (ADC overall)	Acinar	-	-	.222			
Solid	Acinar	2.706	0.883–8.294	.081			
Papillary	Acinar	1.057	0.285–3.920	.934			
Micropapillary	Acinar	0.750	0.095–5.946	.786			
Lepidic	Acinar	0.264	0.034–2.071	.205			
pT category (overall)	pT1	-	-	.387			
T2	pT1	1.831	0.662–5.064	.244			
T3	pT1	2.011	0.657–6.161	.221			
T4	pT1	2.766	0.567–0.724	.137			
Smoking status	Smoker	0.502	0.197–1.276	.147			
STAS distance from tumor edge	≤2.5 mm	0.901	0.287–2.825	.858			
STAS from edge of tumor	≤3 alveoli	0.611	0.159–2.341	.472			
STAS morphological subtype (overall)	Single cells	-	-	.259			
Solid nests	Single cells	554.268	0.233–1,316,585.998	.111			
Micropapillary	Single cells	16.782	0.037–7,547.348	.366			
STAS status	Absent	2.250	0.987–5.129	.054			
Surgical procedure	Lobectomy	1.635	0.717–3.728	.242			
Treatment history (adjuvant)	Treated	0.441	0.190–1.022	.056			
Tumor grade	Grade 1			.126			
Grade 2	Grade 1	5.786	0.744–45.001	.093			
Grade 3	Grade 1	8.096	1.041–62.954	.046			
Tumor location	Left	1.122	0.474–2.658	.794			
Tumor size	≤3 cm	1.171	0.512–2.677	.708			
Visceral pleural invasion	Negative	2.164	0.911–5.141	.080			

$p < .05$ is considered significant.
HR, hazard ratio; CI, confidence interval; SqCC, squamous cell carcinoma; ADC, adenocarcinoma; STAS, spread through air spaces.

tomy specimens. Interestingly, a completion lobectomy may potentially be beneficial for these patients with STAS-positive tumors, reducing the risk of tumor recurrence or progression [43]. In this study, we found that ADC histology, high histological tumor grade, and the presence of LVI were associated with STAS in the univariate analysis. Further, the multivariate analysis proved that high tumor grade is an independent predictor of STAS. Several studies analyzed the correlation between STAS and other clinicopathological parameters. Consistent with our findings, some studies found an association between STAS and high tumor grade/poor differentiation [4,39,40,44,45] or LVI [11,27,40,46]. For example, Lee et al. [40] investigated STAS in

Table 4. Cox proportional hazards regression model for overall survival in patients with adenocarcinoma

Variable	Reference category	Univariate analysis		
		HR	95% CI	p-value
Age	≤60 yr	1.317	0.525–3.578	.519
Sex	Female	1.103	0.332–3.663	.873
Lymphovascular invasion	Absent	2.559	1.041–6.288	.041
Margin status	Negative	2.190	0.868–5.527	.097
Necrosis	Absent	2.200	0.837–5.784	.110
Pathologic stage	Stage I–II	2.121	0.646–6.961	.215
pN category (overall)	pN0	-	-	.516
pN1	pN0	1.969	0.620–6.961	.250
pN2	pN0	0.000	0.000	.983
Predominant growth pattern	Acinar	-	-	.222
Solid	Acinar	2.706	0.883–8.294	.081
Papillary	Acinar	1.057	0.285–3.920	.934
Micropapillary	Acinar	0.750	0.095–5.946	.786
Lepidic	Acinar	0.264	0.034–2.071	.205
pT category (overall)	pT1	-	-	.654
T2	pT1	1.219	0.383–3.880	.737
T3	pT1	1.833	0.579–5.802	.303
T4	pT1	2.040	0.518–8.031	.308
Smoking status	Smoker	0.578	0.200–1.518	.266
STAS distance from tumor edge	≤2.5 mm	1.103	0.332–3.663	.873
STAS from edge of tumor	≤3 alveoli	0.725	0.184–2.861	.646
STAS morphologic subtype (overall)	Single cells	-	-	.411
Solid nests	Single cells	954.001	0.021–44,129,592.574	.211
Micropapillary	Single cells	17.077	0.004–77,386.721	.509
STAS status	Absent	1.474	0.603–3.603	.395
Surgical procedure	Lobectomy	0.985	0.408–2.382	.974
Treatment history (adjuvant)	Treated	0.832	0.339–2.039	.668
Tumor grade	Grade 1			.510
Grade 2	Grade 1	3.226	0.410–25.403	.266
Grade 3	Grade 1	3.361	0.424–26.660	.251
Tumor location	Left	1.658	0.634–4.337	.303
Tumor size	≤3 cm	1.163	0.480–2.816	.738
Visceral pleural invasion	Negative	1.232	0.478–3.175	.666

$p < .05$ is considered significant.
HR, hazard ratio; CI, confidence interval; STAS, spread through air spaces.

316 cases of lung ADC and found that STAS was significantly associated with high-grade histology, LVI, higher stage, and lymph node metastasis. Uruga et al. [27] studied 208 cases of early-stage lung ADC and found a significant association between higher STAS and LVI, solid predominant ADC, visceral pleural invasion, and tumor size ≥ 10 mm. Other studies also reported a significant association between STAS and different parameters, including micropapillary growth pattern, nodal involvement, higher stage, perineural invasion, and pleural invasion; however, none of these variables were associated with STAS in our work [12,16,31,39,40,47]. It is possible that we were not able to identify a statistically significant association between STAS and these variables due to the small sample size.

The association of STAS with poor OS and DFS has been extensively suggested. A meta-analysis involving 3754 patients demonstrated a significant association between STAS and worse RFS and OS in NSCLC [26]. Another meta-analysis, including 47 studies, also concluded that STAS presence is associated with poor prognosis [48]. A study by Chen et al. [23] reported that STAS is significantly associated with lower OS and RFS in stage IB NSCLC. Another study included STAS among the pathological features that adversely affect the OS and progression-free survival (PFS) in stage I lung ADC [49]. Another interesting study reported that STAS presence negatively impacts OS and RFS in stage IB patients. Furthermore, it observed that adjuvant chemotherapy improves RFS outcomes in stage IB STAS-positive patients with high-risk recurrence factors, such as LVI, pleural invasion, and poor differentiation [50]. Moreover, other studies included lung cancer cases of stages I–IV and reported the same adverse effect of STAS on survival [6,7,16,19,21,40,51-54]. On the other hand, a recent study did not find an association between STAS and worse survival or higher recurrence rates; however, they attributed this to a limited follow-up duration [55].

Herein, we included NSCLC cases of stages I–IV and found a significant association between STAS and lower OS but not DFS in a univariate analysis. However, based on our multivariate analysis, STAS was not an independent predictor of prognosis, which is likely due to the small sample size. Furthermore, STAS did not reveal an independent prognostic impact on OS in univariate analysis in the ADC cohort. In line with previous results, we found that STAS presence has a negative impact on OS in subgroups of early-stage lung cancer, defined as tumor stage pT1, tumor size ≤ 3 cm, and negative visceral pleural invasion.

Due to a lack of consensus on measuring the extension of STAS in lung cancer, in this study, we measured the distance between STAS and primary tumor in mm using a cut-off value of 2.5 mm and according to the number of alveoli using a cut-off value of 3 alveoli. In both grading methods, no significant association was found between STAS extension and OS, either in the entire patient cohort or the ADC cohort; however, STAS extension of >2.5 mm from the edge of the primary tumor was significantly associated with lower DFS in the NSCLC cohort. However, this finding could not be further assessed in a multivariate analysis due to the small number of cases showing disease recurrence or progression. Few studies have assessed the prognostic significance of STAS distance using different methodologies to define STAS distance. Han et al. [14] measured the distance between the edge of the primary tumor and the furthest STAS in mm and observed that STAS II, defined as STAS ≥ 2.5 mm away from the edge of the primary tumor, is an independent poor prognostic factor for recurrence in stage I lung ADC, regardless of the extent of resection. Hashinokuchi et al. [53] categorized cases of STAS as limited (≤1 mm) and extended (>1 mm) based on the median maximum spread distance between the edge of the primary tumor and the furthest STAS and demonstrated that extended STAS was an independent prognostic factor for OS and RFS. On the other hand, Yanagawa et al. [9] used a cutoff value of 0.8 mm between the edge of the primary tumor and the furthest STAS and found no difference in OS or RFS between near STAS (<0.8 mm) and far STAS (>0.8 mm).

Similar to the results of this study, Warth et al. [7], Lu et al. [42], Kadota et al. [28], and Dai et al. [41] defined STAS distance as the number of alveoli between the edge of the main tumor and the furthest STAS, and using a cutoff point of 3 alveoli between limited STAS (< 3 alveoli) and extensive STAS (>3 alveoli), they reported no significant prognostic impact of STAS distance in NSCLC. Taken together, these results suggest that the prognostic significance of STAS distance depends on the methodology used and how the cutoff value was determined. Therefore, further research is warranted to explore STAS's biological perspectives, establish a method to measure STAS distance, and determine the clinically significant cutoff value.

Emphasizing the significance of STAS, a large staging study of lung cancer conducted by the International Association for the Study of Lung Cancer (IASLC) supported the recommendation to include STAS as a histological descriptor for the Ninth Edition of the TNM Classification of Lung Cancer [56]. Additionally, the IASLC aims to gather more information in the coming years to assess the relative importance of STAS in comparison to LVI and visceral pleural invasion in the staging of lung cancer, which will aid in the development of the 10th edition of the TNM stage classification.

While our study's strength includes using different classifications of STAS and being the first study to investigate STAS in lung cancer among Jordanian patients, it has several potential limitations. First, this is a retrospective study, which may introduce some selection bias, and some data were missing, which could have negatively affected the results and sample size. Second, the small sample size may have influenced the results, and furthermore, it hindered the proper stratification and analysis of the data based on histological subtypes or different stages, which may have introduced biases in the results, given the different prognoses associated with different tumor histological subtypes or other parameters. Third, formalin fixation may have affected STAS distance. Finally, due to the small number of patients who experienced disease recurrence, no further DFS analysis was performed.

In conclusion, our data indicated that a high histological grade is an independent predictor of STAS in lung cancer. Additionally, the results suggested that STAS may have a negative impact on prognosis. However, it is essential to consider that STAS may be merely a characteristic of high-grade tumors rather than a significant, independent prognostic indicator. Therefore, additional extensive multicenter and prospective studies are necessary to clarify the prognostic role of STAS in lung cancer and to establish a clinically significant cutoff value for STAS distance. This may help clinicians in the prognostic stratification of patients and inform decisions regarding further treatment.

Supplementary Information

The Data Supplement is available with this article at https://doi.org/10.4132/jptm.2025.10.15.

Ethics Statement

This study received approval from the Institutional Review Boards at the Hashemite University (Protocol No.5/1/2023/2024 on 19 November, 2023) and JRMS (Protocol No. 5/2024 on 2 April, 2024). All procedures followed the 1964 Helsinki Declaration and its relevant amendments. Because the study was retrospective and no patient identifications were used, the Institutional Review Board committees waived the need for formally written informed consent.

Availability of Data and Material

The data used and analyzed during the current study are available from the corresponding author upon reasonable request.

Code Availability

Not applicable.

ORCID

Ola Abu Al Karsaneh	https://orcid.org/0000-0001-6064-2548
Amani Al-Rousan	https://orcid.org/0009-0009-6024-5118
Sofian Al Shboul	https://orcid.org/0000-0002-0455-4380
Mohammed El-Sadoni	https://orcid.org/0009-0004-2619-420X
Anas Hayajneh	https://orcid.org/0009-0003-7269-9228
Moath Alrjoub	https://orcid.org/0009-0008-6931-0492
Sura Al-Rawabdeh	https://orcid.org/0000-0002-8237-7631
Tareq Saleh	https://orcid.org/0000-0002-2878-1107

Author Contributions

Conceptualization: OAAK. Data curation: OAAK. Formal analysis: SAS. Investigation: OAAK, AAR, MES, MA, AH, SAR. Funding acquisition: OAAK. Methodology: OAAK, AAR. Project administration: OAAK. Resources: OAAK. Software: SAS. Supervision: OAAK. Validation: OAAK, TS. Visualization: OAAK, TS. Writing—original draft: OAAK. Writing—review & editing: OAAK, TS. Approval of final manuscript: all authors.

Conflicts of Interest

The authors declare that they have no potential conflicts of interest.

Funding Statement

The Deanship of Scientific Research, Hashemite University, Zarqa, Jordan, supported Dr. Ola Abu Al Karsaneh for this work (OAAK: grant no. 746/57/2022).

Acknowledgments

All authors would like to thank the Department of Pathology at King Abdullah University Hospital for granting access to their slide scanner.

REFERENCES

1. Siegel RL, Miller KD, Fuchs HE, Jemal A. Cancer statistics, 2022. CA Cancer J Clin 2022; 72: 7-33.
2. Jordan Cancer Registry. Cancer incidence in Jordan-2022. Amman: Ministry of Health, Jordan, 2022.
3. Shiono S, Ishii G, Nagai K, et al. Predictive factors for local recurrence of resected colorectal lung metastases. Ann Thorac Surg 2005; 80: 1040-5.
4. Onozato ML, Kovach AE, Yeap BY, et al. Tumor islands in resected early-stage lung adenocarcinomas are associated with unique clinicopathologic and molecular characteristics and worse prognosis. Am J Surg Pathol 2013; 37: 287-94.
5. Travis WD, Brambilla E, Nicholson AG, et al. The 2015 World Health Organization classification of lung tumors: impact of genetic, clinical and radiologic advances since the 2004 classification. J Thorac Oncol 2015; 10: 1243-60.
6. Kadota K, Nitadori JI, Sima CS, et al. Tumor spread through air spaces is an important pattern of invasion and impacts the frequency and location of recurrences after limited resection for small stage I lung adenocarcinomas. J Thorac Oncol 2015; 10: 806-14.

7. Warth A, Muley T, Kossakowski CA, et al. Prognostic impact of intra-alveolar tumor spread in pulmonary adenocarcinoma. Am J Surg Pathol 2015; 39: 793-801.
8. Lee MA, Kang J, Lee HY, et al. Spread through air spaces (STAS) in invasive mucinous adenocarcinoma of the lung: incidence, prognostic impact, and prediction based on clinicoradiologic factors. Thorac Cancer 2020; 11: 3145-54.
9. Yanagawa N, Shiono S, Endo M, Ogata SY. Tumor spread through air spaces is a useful predictor of recurrence and prognosis in stage I lung squamous cell carcinoma, but not in stage II and III. Lung Cancer 2018; 120: 14-21.
10. Aly RG, Rekhtman N, Li X, et al. Spread through air spaces (STAS) is prognostic in atypical carcinoid, large cell neuroendocrine carcinoma, and small cell carcinoma of the lung. J Thorac Oncol 2019; 14: 1583-93.
11. Shiono S, Yanagawa N. Spread through air spaces is a predictive factor of recurrence and a prognostic factor in stage I lung adenocarcinoma. Interact Cardiovasc Thorac Surg 2016; 23: 567-72.
12. Alvarez Moreno JC, Aljamal AA, Bahmad HF, et al. Correlation between spread through air spaces (STAS) and other clinicopathological parameters in lung cancer. Pathol Res Pract 2021; 220: 153376.
13. Cao L, Jia M, Sun PL, Gao H. Histopathologic features from preoperative biopsies to predict spread through air spaces in early-stage lung adenocarcinoma: a retrospective study. BMC Cancer 2021; 21: 913.
14. Han YB, Kim H, Mino-Kenudson M, et al. Tumor spread through air spaces (STAS): prognostic significance of grading in non-small cell lung cancer. Mod Pathol 2021; 34: 549-61.
15. Tian Y, Feng J, Jiang L, et al. Integration of clinicopathological and mutational data offers insight into lung cancer with tumor spread through air spaces. Ann Transl Med 2021; 9: 985.
16. Xie H, Su H, Zhu E, et al. Morphological subtypes of tumor spread through air spaces in non-small cell lung cancer: prognostic heterogeneity and its underlying mechanism. Front Oncol 2021; 11: 608353.
17. Xie H, Dou S, Huang X, Wen Y, Yang L. The effect of spread through air spaces on postoperative recurrence-free survival in patients with multiple primary lung cancers. World J Surg Oncol 2024; 22: 75.
18. Liu H, Yin Q, Yang G, Qie P. Prognostic impact of tumor spread through air spaces in non-small cell lung cancers: a meta-analysis including 3564 patients. Pathol Oncol Res 2019; 25: 1303-10.
19. Terada Y, Takahashi T, Morita S, et al. Spread through air spaces is an independent predictor of recurrence in stage III (N2) lung adenocarcinoma. Interact Cardiovasc Thorac Surg 2019; 29: 442-8.
20. Chen D, Wang X, Zhang F, et al. Could tumor spread through air spaces benefit from adjuvant chemotherapy in stage I lung adenocarcinoma?: a multi-institutional study. Ther Adv Med Oncol 2020; 12: 1758835920978147.
21. Jia M, Yu S, Yu J, Li Y, Gao H, Sun PL. Comprehensive analysis of spread through air spaces in lung adenocarcinoma and squamous cell carcinoma using the 8th edition AJCC/UICC staging system. BMC Cancer 2020; 20: 705.
22. Mantovani S, Pernazza A, Bassi M, et al. Prognostic impact of spread through air spaces in lung adenocarcinoma. Interact Cardiovasc Thorac Surg 2022; 34: 1011-5.
23. Chen Z, Wu X, Fang T, et al. Prognostic impact of tumor spread through air spaces for T2aN0 stage IB non-small cell lung cancer. Cancer Med 2023; 12: 15246-55.
24. Wang S, Hao J, Qian C, Wang H. Tumor spread through air spaces is a survival predictor in non-small-cell lung cancer. Clin Lung Cancer 2019; 20: e584-91.
25. Shiono S, Endo M, Suzuki K, Hayasaka K, Yanagawa N. Spread through air spaces in lung cancer patients is a risk factor for pulmonary metastasis after surgery. J Thorac Dis 2019; 11: 177-87.
26. Chen D, Mao Y, Wen J, et al. Tumor spread through air spaces in non-small cell lung cancer: a systematic review and meta-analysis. Ann Thorac Surg 2019; 108: 945-54.
27. Uruga H, Fujii T, Fujimori S, Kohno T, Kishi K. Semiquantitative assessment of tumor spread through air spaces (STAS) in early-stage lung adenocarcinomas. J Thorac Oncol 2017; 12: 1046-51.
28. Kadota K, Kushida Y, Katsuki N, et al. Tumor spread through air spaces is an independent predictor of recurrence-free survival in patients with resected lung squamous cell carcinoma. Am J Surg Pathol 2017; 41: 1077-86.
29. Kodama K, Higashiyama M, Okami J, et al. Oncologic outcomes of segmentectomy versus lobectomy for clinical T1a N0 M0 non-small cell lung cancer. Ann Thorac Surg 2016; 101: 504-11.
30. Wang J, Yao Y, Tang D, Gao W. Spread through air spaces (STAS) in surgically resected lung adenocarcinoma prognosis. Indian J Surg 2023; 85: 483-90.
31. Cao D, Sha J, Cui R, Han S. Advances in research of spreading through air spaces and the effects on the prognosis of lung cancer. Cancer Manag Res 2019; 11: 9725-32.
32. Jia M, Yu S, Gao H, Sun PL. Spread through air spaces (STAS) in lung cancer: a multiple-perspective and update review. Cancer Manag Res 2020; 12: 2743-52.
33. Nicholson AG, Tsao MS, Beasley MB, et al. The 2021 WHO clas-

sification of lung tumors: impact of advances since 2015. J Thorac Oncol 2022; 17: 362-87.

34. Moreira AL, Ocampo PS, Xia Y, et al. A grading system for invasive pulmonary adenocarcinoma: a proposal from the International Association for the Study of Lung Cancer Pathology Committee. J Thorac Oncol 2020; 15: 1599-610.
35. Mirsadraee S, Oswal D, Alizadeh Y, Caulo A, van Beek E Jr. The 7th lung cancer TNM classification and staging system: review of the changes and implications. World J Radiol 2012; 4: 128-34.
36. Detterbeck FC. The eighth edition TNM stage classification for lung cancer: what does it mean on main street? J Thorac Cardiovasc Surg 2018; 155: 356-9.
37. Ma K, Zhan C, Wang S, Shi Y, Jiang W, Wang Q. Spread through air spaces (STAS): a new pathologic morphology in lung cancer. Clin Lung Cancer 2019; 20: e158-62.
38. Huang L, Tang L, Dai L, Shi Y. The prognostic significance of tumor spread through air space in stage I lung adenocarcinoma. Thorac Cancer 2022; 13: 997-1005.
39. Hu SY, Hsieh MS, Hsu HH, et al. Correlation of tumor spread through air spaces and clinicopathological characteristics in surgically resected lung adenocarcinomas. Lung Cancer 2018; 126: 189-93.
40. Lee JS, Kim EK, Kim M, Shim HS. Genetic and clinicopathologic characteristics of lung adenocarcinoma with tumor spread through air spaces. Lung Cancer 2018; 123: 121-6.
41. Dai C, Xie H, Su H, et al. Tumor spread through air spaces affects the recurrence and overall survival in patients with lung adenocarcinoma >2 to 3 cm. J Thorac Oncol 2017; 12: 1052-60.
42. Lu S, Tan KS, Kadota K, et al. Spread through air spaces (STAS) is an independent predictor of recurrence and lung cancer-specific death in squamous cell carcinoma. J Thorac Oncol 2017; 12: 223-34.
43. Eguchi T, Kameda K, Lu S, et al. Lobectomy is associated with better outcomes than sublobar resection in spread through air spaces (STAS)-positive T1 lung adenocarcinoma: a propensity score-matched analysis. J Thorac Oncol 2019; 14: 87-98.
44. Masai K, Sakurai H, Sukeda A, et al. Prognostic impact of margin distance and tumor spread through air spaces in limited resection for primary lung cancer. J Thorac Oncol 2017; 12: 1788-97.
45. Chen X, Zhou H, Wu M, et al. Prognostic impact of spread through air spaces in patients with ≤2 cm stage IA lung adenocarcinoma. J Thorac Dis 2024; 16: 2432-42.
46. Choi S, Kim HS, Min KW, et al. JAK2 loss arising from tumor-spread-through-air-spaces (STAS) promotes tumor progression by suppressing CD8+ T cells in lung adenocarcinoma: a machine learning approach. J Korean Med Sci 2024; 39: e16.
47. Yildirim S, Alan O, Yuksel Yasar Z, et al. Prognostic impact and clinical features of spread through air spaces in operated lung cancer: real-world analysis. Medicina (Kaunas) 2024; 60: 1374.
48. Pyo JS, Kim NY. Clinicopathological impact of the spread through air space in non-small cell lung cancer: a meta-analysis. Diagnostics (Basel) 2022; 12: 1112.
49. Wang S, Li Y, Sun X, et al. Proposed novel grading system for stage I invasive lung adenocarcinoma and a comparison with the 2020 IASLC grading system. Thorac Cancer 2024; 15: 519-28.
50. Lv Y, Li S, Liu Z, et al. Impact of surgery and adjuvant chemotherapy on the survival of stage I lung adenocarcinoma patients with tumor spread through air spaces. Lung Cancer 2023; 177: 51-8.
51. Morimoto J, Nakajima T, Suzuki H, et al. Impact of free tumor clusters on prognosis after resection of pulmonary adenocarcinoma. J Thorac Cardiovasc Surg 2016; 152: 64-72.
52. Liu A, Sun X, Xu J, et al. Relevance and prognostic ability of Twist, Slug and tumor spread through air spaces in lung adenocarcinoma. Cancer Med 2020; 9: 1986-98.
53. Hashinokuchi A, Akamine T, Toyokawa G, et al. Impact of the distance of spread through air spaces in non-small cell lung cancer. Interdiscip Cardiovasc Thorac Surg 2024; 40: ivae181.
54. Toyokawa G, Yamada Y, Tagawa T, et al. Significance of spread through air spaces in resected lung adenocarcinomas with lymph node metastasis. Clin Lung Cancer 2018; 19: 395-400.
55. Huang L, Petersen RH. Tumour spread through air spaces is a determiner for treatment of clinical stage I non-small cell lung cancer: thoracoscopic segmentectomy vs lobectomy. Lung Cancer 2025; 201: 108438.
56. Travis WD, Eisele M, Nishimura KK, et al. The International Association for the Study of Lung Cancer (IASLC) Staging Project for Lung Cancer: recommendation to introduce spread through air spaces as a histologic descriptor in the ninth edition of the TNM classification of lung cancer. Analysis of 4061 pathologic stage I NSCLC. J Thorac Oncol 2024; 19: 1028-51.

JPTM

ORIGINAL ARTICLE

pISSN 2383-7837 · eISSN 2383-7845

Journal of Pathology and Translational Medicine 2026; 60: 107-123
https://doi.org/10.4132/jptm.2025.10.20

PSMA expression in hepatic colorectal cancer metastasis

Eundong Park[1], Michel Kmeid[2], Xin Wang[1], Haiyan Qiu[1], Clifton G. Fulmer[2], Marcello P. Toscano[2], Nusret Bekir Subasi[1], Maciej Gracz[1], Hwajeong Lee[1]

[1]Department of Pathology and Laboratory Medicine, Albany Medical Center, Albany, NY, USA
[2]Department of Pathology, Cleveland Clinic, Cleveland, OH, USA

Graphical abstract

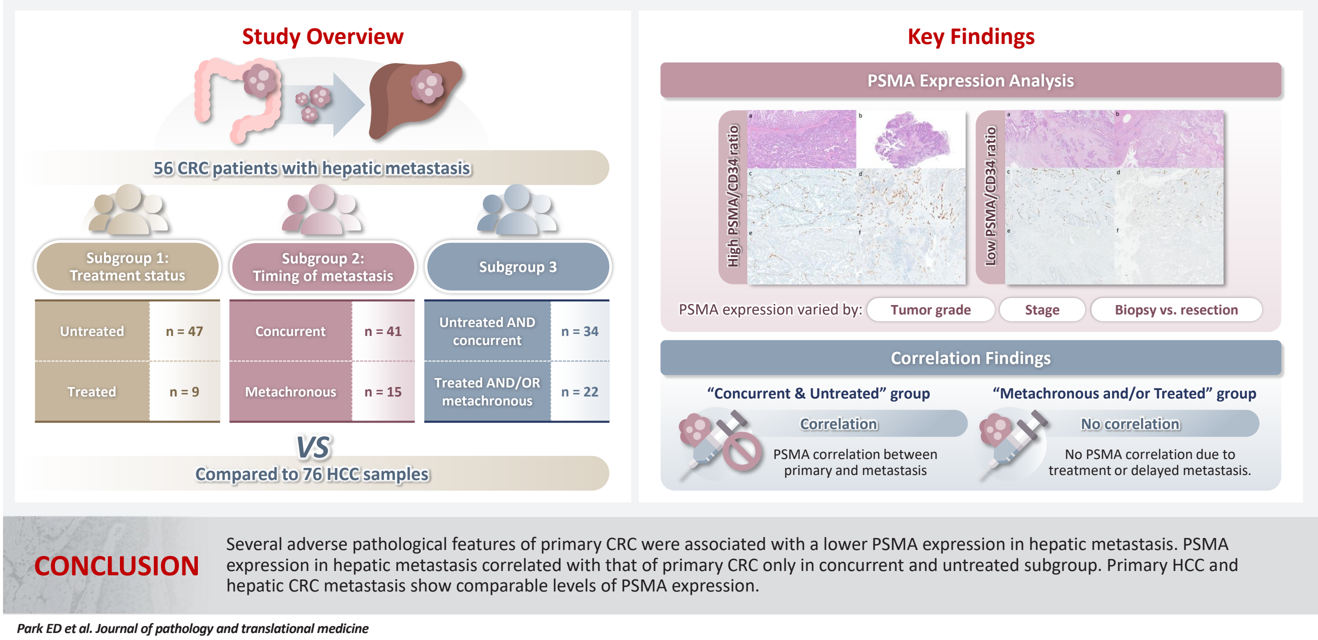

Study Overview

56 CRC patients with hepatic metastasis

Subgroup 1: Treatment status		Subgroup 2: Timing of metastasis		Subgroup 3	
Untreated	n = 47	Concurrent	n = 41	Untreated AND concurrent	n = 34
Treated	n = 9	Metachronous	n = 15	Treated AND/OR metachronous	n = 22

VS

Compared to 76 HCC samples

Key Findings

PSMA Expression Analysis

PSMA expression varied by: Tumor grade · Stage · Biopsy vs. resection

Correlation Findings

"Concurrent & Untreated" group
Correlation
PSMA correlation between primary and metastasis

"Metachronous and/or Treated" group
No correlation
No PSMA correlation due to treatment or delayed metastasis.

CONCLUSION Several adverse pathological features of primary CRC were associated with a lower PSMA expression in hepatic metastasis. PSMA expression in hepatic metastasis correlated with that of primary CRC only in concurrent and untreated subgroup. Primary HCC and hepatic CRC metastasis show comparable levels of PSMA expression.

Park ED et al. Journal of pathology and translational medicine

JPTM

ORIGINAL ARTICLE

pISSN 2383-7837 · eISSN 2383-7845

Journal of Pathology and Translational Medicine 2026; 60: 107-123
https://doi.org/10.4132/jptm.2025.10.20

PSMA expression in hepatic colorectal cancer metastasis

Eundong Park[1], Michel Kmeid[2], Xin Wang[1], Haiyan Qiu[1], Clifton G. Fulmer[2], Marcello P. Toscano[2], Nusret Bekir Subasi[1], Maciej Gracz[1], Hwajeong Lee[1]

[1]Department of Pathology and Laboratory Medicine, Albany Medical Center, Albany, NY, USA
[2]Department of Pathology, Cleveland Clinic, Cleveland, OH, USA

Background: Prostate-specific membrane antigen (PSMA) is expressed in the neovasculature of various malignancies, such as colorectal cancer (CRC) and hepatocellular carcinoma (HCC). However, PSMA expression in hepatic CRC metastasis has not been studied in detail. **Methods:** The PSMA expression in primary CRC and corresponding hepatic metastasis was evaluated by immunohistochemistry in a metastatic CRC cohort (n = 56), which was divided into subgroups according to treatment history and timing of metastasis. Demographic and histological characteristics of primary CRC were collected and their relationships with PSMA expression were examined. Additionally, the PSMA expression in resected HCC (n = 76) was compared with that of hepatic CRC metastasis. **Results:** In primary CRC, PSMA level showed a positive association with tumor size. Lower PSMA expression in hepatic metastasis was associated with higher primary CRC grade, advanced pTNM stage at the time of CRC resection, presence of tumor deposit, and unresectability of metastatic lesion. PSMA expression in primary CRC correlated with that in hepatic metastasis only in concurrent and untreated metastasis subgroup. PSMA expression in primary CRC and hepatic metastasis, regardless of treatment history and timing of metastasis, was not significantly different from that of HCC. **Conclusions:** Several adverse pathological features of primary CRC were associated with a lower PSMA expression in hepatic metastasis. PSMA expression in hepatic metastasis correlated with that of primary CRC only in concurrent and untreated subgroup. Primary HCC and hepatic CRC metastasis show comparable levels of PSMA expression.

Keywords: PSMA; Colorectal neoplasms; Liver neoplasms/secondary; Hepatocellular carcinoma; Immunohistochemistry

INTRODUCTION

Prostate-specific membrane antigen (PSMA) is a transmembrane protein first identified in prostate cancer cell line LNCaP [1]. Although its role in cancer development is unclear, PSMA expression in prostate cancer is significantly higher than in benign prostate tissue [2]. PSMA-directed approaches, one of which was approved by the Food and Drug Administration for use in metastatic castration-resistant prostate cancer, are regarded as promising novel treatments for prostate cancer [3].

Notably, immunohistochemistry (IHC) studies reported PSMA expression in neovasculature of various non-prostatic malignancies [2,4]. Moreover, PSMA expression was found to have diagnostic and prognostic significance in non-prostatic cancers, including hepatocellular carcinoma (HCC) and colorectal cancer (CRC). Compared to conventional CD34 IHC, PSMA IHC can differentiate HCC from benign hepatic lesions more accurately [5]. HCC patients with higher PSMA expression have more aggressive histology and worse prognosis [6,7]. While higher PSMA expression in CRC tumor neovasculature was associated with several unfavorable clinical and histologic features [8,9], our previous study [10] suggested a contrasting trend.

Due to its distinct expression profile, PSMA serves as a diagnostic and therapeutic target for various non-prostatic solid cancers [11], such as HCC and CRC. PSMA–positron emission tomography computed tomography (PET/CT) had a comparable [12] or higher [13] detection rate for HCC than conven-

Received: August 14, 2025 **Revised:** September 29, 2025 **Accepted:** October 20, 2025

Corresponding Author: Hwajeong Lee, MD
Department of Pathology and Laboratory Medicine, Albany Medical Center, Mail Code 81, 47 New Scotland Avenue, Albany, NY 12208, USA
Tel: +1-518-262-6254, Fax: +1-518-262-3663, E-mail: leeh5@amc.edu

This is an Open Access article distributed under the terms of the Creative Commons Attribution Non-Commercial License (https://creativecommons.org/licenses/by-nc/4.0/) which permits unrestricted non-commercial use, distribution, and reproduction in any medium, provided the original work is properly cited.
© 2026 The Korean Society of Pathologists/The Korean Society for Cytopathology

tional fluorodeoxyglucose-PET/CT. A series of case reports have described primary and metastatic CRC being incidentally detected by PSMA-PET/CT [14-17]. Additionally, preliminary analysis suggested that as in prostate cancer patients [18], PSMA-PET/CT radiotracer uptake in HCC patients reflects PSMA IHC results [19], which suggests IHC studies can provide insight into the potential applicability of PSMA theranostics in non-prostatic cancers.

Liver is the most common site for CRC metastasis [20]. 20% of CRC patients have a distant metastasis at diagnosis [21], and 30%–50% of patients develop hepatic metastasis at some time point [22]. Therefore, considering its prevalence, a detailed investigation of PSMA expression in hepatic CRC metastasis could advance the understanding of the disease and support the development of novel treatments. However, currently, there are no comprehensive studies examining PSMA expression and its association with clinical and pathological features in hepatic CRC metastasis. Pilot studies reported that most liver metastasis in CRC patients were PSMA (+), with identical PSMA staining pattern and degrees to that of primary CRC from the same patient [8].

This study aims to evaluate PSMA expression in hepatic CRC metastasis. CRC patients who underwent primary CRC resection without neoadjuvant therapy (n = 56) and with hepatic metastasis were identified and grouped by treatment history (untreated subgroup; n = 47 and treated subgroup; n = 9, see Materials and Methods below) and timing of metastasis (concurrent metastasis subgroup; n = 41 and metachronous metastasis subgroup; n = 15, see Materials and Methods below). Clinicopathological features associated with PSMA expression in primary CRC and hepatic metastasis were identified. PSMA expression in primary CRC and hepatic metastasis were examined to assess their possible correlation. Since PSMA-targeted imaging has shown some promise in HCC, PSMA expression in hepatic CRC metastasis and HCC were compared in an attempt to examine whether such modalities could be applied in hepatic CRC metastasis. To improve readability, hepatic CRC metastasis is referred to as hepatic metastasis in the main text.

MATERIALS AND METHODS

Study populations

The study cohort includes 56 patients with CRC who underwent primary surgical resection without neoadjuvant therapy at Albany Medical Center (AMC) with concurrent or metachronous hepatic metastasis. Cases with available tumor tissue were included. The timing of metastatic tissue sampling was either synchronous (n = 41) or metachronous (metastasis was not detected at the time of initial staging work-up and CRC resection; n = 15) relative to the CRC resection. Hepatic metastases were sampled by Tru-cut/wedge biopsy (n = 23) or resection (n = 33). Patients who underwent needle core biopsy for their hepatic metastasis by vascular and interventional radiology were excluded.

Fig. 1 outlines the patient cohorts, subgroups, and analyses presented in this study. All primary CRC were untreated at the time of resection. Three sets of subgroup analysis were conducted: (1) untreated (n = 47; biopsied or resected) vs. chemotherapy-treated (n = 9; resected following chemotherapy) hepatic metastasis, (2) concurrent (n = 41) vs. metachronous (n = 15) metastasis, and (3) untreated and concurrent metastasis (n = 34) vs. treated and/or metachronous (n = 22) metastasis. The rationale for this grouping was based on our observation that tumor characteristics and treatment status are associated with PSMA expression in CRC [10].

Clinical data were extracted from electronic medical records, which included age, sex, colorectal tumor location, tumor size, and survival outcomes from the time of CRC resection. For hepatic metastasis, presence of multifocal hepatic metastasis, size of hepatic lesion, tissue acquisition method, operability as determined by surgeon and timing of tissue retrieval were recorded. Demographics, primary CRC characteristics, and hepatic metastasis characteristics by treatment status are summarized in Table 1. For the control HCC group, the previously described cohort of 76 HCC patients who underwent hepatic resection in AMC from 2003 to 2019 was used [5].

Histologic review

Hematoxylin and eosin–stained slides of primary CRC and corresponding hepatic metastasis were retrieved for histologic review. Primary CRC was graded according to American Joint Committee on Cancer grading criteria. Examined histologic parameters included pT category, pN category, pTNM stage at the time of primary CRC resection, the number of positive lymph nodes, tumor deposits, tumor budding score, presence of precursor lesions, tumor-stroma ratio, lymphovascular invasion, perineural invasion, and primary CRC resection margin. For each case, representative tumor block was selected for IHC. When available, sections harboring tumor-benign tissue junction were selected.

https://doi.org/10.4132/jptm.2025.10.20

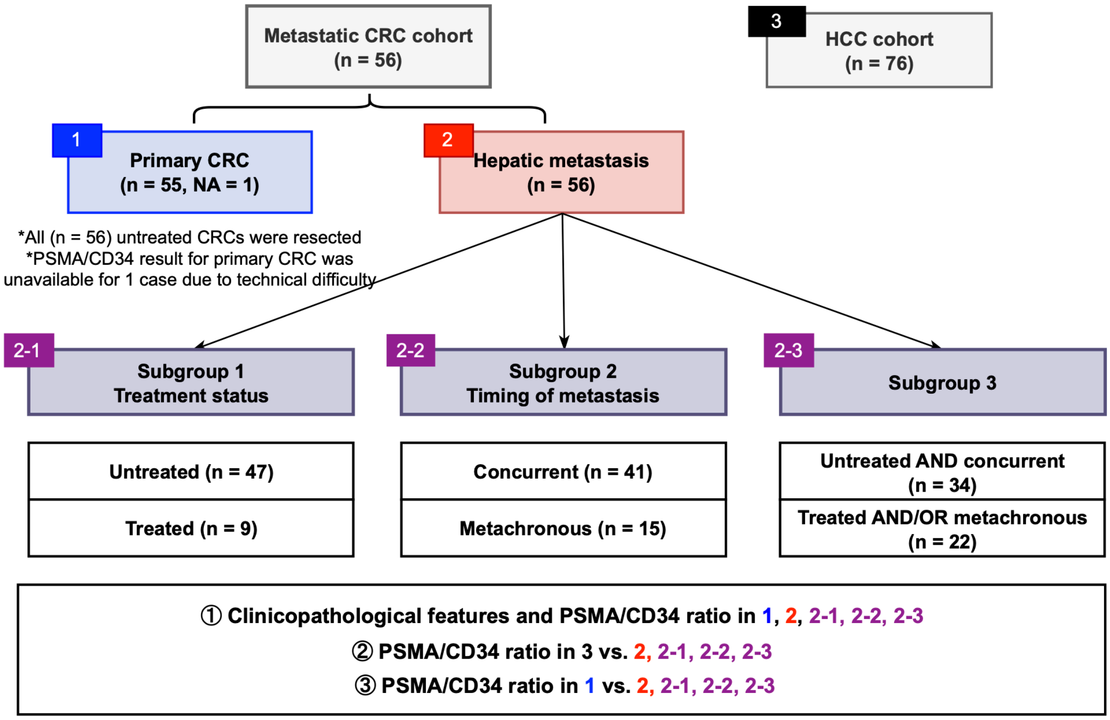

Fig. 1. Schematic diagram of the patient cohorts, subgroups, and analyses. CRC, colorectal cancer; HCC, hepatocellular carcinoma; PSMA, prostate-specific membrane antigen; NA, not available.

PSMA and CD34 IHC analysis

The ratio of PSMA expression to that of pan-endothelial markers, such as CD31 or CD34, has been used as a part of scoring systems [23,24] or a direct measure [25-27] of vascular PSMA expression. In our laboratory, CD34 staining was more robust and easier to interpret than CD31. The PSMA/CD34 ratio, assessed by visual estimation (H.L.), was used as a score of PSMA expression. The ratio was categorized as high (≥50%) and low (<50%) expression for survival analyses, consistent with the threshold used in a previous study of primary CRC across all stages [10]. PSMA and CD34 IHC were performed on 5-μm-thick formalin-fixed paraffin-embedded tissue sections from the selected blocks using the same antibodies, protocols and detection kits as described before [5] (PSMA: 1D6, mouse monoclonal, 1:25, Novocastra, Leica, Buffalo Grove, IL, USA; CD34: QBEnd/10, mouse monoclonal, Ventana Medical Systems, Inc., Tucson, AZ, USA). Staining was carried out with Discovery Ultra Ventana System and OptiView DAB Detection Kit (Ventana Medical Systems, Inc.). Human prostate tissue and tonsillar tissue served as positive controls for PSMA and CD34 IHC, respectively. Benign colon and liver tissue from every inspected slide was PSMA-negative. Representative PSMA and CD34 IHC images of hepatic metastases and their corresponding primary CRCs are shown in Figs. 2 and 3.

Statistical analysis

Statistical analysis was performed using R version 4.3.3 (R Foundation for Statistical Computing, Vienna, Austria). Threshold for statistical significance was set as p-value < .05. Each continuous variable was assessed by Shapiro-Wilk test, with p > .05 as a cutoff for assuming normal distribution. The relationship with the PSMA/CD34 ratio and dichotomous variables were analyzed using the Wilcoxon rank-sum test, ordinal and continuous variables using Kendall's tau (τ), and multi-level categorical variables using the Kruskal-Wallis test. Clinicopathological characteristics according to treatment history were assessed using the Wilcoxon rank-sum test and Fisher's exact test.

Cox proportional hazards (PH) model was used for the time-to-event analysis of overall survival (OS) and recurrence-free survival (RFS) for concurrent metastasis cases. Metachronous metastasis cases were excluded from the time-to-event analysis. Goodness-of-fit test with p > 0.05 was considered to meet the PH assumption. Hazard ratio (HR) and 95% confidence interval (CI) for each Cox PH model was reported. Representative

Table 1. Clinicopathological characteristics of patients with hepatic metastasis

Clinical characteristic	All patients (n = 56)	Previously untreated patients (n = 47)	Chemotherapy-treated patients (n = 9)	p-value (previously untreated patients vs. chemotherapy treated patients)
Demographics				
Sex				
Female	28 (50.0)	22 (46.8)	6 (66.7)	.469
Male	28 (50.0)	25 (53.2)	3 (33.3)	
Age (yr)				
Median (range)	59 (40–87)	59 (40–87)	65 (50–75)	.173
Mean	59.5	58.8	63.0	
Treatment status				
Untreated	47 (83.9)	NA	NA	NA
Treated	9 (16.1)			
Primary CRC characteristics				
Primary CRC size (cm)				
Median (range)	4.5 (1.4–13.5)	4.5 (1.4–13.5)	4.5 (3.0–9.0)	.858
Mean	5.2	5.2	4.9	
Location[a]				
Right	26 (46.4)	21 (44.7)	5 (55.6)	.875
Left	5 (8.9)	5 (10.6)	0	
Rectum	25 (44.6)	21 (44.7)	4 (44.4)	
Grade[a]				
1	2 (3.6)	2 (4.3)	0	.584
2	44 (78.6)	37 (78.7)	7 (77.8)	
3	10 (17.9)	8 (17.0)	2 (22.2)	
pT category				
2	3 (5.4)	2 (4.3)	1 (11.1)	.386
3	35 (62.5)	29 (61.7)	6 (66.7)	
4	18 (32.1)	16 (34.0)	2 (22.2)	
pN category				
0	10 (17.9)	9 (19.1)	1 (11.1)	.951
1	18 (32.1)	14 (29.8)	4 (44.4)	
2	28 (50.0)	24 (51.1)	4 (44.4)	
pTNM stage				
I	1 (1.8)	1 (2.1)	0	.686
II	2 (3.6)	2 (4.3)	0	
III	12 (21.4)	10 (21.3)	2 (22.2)	
IV	41 (73.2)	34 (72.3)	7 (77.8)	
Tumor deposit				
Absent	18 (32.1)	16 (34.0)	2 (22.2)	.703
Present	38 (67.9)	31 (66.0)	7 (77.8)	
Lymphovascular invasion				
Absent	19 (33.9)	15 (31.9)	4 (44.4)	.470
Present	37 (66.1)	32 (68.1)	5 (55.6)	
Perineural invasion				
Absent	29 (51.8)	27 (57.4)	2 (22.2)	.073
Present	27 (48.2)	20 (42.6)	7 (77.8)	

Continued

Table 1. Continued

Clinical characteristic	All patients (n = 56)	Previously untreated patients (n = 47)	Chemotherapy-treated patients (n = 9)	p-value (previously untreated patients vs. chemotherapy treated patients)
Primary CRC margin				
Negative	50 (89.3)	45 (95.7)	5 (55.6)	.004
Positive	6 (10.7)	2 (4.3)	4 (44.4)	
Tumor-stroma ratio				
Stroma low	18 (32.1)	14 (29.8)	4 (44.4)	.448
Stroma high	38 (67.9)	33 (70.2)	5 (55.6)	
Precursor lesion				
Absent	36 (64.3)	31 (66.0)	5 (55.6)	.707
Present	20 (35.7)	16 (34.0)	4 (44.4)	
Tumor budding score				
1	29 (51.8)	26 (55.3)	3 (33.3)	.058
2	15 (26.8)	14 (29.8)	1 (11.1)	
3	12 (21.4)	7 (14.9)	5 (55.6)	
No. of tumor buds				
Median (range)	4 (0–23)	3 (0–17)	11 (0–23)	.072
Mean	5.8	4.9	10.4	
No. of positive lymph nodes				
Median (range)	3.5 (0–13)	4 (0–13)	2 (0–9)	.777
Mean	3.4	3.5	3.0	
No. of tumor deposits				
Median (range)	2 (0–13)	2 (0–13)	2 (0–5)	.891
Mean	2.71	2.9	2.0	
Hepatic metastasis characteristics				
No. of hepatic metastasis				
Single	27 (48.2)	21 (44.7)	4 (44.4)	>.99
Multiple	25 (44.6)	22 (46.8)	5 (55.6)	
Hepatic metastasis size (cm)	NA = 4	NA = 4		
Median (range)	2.9 (0.6–22.5)	2.7 (0.6–22.5)	3.2 (1–8)	.513
Mean	3.5	3.5	3.6	
Tissue acquisition method				
Biopsy	23 (41.1)	23 (48.9)	0	.007
Resection	33 (58.9)	24 (51.1)	9 (100)	
Operability				
Operable	34 (60.7)	25 (53.2)	9 (100)	.008
Inoperable	22 (39.3)	22 (46.8)	0	
Tissue acquisition time				
Synchronous	41 (73.2)	34 (72.3)	7 (77.8)	>.99
Asynchronous	15 (26.8)	13 (27.7)	2 (22.2)	

Values are presented as number (%) unless otherwise indicated.

CRC, colorectal cancer; NA, not applicable,

[a] Percentages for subgroups may not sum to 100 due to rounding.

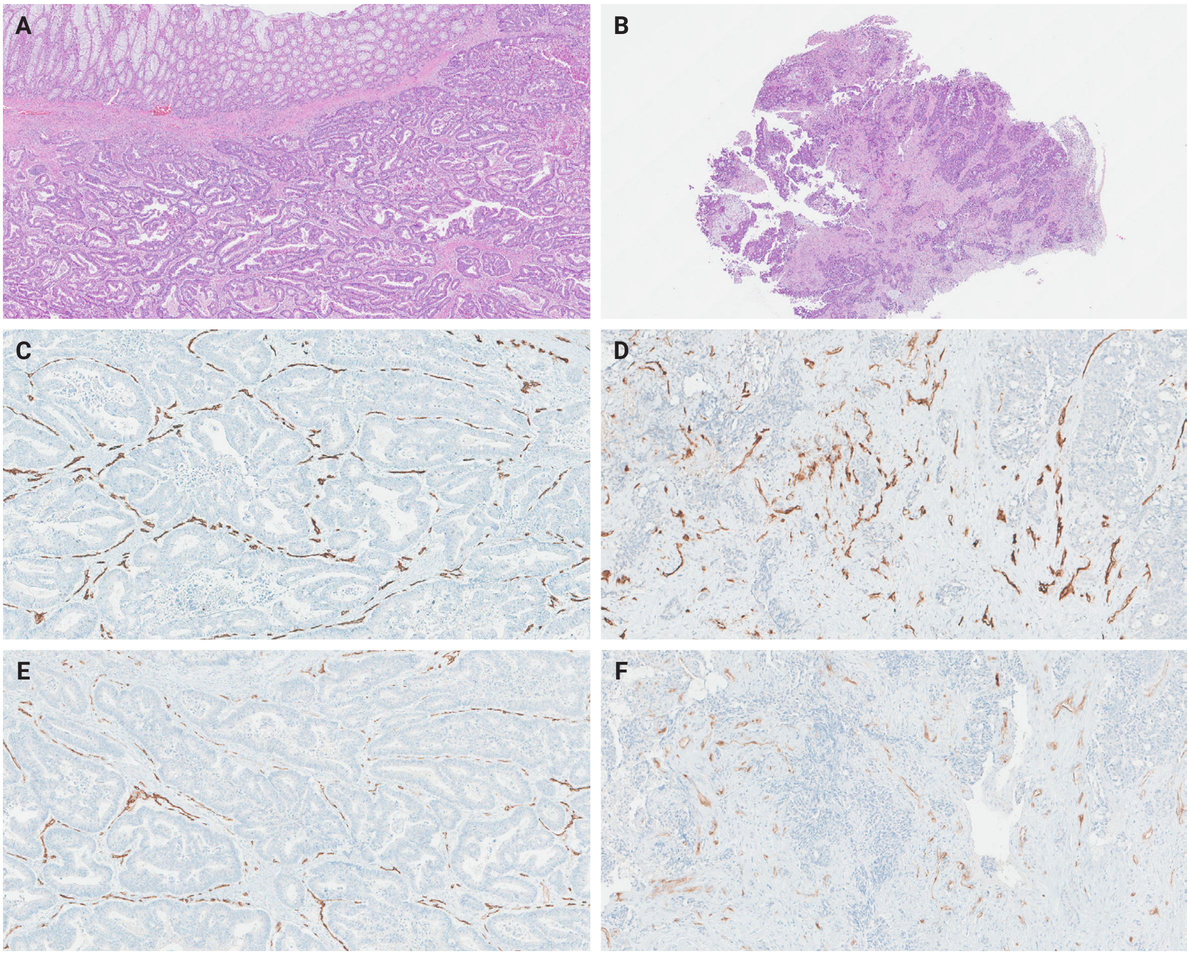

Fig. 2. Representative images for CD34 (C, D) and prostate-specific membrane antigen (PSMA) (E, F) immunohistochemistry in primary colorectal cancer with high PSMA/CD34 ratio (A, C, E) and wedge biopsy of corresponding hepatic metastasis (untreated) (B, D, F).

values for continuous variables were range, mean, and median. Categorical variables were reported as frequencies and percentages (%).

RESULTS

PSMA expression in primary CRC and hepatic metastasis

The summary statistics of the PSMA/CD34 ratio for the entire cohort, as well as subgroups stratified by treatment status and timing of metastasis, as shown in Fig. 1, are outlined in Table 2. In the entire cohort (n = 56), the PSMA/CD34 ratio in primary CRC had a mean of 27.1 (range, 0 to 85.0) and a median of 20.0. For hepatic metastasis, the mean was 29.2 (range, 0 to 95.0), with a median of 20.0.

PSMA expression in primary CRC and clinicopathological features

The associations between the clinicopathological parameters and PSMA expression in the primary CRC are summarized in Table 3. At the time of CRC resection, 1 (2%) case was pTNM stage I, two (4%) were II, 12 (21%) were III, and 41 (73%) were IV (Table 1). Patients with larger CRC ($p = .013$, $\tau = 0.241$) had higher PSMA expression.

PSMA expression in hepatic metastasis and clinicopathological features: entire cohort

The associations between the clinicopathological characteristics and the PSMA expression in the hepatic metastasis are summarized in Table 4 and Supplementary Table S1. In the entire cohort (n = 56), the PSMA expression in hepatic metastasis was lower in high grade primary CRC ($p = .005$, $\tau = -0.318$),

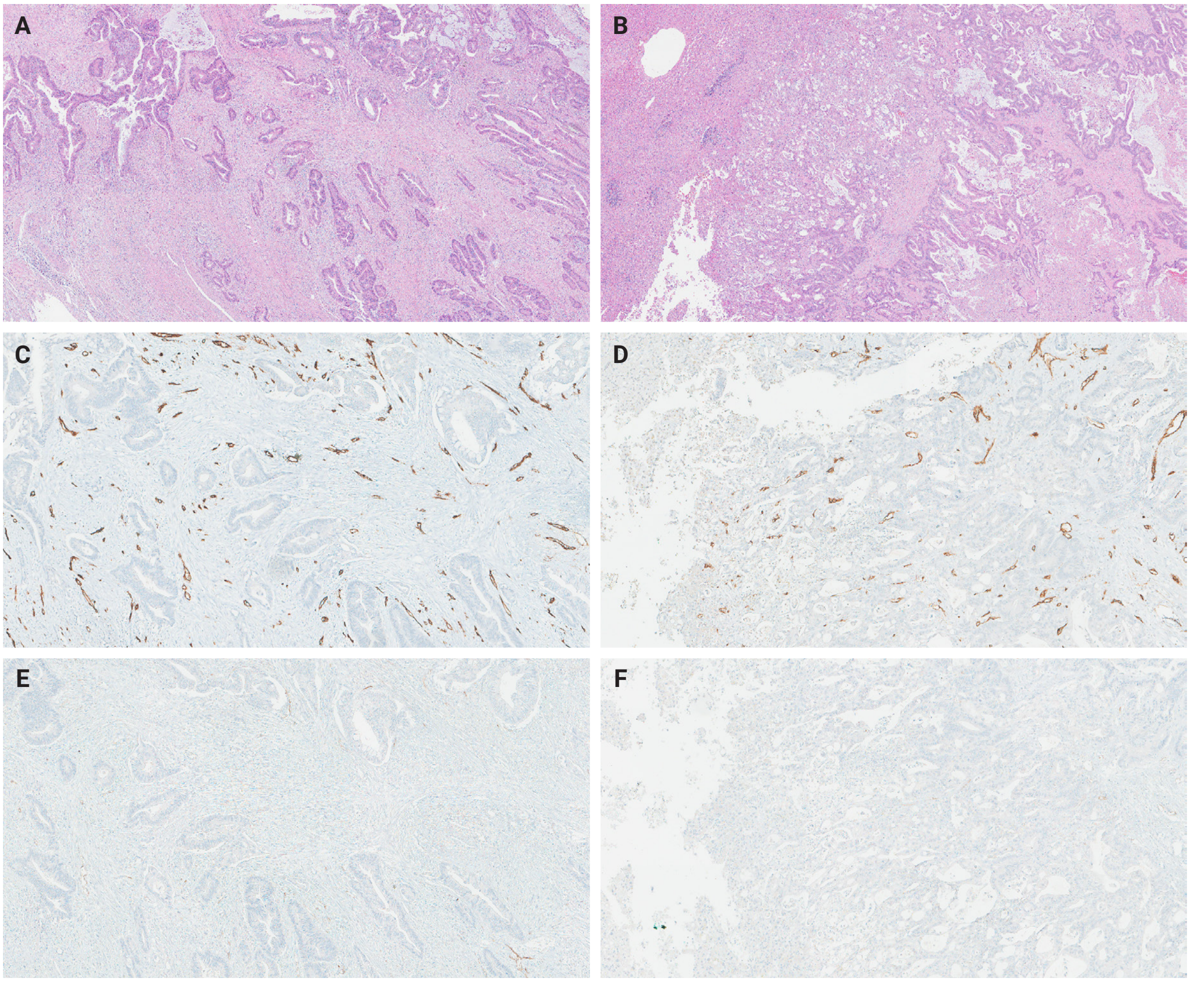

Fig. 3. Representative images for CD34 (C, D) and prostate-specific membrane antigen (PSMA) (E, F) immunohistochemistry in primary colorectal cancer with low PSMA/CD34 ratio (A, C, E) and resected corresponding hepatic metastasis (untreated) (B, D, F).

higher pTNM stage at the time of CRC resection (p = .020, τ = –0.262) and the presence of tumor deposit (p = .037). Although pN stage was not related to PSMA levels, the presence of nodal involvement (pN0 vs. pN1–2) was marginally associated with a lower PSMA level (p = .065) in hepatic metastasis. Regarding the characteristics of hepatic metastasis, biopsy (p = .004), inoperable lesions (p = .005), and lesion acquired synchronously with CRC resection (p = .024) were associated with lower PSMA expression in hepatic metastasis. Prior chemotherapy did not have a significant impact on PSMA expression in hepatic metastasis (p = .653). Boxplots and scatterplots for variables showing significant associations with PSMA expression in primary CRC and hepatic metastasis are presented in Supplementary Fig. S1.

PSMA expression in hepatic metastasis and clinicopathological features: grouped by treatment status

In the untreated subgroup (n = 47), high grade primary CRC (p = .032, τ = –0.267), higher pTNM stage at the time of CRC resection (p = .048, τ = –0.244), the presence of tumor deposit (p = .036), biopsy (p = 0.004), and inoperable metastasis (p = .005) were significantly associated with lower PSMA expression in hepatic metastasis. Patients with nodal involvement (p = .051) tended to exhibit lower PSMA expression. In the chemotherapy-treated patients (n = 9), older age was associated with higher PSMA expression in hepatic metastasis (p = .035, τ = 0.572). Treated patients with higher primary CRC tumor grade tended to exhibit lower PSMA expression in hepatic metastasis; however, the association was marginal (p = .055)

Table 2. PSMA expression in study population

PSMA/CD34 ratio	All patients (n = 56)	Previously untreated patients (n = 47)	Chemotherapy-treated patients (n = 9)	Concurrent metastasis (n = 41)	Metachronous metastasis (n = 15)	Untreated and concurrent metastasis (n = 34)	Treated and/or metachronous metastasis (n = 22)
Primary CRC	NA = 1	NA = 1		NA = 1		NA = 1	
Mean	27.1	27.8	23.8	27.9	25.1	28.5	25
Median (range)	20.0 (0–85.0)[a]	20.0 (0–85.0)[a]	15.0 (2.0–70.0)	17.5 (0–85.0)[a]	20.0 (0–80.0)	20 (0–85.0)[a]	20 (0–80.0)
Hepatic metastasis							
Mean	29.2	29.0	30.2	24.2	43.1	24.4	36.7
Median (range)	20.0 (0–95.0)	20.0 (0–95.0)	20.0 (0–80.0)	10.0 (0–90.0)	40.0 (2–95.0)	10.0 (0–90.0)	27.5 (0–95.0)

PSMA, prostate-specific membrane antigen; CRC, colorectal cancer; NA, not applicable/available.
[a] PSMA expression could not be determined in 1 case due to technical difficulties.

PSMA expression in hepatic metastasis and clinicopathological features: grouped by timing of metastasis

In the concurrent metastasis subgroup (n = 41), lower PSMA expression in hepatic metastasis was associated with higher CRC grade (p = .006, τ = –0.372). However, regarding hepatic lesions, biopsy specimens (p = .045) and inoperable lesions (p = .049) were associated with lower PSMA expression in hepatic metastasis. In metachronous metastasis subgroup (n = 15), no significant associations were found between PSMA expression in hepatic metastasis and clinicopathological characteristics.

PSMA expression in hepatic metastasis and clinicopathological features: concurrent and untreated metastasis vs. metachronous and/or treated metastasis

In the concurrent and untreated metastasis subgroup (n = 34), negative associations between higher primary CRC grade (p = .036, τ = –0.314), biopsy specimens of hepatic lesions (p = .036), inoperable lesions (p = .040), and PSMA expression in hepatic metastasis were maintained. In contrast, in metachronous and/or treated subgroup (n = 22), PSMA expression in hepatic metastasis was not associated with any of the aforementioned clinicopathological parameters.

PSMA expression in primary CRC and concurrent hepatic metastasis vs. survival outcomes

Results for survival analysis are outlined in Supplementary Table S2. PSMA expression was grouped into PSMA-high (PSMA/CD34 ratio ≥ 50%) and PSMA-low (PSMA/CD34 ratio < 50%, see Materials and Methods). In concurrent metastasis cases, PSMA expression in primary CRC was not associated with OS (HR, 2.154; 95% CI, 0.891 to 5.204; p = .088) and RFS (HR, 5.480; 95% CI, 0.496 to 60.52; p = .165). Likewise, PSMA expression in the concurrent hepatic metastasis subgroup was not associated with OS and RFS (OS: HR, 0.546; 95% CI, 0.189 to 1.578; p = .264; RFS: HR, 0.348; 95% CI, 0.041 to 2.961; p = .334). Similarly, no association was found in the concurrent and untreated subgroup (OS: HR, 0.441; 95% CI, 0.131 to 1.490; p = .188, RFS: HR, 0.429; 95% CI, 0.046 to 4.003; p = .458). Sensitivity analyses using different cutoffs showed no significant association between PSMA expression in hepatic metastasis and prognosis (Supplementary Table S3). Kaplan-Meier plots and corresponding p-values from log-rank test are outlined in Supplementary Fig. S2.

Table 3. Associations between clinicopathological characteristics of primary CRC and hepatic metastasis vs. PSMA expression in primary CRC

Characteristic	PSMA/CD34 ratio (n = 56)		
	Mean	Median (range)	p-value
Demographics			
Sex			
Male	31.0	20 (2–85)	.196
Female	23.3	17.5 (0–80)	
Age			.069 (τ = −0.176)
Treatment status			
Untreated	27.8	20 (0–85)	.873
Treated	23.8	15 (2–70)	
Primary CRC characteristics			
Primary CRC size (cm)			.013 (τ = 0.241)
Location			
Right	23.3	15 (2–80)	.530
Left	38.0	20 (15–80)	
Rectum	28.7	20 (0–85)	
Grade			
1	4.5	4.5 (2–7)	.457 (τ = 0.085)
2	27.7	20 (0–85)	
3	28.9	17.5 (2–70)	
pT category			
2	36.7	50 (0–60)	.227 (τ = 0.137)
3	22.9	15 (0–85)	
4	33.6	25 (0–80)	
pN category			
0	38.0	35 (0–80)	.892 (τ = 0.015)
1	18.9	12.5 (0–60)	
2	28.6	20 (0–85)	
pTNM stage at time of CRC resection			
1	0	0 (0–0)	.851 (τ = 0.021)
2	50.0	50 (20–80)	
3	23.0	20 (2–70)	
4	27.9	17.5 (0–85)	
Tumor deposit			
Absent	29.4	20 (0–80)	.732
Present	26.0	20 (0–85)	
Lymphovascular invasion			
Absent	26.0	20 (0–80)	.715
Present	27.7	20 (0–85)	
Perineural invasion			
Absent	23.1	15 (0–80)	.173
Present	31.6	25 (2–85)	
Primary CRC margin			
Negative	26.0	20 (0–85)	.371
Positive	36.2	37.5 (2–70)	
Tumor-stroma ratio			
Stroma high	28.3	15 (0–85)	.935
Stroma low	24.7	20 (0–60)	
Precursor lesion			
Absent	30.4	20 (0–85)	.308
Present	21.4	17.5 (0–80)	
Tumor budding score			
1	29.5	20 (0–85)	.892 (τ = −0.015)
2	18.5	15 (0–40)	
3	32.4	20 (2–80)	
No. of tumor buds			.327 (τ = −0.098)
No. of positive lymph nodes			.397 (τ = 0.086)
No. of tumor deposits			.580 (τ = 0.056)
Hepatic metastasis characteristics			
No. of hepatic metastasis			
Multifocal	30.1	20 (2–85)	.255
Single	24.3	20 (0–80)	
Hepatic metastasis size (cm)			.508 (τ = −0.067)
Tissue acquisition method			
Biopsy	29.0	15 (0–85)	>.99
Resection	25.8	20 (0–80)	
Operability			
Inoperable	30.3	20 (0–85)	.654
Operable	25.0	20 (0–80)	
Tissue acquisition time			
Concurrent	27.9	17.5 (0–85)	.864
Metachronous	25.1	20 (0–80)	

CRC, colorectal cancer; PSMA, prostate-specific membrane antigen; τ, Kendall's tau.

PSMA expression in hepatic metastasis compared to HCC

To evaluate the potential of targeting PSMA in hepatic metastasis, PSMA expression in hepatic metastasis was compared with that of HCC. PSMA expression in hepatic metastasis was not significantly different from HCC in the entire cohort (p = .334). None of the subgroups showed significant differences in PSMA expression in hepatic metastasis compared to HCC (untreated subgroup: p = .313, treated subgroup: p = .818, concurrent metastasis subgroup: p = .084, metachronous metastasis subgroup: p = .327, concurrent and untreated subgroup: p = .096, meta-

Table 4. Associations between clinicopathological characteristics of primary CRC vs. PSMA expression in hepatic metastasis

Clinical characteristic	PSMA/CD34 ratio								
	All patients (n = 56)			Previously untreated patients (n = 47)			Chemotherapy-treated patients (n = 9)		
	Mean	Median (range)	p-value	Mean	Median (range)	p-value	Mean	Median (range)	p-value
Demographics									
Sex									
Male	32.7	20 (0–95)	.478	31.4	20 (0–95)	.746	43.3	30 (20–80)	.214
Female	25.8	12.5 (0–80)		26.3	15 (2–80)		23.7	12.5 (0–80)	
Age			.568 (τ = −0.055)			.140 (τ = −0.157)			.035 (τ = 0.572)
Treatment status			.653			NA			NA
Untreated	29.0	20 (0–95)		29.0	20 (0–95)				
Treated	30.2	20 (0–80)					30.2	20 (0–80)	
Primary CRC characteristics									
Primary CRC size (cm)			.314 (τ = 0.097)			.329 (τ = 0.104)			.596 (τ = 0.145)
Location			.287			0.460			.323[a]
Right	21.0	12.5 (0–80)		20.2	10 (2–80)		24.4	15 (0–80)	
Left	39.6	50 (0–80)		39.6	50 (0–80)				
Rectum	35.7	25 (0–95)		35.3	20 (0–95)		37.5	30 (10–80)	
Grade			.005 (τ = −0.318)			.032 (τ = −0.267)			(Grade 2 vs. 3) .055[b]
1	2.0	2 (2–2)		2.0	2 (2–2)				
2	36.3	20 (0–95)		36.0	20 (0–95)		37.9	30 (10–80)	
3	3.4	2 (0–10)		3.4	2 (0–10)		3.5	3.5 (0–7)	
pT category			.170 (τ = −0.155)			.103 (τ = −0.203)			.702 (τ = 0.115)
2	61.7	75 (20–90)		82.5	82.5 (75–90)		20.0	20 (20–20)	
3	29.4	20 (0–95)		29.9	20 (0–95)		27.0	22.5 (0–80)	
4	23.5	12.5 (0–80)		20.8	12.5 (0–70)		45.0	45 (10–80)	
pN category			.579 (τ = −0.061)			.791 (τ = −0.032)			.559 (τ = −0.175)
0	44.0	32.5 (2–90)		46.7	40 (2–90)		20.0	20 (20–20)	
1	18.9	8.5 (0–90)		13.9	4.5 (0–90)		36.8	30 (7–80)	
2	30.5	17.5 (0–95)		31.2	20 (0–95)		26.2	12.5 (0–80)	
pTNM stage at time of CRC resection			.020 (τ = −0.262)			.048 (τ = −0.244)			.184[c]
1	75.0	75 (75–75)		75.0	75 (75–75)				
2	32.5	32.5 (25–40)		32.5	32.5 (25–40)				
3	42.2	35 (2–95)		39.6	30 (2–95)		55.0	55 (30–80)	
4	24.1	10 (0–90)		24.4	10 (0–90)		23.1	15 (0–80)	

Continued

Table 4. Continued

Clinical characteristic	PSMA/CD34 ratio								
	All patients (n = 56)			Previously untreated patients (n = 47)			Chemotherapy-treated patients (n = 9)		
	Mean	Median (range)	p-value	Mean	Median (range)	p-value	Mean	Median (range)	p-value
Tumor deposit			.037			.036			.639
Absent	40.9	27.5 (2–95)		42.9	32.5 (2–95)		25.0	25 (20–30)	
Present	23.7	10 (0–80)		21.8	10 (0–80)		31.7	15 (0–80)	
Lymphovascular invasion			.351			.755			.138
Absent	33.3	20 (2–95)		31.5	20 (2–95)		40.0	30 (20–80)	
Present	27.1	15 (0–90)		27.8	17.5 (0–90)		22.4	10 (0–80)	
Perineural invasion			.433			.174			.555
Absent	32.1	20 (0–95)		33.4	20 (2–95)		15.0	15 (0–30)	
Present	26.1	10 (0–90)		23.1	9 (0–90)		34.6	20 (7–80)	
Primary CRC margin			.894			>.99			.805
Negative	29.8	20 (0–95)		29.6	20 (0–95)		31.0	30 (0–80)	
Positive	24.5	15 (7–80)		15.0	15 (10–20)		29.2	15 (7–80)	
Tumor-stroma ratio			.219			.241			.138
Stroma high	25.3	12.5 (0–90)		25.8	15 (0–90)		22.4	10 (0–80)	
Stroma low	37.4	25 (0–95)		36.6	20 (0–95)		40.0	30 (20–80)	
Precursor lesion			.335			.126			.387
Absent	34.1	20 (0–95)		35.5	20 (0–95)		25.4	10 (0–80)	
Present	20.4	17.5 (0–80)		16.4	12.5 (0–80)		36.2	25 (15–80)	
Tumor budding score			.298 (τ = –0.114)			.435 (τ = –0.095)			.404 (τ = –0.250)
1	34.3	20 (0–90)		33.2	20 (0–90)		43.3	30 (20–80)	
2	28.1	20 (2–95)		29.6	20 (2–95)		7.0	7 (7–7)	
3	18.3	10 (0–80)		12.1	8 (2–30)		27.0	15 (0–80)	
No. of tumor buds			.655 (τ = –0.044)			.866 (τ = –0.018)			.523 (τ = –0.176)
No. of positive lymph nodes			.491 (τ = –0.069)			.727 (τ = –0.039)			.335 (τ = –0.269)
No. of tumor deposits			.117 (τ = –0.159)			.110 (τ = –0.178			.915 (τ = –0.030)

CRC, colorectal cancer; PSMA, prostate-specific membrane antigen; τ, Kendall's tau; NA, not applicable.

[a]Only right-sided and rectal CRCs were present; [b]Only grade 2 and grade 3 CRCs were present; [c]Only pTNM stage 3 and 4 CRCs were present.

chronous and/or treated subgroup: p = .699) (Supplementary Fig. S3).

Correlation of PSMA expression between hepatic metastasis and primary CRC

The PSMA expression in primary CRC and matched hepatic metastasis from the same case were compared to assess possible association. A significant correlation in PSMA expression in primary CRC and hepatic metastasis was found in the entire cohort (p = .022, τ = 0.227) and untreated subgroup (p = .045, τ = 0.219), while no significant association was observed in the treated subgroup (p = .392, τ = 0.239) (Figs. 2, 3).

When stratified by the timing of metastasis, a significant correlation in PSMA expression between primary CRC and hepatic metastasis was observed in the concurrent metastasis subgroup (p = 0.022, τ = 0.270), but not in the metachronous metastasis subgroup (p = 0.544, τ = 0.123). As expected, a similar pattern was observed when comparing concurrent and untreated metastasis subgroup (p = 0.033, τ = 0.279) with metachronous and/or treated subgroup (p = 0.302, τ = 0.167).

DISCUSSION

Unlike previous studies that included CRC patients with or without metastasis, our cohort consists solely of hepatic metastasis cases. Haffner et al. [8] reported 16 (84.2%) of 19 liver CRC metastases were PSMA-positive, when low intensity staining in less than <10% of endothelium was considered negative [8]. Study by Abdel-Hadi et al. [9] included 13 CRC patients with distant metastasis and their results paralleled that of Haffner et al. [8]. However, tissue collection methods and treatment history were not specified in Haffner et al.'s study [8]. Abdel-Hadi et al. [9] excluded previously treated CRC cases but did not specify sites of sampled metastatic lesions. Our cohort consists of a larger number of patients (n = 56) with defined hepatic metastasis, treatment history, tissue collection method, and timing of metastasis. Further, correlation between PSMA expression in hepatic metastasis and pathological variables of primary CRC was examined in this study.

Although it is relatively well documented that PSMA is upregulated as the cancer progresses [6,28-30], several conflicting findings have been reported [10,31]. PSMA expression in CRC patients was reported to be associated with higher CRC grade, male sex, presence of distant metastasis, and vascular invasion [8,9]. However, our previous study on a larger CRC cohort found that unfavorable prognostic features, such as higher pT, pN, and pTNM stage; the presence and greater number of tumor deposits; and the use of post-operative adjuvant treatment, were associated with lower PSMA expression [10]. In our current CRC cohort with concurrent or metachronous hepatic metastasis, except for tumor size, most clinicopathological variables previously reported to be associated with PSMA expression did not show statistically significant association. The discrepancy might stem from differences in study populations, or other factors may alter/impact PSMA expression in CRC with hepatic metastasis.

In our entire cohort, PSMA level in hepatic metastasis was lower in high-grade primary CRC, advanced pTNM stage at the time of primary CRC resection and the presence of tumor deposit. In addition, nodal involvement in primary CRC showed a modest association with a lower PSMA expression in hepatic metastasis (p = .065). In terms of clinicopathological characteristics of hepatic lesions, biopsy, inoperable hepatic lesion and synchronous sampling with CRC resection were associated with lower PSMA expression in hepatic metastasis. The presence of tumor deposit is an independent adverse prognostic factor in CRC patients who undergo radical resection [32]. High pTNM stage, lymph node involvement and higher tumor grade are unfavorable prognostic features. Inoperable hepatic metastasis invariably portends a grim prognosis [33]. In our cohort, all inoperable hepatic metastasis underwent biopsy, which may account for a lower PSMA expression in biopsied tissues. It appears that several adverse pathological and clinical features are associated with a lower PSMA expression in hepatic metastasis, as it is the case in primary CRCs [10]. One possible explanation for this pattern is that PSMA regulation may be site- (primary versus metastatic) or tumor-dependent. Endothelial cells from different anatomic locations exhibit considerable differences in gene expression profiles [34]. Furthermore, studies comparing benign and tumor-associated vasculature found that most differentially regulated genes were organ- or stage-specific [35,36]. Thus, although PSMA is widely expressed in the neovasculature of non-prostatic cancers, its regulatory mechanism in CRC and its hepatic metastases may differ from that in other cancers, potentially reflecting variations in the tumor microenvironment. This notion is supported by an animal study showing that protein expression profiles in the tumor vasculature of pancreatic islet tumor cells differed by anatomic sites (orthotopic vs. heterotopic), highlighting the influence of the tumor microenvironment on endothelial cell phenotypes [37].

To evaluate the effect of treatment status and timing of metastasis in PSMA expression, we performed a subgroup analysis (Fig. 1). The impact of chemotherapy on PSMA expression is yet to be investigated in detail. In a study of serous epithelial ovarian carcinoma, there was no change in PSMA expression between pre- and post-chemotherapy samples, although PSMA staining was nearly absent in their cohort [38]. In our previous analysis of rectal adenocarcinoma, the chemoradiotherapy-treated subgroup exhibited lower PSMA expression compared to the untreated subgroup [10]. However, in hepatic metastasis, no significant difference in PSMA expression was observed between chemotherapy-treated and untreated subgroups. It appears that the impact of chemotherapy on PSMA expression is dependent on tumor type, location, setting (primary vs. metastasis), and possibly the treatment regimen, warranting further investigations.

In the untreated subgroup, clinicopathological features of primary CRC previously linked to lower PSMA expression in the hepatic metastasis in the entire cohort-such as higher primary CRC grade, advanced pTNM stage, presence of tumor deposit, biopsied hepatic lesions, and inoperable hepatic lesions-remained significantly associated. However, none of the aforementioned features showed a significant association with PSMA expression in hepatic metastasis from the treated subgroup. Although older patients showed higher PSMA expression in the treated subgroup, due to a small number of cases (n = 9), we cannot confirm the clinical significance of this observation or hypothesize the pathophysiologic mechanism behind it. However, a marginal association with higher primary CRC grade and lower PSMA scores ($p = .055$) was still observed in the treated subgroup. This raises the possibility that the association between adverse pathological features and lower PSMA expression persists to a certain extent in treated subgroup, as they are in the entire cohort and untreated subgroup.

When stratified by the timing of metastasis, concurrent metastasis subgroup with the above adverse prognostic features exhibited a lower PSMA expression in hepatic metastasis. However, in metachronous metastasis subgroup, no such association was observed. In addition, in the same subgroup with metachronous metastasis, no association between pTNM stage at the time of primary CRC resection and PSMA expression in hepatic metastasis was observed ($p = .615$, $\tau = -0.112$). A similar trend was found when concurrent and untreated subgroup versus treated and/or metachronous subgroup were compared.

These findings suggest that PSMA expression profiles differ between concurrent and untreated cases versus metachronous and/or treated cases. Concurrent metastasis cases presented with hepatic lesions at the time of CRC resection, whereas metachronous cases developed metastasis later. This time lag between CRC resection and the development of hepatic lesions may alter the relationship between PSMA expression in metastasis and the clinicopathological features of the primary CRC. In other words, PSMA expression in metachronous hepatic metastasis may no longer reflect the tumor biology of primary (previous) CRC. Likewise, treatment status is likely to influence PSMA expression in hepatic metastasis, similar to our observation in treated rectal cancer [10].

In our entire cohort, the PSMA expression in hepatic metastasis exhibited a positive correlation with that of primary CRC. This finding suggests that PSMA expression in primary CRC specimen may be used to estimate that in hepatic metastasis. However, these correlations remained significant only in concurrent and untreated subgroup, but not in metachronous and/or treated subgroup, indicating that the time interval and treatment history influence PSMA expression in hepatic metastasis. A recent study compared the gene mutation profiles of synchronous and metachronous hepatic metastases with their corresponding primary CRCs [39]. Primary CRCs giving rise to concurrent metastases harbored a distinct set of mutations compared with those leading to metachronous metastases. Likewise, the mutational landscapes of hepatic metastases differed by metastasis timing. Notably, when mutation profiles were compared between primary CRCs and paired hepatic metastases from the same individual, the genes showing the greatest discrepancies varied according to the timing of metastasis. These findings indicate that primary CRCs leading to concurrent versus metachronous metastases are biologically distinct, which could account for observed differences in the association of PSMA expression between primary CRC and hepatic metastases by the timing of metastasis. Regarding treatment history, it is possible that chemotherapy-induced alterations in tumor microenvironment could be the cause of the observed discrepancy. Neoadjuvant chemotherapy induces various stromal histologic changes across multiple cancers, including CRC hepatic metastases [40-42]. Additionally, chemotherapeutic agent modifies tumor immune microenvironment [43,44], which contributes to tumor neoangiogenesis [45,46] and is associated with intratumoral PSMA expression [47]. A schematic diagram outlining how chemotherapy and metastasis timing may influence the association of PSMA expression between primary

CRC and metastatic lesions is shown in Fig. 4.

Haffner et al. [8] reported among 11 cases with both primary CRC and nodal/hepatic metastasis available, eight pairs (73%) showed identical PSMA staining patterns and scores. Treatment history and the timing of metastasis were not provided in their manuscript and their scoring system involved staining extent and intensity, while the PSMA/CD34 ratio in our study is based on the staining extent. Despite the differences in scoring methods, their findings align with our results for entire cohort, as well as concurrent and untreated subgroup. A lack of such association in metachronous and/or treated subgroup is possibly due to altered PSMA expression in these cases related to progression of the disease (time lag) or treatment. Alternatively, it is also possible that the previous study did not include treated patients.

In our study, PSMA expression in hepatic metastasis, regardless of treatment history and timing of metastasis, was not markedly different from HCC. This suggests that hepatic metastasis is expected to sequester PSMA-targeted radiotracer to a similar extent as HCC does, making PSMA-PET/CT a potential option in detecting hepatic metastasis. Preliminary studies in HCC demonstrated that PSMA-PET/CT can detect primary and metastatic HCC [19,48,49], and the degree of tracer uptake tends to correlate with PSMA IHC [19]. Given that some adverse features of CRC are associated with lower PSMA levels in hepatic metastasis, PSMA-targeted modalities might be more useful for patients with seemingly less aggressive CRC with occult metastasis.

However, it is worthy of noting that PSMA expression is generally lower in non-prostatic cancers, potentially complicating imaging [50]. Indeed, Cuda et al. [51] argued that liver metastasis in CRC patients does not avidly sequester PSMA-targeted radiotracer, limiting the utility of PSMA-based therapy in such patients. However, a small number of patients (n = 10) were enrolled for PSMA-targeted imaging, and neither resected tumors nor their IHC data were available in their 10 patients. Thus, we believe that the clinical utility of PSMA-directed imaging in metastatic CRC should be validated in a larger cohort with corresponding IHC results obtained using a standardized protocol. Also, intratumoral staining heterogeneity needs to be addressed and assessed in a systematic manner to validate the clinical applicability of this tool, given that metastatic lesions will likely be biopsied for biomarker testing.

There are several limitations in this study. Non-prostate cancers may show heterogenous PSMA expression within a single specimen [5,52], thus small biopsies of hepatic metastasis could be subjected to sampling error. However, we used Tru-cut/wedge biopsies or resected specimens, rather than thin image-guided biopsies, to mitigate this limitation. In addition, relatively small cohort size, especially the treated subgroup (n = 9), may account for the limited statistical power. Thirdly, methods for more precise quantification of PSMA IHC results, such as double staining techniques or digital pathology modalities, were not available due to limited resources. Similarly, the IHC slides were reviewed by one author; thus, potential interobserver variability could not be addressed.

To the best of our knowledge, this is the first study to systematically analyze the association of the PSMA expression and clinicopathological attributes in metastatic CRC cohort, with clearly defined tissue acquisition methods, metastatic site (all liver), and treatment history. Lower PSMA expression in hepatic metastasis is associated with several adverse features of

	Discrepancies in PSMA Expression Between Primary CRC and Hepatic Metastases
Treatment history	Chemotherapy-induced changes in tumor immune microenvironment → Altered tumor neoangiogenesis → PSMA expression in primary CRC and hepatic metastsis **does not correlate in treated cases**
Timing of metastasis	Genetic differences in concurrent vs. metachronous cases → Distinct sets of genes are differentially regulated in primary CRC and hepatic metastasis → PSMA expression in primary CRC and hepatic metastsis **does not correlate in metachronous cases**

Fig. 4. Schematic diagram of potential causes of discrepancies in prostate-specific membrane antigen (PSMA) expression between primary colorectal cancer (CRC) and hepatic metastasis, based on treatment history and metastasis timing.

the primary CRC. PSMA expression in hepatic metastasis correlates with that of the primary CRC, only in concurrent and untreated metastasis. Regardless of treatment history or timing of metastasis, PSMA expression in hepatic metastasis is similar to that in primary HCC. Further research is needed to evaluate the clinical potential of PSMA-targeted modalities in hepatic CRC metastasis.

Supplementary Information

The Data Supplement is available with this article at https://doi.org/10.4132/jptm.2025.10.20.

Ethics Statement

The study was conducted according to the guidelines of the Declaration of Helsinki and approved by the Institutional Review Board at Albany Medical College (protocol #5718, Approval date 06/18/2020) with a waiver of informed patient consent. Patient consent was waived as IRB granted a waiver of patient consent, determining that the study qualified as secondary research for which patient consent is not required.

Availability of Data and Material

The data that support the findings of this study are available from the corresponding author upon reasonable request.

Code Availability

Not applicable.

ORCID

Eundong Park	https://orcid.org/0009-0007-9530-5243
Michel Kmeid	https://orcid.org/0000-0001-8546-5744
Xin Wang	https://orcid.org/0009-0007-9132-405X
Haiyan Qiu	https://orcid.org/0009-0004-1439-1046
Clifton G. Fulmer	https://orcid.org/0000-0003-1453-9421
Marcello P. Toscano	https://orcid.org/0000-0002-6316-3566
Nusret Bekir Subasi	https://orcid.org/0009-0000-3461-4658
Maciej Gracz	https://orcid.org/0000-0001-5580-7280
Hwajeong Lee	https://orcid.org/0000-0001-7005-6278

Author Contributions

Conceptualization: HL. Data acquisition and analysis: EP, MK, XW, HQ, NBS, MG, HL. Writing—original draft: EP. Writing—review & editing: MK, XW, HQ, CGF, MPT, NBS, MG, HL. Approval of final manuscript: all authors.

Conflicts of Interest

The authors declare that they have no potential conflicts of interest.

Funding

No funding to declare.

Acknowledgments

We thank Ms. Rebecca Pirri and Dr. Timothy Jennings for their support.

REFERENCES

1. Horoszewicz JS, Leong SS, Kawinski E, et al. LNCaP model of human prostatic carcinoma. Cancer Res 1983; 43: 1809-18.
2. Silver DA, Pellicer I, Fair WR, Heston WD, Cordon-Cardo C. Prostate-specific membrane antigen expression in normal and malignant human tissues. Clin Cancer Res 1997; 3: 81-5.
3. Sartor O, de Bono J, Chi KN, et al. Lutetium-177-PSMA-617 for metastatic castration-resistant prostate cancer. N Engl J Med 2021; 385: 1091-103.
4. Chang SS, O'Keefe DS, Bacich DJ, Reuter VE, Heston WD, Gaudin PB. Prostate-specific membrane antigen is produced in tumor-associated neovasculature. Clin Cancer Res 1999; 5: 2674-81.
5. Kmeid M, Park YN, Chung T, et al. PSMA Immunohistochemistry in hepatic neoplasms: a promising diagnostic marker with potential theranostic applications. Am J Surg Pathol 2022; 46: 1688-99.
6. Chen LX, Zou SJ, Li D, et al. Prostate-specific membrane antigen expression in hepatocellular carcinoma, cholangiocarcinoma, and liver cirrhosis. World J Gastroenterol 2020; 26: 7664-78.
7. Jiao D, Li Y, Yang F, et al. Expression of prostate-specific membrane antigen in tumor-associated vasculature predicts poor prognosis in hepatocellular carcinoma. Clin Transl Gastroenterol 2019; 10: 1-7.
8. Haffner MC, Kronberger IE, Ross JS, et al. Prostate-specific membrane antigen expression in the neovasculature of gastric and colorectal cancers. Hum Pathol 2009; 40: 1754-61.
9. Abdel-Hadi M, Ismail Y, Younis L. Prostate-specific membrane antigen (PSMA) immunoexpression in the neovasculature of colorectal carcinoma in Egyptian patients. Pathol Res Pract 2014; 210: 759-63.
10. Park E, Wang X, Kmeid M, et al. Prostate-specific membrane antigen expression in colorectal cancer and its potential implication

in disease monitoring in rectal cancer. J Gastrointest Cancer 2025; 56: 159.

11. Backhaus P, Noto B, Avramovic N, et al. Targeting PSMA by radioligands in non-prostate disease-current status and future perspectives. Eur J Nucl Med Mol Imaging 2018; 45: 860-77.
12. Kuyumcu S, Has-Simsek D, Iliaz R, et al. Evidence of prostate-specific membrane antigen expression in hepatocellular carcinoma using 68Ga-PSMA PET/CT. Clin Nucl Med 2019; 44: 702-6.
13. Kesler M, Levine C, Hershkovitz D, et al. (68)Ga-PSMA is a novel PET-CT tracer for imaging of hepatocellular carcinoma: a prospective pilot study. J Nucl Med 2019; 60: 185-91.
14. Arcay A, Eiber M, Langbein T. Incidental finding of colon carcinoma related to high uptake in 18F-PSMA-1007 PET. Clin Nucl Med 2020; 45: 561-2.
15. Aras O, Demirdag C, Kommidi H, Ting R, Sayman HB. Radiopharmaceutical for detecting PSMA-positive metastatic colon cancer: matched-pair comparison of 18F-BF3-Cy3-ACUPA and 68Ga-PSMA PET/MRI. Nucl Med Rev Cent East Eur 2022; 25: 129-30.
16. Hangaard L, Jochumsen MR, Vendelbo MH, Bouchelouche K. Metastases from colorectal cancer Avid on 68Ga-PSMA PET/CT. Clin Nucl Med 2017; 42: 532-3.
17. Doroudinia A, Chekuri S. 68 Ga-PSMA-Avid liver metastases from colon cancer, not visualized on FDG PET scan. Clin Nucl Med 2023; 48: e547-8.
18. Woythal N, Arsenic R, Kempkensteffen C, et al. Immunohistochemical validation of PSMA expression measured by (68) Ga-PSMA PET/CT in primary prostate cancer. J Nucl Med 2018; 59: 238-43.
19. Thompson SM, Suman G, Torbenson MS, et al. PSMA as a theranostic target in hepatocellular carcinoma: immunohistochemistry and (68) Ga-PSMA-11 PET using cyclotron-produced (68) Ga. Hepatol Commun 2022; 6: 1172-85.
20. Hess KR, Varadhachary GR, Taylor SH, et al. Metastatic patterns in adenocarcinoma. Cancer 2006; 106: 1624-33.
21. Leufkens AM, van den Bosch MA, van Leeuwen MS, Siersema PD. Diagnostic accuracy of computed tomography for colon cancer staging: a systematic review. Scand J Gastroenterol 2011; 46: 887-94.
22. Tsilimigras DI, Brodt P, Clavien PA, et al. Liver metastases. Nat Rev Dis Primers 2021; 7: 27.
23. Moore M, Panjwani S, Mathew R, et al. Well-differentiated thyroid cancer neovasculature expresses prostate-specific membrane antigen: a possible novel therapeutic target. Endocr Pathol 2017; 28: 339-44.
24. Crowley MJ, Scognamiglio T, Liu YF, et al. Prostate-specific membrane antigen is a potential antiangiogenic target in adrenocortical carcinoma. J Clin Endocrinol Metab 2016; 101: 981-7.
25. Holzgreve A, Biczok A, Ruf VC, et al. PSMA expression in glioblastoma as a basis for theranostic approaches: a retrospective, correlational panel study including immunohistochemistry, clinical parameters and PET imaging. Front Oncol 2021; 11: 646387.
26. Tubre T, Hacking S, Alexander A, et al. Prostate-specific membrane antigen expression in meningioma: a promising theranostic target. J Neuropathol Exp Neurol 2022; 81: 1008-17.
27. Morgantetti G, Ng KL, Samaratunga H, Rhee H, Gobe GC, Wood ST. Prostate specific membrane antigen (PSMA) expression in vena cava tumour thrombi of clear cell renal cell carcinoma suggests a role for PSMA-driven tumour neoangiogenesis. Transl Androl Urol 2019; 8(Suppl 2): S147-55.
28. Spatz S, Tolkach Y, Jung K, et al. Comprehensive evaluation of prostate specific membrane antigen expression in the vasculature of renal tumors: implications for imaging studies and prognostic role. J Urol 2018; 199: 370-7.
29. Wernicke AG, Varma S, Greenwood EA, et al. Prostate-specific membrane antigen expression in tumor-associated vasculature of breast cancers. APMIS 2014; 122: 482-9.
30. Nomura N, Pastorino S, Jiang P, et al. Prostate specific membrane antigen (PSMA) expression in primary gliomas and breast cancer brain metastases. Cancer Cell Int 2014; 14: 26.
31. Wang HL, Wang SS, Song WH, et al. Expression of prostate-specific membrane antigen in lung cancer cells and tumor neovasculature endothelial cells and its clinical significance. PLoS One 2015; 10: e0125924.
32. Basnet S, Lou QF, Liu N, et al. Tumor deposit is an independent prognostic indicator in patients who underwent radical resection for colorectal cancer. J Cancer 2018; 9: 3979-85.
33. Eng C, Yoshino T, Ruiz-Garcia E, et al. Colorectal cancer. Lancet 2024; 404: 294-310.
34. Chi JT, Chang HY, Haraldsen G, et al. Endothelial cell diversity revealed by global expression profiling. Proc Natl Acad Sci U S A 2003; 100: 10623-8.
35. Aird WC. Molecular heterogeneity of tumor endothelium. Cell Tissue Res 2009; 335: 271-81.
36. Dudley AC. Tumor endothelial cells. Cold Spring Harb Perspect Med 2012; 2: a006536.
37. Joyce JA, Laakkonen P, Bernasconi M, Bergers G, Ruoslahti E, Hanahan D. Stage-specific vascular markers revealed by phage display in a mouse model of pancreatic islet tumorigenesis. Can-

cer Cell 2003; 4: 393-403.
38. Aide N, Poulain L, Elie N, et al. A PSMA-targeted theranostic approach is unlikely to be efficient in serous ovarian cancers. EJNMMI Res 2021; 11: 11.
39. Rajtmajerova M, Ambrozkiewicz F, Hlavac V, et al. Genetic differences between primary colorectal cancer and its paired synchronous and metachronous metastases. Int J Cancer 2025; 158: 120-30.
40. Moll UM, Chumas J. Morphologic effects of neoadjuvant chemotherapy in locally advanced breast cancer. Pathol Res Pract 1997; 193: 187-96.
41. McCluggage WG, Lyness RW, Atkinson RJ, et al. Morphological effects of chemotherapy on ovarian carcinoma. J Clin Pathol 2002; 55: 27-31.
42. Fernandez-Acenero MJ, Cortes-Guiral D, Munoz LE, Martinez-Useros J, Pastor-Idoate C. Morphological aspects of the hepatic response to neoadjuvant therapy. Pathol Res Pract 2015; 211: 665-70.
43. Bracci L, Schiavoni G, Sistigu A, Belardelli F. Immune-based mechanisms of cytotoxic chemotherapy: implications for the design of novel and rationale-based combined treatments against cancer. Cell Death Differ 2014; 21: 15-25.
44. Zitvogel L, Galluzzi L, Smyth MJ, Kroemer G. Mechanism of action of conventional and targeted anticancer therapies: reinstating immunosurveillance. Immunity 2013; 39: 74-88.
45. Albini A, Bruno A, Noonan DM, Mortara L. Contribution to tumor angiogenesis from innate immune cells within the tumor microenvironment: implications for immunotherapy. Front Immunol 2018; 9: 527.
46. Fu LQ, Du WL, Cai MH, Yao JY, Zhao YY, Mou XZ. The roles of tumor-associated macrophages in tumor angiogenesis and metastasis. Cell Immunol 2020; 353: 104119.
47. Park E, Subasi NB, Wang X, et al. CXCR2 expression is associated with prostate-specific membrane antigen expression in hepatocellular carcinoma: reappraisal of tumor microenvironment and angiogenesis. Clin Transl Oncol 2025; 27: 2544-56.
48. Shamim SA, Kumar N, Arora G, et al. A prospective study of (68) Ga-PSMA PET/CT imaging of HCC as diagnosed on conventional imaging to evaluate for potential (177)Lu-PSMA therapy. Ann Nucl Med 2024; 38: 103-11.
49. Hirmas N, Leyh C, Sraieb M, et al. (68)Ga-PSMA-11 PET/CT improves tumor detection and impacts management in patients with hepatocellular carcinoma. J Nucl Med 2021; 62: 1235-41.
50. Wang JH, Kiess AP. PSMA-targeted therapy for non-prostate cancers. Front Oncol 2023; 13: 1220586.
51. Cuda TJ, Riddell AD, Liu C, et al. PET imaging quantifying (68) Ga-PSMA-11 uptake in metastatic colorectal cancer. J Nucl Med 2020; 61: 1576-9.
52. Bychkov A, Vutrapongwatana U, Tepmongkol S, Keelawat S. PSMA expression by microvasculature of thyroid tumors: potential implications for PSMA theranostics. Sci Rep 2017; 7: 5202.

JPTM

CASE STUDY

pISSN 2383-7837 · eISSN 2383-7845

Journal of Pathology and Translational Medicine 2026; 60: 124-128
https://doi.org/10.4132/jptm.2025.12.10

Drug-induced phospholipidosis of the kidney suspected to be caused by atomoxetine

Sung-Eun Choi[1], Kee Hyuck Kim[2], Minsun Jung[3], Jeong Hae Kie[1]

[1]Department of Pathology, National Health Insurance Service Ilsan Hospital, Goyang, Korea
[2]Department of Pediatrics, National Health Insurance Service Ilsan Hospital, Goyang, Korea
[3]Department of Pathology, Yonsei University College of Medicine, Seoul, Korea

Drug-induced phospholipidosis (DIP) is characterized by intracellular accumulation of phospholipids with lamellar body formation secondary to drug-altered lipid metabolism, which can trigger inflammation and histopathological changes. Fabry disease and DIP both exhibit zebra bodies on electron microscopy, complicating differential diagnosis. A 17-year-old male with microscopic hematuria and proteinuria had received atomoxetine (40 mg) for 11 months to treat attention-deficit hyperactivity disorder. Light microscopy showed one glomerulus with perihilar sclerosis and periglomerular fibrosis. Kidney biopsy revealed zebra bodies in podocytes, initially suggesting Fabry disease. However, α-galactosidase A enzyme activity was normal on tandem mass spectrometry. Next-generation sequencing of *GLA* identified only three benign variants. This represents the first reported case of atomoxetine-induced DIP. When zebra bodies are observed, clinicians should consider DIP caused by cationic amphiphilic drugs alongside Fabry disease. Atomoxetine meets the structural criteria for inducing DIP, and awareness of this potential complication is essential.

Keywords: Lysosomal storage diseases; Fabry disease; Podocytes; Biopsy; Atomoxetine hydrochloride

INTRODUCTION

Fabry disease is a rare metabolic disorder characterized by systemic glycosphingolipid accumulation. As it is X-linked, males generally have more severe symptoms and faster progression than females [1]. However, there have been many reports of atypical variants in males with late onset and involvement of a single organ [2]. It is thought that this milder disease phenotype is due to a certain level of residual enzyme activity associated with missense mutations [3]. Pathological findings on kidney biopsy include enlarged and vacuolated podocytes on light microscopy, along with lamellated lipid inclusions (known as “zebra bodies”) in the vacuoles, which can be seen under an electron microscope [4]. Therefore, if zebra bodies are observed on kidney biopsy of a pediatric patient with proteinuria, Fabry disease should generally be considered the primary diagnosis.

However, drug-induced phospholipidosis (DIP) exhibits almost identical pathological findings to Fabry disease [5]. It is diagnosed by first ruling out Fabry disease and then identifying any suspected drugs, which may include hydroxychloroquine [5-8] or amiodarone [9,10]. Herein, we describe a case of DIP in association with atomoxetine (Strattera, Eli Lilly and Company, Indianapolis, IN, USA), a treatment for attention-deficit hyperactivity disorder (ADHD). To the best of our knowledge, this is the first report of atomoxetine as a possible causative agent for DIP.

CASE REPORT

A 17-year-old male patient visited our outpatient clinic after a

Received: August 22, 2025 **Revised:** December 1, 2025 **Accepted:** December 10, 2025

Corresponding Author: Jeong Hae Kie, MD, PhD
Department of Pathology, National Health Insurance Service Ilsan Hospital, 100 Ilsan-ro, Goyang 10444, Korea
Tel: +82-31-780-0892, Fax: +82-31-900-0899, E-mail: jhkie88@nhimc.or.kr

This is an Open Access article distributed under the terms of the Creative Commons Attribution Non-Commercial License (https://creativecommons.org/licenses/by-nc/4.0/) which permits unrestricted non-commercial use, distribution, and reproduction in any medium, provided the original work is properly cited.
© 2026 The Korean Society of Pathologists/The Korean Society for Cytopathology

school urine test showed microscopic hematuria and proteinuria. There were no specific symptoms. Prior to this visit, he had taken 40 mg of atomoxetine daily for 12 months as a treatment for ADHD. Proteinuria persisted for 28 months in urine tests conducted every 6 months; urine albumin-to-creatinine ratio gradually increased from 412 µg/mgCr to 474.6 µg/mgCr over 17 months, while the urine protein-to-creatinine ratio (UPCR) increased from 629.9 mg/g to 666.7 mg/g over the same period. A kidney biopsy was performed to determine the cause of proteinuria.

At the time of renal biopsy, the patient was normotensive (120/70 mmHg of blood pressure) with a normal heart rate (61 beats per minute) and a body mass index of 26.7. There was no edema. Physical examination was unremarkable otherwise. Urine analysis showed proteinuria (3+) and microscopic hematuria (1+, red blood cell [RBC] 6–10/high-power field) with dysmorphic RBCs (13%). UPCR was 1,392.5 mg/g. Serum creatinine was 0.78 mg/dL. Serum albumin was 4.4 g/dL. Cholesterol level was 195 mg/dL. C-reactive protein was not elevated at less than 0.2 mg/dL. C3 level was normal at 113 mg/dL. Anti-nuclear antibody and anti-neutrophil cytoplasmic antibody were not detected.

On light microscopy, a total of 20 glomeruli were present. A glomerulus with perihilar sclerosis was noted; it also had periglomerular fibrosis with Bowman's capsule wrinkling (Fig. 1). The other glomeruli were normocellular without mesangial expansion or size enlargement. The capillary loops were patent without collapse. The glomerular basement membrane was not thickened or duplicated. Tubules showed mild atrophy with focal proteinaceous casts. Mild interstitial fibrosis was present with mild inflammatory infiltrates. Vessels were unremarkable. On immunofluorescent microscopy, six glomeruli were present. Minimal to mild deposits of C3 were present in the mesangium of the glomeruli. No deposits of IgG, IgA, IgM, C4, C1q, fibrin-

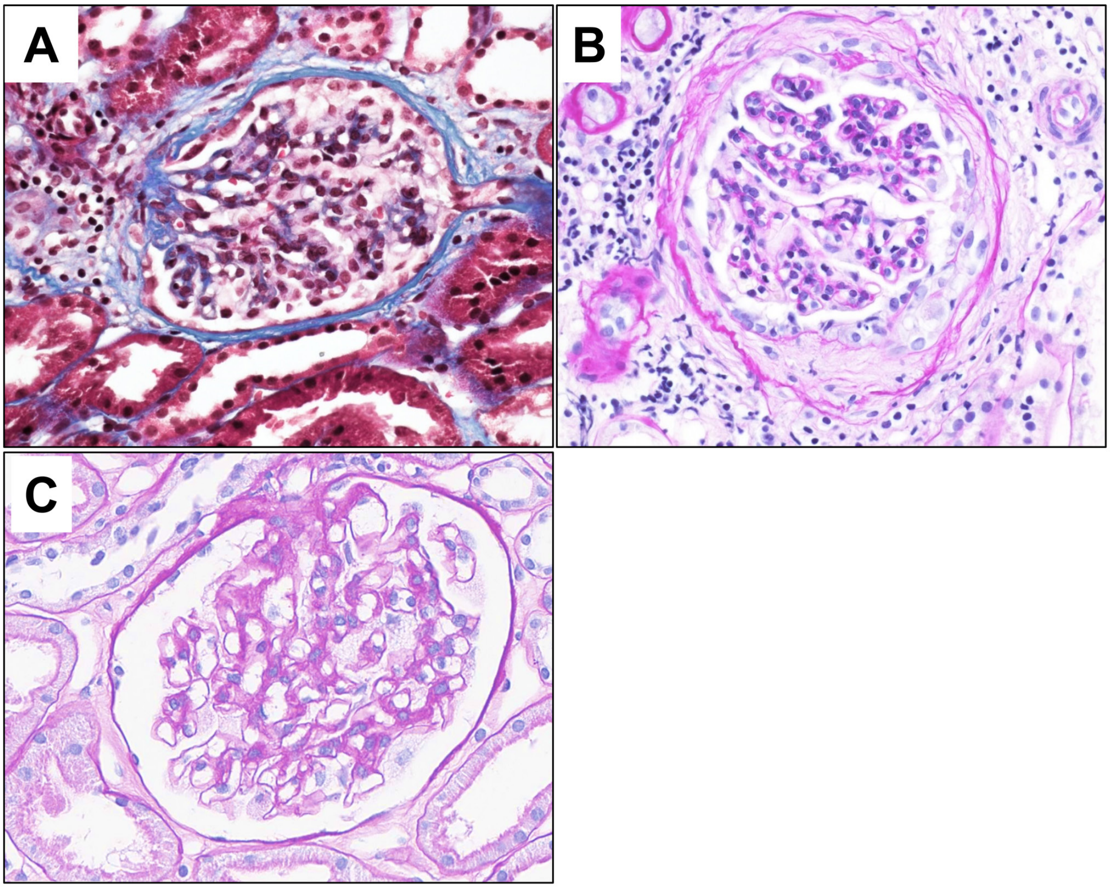

Fig. 1. Light microscopy reveals a glomerulus showing focal perihilar sclerosis (A, Masson's trichrome) and periglomerular fibrosis with Bowman's capsule wrinkling (B, periodic acid-Schiff). A glomerulus from Fabry disease, characterized by the presence of foamy histiocytes, is presented (C).

ogen, kappa, or lambda were identified. On electron microscopy (EM), alternating lamellar structures of electron-dense and electron-lucent area, known as myeloid or zebra bodies, were identified in the cytoplasm of podocytes (Fig. 2). The foot processes were diffusely effaced, covering around 100% of the area. Based on histopathology findings, Fabry disease with secondary focal segmental glomerulosclerosis was suspected.

To confirm the diagnosis, the activity level of α-galactosidase A enzyme was measured using tandem mass spectrometry. The enzyme activity was within normal limits. Next-generation sequencing was performed on *GLA*, encompassing the coding region and the ±25 base pairs of the flanking region. The result was negative for all pathogenic, likely pathogenic, and variants of undetermined significance; only three benign variants were identified. Thorough family history taking was done, but none of the family members had typical symptoms or signs of Fabry disease, including paresthesia, renal dysfunction, cardiac arrythmia, or myocardial infarction. The patient also had no industrial exposure to silicon, which ruled out the possibility of silicon nephropathy. Taken together, the final diagnosis was DIP.

He was started on losartan, an angiotensin II receptor blocker, at a dose of 50 mg daily. He has been attending the outpatient clinic regularly every 6 months, with proteinuria and renal function remaining stable. Hematuria remained at 1+, and UPCR increased slightly to 1,948.3 mg/g at the last visit.

DISCUSSION

Fabry disease is an X-linked inherited disorder characterized by multiple systemic manifestations due to inherent shortages of an enzyme, α-galactosidase A, or its inactivity. α-galactosidase A is a hydrolase that resides in lysosomes and its deficiency leads to the progressive accumulation of glycosphingolipids such as globotriaosylceramide (GL-3), which impairs the function of tissues and organs. The symptoms of Fabry disease include paresthesias in the extremities, angiokeratomas, corneal opacity, anhidrosis, and heart and cerebrovascular dysfunction. When the kidney is affected, proteinuria and hematuria may occur, and in most cases, it progresses to renal failure when patients reach their 30s to 40s [11]. Typical light microscopic findings include foamy and vacuolated podocytes. On EM, enlarged lysosomes are filled with osmiophilic and lamellated

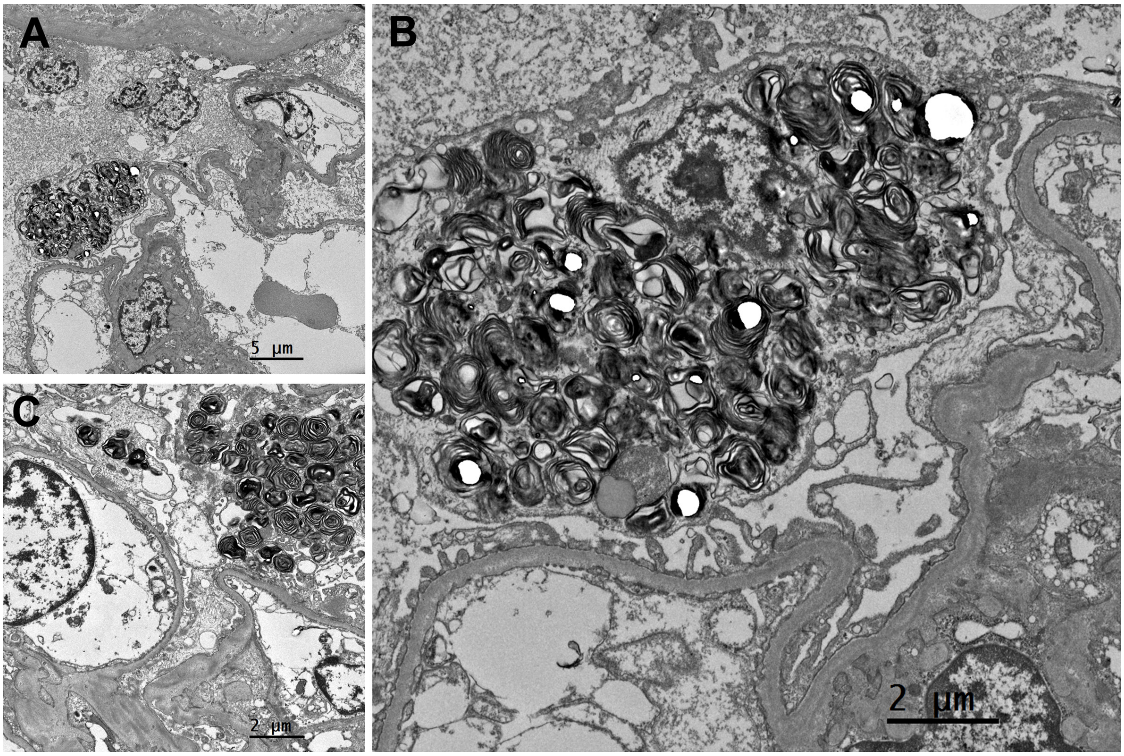

Fig. 2. Electron microscopy demonstrates zebra bodies (myeloid bodies) within the podocytes and diffuse effacement of the foot processes (A, ×800; B and C, ×2,000).

membrane structures showing an onion skin-like appearance or parallel dense layers, so called myeloid or "zebra" bodies. Inclusions related to accumulated GL-3 are typically present in podocytes. They are also present in the mesangium, parietal epithelium, tubular epithelium, and vascular myocytes. In this case, although the patient had zebra bodies on EM, there were no relevant symptoms or family history.

Although rare, atypical Fabry disease must also be considered in the differential diagnosis. The distinguishing features of this condition include a later onset, milder symptoms, and higher α-galactosidase A activity (ranging from 1% to 35% compared to less than 1% in the classic form). While the condition is primarily observed in females due to its X-linked nature, it has been documented in 1.2% of males with end-stage kidney disease on hemodialysis [2]. It is possible for patients with atypical Fabry disease to exhibit near-normal α-galactosidase A activity, which is consistent with the observations made in this case. In such case, measuring GL-3 levels would be informative. We were unable to measure GL-3 levels due to practical constraints, which is a limitation. Despite the fact that routine sequence analysis is reported to encompass up to 95% of pathogenic variants [2], approximately 5% are likely to be identified exclusively through gene-targeted deletion/duplication analysis [2]. Although there are limitations to our analysis, including the absence of GL-3 level measurement and deletion/duplication assays, which prevent the complete exclusion of atypical Fabry disease, the absence of abnormalities in other organs, especially the heart, and the patient's relatively young age of 17 years at the time of biopsy led to a diagnosis of DIP.

Another differential diagnosis that causes zebra bodies is DIP. Due to their physicochemical structure, cationic amphiphilic drugs (CADs) can easily pass through cell membranes, as they have both hydrophobic and hydrophilic domains. The acidic nature of the lysosome appears to provide a favorable environment for basic CADs to accumulate and become entrapped through protonation [12]. CADs inhibit lysosomal phospholipase activity by forming indigestible complexes with phospholipids [13], or by directly inhibiting phospholipase [14]. This leads to phospholipids accumulating in lysosomes [12]. Patients with DIP related to CADs may exhibit less extensive zebra bodies than those with Fabry disease [6] or curvilinear bodies (i.e., twisted microtubular structure). However, neither of these is a definitive distinguishing factor.

Drugs such as hydroxychloroquine [7,8], amiodarone [9], and ranolazine [15] have been reported to cause phospholipidosis in the kidney. Atomoxetine is a selective norepinephrine reuptake inhibitor that has been used to treat ADHD since 2002. Although atomoxetine has not been reported to cause DIP, its structure meets the criteria of CADs. It has a primary amine group corresponding to the hydrophilic domain, as well as two aromatic rings—a phenyl ring and an o-tolyl ether—corresponding to the hydrophobic domain [16]. The circumstances in which CADs can cause phospholipidosis are not well understood. The cumulative dose of the drug may be associated with this condition [17], but experiments in animals and in vivo to verify this have not yet been conducted. Similarly, the time to recover renal function following drug withdrawal varies, and full recovery does not always occur [8]. In this case, almost all the foot processes of the podocytes were effaced, and perihilar sclerosis progressed. The patient discontinued atomoxetine at age 8 after 1 year of treatment. At the current follow-up (age 17, 10 years post-discontinuation), proteinuria persists, likely reflecting irreversible podocyte injury as evidenced by the extensive foot process effacement and perihilar sclerosis on the initial biopsy.

Various types of drugs, such as antidepressants, antibiotics, antiarrhythmics, and antimalarials, belong to the CAD category, but their association with phospholipidosis and the mechanisms that cause cellular and clinical toxicity are relatively poorly understood. Although a predictive biomarker for phospholipidosis (i.e., urine di-22:6-BMP [18]) has been discovered, it is expected to be some time before it is introduced into drug monitoring in practice.

Zebra bodies were once considered a definitive finding of Fabry disease [19], but are now considered not uncommon in cases of DIP or silicon nephropathy [20]. Since many drugs belong to the CAD class, if zebra bodies are found in EM, DIP should be considered alongside Fabry disease.

Ethics Statement

All procedures performed in the current study were exempted from review by the Institutional Review Board (NHIMC IRB 2025-08-012, 2025-08-21) in accordance with the 1964 Helsinki declaration and its later amendments, and written informed consent was obtained from the patient.

Availability of Data and Material

The datasets generated or analyzed during the study are available from the corresponding author on reasonable request.

Code Availability

Not applicable.

ORCID

Sung-Eun Choi	https://orcid.org/0000-0002-6955-658X
Kee Hyuck Kim	https://orcid.org/0000-0003-4720-6455
Minsun Jung	https://orcid.org/0000-0002-8701-4282
Jeong Hae Kie	https://orcid.org/0000-0003-1782-5650

Author Contributions

Conceptualization: JHK. Investigation: JHK, KHK, SEC. Visualization: JHK, MJ, SEC. Writing—original draft: SEC. Writing—review & editing: all authors. Approval of final manuscript: all authors.

Conflicts of Interest

The authors declare that they have no potential conflicts of interest.

Funding Statement

No funding to declare.

REFERENCES

1. Mehta A, Widmer U. Natural history of Fabry disease. In: Mehta A, Beck M, Sunder-Plassmann G, eds. Fabry disease: perspectives from 5 years of FOS. Oxford: Oxford PharmaGenesis, 2006.
2. Nakao S, Kodama C, Takenaka T, et al. Fabry disease: detection of undiagnosed hemodialysis patients and identification of a "renal variant" phenotype. Kidney Int 2003; 64: 801-7.
3. Ries M, Gal A. Genotype-phenotype correlation in Fabry disease. In: Mehta A, Beck M, Sunder-Plassmann G, eds. Fabry disease: perspectives from 5 years of FOS. Oxford: Oxford PharmaGenesis, 2006.
4. Woywodt A, Hellweg S, Schwarz A, Schaefer RM, Mengel M. A wild zebra chase. Nephrol Dial Transplant 2007; 22: 3074-7.
5. Bracamonte ER, Kowalewska J, Starr J, Gitomer J, Alpers CE. Iatrogenic phospholipidosis mimicking Fabry disease. Am J Kidney Dis 2006; 48: 844-50.
6. Costa RM, Martul EV, Reboredo JM, Cigarran S. Curvilinear bodies in hydroxychloroquine-induced renal phospholipidosis resembling Fabry disease. Clin Kidney J 2013; 6: 533-6.
7. Khubchandani SR, Bichle LS. Hydroxychloroquine-induced phospholipidosis in a case of SLE: the wolf in zebra clothing. Ultrastruct Pathol 2013; 37: 146-50.
8. de Menezes Neves PD, Machado JR, Custodio FB, et al. Ultrastructural deposits appearing as "zebra bodies" in renal biopsy: Fabry disease? Comparative case reports. BMC Nephrol 2017; 18: 157.
9. Pintavorn P, Cook WJ. Progressive renal insufficiency associated with amiodarone-induced phospholipidosis. Kidney Int 2008; 74: 1354-7.
10. Duineveld MD, Kers J, Vleming LJ. Case report of progressive renal dysfunction as a consequence of amiodarone-induced phospholipidosis. Eur Heart J Case Rep 2023; 7: ytad457.
11. Najafian B, Mauer M, Hopkin RJ, Svarstad E. Renal complications of Fabry disease in children. Pediatr Nephrol 2013; 28: 679-87.
12. Lullmann H, Lullmann-Rauch R, Wassermann O. Lipidosis induced by amphiphilic cationic drugs. Biochem Pharmacol 1978; 27: 1103-8.
13. Lullmann-Rauch R. Drug-induced lysosomal storage disorders. Front Biol 1979; 48: 49-130.
14. Kubo M, Hostetler KY. Mechanism of cationic amphiphilic drug inhibition of purified lysosomal phospholipase A1. Biochemistry 1985; 24: 6515-20.
15. Scheurle C, Dammrich M, Becker JU, Baumgartel MW. Renal phospholipidosis possibly induced by ranolazine. Clin Kidney J 2014; 7: 62-4.
16. Reasor MJ, Hastings KL, Ulrich RG. Drug-induced phospholipidosis: issues and future directions. Expert Opin Drug Saf 2006; 5: 567-83.
17. Vater M, Mockl L, Gormanns V, et al. New insights into the intracellular distribution pattern of cationic amphiphilic drugs. Sci Rep 2017; 7: 44277.
18. Tengstrand E, Zhang H, Liu N, Dunn K, Hsieh F. A multiplexed UPLC-MS/MS assay for the simultaneous measurement of urinary safety biomarkers of drug-induced kidney injury and phospholipidosis. Toxicol Appl Pharmacol 2019; 366: 54-63.
19. Alroy J, Sabnis S, Kopp JB. Renal pathology in Fabry disease. J Am Soc Nephrol 2002; 13 Suppl 2: S134-8.
20. Banks DE, Milutinovic J, Desnick RJ, Grabowski GA, Lapp NL, Boehlecke BA. Silicon nephropathy mimicking Fabry's disease. Am J Nephrol 1983; 3: 279-84.